

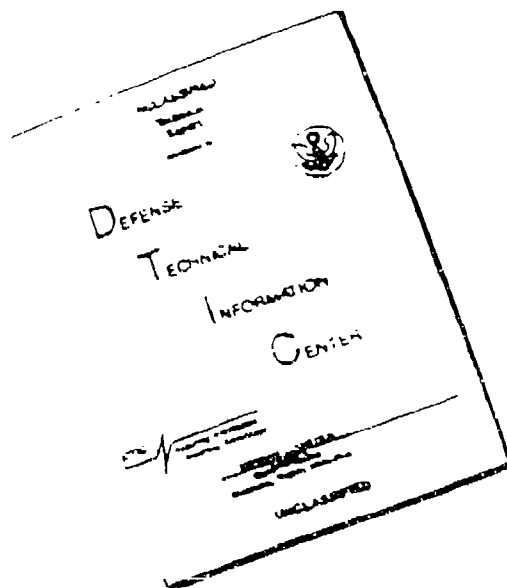


REPORT D		AD-A255 967		m Approved OMB No. 0704-0188 (2)	
<small>Public reporting burden for this collection of information is estimated to average 1 hour per response, including the time for reviewing instructions, searching existing data sources, gathering and maintaining the data needed, reviewing and collecting the information, and reviewing and editing the collection of information. Send comments regarding this burden estimate or any other aspect of this collection of information, including suggestions for reducing this burden, to Washington Headquarters Service, Project (0704-0188), Washington, DC 20503.</small>				<small>For reviewing instructions, searching existing data sources, gathering and maintaining the data needed, reviewing and collecting the information, and reviewing and editing the collection of information, including suggestions for reducing this burden, to Washington Headquarters Service, Project (0704-0188), Washington, DC 20503.</small>	
1. AGENCY USE ONLY (Leave blank)		2. REPORT DATE 30 June 1992		3. REPORT TYPE AND DATES COVERED Final Technical 5/1/90-4/30/92	
4. TITLE AND SUBTITLE Control of Asymmetric Jet		DTIC SELECTE S D OCT 07 1992		5. FUNDING NUMBERS AFOSR- 90-0301 2307/BS	
6. AUTHOR(S) Ho, Chih-Ming				8. PERFORMING ORGANIZATION REPORT NUMBER 2 0864	
7. PERFORMING ORGANIZATION NAME(S) AND ADDRESS(ES) Department of Aerospace Engineering University of Southern California Univeristy Park, RRB 101 Los Angeles, CA 90089-1191		* AFOSR-TR-		10. SPONSORING/MONITORING AGENCY REPORT NUMBER AFOSR 90-0301	
9. SPONSORING/MONITORING AGENCY NAME(S) AND ADDRESS(ES) Air Force Office of Scientific Research Bolling AFB, D.C. 20332-6448		N/A			
11. SUPPLEMENTARY NOTES					
12a. DISTRIBUTION/AVAILABILITY STATEMENT Approved for publication and release; distribution unlimited			12b. DISTRIBUTION CODE		
13. ABSTRACT (Maximum 200 words) A passive method of enhancing the rate of entrainment by as much as 500% in subsonic open nozzle flows has been obtained by modifying axisymmetric nozzle geometry to a 2:1 aspect-ratio elliptic nozzle. Small aspect-ratio elliptical nozzles have been demonstrated to more efficiently control mixing processes and to exhibit increased rates of spreading, entrainment and fine-scale mixing than axisymmetric nozzles at subsonic and supersonic conditions in a confined dump combustor and in high-temperature ramjets. Vortex self-induction is the principle mechanism controlling mixing processes in asymmetric jet nozzles.					
92 10 000				92-26586/91  43	
14. SUBJECT TERMS Small aspect-ratio elliptic jet, vortex self-induction bulk mixing, small-scale mixing, axis switching				15. NUMBER OF PAGES 124	
17. SECURITY CLASSIFICATION OF REPORT unclassified		18. SECURITY CLASSIFICATION OF THIS PAGE unclassified		19. SECURITY CLASSIFICATION OF ABSTRACT unclassified	
20. LIMITATION OF ABSTRACT UNCLASSIFIED					

DISCLAIMER NOTICE



THIS DOCUMENT IS BEST QUALITY AVAILABLE. THE COPY FURNISHED TO DTIC CONTAINED A SIGNIFICANT NUMBER OF PAGES WHICH DO NOT REPRODUCE LEGIBLY.

Grant No. AFOSR-90-0301

CONTROL OF ASYMMETRIC JET

*Principal Investigator:
Ho, Chih-Ming*

*Department of Aerospace Engineering
University of Southern California
University Park
Los Angeles, California 90089-1191*

30 June 1992

*Final Technical Report
Period: 01 May 1990 to 30 April 1992*

*Air Force Office of Scientific Research
Bolling Air Force Base
Washington, D.C. 20332-6448*

Control of Asymmetric Jets

FINAL REPORT

AFOSR-90-0301

Principal Investigator: Chih-Ming Ho

Department of Aerospace Engineering

University of Southern California

Los Angeles, CA 90089-1191

INTRODUCTION

The study of turbulent jet shear flow plays an important role in numerous engineering applications. Free and confined jets are common devices present in mixing processes and the production of thrust. Jets form due to flow issuing from a nozzle and the resultant velocity difference forms a shear layer consisting of coherent toroidally shaped vortical structures whose dynamics are responsible for entraining surrounding fluid and the generation of fine scale mixing requisite for the initiation of chemical reactions. It is therefore desirable to control the transfer of mass, heat and momentum via large-scale and small-scale mixing processes.

A passive method of enhancing the rate of entrainment by as much as 500% in subsonic open nozzle flows has been obtained by modifying axisymmetric nozzle geometry to a 2:1 aspect-ratio elliptic nozzle.¹ Small aspect-ratio elliptical jet nozzles have been demonstrated to more efficiently control mixing processes and to exhibit increased rates of spreading and entrainment than axisymmetric nozzles at subsonic² and supersonic conditions,³ in a confined dump combustor,⁴ and in high-temperature ramjet facilities.⁵

Toroidal elliptic vortices in asymmetric jet shear layers are characterized by azimuthally varying radii of curvature. The section of the vortex ring occupying the major axis plane with minimum radius of curvature is convected faster downstream by nature of the *Biot-Savart Law* of induction than the minor axis plane section which has maximum radius of curvature. The faster moving section of the major axis section convects forward as it bends inward decreasing its local radius of curvature until it matches the radius of curvature of the minor axis section which is simultaneously moving outwards. This asymmetric process called *vortex self-induction* is the principle mechanism driving entrainment in small aspect-ratio elliptic jets which entrain ten times more mass in the minor axis region than the major axis region.¹ These vortex dynamics unique to three-dimensional nozzles severely deform the topology of the large-scale structures and are responsible for the elliptic jet's enhanced mixing properties. The phenomenon of *axis switching* occurs when the original elliptically contoured ring briefly sustains a symmetric configuration following a series of downstream deformations and its distance from the nozzle exit reflects increased levels of large-

<input checked="" type="checkbox"/>
<input type="checkbox"/>
<input type="checkbox"/>

and/or

ity Codes
and/or
ial

A-1

scale mixing.

Results at the University of Southern California demonstrate that the initial frequency content, velocity, temperature, upstream geometry of the exit nozzle and its aspect-ratio governs the hydrodynamic instabilities responsible for the creation and evolution of the elliptic jet's shear layer. These initial parameters modify the boundary layer momentum thickness at the jet exit creating an asymmetric distribution of vorticity throughout the elliptical nozzle's contour. This alteration in the initial Kelvin-Helmholtz instability wave strongly modifies the downstream self-induction process of the ensuing large-scale structures. Current investigations have determined that the mechanism of self-induction which controls the large scale evolution of the elliptic jet is also the principle source of small-scale production in the shear layer. Whereas vortex merging is responsible for small-scale production in two-dimensional and axisymmetric free shear layers.⁶ Therefore, the entire spectrum of mixing from the large inviscid structures down to the smallest viscous dominated fine scales are controllable either directly or indirectly via the self-induction mechanism.

ELLIPTIC JET FACILITY

The experimental jet facility is driven by four centrifugal blowers in parallel and heated by two electric heaters in parallel. The flow enters an anechoically treated settling chamber, contracts into an aluminum stagnation chamber of constant diameter and passes through a series of aluminum honeycomb, aluminum foam, and fine wire mesh screen sections enhancing flow uniformity and reducing turbulence. An aluminum composite nozzle smoothly contracts to a 2:1 aspect-ratio elliptical orifice whose major and minor axes' dimensions are 50.8 cm ($= 2a$) by 25.4 cm ($= 2b$), respectively. The semimajor axis length, a , will be the typical scale for nondimensionalizing lengths. The operational conditions of the jet facility are bounded by a maximum velocity of 85 m/s and a maximum temperature of 220 C.

Instantaneous velocity signals are sampled by high temperature hot-wire probes connected to multi-channel constant-temperature circuits providing a flat frequency response to 30 kHz. Instantaneous temperature signals are sampled by a cold-wire probe that is digitally frequency compensated to 3 kHz. The single wire sensor element consists of 5.08 μ m diameter platinum-10% rhodium wire attached to a 1 mm wide probe and the parallel wire probe has two elements 0.4 mm wide separated by 0.5 mm allowing enhanced resolution in detecting small structures. The probes are mounted on a microcomputer controlled traverse system translatable in three-dimensions. Fluctuating multiple-channel data is digitized by a 33 MHz 80386 PC microcomputer at acquisition rates up to 1 MHz and recorded on a 650 Mb erasable optical disk and an ethernet networked 1 Gb Winchester disk. Data is subsequently processed and transferred between Localtalk networked 80386 PCs and a 40 MHz Macintosh IIx workstation.⁷

Sampling along the major and minor axes provides mean and fluctuating profiles of velocity or temperature, respectively, which indicate jet spreading rates and axis switching locations. The massflow, small-scale distribution and streamwise velocity gradients are investigated throughout one

quadrant at respective downstream cross-sections by sampling velocities and temperature across a rectangular grid. Measurements of the total massflow are determined by sampling the velocity and temperature across an entire surface normal to the free stream direction and indicate the amount of ambient fluid entrained into the flow by the large-scale vortices. Instantaneous velocities are phase-averaged with respect to a second hot-wire probe recording the passing of large scale structures. Large-scale information is obtained by smoothing raw data with a finite-impulse response digital filter. Frequency content is determined with the 1-D fast Fourier algorithm and both physical and spectral information are obtained with the 1-D Wavelet Transform algorithm. Small-scale structures are detected through a series of conditional statements employed in the Peak-Valley Counting Technique developed at the University of Southern California.⁸

TECHNICAL DISCUSSIONS

I. Initial Conditions

The effects of exit velocity, temperature and frequency upon the elliptic jet's development were investigated at the jet exit to understand what factors influence vortex self-induction. The initial momentum thickness in the major and minor axes' regions confirmed previous findings of the existence of an asymmetric distribution of momentum thickness about the nozzle perimeter.¹ At the lowest velocity measured, $U_0 = 20$ m/s, the momentum thickness is narrower in the minor axis region than the major axis region such that $\theta_a/\theta_b \approx 6$ inferring the existence of intense vorticity distribution in the minor axis region due in part to a smaller radius of curvature along the upstream nozzle wall contour in the minor axis plane which induces a larger transverse pressure gradient in that region of the boundary layer. At higher exit velocities the momentum thickness decreases in the major axis to match the minor axis momentum thickness and create a more symmetric distribution of vorticity that retards the effects of vortex self-induction.

The influence of frequency content was investigated through forcing at the *Preferred Mode* frequency, the characteristic passage frequency of the large scale structures at the end of the jet's *potential core* region approximately five exit diameters downstream. Under forcing the momentum thickness increases by 100% due to additional flow acoustically driven from the forcing chambers adjacent to the jet exit. However, the momentum thickness ratios decrease to half the natural values and θ_a/θ_b decreases from three to unity with increasing exit velocity. Therefore, Preferred Mode forcing enhances the initial vorticity distribution in the major axis region.

Dramatic increases in flow spreading are achievable by forcing at the Preferred Mode because the initial vortices amalgamate into larger structures at a frequency approximately one-tenth their 'natural' value resulting in a *Collective Interaction* phenomenon.⁹ Spectral analysis of the instability waves near the jet exit confirm the ability of Preferred Mode forcing to suppress vortex merging. Preferred Mode forcing is a useful diagnostic means of investigating the isolated effects of vortex self-induction in asymmetric jet flows.¹⁰

Exit velocity and temperature profoundly alter the elliptic jet's flow field. Mean velocity profiles in the major and minor axes exhibit greater shear layer spreading rates at lower exit velocities and higher exit temperatures. Jet growth may be properly illustrated by plotting the *velocity halfwidth*, the radial location at which the local velocity is half the centerline, for varying streamwise stations. The elliptic jet's spreading is greater and hence its bulk mixing properties improve when the axis switching location is nearer to the nozzle exit because the outward radially growing minor axis region entrains more ambient upstream. The length of the axis switching location is a strong indicator of the efficiency of vortex self-induction and is dependent upon the exit Reynolds number, and the exit density ratio, $\Gamma = \rho/\rho_\infty$.¹¹ Axis switching locations occur farther downstream in larger aspect-ratio asymmetric jets and consequently these nozzle configurations offer lower rates of mixing.¹² Refer to Figure 1.

Entrainment ratios obtained by normalizing the local massflow to the exit massflow demonstrated the elliptic jet to entrain more fluid than an axisymmetric jet of equivalent exit hydraulic diameter at varying velocity and temperature conditions thereby extending its operating range. The minor axis region entrains more than the major axis region for all velocity and temperature cases studied confirming the existence of an asymmetric massflow distribution due to self-induction dynamics rather than vortex merging.¹ Entrainment ratios in the elliptic jet decrease with increasing exit velocity and increase at higher flow temperatures which correlates remarkably well with the axis switching location. High temperature *nonhomogeneous* flows entrain as much as 30% more at $T_0 = 480$ K than ambient flows inferring that density effects exert stronger instability influences than the Reynolds number upon vortex self-induction dynamics. The near-field region of a nonhomogeneous elliptic jet entrains up to six times more than a homogeneous axisymmetric jet and entrains up to three and a half times more than a nonhomogeneous axisymmetric jet.¹¹ Refer to Figure 2. These findings are promising in view of the fact that combustion processes are typically initiated in the near-field region. Stability calculations reveal greater deformations in the initial vortices at increased exit temperatures supporting experimental observations, and increased temperatures improve bulk mixing characteristics in an elliptic jet.¹³

The initial exit conditions, including velocity, temperature and frequency content in addition to the nozzle geometry, together significantly modify the initial momentum thickness and hence the initial vorticity content of the large scales. The momentum thickness is an important length scale and coupled with velocity and the initial instability frequency through a constant Strouhal number relationship for jet free shear layers dictates initial conditions.¹⁴ The degree of asymmetry in the vorticity distribution is responsible for the azimuthally varying induced velocity distribution that determines the rate of growth of the shear layer by inviscidly controlled dynamics of vortex self-induction.

II. Self-induction Dynamics¹¹

The mean velocity profiles emerging from asymmetric nozzle possess top-hat profiles and evolve

into bell-shaped profiles downstream. However, three-dimensional jets are distinguished from their axisymmetric counterparts by displaying unique velocity profiles and spread rates in the planes of their major and minor axes regions, respectively. The minor axis velocity profiles display considerably higher spreading than the major axis velocity profiles. The Reynolds number dependence of vortex self-induction is evident in the degree of asymmetry of the mean velocity contours at two extreme exit velocities. Increased spreading of the minor axis shear layer into the ambient and near-circular topologies characterize the lower velocities and at higher velocities spreading rates are less pronounced in both axes' regions and contours of constant velocity retain their elliptical nature signifying delayed axis switching. Refer to Figure 3(a).

Preferred Mode forcing severely distorts the mean flow field from an elliptical to a rectangular distribution and downstream of the potential core the acoustically modified azimuthal modes severely distort the vortex ring into a 'cloverleaf' distribution possibly as a result of the toroidal vortices interacting with enhanced streamwise vortices.¹⁵ Lower degrees of spreading characterize the minor axis region: prolonging the onset of axis switching, thus Preferred Mode forcing appears to strengthen the vorticity content of the major axis region at the expense of the minor axis region. Refer to Figure 3(b).

An approximation of the large scale vorticity field in the natural and Preferred Mode forced cases was obtained from low-frequency bandpassed, time-averaged and phase-averaged analyses of the velocity strain rate field, $\partial u/\partial x$, $\partial u/\partial y$ and $\partial u/\partial z$. Two of the three vorticity components lie parallel to the vortex ring plane and are approximated by two of the velocity strain quantities, $\omega_y = \partial u/\partial z - \partial w/\partial x - \partial u/\partial z$, and $\omega_z = \partial v/\partial x - \partial u/\partial y - \partial u/\partial y$. Vorticity in the major axis region may be approximated by values of $-\partial u/\partial y$, and similarly, vorticity in the minor axis region by values of $\partial u/\partial z$. Intersections of phase-averaged $\partial u/\partial y$ with the major axis plane and phase-averaged $\partial u/\partial z$ with the minor axis plane, respectively, readily visualize vortex cores. Near the jet exit at the second vortex merging location the major axis section of the ring is shifted downstream of the minor axis section in agreement with flow visualization¹ and the Biot-Savart Induction Law. At the location of axis switching the minor axis core surpasses the major axis core accompanied by an increase in its local ring radius. Far downstream in the fully turbulent region both core sections exhibit weakened vorticity of one-fifth their initial value due to phase decorrelation of the large scale structures.¹⁶ The major axis vortex cross-sections are approximately 100% larger in dimension and as much as 50% weaker in magnitude than the respective minor axis cores confirming the presence of more intense vorticity in the minor core. Preferred Mode forcing intensifies the vortex cores by reducing their cross-section 20% and increasing peak vorticity by 100% by more efficiently imparting energy from the mean flow into the large-scale vortices. The forced major cores are of approximate strength as the minor cores adding evidence to the existence of an enhanced major axis region under Preferred Mode forcing.

The temperature field was investigated at nonhomogeneous conditions and displayed regions of cooler ambient fluid penetrating into the potential core along the minor axis. Investigations revealed greater rms temperature peaks in the minor axis section and a conspicuous bifurcation of the

centerline temperature peak in the mean temperature field at the end of the potential core together substantiated the existence of larger mixing rates in the minor axis region. Probability density function analyses of the turbulent temperature field identified broader, more evenly distributed temperature profiles along the minor axis skewed towards ambient temperatures. In contrast the major axis profiles were characterized by narrower peaks skewed towards centerline temperatures.¹⁷

Density fluctuations in the nonhomogeneous elliptic jet was visualized by conventional shadowgraph, schlieren and focused schlieren optical diagnostic methods.¹⁸ The wrinkled turbulent three-dimensional outer structure of the shear layer, streamwise vortices and toroidal structures were imaged at various velocities and temperatures confirming the existence greater spreading in the minor axis plane. Focused schlieren techniques imaged planar sections of finite depth within the shear layer and individual cross-sections of tilting large scale vortices albeit at reduced levels of contrast.

III. Small Scale Topology^{11, 19}

The three-dimensional topology of the small-scale structures in the elliptic jet shear layer was investigated for the case $U_0 = 20$ m/s to document small-scale production regions and to identify the physical mechanism of small-scale generation. Small-scale structures designate regions of small-scale mixing where large parcels of ambient fluid are homogenized and broken down to progressively smaller scales by complex large-scale vortex interactions and infer the existence of combustion regions in reacting flows possible under required thermodynamic and stoichiometric conditions. The flow was forced at the Preferred Mode frequency to isolate vortex self-induction effects from vortex merging on small-scale generation and compared against the natural case.

Within the first five semimajor axis diameters downstream the small-scale structures are asymmetrically distributed in the vortex ring regions in the natural case with as much as 40% larger populations in the minor axis region. In the Preferred Mode forced case the modified rectangular vortices contain a more symmetric small-scale distribution with only 10% greater small-scale activity in the major axis region. Farther downstream in the natural case the small-scale structures spread inwards to the jet center taking on a symmetric near-circular distribution and similar events characterize the forced case except that the small-scale contour levels take on rectangular contours and further downstream 'cloverleaf' distributions characteristic of the mean velocity field in the distorted shear layer. In the natural case the distributions are maximum in the near-field minor axis region by as much as 40% more than the surrounding shear layer with the reverse occurring in the Preferred Mode forced case where they are more symmetric with less prominent peaks which are 10% greater than levels occupying the vortex ring downstream of $x/a = 4$ in the forced case. Maxima in the number small scales per number of local large scales increases parabolically in the natural case downstream because the large scale populations decrease downstream due to successive vortex mergings. However, in the forced case vortex merging is suppressed and consequently the number of small scales per local large scales remains nearly constant with a small peak at $x/a=5$. Refer to

Figures 4(a) & 4(b).

Preferred Mode forcing distributes more small scales over a greater cross-section and overall small-scale population increases by 25% than the natural case possibly due to enhanced interactions between larger, concentrated toroidal vortices and streamwise structures. Therefore, the mechanism of vortex self-induction rather than vortex merging is principally responsible for small-scale generation in a subsonic 2:1 aspect-ratio elliptic jet.¹⁹ Small scales are produced one semimajor axis diameter closer to the jet exit under forcing thereby decreasing the distance to turbulent transition and shifting higher levels of small-scale mixing activity nearer upstream to the exit. In the natural case both major and minor axis regions generate equivalent numbers of total small scales, whereas the forced major axis region produces as much as 50% more small scales than the minor axis region. Self-induction enhances vorticity in the major axis region. Refer to Figure 5. In the natural case the number of small scales peaks at $x/\lambda_0 = 8$, the second vortex merging location similar to that of a subsonic mixing layer⁸ and at higher exit velocities the peak in the streamwise small-scale population shifts upstream to $x/\lambda_0 = 4$. The small-scale levels steadily decrease downstream due to the dissipation of decreasing turbulent kinetic energy in the decaying free shear layer at the wavelength of the small-scale structures.⁸ The peak in the forced case occurs upstream of the natural peak at $x/\lambda_F = 0.3$, where λ_F is the Preferred Mode wavelength, for all velocity cases due to increased turbulence levels nearer to the jet exit. Downstream the numbers decrease, then gradually increase to a small peak at the end of the potential core and finally decay downstream in a fashion similar to the natural case. Refer to Figures 6(a) & 6(b).

A frequency histogram analysis of the small-scale content in the shear layer reveals peaks identifying the most probable small-scale frequency whose values increase linearly with greater Reynolds number. For a given velocity the peak of the small-scale frequency distribution decreases very gradually downstream along the decaying shear layer for both the natural and Preferred Mode forced cases. In addition, these distributions are identical in both axes' regions for both flow cases indicating that forcing only modifies the large-scale structures and the population of small scales but it does not *directly* affect the physical nature of the viscous-dominated small scales. The dimension of the small-scale structures are about one order of magnitude larger than the Kolmogorov length scale and 1/2 to 3/4 smaller than the Taylor microscale.

Time-averaged and phase-averaged population densities of the small-scale and velocity strain rate distributions suggest the minor axis region of the vortices control small-scale processes. Two-dimensional raster imaging demarcates regions of small-scale activity during successive phases of the passage of one large scale structure.¹⁴ Contours of constant $\partial u/\partial z$ representing the partial vorticity component in the minor axis region correlate with the small-scale topology in the natural case than contours of $\partial u/\partial y$ representing the partial vorticity component in the major axis region. Small-scale production by the correlated and stronger vorticity field in the minor axis region complements the existence of greater entrainment values and maxima of the small-scale distribution in the minor axis region. In the Preferred Mode forced case the $\partial u/\partial z$ distribution also correlates more strongly with

the distorted albeit more symmetric small-scale distribution. Phase-averaged analyses confirmed the occurrence of small scales and both $\partial u/\partial y$ and $\partial u/\partial z$ velocity strain rates within the vortex core cross-sections. The maximum number of small scales occur in the downstream circumferential section of the vortex core for the natural case and in the center of the vortex core for the forced case. Furthermore, the regions of velocity strain rate extend upstream into the 'braid' region in the natural case but do not under forcing. Observations of natural and forced small-scale mixing activity in the subsonic elliptic jet correlate well with combustion product concentrations visualized in natural and Preferred Mode forced chemically reacting nozzle flows.²⁰ Refer to Figures 7(a) & 7(b).

CONCLUSION

By *passively* changing nozzle contour geometry and aspect-ratio and *actively* varying the initial frequency content, velocity and temperature, the initial asymmetric vorticity distribution in the elliptic nozzle boundary layer has been demonstrated to modify the dynamics of vortex self-induction. Preferred Mode forcing effectively suppresses vortex merging in the elliptic jet by driving many large-scale structures to roll-up into one larger vortex via the Collective Interaction mechanism. The three-dimensionally deforming, mutually self-inducting coherent vortex structures control the large- and small-scale mixing properties of the elliptic jet. Two related jet properties, the location of the first axis switching and mass entrainment, demonstrate increased large-scale mixing at decreased exit velocity and increased exit temperature. Phase-averaged mean velocity strain rates visualize the topology of the coherent vortex rings and illustrate phase decorrelation of the vortices downstream. The temperature field in the nonhomogeneous elliptic jet displays regions of strong mixing in the minor axis region confirming the existence of asymmetric mixing. These results reaffirm an excellent correlation between elliptic vortex ring dynamics and their associated axis switchings with mass entrainment verifying that the flow is indeed driven by azimuthally deforming, self-inducting elliptic vortices.

The small-scale topology of the elliptic jet has been investigated by the Peak-Valley-Counting method and the small-scale mixing region is asymmetrically distributed with maxima occurring in the minor axis region. The small-scale production regions correlate with the $\partial u/\partial z$ velocity strain rate field—the minor axis vorticity field. Small scales are concentrated within the cores of the large-scale vortices and peak between the first and second vortex merging over the range of Reynolds numbers studied from 2×10^4 - 1.3×10^5 . Small-scale activity is decreased downstream of this location due to decaying flow conditions. Acoustic forcing at the Preferred Mode severely deforms the large scales inducing larger spreading of the mean flow field and 25% increased small-scale levels over the natural case. The most probable frequency associated with the viscous-dominated small scales varies linearly with the Reynolds number, but it is independent of initial frequency content.

2:1 aspect-ratio elliptic jets appear by many accounts to be very promising improvements over axisymmetric jet configurations because of their enhanced mixing characteristics. The mechanism of

vortex self-induction, which is influenced by nozzle geometry, Reynolds number and density ratio, enhances large scale mixing more efficiently than vortex merging and it is the dominant small-scale production mechanism in the elliptic jet. The vortex self-induction mechanism is the principle means responsible for large scale mixing and small-scale production, therefore, bulk entrainment processes and fine-scale mixing necessary in combustion systems are controllable via this mechanism.

Research Assistant: Thomas Austin

PH.D. THESIS

1. "Small Scale Topology of a 2:1 Aspect-Ratio Elliptic Jet," T. Austin, 1992.

PUBLICATIONS

1. Austin, T. "Temperature Measurements in a Heated Elliptic Jet," A.I.A.A. 6th Annual Region VI Student Conference, 1986.
2. Austin, T., Ho, C.M. "Temperature Effects on Entrainment of an Elliptic Jet," *Bulletin of the American Physical Society*, 1988, 33: 2237.
3. Ho, C.M., Austin, T. "Entrainment of Asymmetric Jets," Proceedings of Research on Turbulence A.F.O.S.R. Contractor's Meeting, 1988.
4. Ho, C.M., Austin, T. & J. "Hertzberg Entrainment of 3-D Shear Layers," Proceedings of The Fourth Asian Congress of Fluid Mechanics, 1989.
5. Austin, T., S. Schreck "Planar Imaging of a heated Elliptic Jet," Proceedings of The Western States Section of The Combustion Institute 1990 Fall Meeting, 1990.
6. Austin, T., Ho, C.M. "Controlled Small-Scale Mixing in a 2:1 Aspect-Ratio Elliptic Nozzle," paper 91-81, The Western States Section of The Combustion Institute 1991 Fall Meeting.
7. Austin, T., Ho, C.M. "Small Scale Topology of a 2:1 Aspect-Ratio Elliptic Jet," *Bulletin of the American Physical Society*, 1991, 36: 2710.
8. Austin, T., Ho, C.M. "Controlled Entrainment in a 2:1 Aspect-Ratio Subsonic Elliptic Nozzle," paper 92-0537, 30th A.I.A.A. Aerospace Sciences Meeting, 1992.
9. Austin, T. "Three-Dimensional Portraiture of the Turbulent Topology of a Subsonic Elliptic Nozzle," 1st Annual Scientific & Engineering Applications fMacintosh Conference, 1992.

FOOTNOTES

1. Ho, C. M., Gutmark, E. "Vortex Induction and mass entrainment in a small-aspect ratio elliptic jet" *Journal of Fluid Mechanics*, 1987, 179: 383-405
2. Ho, C.M, Austin, T. "Entrainment of Asymmetric Jets" A.F.O.S.R. Turbulence Research Contractor's Meeting, 1988.
3. Schadow, K., Gutmark, E. "Review of Passive Shear-Flow Control Research for Improved Subsonic and Supersonic Combustion" AIAA paper, 1989, 89-2786.
4. Hertzberg, J., Ho, C.M. "Time averaged 3d flow in a rectangular sudden expansion" AIAA paper,

Jan. 1991, 91-0040.

5. Schadow, K., Wilson, K., Lee, M., Gutmark, E. "Enhancement of Mixing in Ducted Rockets with Elliptic Gas-Generator Nozzles" AIAA paper, 1984, 84-1260.
6. Winant, C., Browand, F. "Vortex pairing: the mechanism of turbulent mixing layer growth at moderate Reynolds number" *Journal of Fluid Mechanics*, 1974, 63: 237-255.
7. Austin, T. "Three-Dimensional Portraiture of the Turbulent Topology of a Subsonic Elliptic Nozzle" 1st Annual Scientific & Engineering Applications Macintosh Conference, 1992.
8. Ho, C. M., Zohar, Y., "The dissipation length scale of turbulent shear flows" *Journal of Fluid Mechanics*, 1993, to be published.
9. Ho, C. M., Huang, L. "Subharmonics and vortex merging in mixing layers" *Journal of Fluid Mechanics*, 1982, 119: 443-473.
10. Austin, T., Ho, C.M. "Controlled Small-Scale Mixing in a 2:1 Aspect-Ratio Elliptic Nozzle" paper 91-81, Western States Section of The Combustion Institute 1991 Fall Meeting.
11. Austin, T., Ho, C.M. "Controlled Entrainment in a 2:1 Aspect-Ratio Subsonic Elliptic Nozzle" paper 92-0537, 30th A.I.A.A. Aerospace Sciences Meeting, 1992.
12. Krothapalli, A., Baganoff, D., Karamcheti, K. "On the Mixing of a Rectangular Jet" *Journal of Fluid Mechanics*, 1981, 107: 201-220.
13. Koshigoe, S., Ho, C.M., Tubis, A. "Application of a generalized shooting method to the linear instability analysis of elliptic core jets" AIAA paper, Oct. 1987, 87-2733.
14. Michalke, A. "On spatially growing disturbances in an inviscid shear layer" *Journal of Fluid Mechanics*, 1965, 23: 521-544.
15. Ashurst, W., Meiburg, E. "Three-dimensional shear layers via vortex dynamics" *Journal of Fluid Mechanics*, 1988, 189: 87-116.
16. Zohar, Y., Foss, J., Ho, C.M., Buell, J. "Phase decorrelation of coherent structures in a free shear layer" *Journal of Fluid Mechanics*, 1991 230: 319-337.
17. Austin, T., Ho, C.M. "Temperature Effects on Entrainment of an Elliptic Jet" *Bulletin of the American Physical Society*, 1988, 33: 2237.
18. Austin, T., S. Schreck "Planar Imaging of a heated Elliptic Jet" Proceedings of The Western States Section of The Combustion Institute 1990 Fall Meeting, 1990.
19. Austin, T., Ho, C.M. "Small Scale Topology of a 2:1 Aspect-Ratio Elliptic Jet" *Bulletin of the American Physical Society*, Vol. 36, p. 2710, 1991.
20. Gutmark, E., Parr, T., Hanson-Parr D., Schadow, K. "Coherent and random structure in reacting jets" *Experiments in Fluids*, 1990, vol. 10, pp. 147-156.

Asymmetric Jet Axis Switching Location

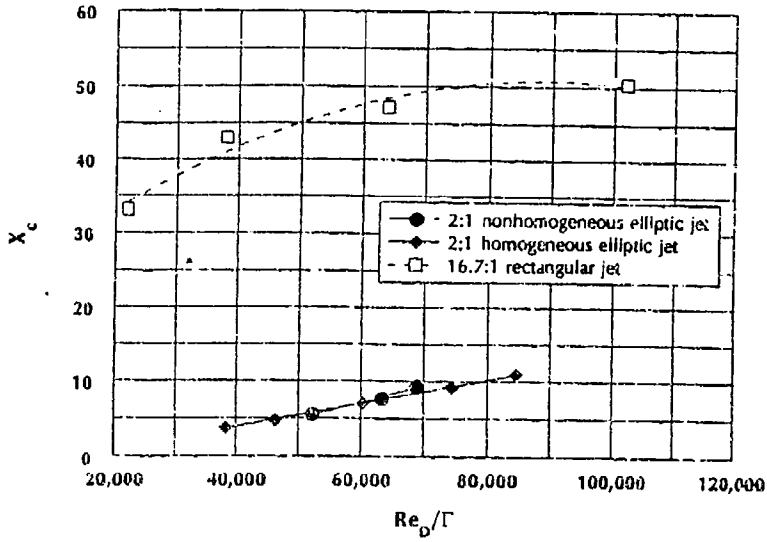


Figure 1.

Subsonic Jet Entrainment Ratios
Reynolds Number and Density Ratio effects

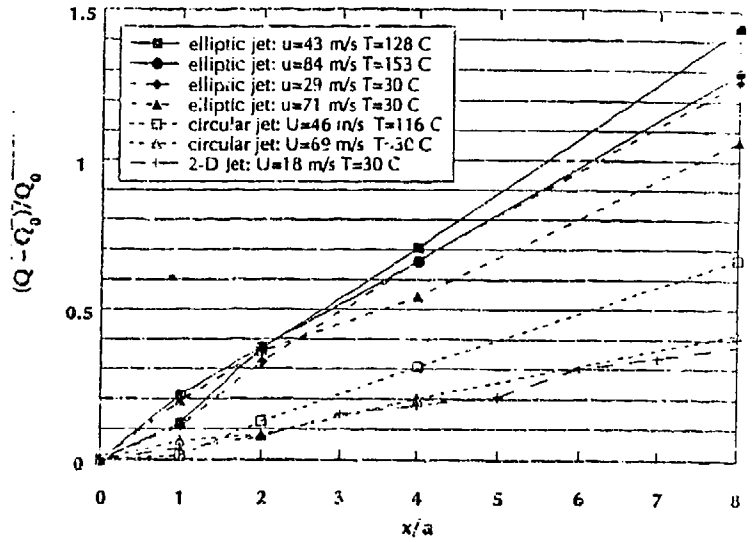


Figure 2.

MEAN VELOCITY FIELD

$U_0 = 20$ m/s natural case

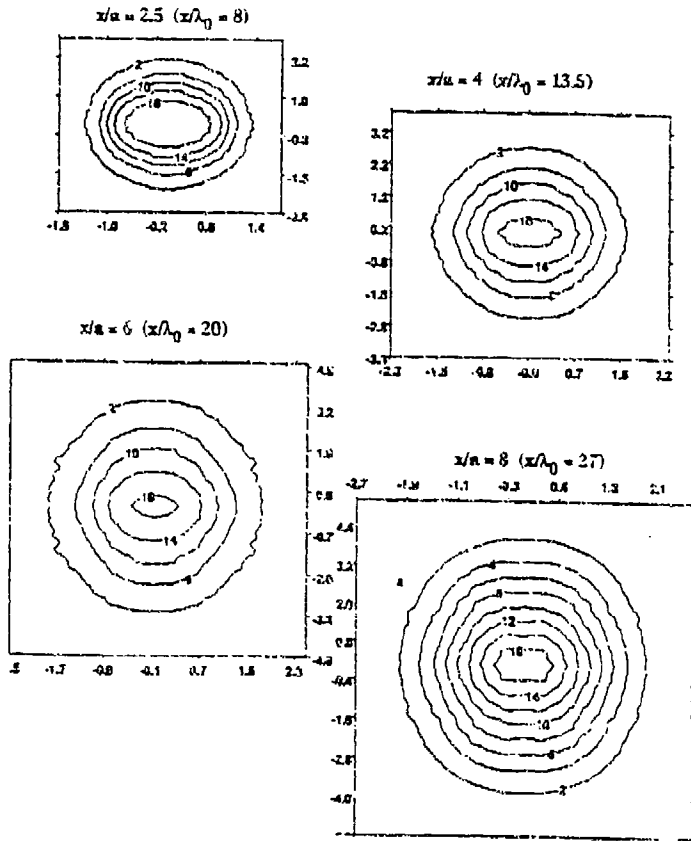


Figure 3(a).

MEAN VELOCITY FIELD

$U_0 = 20$ m/s Preferred Mode forced case

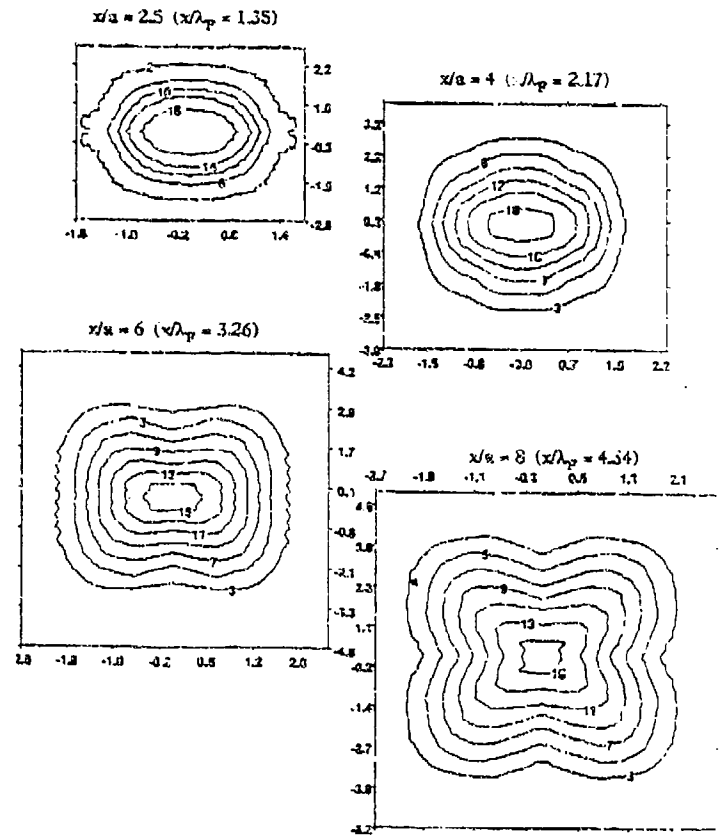


Figure 3(b).

Small scale activity per local large scale structure
 $U_0 = 20 \text{ m/s}$ natural case

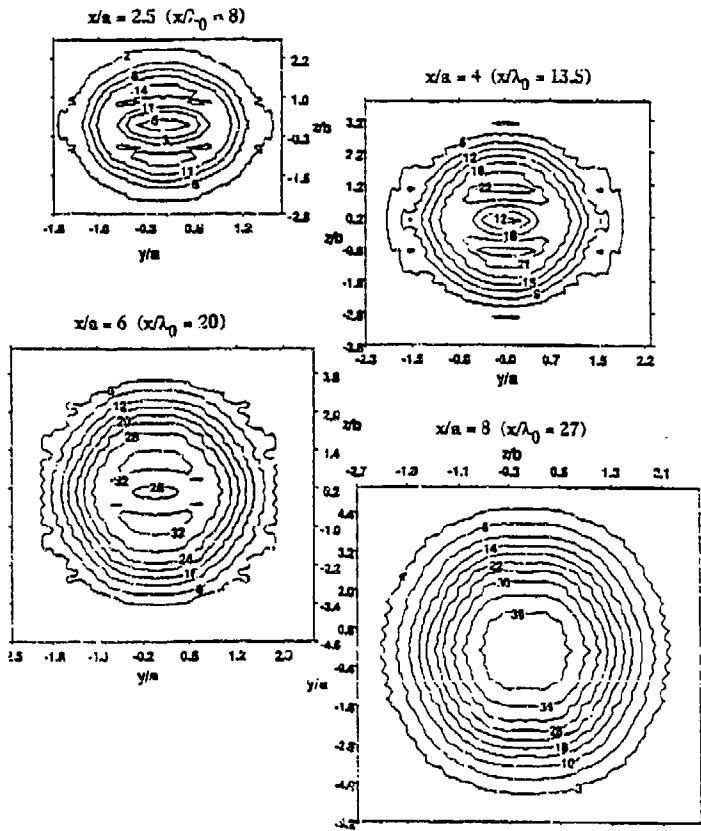


Figure 4(a).

Small scale activity per local large scale structure
 $U_0 = 20 \text{ m/s}$ Preferred Mode forced case

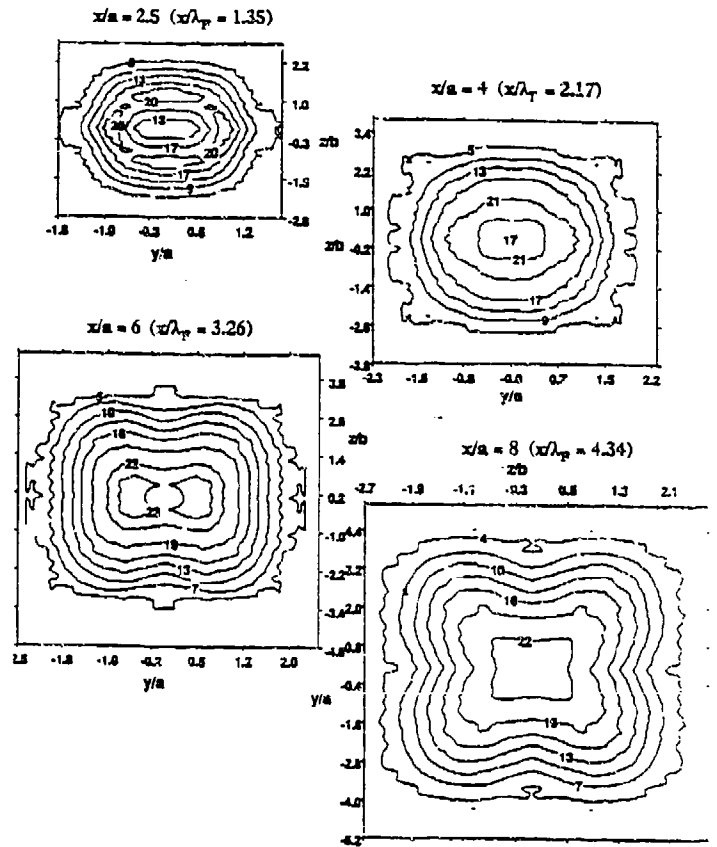


Figure 4(b).

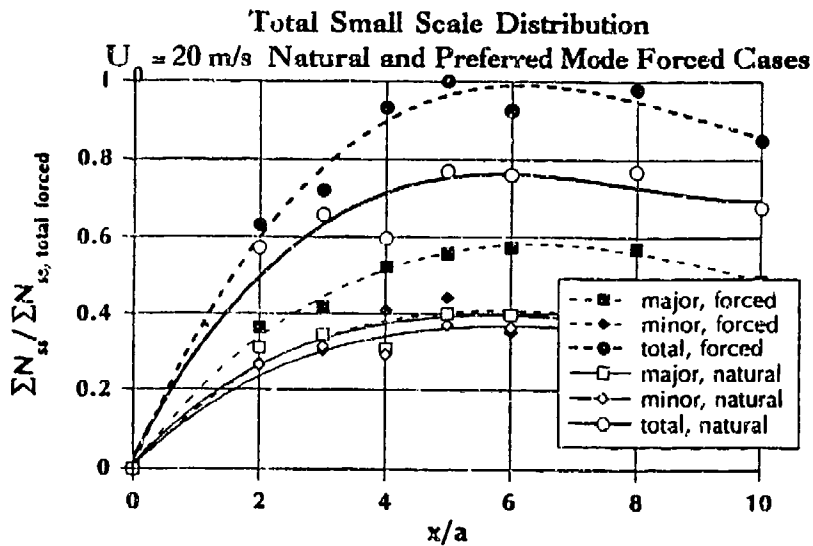


Figure 5.

Streamwise Shear Layer Small Scale Population

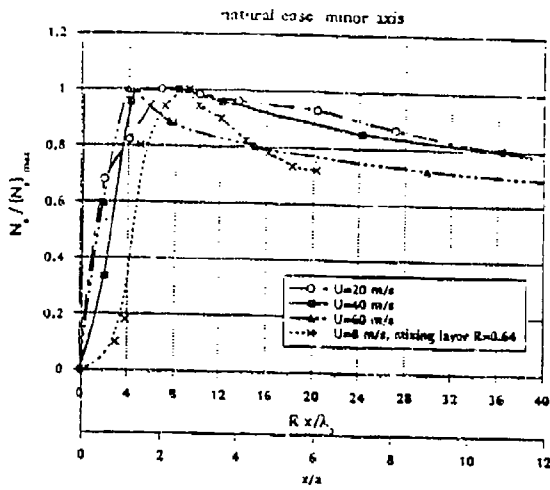


Figure 6(a).

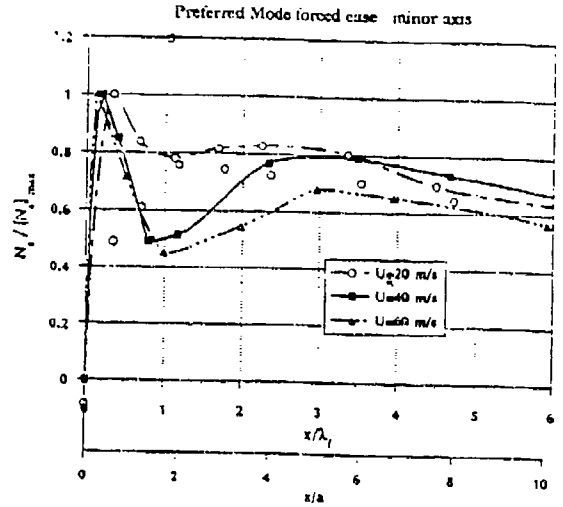


Figure 6(b).

Natural Case $\omega/\alpha = 4$ $\omega/\lambda_0 = 13.5$ $U_0 = 19$ m/s
phase averaged sequence

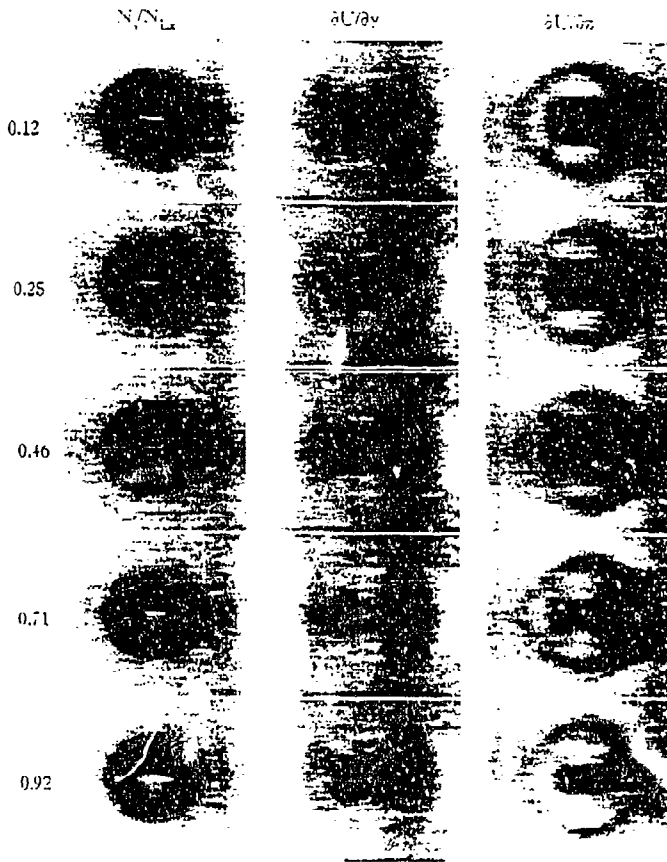


Figure 7(a).

Preferred Mode forced case $\omega/\alpha = 4$ $\omega/\lambda_0 = 2.17$ $U_0 = 19$ m/s
phase averaged sequence

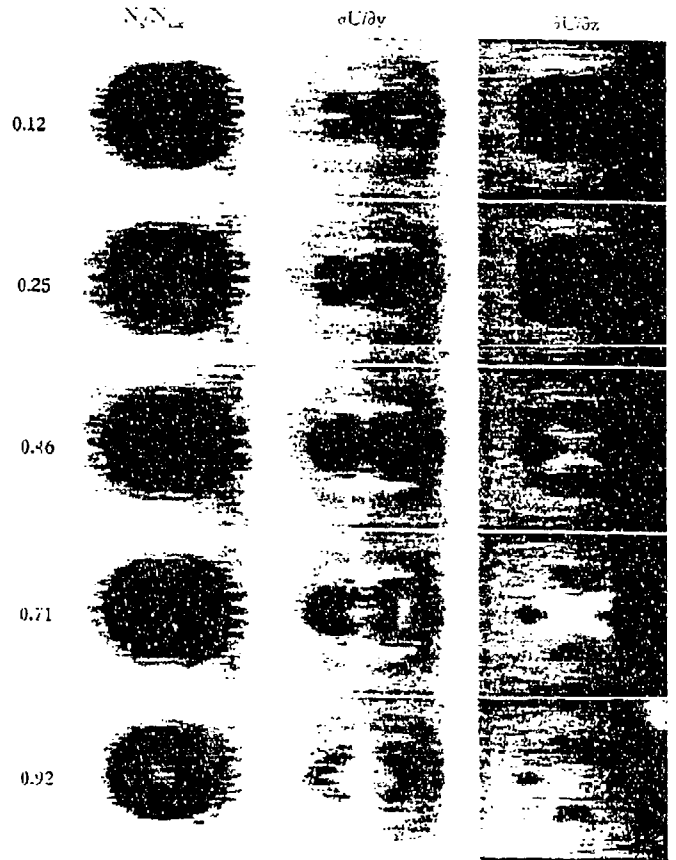


Figure 7(b).

SESSION BD: INSTABILITIES OF JETS AND WAKES I

Sunday morning, 20 November 1988

214 Norton Hall at 11:00

F. W. Roos, presiding

11:00

BD 1

The low-Froude number wake of floating bluff objects* G. Triantafyllou and A. Dimas, MIT - The stability of the viscous wake behind floating bluff objects is analyzed. For a fully submerged object, it is well known that the flow separates and forms a region of recirculating flow behind the object; after a critical Reynolds number, the flow in the wake becomes absolutely unstable, and the bubble is destroyed creating a vortex street. For a floating object at low Froude numbers, however, it is shown that the instability is of the convective type for all Reynolds numbers. As a result, behind floating objects the recirculating flow region remains intact and no vortex street is formed. This result is verified experimentally for the flow past a half-submerged circular cylinder at Reynolds number based on the cylinder radius equal to 25000. The flow is visualized through bubbles, produced by dropping the pressure in the tunnel. The presence of a region of steady recirculating flow is clearly visualized, reminiscent of the flow in infinite fluid at low Reynolds numbers. It is concluded that, for low Froude numbers, the presence of the free surface has a stabilizing effect on the wake, suppressing unsteady effects.

*Work supported by ONR, Contract N00014-87-K-0356

11:13

BD 2 Nonlinear Stability of a Viscous Axisymmetric Jet. J. HORWITZ, S. ROSENBLAT, IL INST OF TECHNOLOGY* - The temporal stability of a viscous circular jet with respect to axisymmetric disturbances is studied. First, the Stuart-Watson method is used to study the weak nonlinear interactions. The Landau constant is positive indicating there is a supercritical Hopf bifurcation at $R=58.3$. This method also reveals the nature of the 2 additional modes arising from the self interaction of the fundamental and provides a basis for studying the more strongly nonlinear interactions. Finally, a truncated Fourier-eigenfunction expansion leads to a system of 5 o.d.e.'s. Numerical results show that the periodic solution appearing at 58.3 is stable when $R < 76.2$. There is a secondary bifurcation at $R=76.2$ to a quasiperiodic solution with 2 incommensurate frequencies which ends in a homoclinic orbit at $R=79.5$. A search for solutions when $R > 79.5$ results in only unbounded ones indicating limitations of this model.

*Supported by AFOSR Grant 86-0165

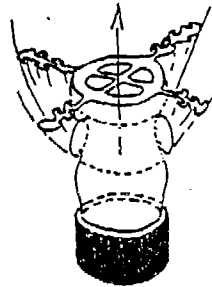
11:26

BD 3 Instability in a Vortex Jet at High Reynolds Number. M. R. FOSTER, Ohio State U. - A particular slender vortex--a member of a family of exact solutions found by R. R. Long¹--consists of a ring jet across which the swirl velocity changes from rigid rotation to a potential vortex. Such a structure occurs when the axial flux of axial momentum is much larger than the axial flux of angular momentum. At axial wave lengths comparable to the vortex width, the instability at infinite Reynolds number is governed by sinuous and varicose Bickley modes. Long-wave instabilities, however, involve the three-dimensionality of the vortex, and so deviate from the Bickley modes. Modifications of these long-wave inviscid modes at large but finite Reynolds number are presented. Because the exact vortex solution has radial velocity larger than $1/Re$, such viscous corrections to the inertial modes are never solutions of a parallel-flow equation.

¹Long, R. R., J. Fluid Mech. 11, 611 (1961)

11:39

BD 4 Heated jets are different. D.W. BECHERT, B. LERHMANN, B. BARSIKOW*, DFVLR Berlin, F.R.G., and P.A. MONKEWITZ, U.C.L.A., Los Angeles, U.S.A. -- Heated axisymmetric jets are investigated ($t=150-400^{\circ}\text{C}$, $Re=5 \cdot 10^3-10^5$). The absolute instability causes dramatic changes: (i) The spectrum of the fluctuations changes from broad band of a cold jet to a line spectrum of a heated jet as predicted. A regular vortex ring structure appears. (ii) strong planar quasi-steady side jets occur. These side jets distort



the cross section towards a star-shaped structure with 2-6 lobes. Spreading rate and mixing are enhanced dramatically by the side jets. The side jets are considered to be caused by a lobe-like instability of the ring vortices. Thus, side jets can be generated also in a forced cold jet.

*supported by TECFLAM

11:52

BD 5

Energy Budget for Atomization*

B. CREIGHTON and S.P. LIN, Clarkson University. --** An equation of mechanical energy balance in a viscous liquid jet is derived. Numerical evaluations of each term involved in the equation reveal that the work by the fluctuating ambient gas pressure is responsible for the convective instability in the atomization mode. Atomization is a process of breaking up a jet into small droplets of sizes much smaller than the jet diameter. The atomization mode is distinct from the Rayleigh mode for which the capillary pinching is responsible for the instability.

* Submitted by S.P. LIN

** Supported by ARO DAAL03-86-K-0072

SESSION BD: INSTABILITIES OF JETS AND WAKES I

Sunday morning, 20 November 1988

214 Norton Hall at 11:00

F. W. Roos, presiding

11:00

BE 1

Influence of Turbulence on Instability Pressure Waves in an Axisymmetric Jet. J. H. MILES and G. RAMAN* NASA Lewis Research Center, Cleveland, OH. -- The influence of turbulence due to a circular grid on shear layer instability pressure waves is investigated. Auto-spectra, transfer-function, and coherence measurements are made to investigate instability pressure waves in a 8.89-cm diameter jet for an untripped initial condition, an initial condition due to a trip ring, and an initial condition due to a circular grid. The transfer-function and the coherence are measured with a pair of microphones at the same distance from the jet centerline but separated axially by 5.08-cm.

*Sverdrup Technology, Inc.

11:13

BE 2

Temperature Effect on Entrainment of an Elliptical Jet. AUSTIN, TOM & HO, CHIH-MING, Univ. So. Calif. *--Previous studies on an elliptical jet having an aspect ratio of 2.1 have revealed a phenomenal difference of as much as 500% increased entrainment compared to an ordinary circular jet. Presently we are examin-

ing the effects of temperature on the development of a jet. Preliminary studies of the elliptical jet at exit temperatures up to 250 C have shown a further increase of 30% in the elliptical jet's entrainment rate over the unheated case. We will measure the jet's mean and fluctuating temperature field along with its associated velocity components by means of a combined hot-wire and cold-wire probe. A correlation will be deduced to determine the significance that temperature has upon an elliptical jet's inherent entrainment.

*Supported by the AFOSR Grant No. F49620-85-C-0080.

11:26

BE3 Dynamics of Turbulent Jets near a Free Surface.* K. Madnia and L.P. Bernal, Univ. of Michigan. -- The interaction of the free surface with a turbulent round underwater jet has been studied experimentally. Hot film axial velocity measurements were conducted to study the effect of the free surface on the jet turbulence. Mean and rms values of the velocity fluctuation were measured along directions parallel and perpendicular to the surface for several jet depths. The jet flow structure is altered by the interaction with the free surface. The velocity profiles show an increase of the maximum mean velocity compared to the free jet. The jet growth rate in the direction parallel to the free surface is larger by a factor of 1.4 compared to the growth in the direction perpendicular to the surface. Simultaneous measurements of the surface curvature and the jet axial velocity are being conducted to gain additional insight on the mechanisms of generation of surface waves and motions by the jet turbulence.

*Supported by ONR Contract no. N000184-86-K-0684.

11:39

BE 4 Excitation of an Axisymmetric Jet at Fundamental and Subharmonic Frequencies G. RAMAN* and E. J. RICE NASA Lewis Research Center, Cleveland, OH. -- The axisymmetric jet mixing layer can be controlled by generating resonant interactions, such as the resonance between a fundamental wave and its subharmonic. Experiments were performed at a Mach number of 0.45 with fundamental and subharmonic excitations at Strouhal numbers of 0.4 and 0.2 respectively. The initial phase difference between the two excitation components was varied at intervals of 45 degrees for one full cycle of the fundamental. The fundamental velocity excitation level was equal to 7 percent of the jet exit velocity and the ratio of fundamental/subharmonic was 15. Phase averaged coherent velocities were recorded at the two frequencies along the jet centerline. At certain values of the initial phase difference the growth of the subharmonic was significantly augmented, while the growth of the fundamental remained unaffected. Mean velocity measurements along the jet centerline showed that the initial phase difference which produced the largest subharmonic augmentation also produced the highest centerline mean velocity decay rate.

*Sverdrup Technology, Inc.

11:52

BE 5 Effect of Dual-Mode Excitation on Jet Entrainment.* P.J. Juvel and W.C. Reynolds Stanford University. - Round jets subject to dual-mode dual-frequency acoustic excitation have been shown to spread more rapidly than natural jets. When the ratio of symmetric to helical excitation frequencies is a non-integer, the jet blooms and sends vortex rings in all directions. Blooming occurs in both

free and shrouded jets (ejectors or thrust augmentors). Hot-wire measurements were made at the exit of a shrouded jet at Re of 100,000. The mean velocity profiles show a significant increase of entrainment for the shrouded blooming jet compared to the shrouded natural jet. The jet response to different amplitudes of both the axial and the helical excitation is documented by velocity and temperature profiles. Flow visualization reveals the robust nature of the shrouded blooming jet.

*Work supported by AFOSR Contract F49620-86-K-0020.

SESSION BF: TURBULENCE—MODELING I

Sunday morning, 20 November 1988

110 Knox Hall at 11:00

P. S. Bernard, presiding

11:00

BF 1 Second order modeling of low Reynolds number turbulence near walls. T.H. SHIH Center for Turbulence Research and N.N. MANSOUR NASA-Ames. A set of second order closure models for low-Reynolds number turbulence is proposed for the simulation of wall bounded flows without using wall functions. The wall effect is built in the pressure-strain correlation term of the Reynolds-stress equation and in the modeled terms of the dissipation rate equation. We find that realizability is particularly important for modeling the near wall turbulence, and is used in the present models to ensure that the modeled equations will have no unphysical behavior near the wall. The present models are particularly suitable for surfaces of arbitrary topology since they do not use the wall distance as a parameter. The models are tested by computing the fully developed channel flow. The full set of equations are used to compute the mean velocity, all the Reynolds stresses and the dissipation rate of the turbulent kinetic energy. We find reasonable agreement between the predictions and the data for a fully-developed turbulent channel flow.

11:13

BF 2 Turbulence Modeling in Rotating Frames of Reference. C.G. SPEZIALE, ICASE-NASA Langley Research Center. -- The effect of an arbitrary, time-dependent change of frame on the structure of turbulence models is examined from a basic theoretical standpoint. It is proven from the Navier-Stokes equations that turbulence models must be form invariant under arbitrary translational accelerations of the reference frame. More importantly, it is shown that turbulence models should only be affected by rotations of the reference frame through the intrinsic mean vorticity—a rotational dependence that must vanish if the flow becomes two dimensional (the constraint referred to as material frame-indifference in the limit of two-dimensional turbulence). A direct application of these invariance properties along with the Taylor-Proudman Theorem and Rapid Distortion Theory are shown to yield powerful constraints on the allowable form of turbulence models which are seriously violated by most of the commonly used models. Alternative turbulence models with improved properties in rotating frames are developed and some simple applications are considered.

*Partially supported by ONR Contract N00014-85-K-0238

11:26

BF 3 Analysis of Turbulent Flows by a Thermodynamically Consistent Rate-dependent Model. S.J. CHOWDHURY and

Tuesday Afternoon

up to ten percent exists for the riblet-mounted wall in comparison with the smooth wall of the channel. For the first time, we present detailed turbulent statistics in a complex geometry. These results are in excellent agreement with available experimental data and provide a quantitative picture of the drag reduction mechanism of the riblets.

Work supported by NSF.

16:34

JA 4 Numerical Simulation of Two-Dimensional Vortices*. DANIEL C. CHAN, University of Southern California -- We used a pseudo-spectral method to simulate the interactions of two-dimensional vortices inside a spatially periodic square domain, which was initially filled with an array of 6×6 counter-rotating vortices. Reynolds numbers, based on the diameter and rotational speed of the vortices, of 100, 1,000 and 10,000 were used, respectively in conjunction with 1024×1024 collocation points. Temporal integration equal to approximately 50 large eddy turnover time was performed. Vortex pairing was observed at Reynolds number of 100. For Reynolds numbers which were higher than 1000, turbulent flow field was generated by the onset of hydrodynamic instability and inverse cascading was observed in the later stage of the interactions. The slope of the energy spectrum at the inertial subrange changed with time and in some instances, the theoretical value of -3 was predicted.

*work supervised by Prof. Tony Maxworthy and J.A. Domaradzki

16:47

JA 5 Direct Numerical Simulation of a Turbulent Boundary Layer with Heat Transfer*. D.M. BELL, J.H. FERZIGER, Stanford Univ., P. R. SPALART, Boeing. -- The unsteady, three-dimensional, incompressible Navier-Stokes equations, and the passive scalar form of the energy equation, are solved numerically for the spatially-developing flat-plate boundary layer. The solution for several Prandtl numbers is computed simultaneously with a single flow field solution. Results have been obtained for momentum thickness Reynolds numbers $300 < Re_\theta < 700$, and $Pr = 0.1, 0.71, \text{ and } 2.0$. The computed mean profiles, integral quantities and turbulence quantities agree very well with experiments. The results also support the Reynolds analogy for $Pr = 0.7$ and 2.0 , but not for $Pr = 0.1$, at these Reynolds numbers.

*This work is supported with funding from Wright Patterson and NAS.

17:00

JA 6 Large Scale Structures in Periodically Forced 2-D Flows. B. NICOLAENKO, Arizona State Univ., Z.S. SHE, Princeton Univ. -- The dynamics of large scale structures in 2-D flow, is related to both enstrophy cascade and inverse energy cascade. We present results from large-scale simulations of 2-D generalized Kolmogorov flows at $Re \sim 10,000$. These are forced flows with shear instabilities, with a force periodically modulated in space. Specific forces considered are i) anisotropic forces with a single large-scale Fourier wave-vector component, and ii) isotropic forces with a random Fourier wave vector distribution on a fixed spherical shell. Both cases are simulated with and without stochastic noise. The anisotropic case is characterized by strong competing dynamics between large-scale rotating coherent vortices and Saffman vortex sheets. The local shearing effects result in localized enstrophy cascades, which we demonstrate as a wave-like propagation of enstrophy toward small scales. The isotropic case exhibits large-scale structures in the streamline patterns, with some evidence of inverse energy cascade, whereas vorticity remains turbulent at small scales.

17:13

JA 7 Direct Numerical Simulation of Turbulent Flow in a Square Channel. A. HUSER and S. BIRINGEN, Univ. of Colorado-Boulder. -- A study for generating an accurate description of a fully developed, low Reynolds number, anisotropic turbulent flow in a square channel is presented. The numerical scheme employs a time-splitting method to integrate the full Navier-Stokes equations using spectral/finite difference discretization on a staggered mesh.

Time-averaged results are compared with the available experimental results. Higher order correlations are presented with emphasis on the behavior of the Reynolds stress and the dissipation rate budgets along

the two intersecting walls. These results are used to investigate anisotropic turbulence models and boundary-conditions for modeling of such flows. The vortex dynamics responsible for generation of the secondary flow are discussed.

SESSION JB: TURBULENT JETS III

Tuesday afternoon, 26 November 1991

Grande Ballroom B at 15:55

J. G. Brasseur, presiding

15:55

JB 1 Small-Scale Topology of a 2:1 Aspect-Ratio Elliptic Jet. THOMAS AUSTIN and HO, CHIH-MING, Univ. So. Calif. -- The small-scale topology of a homogeneous, subsonic elliptic jet is investigated for the purpose of controlling small-scale transition and, ultimately, fine-scale mixing. The length scale of the small structures responsible for energy dissipation is found to be larger than the Kolmogorov scale and smaller than the Taylor microscale. The streamwise velocity fluctuations are measured within the first ten jet exit diameters in the shear layer over the range, $Re_{jet} = 3 \times 10^4 - 1.7 \times 10^5$. The data is analyzed by the Peak-Valley-Counting method, which yields population distributions and length scales of the small-scale activity. The flow will be actively controlled by acoustic forcing at the jet exit to increase small-scale production and enhance fine-scale mixing.

Supported by AFOSR Grant No. 90-0301.

16:08

JB 2 Instantaneous Spatial Structure of a Confined Swirling Flow. DUNSKY & C.F. EDWARDS, Sandia National Laboratories. -- Instantaneous spatial structure of a confined swirling flow downstream various throat geometries is investigated via transient planar Mie scattering imaging. The flow corresponds to the cold flow conditions in the axisymmetric optical access research furnace. This furnace is used for swirl-stabilized combustor sprays, and has an octagonal cross section area-equivalent diameter of 58.5 cm, and throat diameters ranging from 1 cm. Previous LDV studies indicate that typical time-averaged axial tangential velocity components in the turbulent flow are 10 and respectively. The planar Mie scattering technique allows for unambiguously visualization of flow structure by slicing through the flow with a thin laser light sheet at various locations in the axial/radial and radial/azimuthal planes. Typical images obtained in a diametral plane of the flow structures of various scales not resolved by time-averaged measurements suggest that a vorticity description may be appropriate for characterizing type of flow.

16:21

JB 3 The Effect of Velocity and Density Ratio on the Mixing of Subsonic Jets. P.J. STRYKOWSKI, Univ. of Minnesota, and A. KROTHAPALLI, Florida A&M Univ. & Florida State Univ. -- Recent studies in low-speed jets indicate that mixing and entrainment can be effectively controlled by establishing counter-current mixing in the jet shear layers; counter-current mixing is created by applying suction around the jet periphery. In the present investigation the effect of suction (velocity ratio) on jet mixing is examined in a subsonic circular jet up to a Mach number of unity. In addition, experiments were performed at density ratios $\rho_{jet}/\rho_{ambient}$ between 0.5 and 1 by heating the jet. The experiments were designed to map the mixing properties of the jet in the velocity-ratio/density-ratio plane at several subsonic Mach numbers. Measurements reveal that above a critical velocity ratio the jet mixing can be significantly enhanced. This enhancement is due to a strong forcing of the jet at supercritical velocity ratios, which we believe is related to the absolutely unstable nature of the velocity profiles in the near field of the jet.

¹Strykowski, P.J. & Niccum, D.L. 1991 *J. Fluid Mech.* 227, 309-343.

16:34

JB 4 Differential Molecular Diffusion at High Schmidt Numbers in Turbulent Water Jets. J.R. SAYLOR & K.R. SREENIVASAN, Yale U. -- Two-dimensional laser induced fluorescence imaging was used to determine whether differences in the molecular diffusivity of passive

ENTRAINMENT OF ASYMMETRIC JETS

AFOSR CONTRACT NO. F49620-82-K-0019

Chih-Ming Ho and Thomas Austin
Department of Aerospace Engineering
University of Southern California
Los Angeles, California 90089-1191

SUMMARY

The control of mass transfer between two streams of fluids is an important technological problem in turbulence research. Ho and Gutmark [1987] found that a small aspect ratio elliptic jet can entrain approximately five times more mass as compared with a circular jet. This efficient passive control technique was due to a new entrainment mechanism - unsteady deformation of vortical structures caused by self-induction. In this presentation, we summarize some recent studies in this area.

TECHNICAL DISCUSSIONS

Homogeneous Elliptic Jet:

In many engineering devices, the efficiency will be much improved, if the mass transfer in the transverse direction can be increased. The large vortical structures are responsible for engulfing fluids from both streams and mix them in the shear region. In a two-dimensional flow, the coalescence of these structures was identified to be the main entrainment mechanism [Winant and Browand 1974].

Ho and Gutmark [1982, 1987] found that an elliptic jet can entrain several times more fluid than a two-dimensional jet, either a circular or a plane jet [Fig. 1]. More importantly, they identified a new mechanism, other than vortex merging, for mass transfer. The self-induction of an elliptic vortex ring will make the structure switch its axis orientation. The vortex element near the minor axis moves outward and the vortex near the major axis moves toward the jet axis. This process makes a large amount of ambient fluid move into the jet near the original minor axis region.

Hot Elliptic Jet:

One of the main applications of entrainment enhancement is to improve the efficiency of combustion. The high temperature gradient between the ambient cold fluid and the hot combustion jet will certainly modify the vorticity distribution of the coherent structures. Hence the self-induction will also be affected. In order to examine the temperature effects on the entrainment, we installed electric heaters in the elliptic jet and can heat the jet upto 500° F. In this way, we can isolate the influences of the temperature and the chemical reaction on the vortex deformation.

The entrainment rate of the hot jet was found to be about 25% above the cold elliptic jet [Fig. 2]. Apparently, the axis-switching must be modified by the temperature gradient. Based upon the time averaged velocity profiles, we found that the switching position is changed [Fig. 3]. The reasons for the changes of switching position and the more efficient mass entrainment are not clear yet. However, it is obvious that a fundamental understanding of this process will lead to further development of the entrainment control techniques.

Elliptic Jet with Combustion:

The advantages of using an elliptic jet in combustion is also phenomenal. Schadow et al. [1984] used a 3:1 elliptical nozzle in a premixed jet flame. They found that the centerline temperature increased sharply a short distance from the elliptic nozzle. At end of the test section, the temperature was much higher than that of a circular jet [Fig. 4]. By using some other asymmetric nozzles, they were not only able to increase the combustion efficiency but also minimize the combustion instability.

Supersonic Asymmetric Jet:

The spreading rate of a supersonic shear layer is much slower than that of a subsonic flow. Obviously, the combustion efficiency of supersonic flame is hindered much by the low mixing rate. This is the most pressing problem in developing a hypersonic aircraft. In a preliminary experiment, we found that by using the small aspect rectangular nozzle it was possible to enhance the entrainment as it did in the subsonic flow. Fig. 5 shows the spreading of several shear layers. The $M = 2.4$ flows spread slower than the $M = 0.6$ flows. However, the improvement of the rectangular nozzle over the circular nozzle is about the same for both supersonic and subsonic jets in the far downstream locations. In the near field, we did not measure the mass flow rate, but the variations of the cross-section area ratios are similar for supersonic and subsonic cases [Fig. 6]. Hence, we expect that the supersonic rectangular jet will entrain much more mass than that of a supersonic circular jet in the region near the nozzle.

REFERENCES

- Ho, C.M. and Gutmark, E., "Visualization of a Forced Elliptic Jet", Bull. Am. Phys. Soc., V. 27, pp 1184, 1982.
- Ho, C.M. and Gutmark, E., "Vortex Induction and Mass Entrainment in a Small-aspect-ratio Elliptic Jet", J. of Fluid Mech. V.179, pp 383-405, 1987.
- Jou, W.H., Knoke, G.S. and Ho, C.M., "Entrainment Enhancement of a Supersonic Jet for Advanced Ejectors", DOE Ejector Conf. 1988.
- Schadow, K.C., Wilson, K.J., Lee, M.J. and Gutmark, E., "Enhancement of Mixing in Ducted Rockets with Elliptic Gas-Generator Nozzles", AIAA paper No. 84-1260, 1984.
- Winant, C.D. and Browand, F.K. "Vortex Pairing: the Mechanism of Turbulent Mixing layer Growth at Moderate Reynolds Number", J. Fluid Mech., v. 63, pp 237-255, 1974.

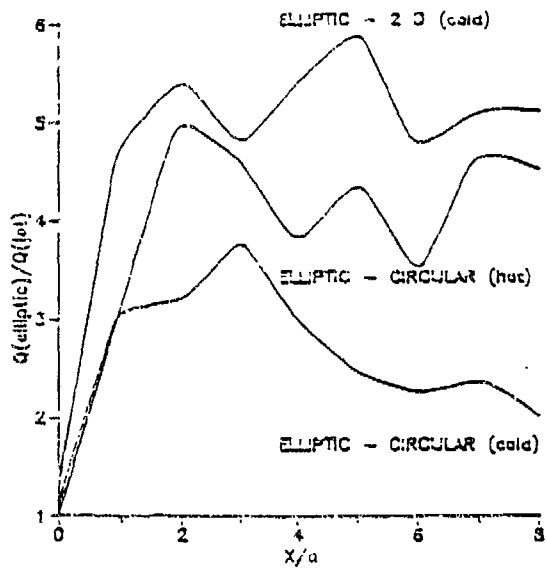


Fig. 1 Improvement of mass entrainment of an elliptic jet

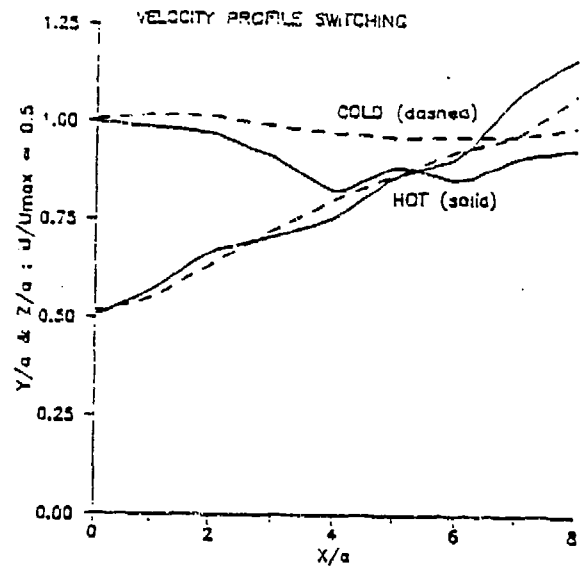


Fig. 3 Positions of axis-switching

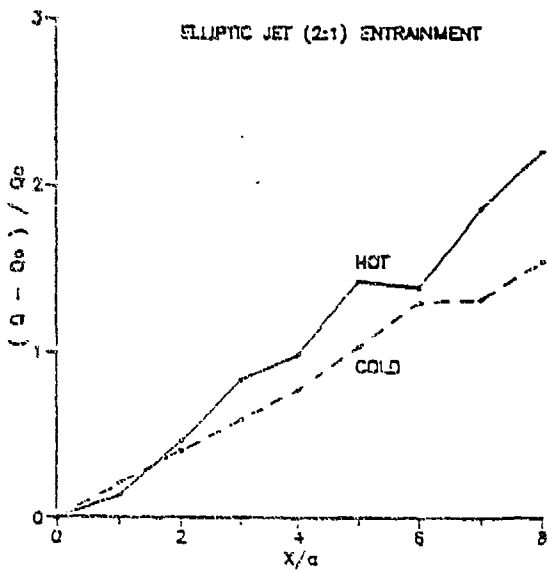


Fig. 2 Entrainment rates of a hot and a cold elliptic jet

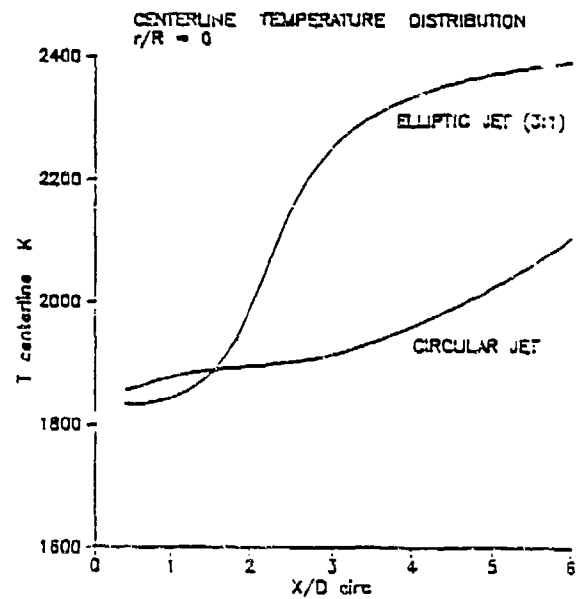


Fig. 4 Centerline temperature of an elliptic and a circular jet

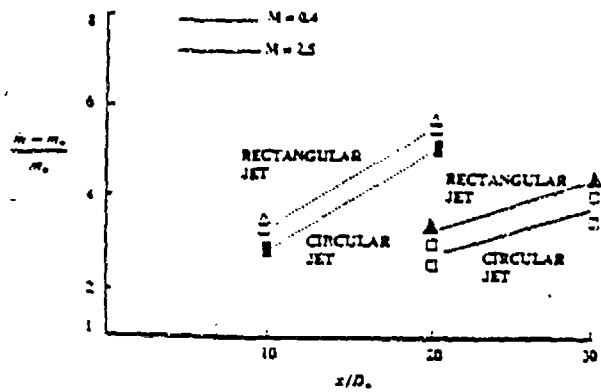


Fig 5 Far field mass entrainment rate

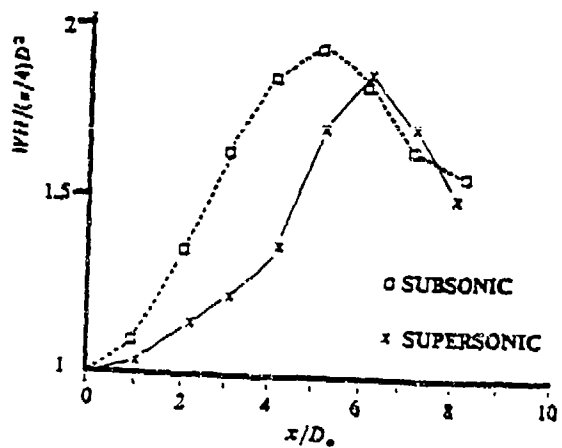


Fig 6 Area ratios of an elliptic jet over a circular jet

August 19-23, 1989 Hong Kong

ENTRAINMENT OF 3-D SHEAR LAYERS

C. M. Ho, T. Austin and J. Hertzberg

Department of Aerospace Engineering
University of Southern California
Los Angeles, California 90089-1191

ABSTRACT In engineering devices involving chemical reaction, it is important to be able to control the mass transfer between two streams of fluids. Ho and Gutmark [1] used a small aspect ratio elliptic jet which can significantly enhance the entrainment. This efficient passive control technique is due to the unsteady deformation of 3-D vortical structures caused by self-induction.

1. Passive and Active Control of Free Shear Layers

The possibility of controlling the mass transfer in the transverse direction of a shear layer is important in improving the efficiency of devices with chemical reaction. In a two-dimensional flow, the coalescence of the vortical structures in the shear layer was identified to be the main entrainment mechanism [2]. If the vortex merging is prohibited, the growth of the mixing layer is stopped or even decreased [3]. On the other hand, if the shear layer is actively perturbed by the subharmonics of the most amplified frequency, multiple vortices will merge simultaneously [4]. The growth of the shear layer is increased.

The spatial development of the shear layer is extremely sensitive to the initial perturbations or the boundary conditions. The alternative approach of controlling the enhancement is to change the upstream boundary condition of the shear layer. Ho and Gutmark [1, 5] found that a jet with an elliptic nozzle can entrain much more fluid than that of a circular or a plane jet [Fig. 1]. This passive control method is even more advantageous for engineering applications, because no delicate forcing arrangement is required. More importantly, they identified a new entrainment mechanism; the self-induction of an elliptic vortex ring makes the structure switch its axis orientation, the vortex element near the minor axis moves outward and makes a large amount of ambient fluid move into the jet near the minor axis region. This concept can be generalized and used in other flow configurations, such as combustion chamber.

2. Applications in Combustion

The ramjet is a device which can be benefited by the entrainment control technique. There is a short distance from the flame holder to the exhaust nozzle. Combustion needs to be accomplished during a short residence time and combustion

instability has been a troublesome problem. The advantages of using an elliptic jet in the ramjet has been shown to be phenomenal. Schadow et al. [6] used a 3:1 elliptical nozzle in a jet with combustion. They found that the centerline temperature increased sharply a short distance from the elliptic nozzle. At the end of the jet potential core, the temperature was much higher than that of a circular jet [Fig. 2].

The combustion instability problem was alleviated by using another type of asymmetric nozzle. They used a triangular nozzle and injected fuel near the tips of the triangle [7]. In this way, the fuel is mixed by the small eddies near the tips and the large structures do not trigger the combustion instability.

3. Supersonic Asymmetric Jet

The spreading rate of a supersonic shear layer is much slower than that of a subsonic flow and the combustion efficiency of supersonic flame is hindered by the low mixing rate. Actually, this is the most pressing problem in developing a hypersonic aircraft. In a preliminary experiment, we found that the small aspect ratio rectangular nozzle could enhance the entrainment as it did in the subsonic flow [8].

In general, the supersonic flows spread slower than that of subsonic flows. However, the entrainment improvement of the rectangular nozzle over the circular nozzle is about the same for both supersonic and subsonic jets in the far downstream locations. Near the Nozzle, the variations of the cross-section area ratios, indicating the shear layer spreading, are similar for supersonic and subsonic cases. Hence, we expect that the supersonic rectangular jet will entrain more mass than that of a supersonic circular jet in the region near the nozzle.

4. Asymmetric Jet in Confinement

Most of the combustion is taking place inside a confined space. The entrainment process is very different from a shear layer in the free space. As has been pointed out in our previous findings [1] the unsteady evolution of the vortex structures can engulf the fluids into the mixing region. We used a 2:1 aspect ratio rectangular jet in a confined environment. The deformation of the vortical structures was found to be much more convoluted than those in a free jet. These deformations are produced by the local 3-D shear layer and the induction of the image vortex. In other words, a properly designed confinement should be able to facilitate the mixing process.

References

- [1] Ho, C.M. & Gutmark, E. : J. Fluid Mech. 179, 383 (1987).

- [2] Winant, C.D. & Browand, F.K. : J. Fluid Mech. 63, 237 (1974).
- [3] Oster, D. & Wygnanski, I. : J. Fluid Mech. 123, 91 (1982).
- [4] Ho, C.M. & Huang, L.S. : J. Fluid Mech. 119, 443 (1982).
 Jou, W.H., Knoke, G.S. & Ho, C.M. : DOE Ejector Conf. (1988).
- [5] Ho, C.M. & Gutmark, E. : Bull. Am. Phys. Soc. 27, 1184 (1982).
- [6] Schadow, K.C., Wilson, K.J., Lee, M.J. & Gutmark, E. : AIAA paper No. 84-1260, (1984).
- [7] Schadow, K.C., Gutmark, E., Parr, T.P., Parr, D.M., & Wilson, K.J. : JANNAF Combustion Conf. (1986).
- [8] Jou, W.H., Knoke, G.S. & Ho, C.M. : DOE Ejector Conf. (1988).

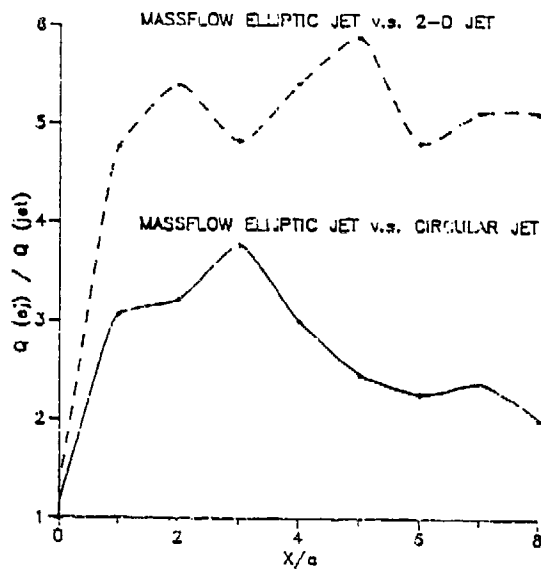


Fig. 1 Mass entrainment rate

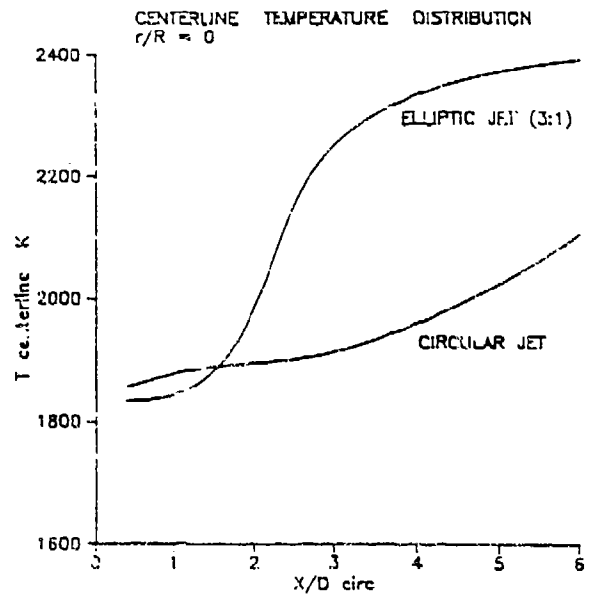


Fig. 2 Centerline temperature

**CONTROLLED SMALL-SCALE MIXING IN A
2:1 ASPECT-RATIO ELLIPTIC NOZZLE**

Austin, Thomas & Ho, Chih-Ming

Department of Aerospace Engineering
University of Southern California
Los Angeles, CA 90089-1191

1. Introduction

The study of turbulent jet shear flow plays an important role in numerous engineering applications. Free and confined jets are common devices present in mixing processes and the production of thrust. It is therefore desirable to control mixing, or the transfer of mass, heat and momentum. Combustion is an extremely complicated process involving fluid dynamics, chemical kinetics and acoustic interactions. Heat release in subsonic and supersonic chemically reacting flows is believed to be associated with vortex dynamics in which large scales provide the bulk of mixing between the fuel and oxidizer. Successive interactions among large scales produce smaller scales which in turn give rise towards finer mixing and initiate reactions leading to combustion at the molecular level. When heat is released in a chemically reacting turbulent shear layer the resulting flow is characterized by a nonconstant density field whose imposed nonhomogeneity couples the effects of fluid dynamics to chemistry. It is important to understand the directly coupled effects that turbulent shear flow and combustion processes have upon each other. Therefore, to control and to improve combustion characteristics one needs to passively, if not actively, direct the developmental processes of large- and small-scale structures in shear flows.

1.1 Elliptic Jet

A passive method of enhancing the rate of entrainment by as much as 500% in subsonic open nozzle flows has been obtained by modifying circular nozzle geometry to a 2:1 aspect-ratio ellipse.¹ (figure 1) This design offers a passive mixing control device and, more importantly, it is more efficient than either a conventional two-dimensional or axisymmetric nozzle. Small aspect-ratio elliptic nozzles have exhibited significantly higher spreading and entrainment

rates providing improved large-scale mixing properties. This concept has been successfully demonstrated at both subsonic² and supersonic conditions,³ in a confined dump combustor,⁴ and in high-temperature ramjet facilities yielding increased combustion efficiency.⁵

Toroidal elliptic vortices are shed at the elliptic nozzle exit. They are characterized by varying radii of curvature such that the section of the ring in the major axis plane with minimum radius of curvature is convected faster downstream by nature of the Biot-Savart Law of induction than the minor axis section of maximum radius of curvature. The faster moving section of the major axis section convects forward as it bends inward decreasing its local radius of curvature until it matches the radius of curvature of the minor axis section which is concurrently moving outwards. This process of *self-induction* is the principle mechanism driving entrainment in a 2:1 aspect-ratio elliptic jet by measurements which indicate as much as ten times more entrainment in the minor axis than the major axis region of a 2:1 aspect-ratio elliptic jet. The phenomenon of *axis switching* occurs when the initially elliptic ring momentarily sustains a circular configuration following a series of downstream distortions. These dynamics which are unique to three-dimensional nozzles dramatically enhance spreading and mixing in small-aspect ratio elliptic jet flows.

Recent measurements reveal that initial conditions in three-dimensional jet nozzles profoundly alter the downstream evolution of the flow. Two prominent features associated with the flow, the location of the first axis switching and mass entrainment, were found to vary significantly with exit velocity and exit temperature. The location of the first axis switching of the elliptic vortices increased downstream in direct proportion to the mean exit velocity and in inverse proportion to the mean exit temperature. Accordingly, measurements of the mass entrainment increased with higher exit temperatures and decreased with higher exit velocities. These results reaffirm the existence of a strong correlation between the dynamics of the elliptic vortex rings and their associated axis switchings with mass entrainment by the large scales verifying that the flow is driven by self-inducting elliptic vortices.⁶

1.2 The Structure of Turbulence

Turbulent shear flows are now known to be composed of structures of varying dimension and are characterized by a specific phase coherency.⁷ The process of turbulent mixing begins with the entrainment of ambient fluid into the flow by either merging or self-inducting large-scale vortices. In plane mixing layers⁸ and axisymmetric jet flows⁹ the dynamics of vortex merging is responsible for the growth of the turbulent shear layer in both homogeneous flows and chemically reacting mixing layers.¹⁰ However, in the three-dimensional flow fields characteristic of elliptic jets a second mechanism caused by the self-induction motions of the azimuthally deformed elliptic vortices controls large-scale mixing. Self-induction is responsible for the elliptic jet's large rate of entrainment, and its effect upon the mean flow is evident in the constant velocity contours at downstream jet cross-sections. (figure 2)

Successive interactions among the energetic, coherent spanwise (or toroidal) and streamwise large-scale structures,

respectively, instigate the production of smaller, three-dimensional scales within the cores of the vortices coinciding with the turbulent transition region.¹¹ The onset of small scales convolutes the topology of the large scales thereby increasing their interfacial surface area. The engulfed material is broken down into smaller homogeneous parcels and the process concludes at scales below the Kolmogorov microscale where molecular diffusion smears out remaining velocity gradients and chemical processes are initiated. The most probable length scale of the small structures lies between the Kolmogorov microscale and the Taylor microscale and this small scale appears to be responsible for dissipating most of the kinetic energy of the mean flow into heat thereby steering the mixing process towards completion.¹² Products of chemical reactions concentrate within the large scales and in particular among the small-scale regions¹³. Planar laser induced fluorescence flow visualization of hydroxyl concentrations reveal the existence of combustion products within vortex cores.¹⁴ Therefore, small scale concentrations appear to overlap zones of combustion in reacting shear layers and increased small-scale production increases fine-mixing which enhances combustion.

1.3 Excitation Effects

Non-reacting turbulent free shear layers¹⁵ and combustion processes¹⁶ have been shown to be sensitive to the external excitation corresponding to the initial instability frequency dictating their formation. This fact reinforces the possibility of indirectly controlling combustion by the passive and active methods successfully employed in controlling coherent structures in non-reacting shear layers. The reasons for controlling combustion are three-fold, to raise the amount of energy released and increase thrust, to extend flammability limits thereby broadening the operational range and to eliminate potentially disastrous combustion instabilities. Zohar has enhanced small-scale production in a plane mixing layer by forcing at the shear layer mode plus its first subharmonic.¹² (figure 3) Jets are uniquely characterized by two length scales, their initial momentum thickness and exit diameter. *Preferred mode* forcing involves acoustic forcing at the frequency corresponding to a constant Strouhal number (nondimensional frequency) based on the exit diameter, $St_D = 0.4$.¹⁷ Its global effect on the ensuing shear layer is to delay vortex merging by driving the creation of larger structures and isolating the effects of self-induction from vortex pairing in an elliptic jet.

1.4 Motivation

Operation of hypersonic aerospace vehicles, the United States National Aerospace Plane and vehicles similar to it, will require supersonic mixing inside scramjet combustors. Potential benefits arising from the application of elliptic shaped nozzles include, improved combustion efficiency; the alleviation of combustion instability; subsonic and supersonic exhaust noise reduction; vectored thrust for increased aircraft agility; thrust augmentation ejectors for Vertical/Short Takeoff or Landing aircraft; aircraft engine infrared signature reduction contributing towards stealth;¹⁸ laser ejector pumps; and improved steam ejectors in heat-actuated heat pumps¹⁹.

The importance of understanding the role of the smaller structures in mixing processes motivates our current research. In two-dimensional flow, including plane mixing layers and axisymmetric jets, the process of vortex merging is responsible for entrainment and small-scale production. However, in three-dimensional flow fields vortex self-induction dominates entrainment. Therefore, it is important to study the effect of self-induction on the generation of small scales in elliptic jets. It is proposed to actively excite the flow field by means of acoustic forcing in an attempt to control small-scale production and improve fine-scale mixing. In this light the small-scale topology of a homogeneous, subsonic 2:1 aspect-ratio elliptic jet is investigated for the purpose of controlling small-scale transition and, ultimately, fine-scale mixing. Streamwise velocity fluctuations are measured and analyzed by phase-averaging and Peak-Valley-Counting methods in a region four semimajor, a , axis diameters downstream of the exit where the flow is becoming fully turbulent.

2. Experimental Procedure

2.1 Jet Facility

The experimental subsonic jet facility is driven by multiple centrifugal blowers in parallel and operates at a maximum exit velocity of 85 m/s bordering the upper limit of incompressibility. The flow enters an anechoically treated cylindrical chamber, contracts into an aluminum stagnation chamber of constant diameter and passes through aluminum honeycomb, aluminum foam, and a series of fine wire mesh screens where the flow field becomes more uniform and less turbulent. An aluminum composite nozzle smoothly contracts to a 2:1 aspect-ratio elliptical orifice with dimensions of 2" (major axis, $2a$) by 1" (minor axis, $2b$). (see figure 4).

A small azimuthally symmetric forcing chamber is machined into the nozzle exit permitting complete circumferential acoustic forcing of the initial shear layer. (figure 5) Four Realistic 13 speakers with a response range between 100 Hz and 15 kHz emit at opposed ends of the major and minor axes, respectively, at the nozzle exit to perturb the flow. The speakers are powered by a pair of two-channel Carver M-200t 120W per channel power amplifiers. The output is synthesized by either a B&K function generator which sends continuous sinewaves, a simple arbitrary waveform transmitted by an RC Electronics Waveform Generator or a more complicated high-frequency waveform sent via a 12-channel Data Translation DT-2814 digital-to-analog converter. The acoustic field generated by the azimuthally positioned speakers was uniform across the span to within 5% of the RMS pressure levels measured by a microphone at the exit.

Turbulent velocity signals containing the signatures of the large and small scales in the shear layer as well as the irrotational fluctuations induced into the quiescent fluid by the passage of the large scales are sampled by two Dantec 55P71 hot-wire probes connected to a constant-temperature circuit which provides a flat frequency response to 30 kHz. The sensor consists of a 0.0001" diameter platinum-10% rhodium wire attached to 0.75 mm wide probes mounted on a

microcomputer controlled traverse system translatable in three-dimensions. Hence, small scales larger than the probe separation with frequencies smaller than the operating range of the hot-wire circuit are resolvable. This places an effective upper limit of 50 m/s at the exit upon the operation of the facility. The fluctuating data is digitized, recorded and analyzed by a PC AT microcomputer-controlled analog-digital converter at acquisition rates up to 1 MHz. Final processing is performed on a Macintosh IIfx workstation.

2.2 Peak-Valley-Counting Method

Measurements of longitudinal velocity fluctuations are undertaken throughout a cross-sectional cut orthogonal to the mean flow four semimajor axis lengths downstream. Every data time record contained at least 15,000 small scales and 2,000 large scale structures to insure statistical reliability. The velocity traces contain low-frequency fluctuations caused by the large-scale structures and higher frequency fluctuations some of which are due to the presence of small scales. Phase-averaged data from the second hot-wire provides local large-scale statistics allowing for the purposes of conditional averaging. The Peak-Valley-Counting method developed by Huang²⁰ and Hsiao²¹ and improved by Zohar¹² was used to detect the small-scale structures. This algorithm generates a pulse train corresponding to the proper local extrema associated with small-scale fluctuations in a turbulent velocity signal by employing a series of logical conditions. (figure 6) The final locations of the actual small-scale fluctuations are obtained by discriminating among the 'peaks' and 'valleys' of the time signal which includes the removal of false fluctuations, erroneous consecutive maxima (or minima), analog-digital-converter noise components and random high-frequency noise by incorporating specific amplitude and temporal threshold levels throughout the five stages of the algorithm.

3. Results and Discussion

3.1 Initial Conditions

The small-scale topology of the elliptic jet was investigated at an exit velocity, $U_0 = 45$ m/s, corresponding to a Reynolds number based on hydraulic diameter of 10^5 . Two cases are considered, first the natural flow and second, the jet excited at its Preferred Mode by forcing at $f_p = 570$ Hz with an amplitude of 1.2% of the free stream mean velocity at the centerline of the jet exit. The initial momentum thickness, θ , for the unforced case is 0.12 mm corresponding to a Reynolds number based on initial momentum thickness of 10^3 , and increases to 0.33 mm under forcing.

The shear layer initially rolls-up via the Kelvin-Helmholtz instability mechanism into vortices two instability wavelengths, λ_0 , downstream at the frequency corresponding to shear layer Strouhal number, $St_0 = f \theta / U_0 = 0.017$ in accordance with linear instability theory.²² The power spectra obtained from a fast fourier transform analysis of the initial unforced flow reveals the initial frequency and its first subharmonic indicative of vortex pairing at four λ_0 downstream. (figures 7a, 7b) Preferred mode forcing effectively suppresses vortex pairing at the first instability frequency

subharmonic and instead pumps energy from the mean flow to form larger more coherent vortices at 570 Hz by the *collective interaction* process.²⁰ (figures 7c, 7d) Therefore, in the forced case only the effects of self-induction dictate the evolution of the flow as well as production of the small scales.

3.2 Streamwise Measurements

The mean centerline velocity distribution with respect to downstream distance illustrates the dramatic effect of forcing by the decreased length of the potential core region in the elliptic jet from $x/a = 5$ to $x/a = 3$ and a 33% smaller mean velocity further downstream in the turbulent region. (figure 8a) A similar plot of the root-mean-square velocity shows twice as much fluctuating energy in the center of the flow in the transitional region at the end of the potential core between $x/a = 4$ to $x/a = 7$ which also coincides with the region of very large entrainment into the mean flow. (figure 8b)

Small-scale populations in the streamwise direction for the unforced case are measured by the Peak-Valley-Counting method and reveal a similar picture similar to the plane mixing layer. (figure 9) The number of small scales increases sharply from the first vortex merging position at $x/\lambda_0 = 4$ to the second merging position at $x/\lambda_0 = 8$. The distribution peaks at the third merging position, $x/\lambda_0 = 16$, and gradually decreases downstream --there is no downstream asymptotic plateau-like region. In the case of the plane mixing layer energy is constantly supplied to the mean flow from nonzero velocity regions above and below the shear layer. A turbulent jet with zero co-flow does not receive energy beyond the exit nozzle and hence the kinetic energy of the flow field, which is imparted to the small-scale structures from the large-scale structures via an *energy cascade* fashion, steadily decays downstream and is dissipated into heat by the small scales.

A still unknown nonlinear secondary instability triggers production of small scales within the cores of the spanwise large scales and may be in part due to complex stretching and tilting process among the large scales. The region of transition to full turbulence appears to follow the first vortex merging and approaching completeness after the second vortex merging. Evidence of this is provided by the number of small scales per initial large scale as calculated by the Peak-Valley-Counting method^{12, 20}, the $-5/3$ slope of the roll-off exponent of the one-dimensional energy spectrum²³, and increased chemical product concentration.²⁴ (figure 10) Hence the location $x/a = 4$ in the elliptic jet flow was qualified for detailed investigation of the small-scale topology because it is at the third vortex merging location and is a region approaching fully turbulent conditions.

3.3 Small-scale Topology

At four semimajor axis lengths downstream the small-scale population densities were mapped out over a 12 by 12 grid encompassing a spatial cross-section intersecting the entire mean flow. Following symmetry checks only one

quadrant in the flow cross-section is measured. The Peak-Valley-Counting method detects and extracts spatial, temporal and velocity information associated with the small-scale structures embedded in the coherent large scales yielding population distributions, length scales and frequencies pertaining to the small-scale activity.

The mean velocity profile across the major and minor axes, respectively, at $x/a = 4$ show distortions in the profile when the flow is forced at the Preferred Mode. These distortions vary with the forcing level and one observes in general an increase in the jet width resulting in greater spreading of the flow field, in the minor axis in particular. (figure 11) Density plots overlaid by constant population contours of the number of small scales per local large scale show greatest concentrations of the small scales in the shear layer of the jet for both cases. (figure 12) The population distribution in the unforced case appears 'fuller' with more curvature than the forced case. In general both contour plots appear similar in shape and density strongly suggesting that self-induction dynamics govern the evolution of the elliptic jet rather than the mechanism of vortex merging. The maximum number of small scales per local large scale attains a value of 8.8 in the forced case and is 10% greater than the peak of 8.1 in the natural flow. Forcing at the frequency predicted by linear instability theory² increases the coherence of the large scale structures by phase-locking them into a more unique frequency and pattern. This would increase the capacity of the large scale structures to contain more smaller scales as described here. It is interesting to note that for both natural and forced cases the maximum number of small scales are located in the major axis region of the shear layer rather than the minor axis. Previous measurements have shown that the minor axis region of an elliptic jet flow are characterized by larger spreading rates and consequently entrain more fluid. However, due to the nature of the unsteadily deforming elliptic vortices which comprise the annular shear layer other cross-sectional further measurements at upstream and downstream streamwise locations are necessary before the flow topology can be fully understood.

The volume integral of the population density contours representing the total number of small-scale structures throughout the cross-section revealed that the forced case produced 25% fewer total small scales than the natural case. This finding is significant because vortex merging has been believed to perform an important role in the evolution of all turbulent free shear layers, however, now it appears that in the case of the three-dimensional elliptic flow field the dynamics of vortex self-induction is responsible for 75% of the small-scale production. As the natural case did produce 25% more small scales than the forced case one can surmise that the strain rate produced by vortex merging is more effective in the generation of small scales than that produced by the self-induction process. To increase the production of small scales in an elliptic jet flow would therefore suggest forcing at the initial instability frequency and its related subharmonics rather than the Preferred Mode frequency thereby promoting more energetic vortex merging.

Further analysis of the small-scale populations were performed by examining slices along the major axis direction at equivalent minor axis (z/b) stations. (figure 13) At first glance it appears that the forced case ($f=f_p$) populations are similar if not greater than their natural ($f=0$) counterparts. Careful observation at stations within the shear layer, $z/b =$

0.76 through $z/b = 1.4$, reveal greater population levels near the core of the flow which account for the 25% larger number of small scales in the natural flow.

At every station in the measured region the Peak-Valley-Counting method builds up a statistically meaningful histogram of the number of small scales corresponding to a specific frequency associated with the fluctuations of the small scales. The small-scale frequency histograms illustrate the existence of a most probable frequency associated with the small scales and that it is constant throughout the entire cross-sectional region of the flow. In the current investigation where the $Re_D = 10^5$ the most probable frequency of the small scales is 13,900 Hz. Previous measurements reveal the frequency to increase with Reynolds number. At the center of the flow there is little or no small-scale activity, but at increasing radially outward locations along the major axis the histogram begins to take on a recognizable shape with a discernible constant peak of the most probable small-scale frequency. Finally at towards the edge of the shear layer the small-scale frequency histograms diminish. (figure 14) The forced case shows similar progression along the major axis with the same most probable small-scale frequency. (figure 15) A characteristic small-scale length can be estimated as $l_s = U_c/f_s = 1.6$ mm, where f_s represents the most probable small-scale frequency and convection velocity is $U_c = U_0 \times 0.6$.

4. Conclusion

Preliminary investigations upon the small-scale topology of a 2:1 aspect-ratio elliptic jet have been performed by the Peak-Valley-Counting method. At an exit velocity of 45 m/s the unforced elliptic jet transitions to full turbulence at the third vortex merging. Downstream of this location energy dissipation becomes greater than the level of kinetic energy remaining in the flow. Small scales are distributed mainly within the shear layer region and exhibit a preference towards the major axis region. Acoustic forcing at the Preferred Mode effectively suppresses vortex merging and isolates the effects of self-induction and causes greater spreading of the mean flow field. Forcing created a 25% decrease in the small-scale populations but did not significantly alter the topology of the turbulent structures. Therefore, the mechanism of self-induction is more desirable than vortex merging in turbulent jet flows because it is responsible for improved large-scale mixing and appears to be the dominant mechanism in the production of small scales in the elliptic jet. These results support the encouraging reports involving elliptic nozzles over circular nozzles in chemically reacting experiments.

Quantitatively, Preferred Mode forcing decreased the number of small scales by 25% thereby reducing the small-scale mixing process. The peaks of the frequency histograms throughout the entire region of interest for both natural and forced cases yielded a most probable small-scale frequency, $f_s = 13,900$ Hz, translating into a characteristic small-scale length, $l_s = 1.6$ mm. Therefore the scale of fine turbulence is unchanged by forcing and it is constant at a given Reynolds number similar to the Taylor and Kolmogorov microscales.

2:1 aspect-ratio elliptic jets appear by many accounts to be very promising improvements over axisymmetric jet

configurations because of their enhanced large-scale and small-scale mixing characteristics. Further investigation of the topology of the small-scale structures and the mechanism governing their formation by the self-interacting large-scale structures will significantly aid in the understanding of controlling and increasing production of the small scales. This endeavor will promote an understanding of the effects of fine-scale mixing which is essential to subsonic and supersonic combustion processes.

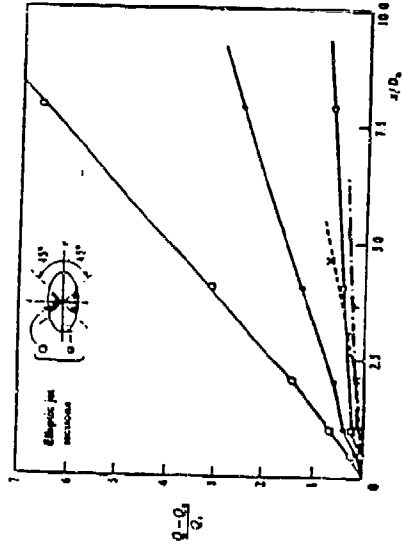
This work is supported by the Air Force Office of Scientific Research under Grant No. AFOSR-90-0301

References

- [1] Ho, C. M., Gutmark, E. Vortex Induction and mass entrainment in a small-aspect ratio elliptic jet. *Journal of Fluid Mechanics*, 1987, 179: 383-405.
- [2] Austin, T., Ho, C.M. Entrainment of Asymmetric Jets. A.F.O.S.R. Turbulence Research Contractor's Meeting, 1988.
- [3] Schadow, K., Gutmark, E. Review of Passive Shear-Flow Control Research for Improved Subsonic and Supersonic Combustion. AIAA paper, 1989, 89-2786.
- [4] Hertzberg, J., Ho, C.M. Time averaged 3d flow in a rectangular sudden expansion. AIAA paper, Jan. 1991, 91-0040.
- [5] Schadow, K., Wilson, K., Lee, M., Gutmark, E. Enhancement of Mixing in Ducted Rockets with Elliptic Gas-Generator Nozzles. AIAA paper, 1984, 84-1260.
- [6] Austin, T., Ho, C.M. Controlled Entrainment in a 2:1 Aspect-ratio Subsonic Elliptic Nozzle to be presented at AIAA 30th Aerospace Sciences Meeting, Jan. 1992.
- [7] Ho, C. M., Huerre, P. Perturbed Free Shear Layers *Annual Review of Fluid Mechanics*, 1984, 16: 365-424.
- [8] Winant, C., Browand, F. Vortex pairing: the mechanism of turbulent mixing layer growth at moderate Reynolds number. *Journal of Fluid Mechanics*, 1974, 63: 237-255.
- [9] Browand, F., Laufer, J. The Role of Large Scale Structures in the Initial Development of Circular jets. Proceedings of 4th Biennial Symposium on Turbulence in Liquids, Univ. of Missouri-Rolla, Sept. 1975: 333-344.
- [10] Masutani, S., Bowman, C. The structure of a chemically reacting plane mixing layer *Journal of Fluid Mechanics*, 1986, 172: 93-126.
- [11] Moser, R.D. & Rogers, M.M. 1991 The three-dimensional evolution of a plane mixing layer Part 2: Pairing and transition to turbulence. In preparation.
- [12] Zohar, Y., Fine scale mixing in a free shear layer. Ph.D. Thesis, University of Southern California, 1990.
- [13] Breidenthal, R. Structure in turbulent mixing layers and wakes using a chemical reaction *Journal of Fluid Mechanics*, 1981, 109: 1-24.
- [14] Gutmark, E., Parr, D., Hanson-Parr T., Schadow, K. On the Role of Large and Small-Scale Structures in Combustion Control *Combustion Science & Technology*, 1989, 66: 107-126.

- [15] Ho, C. M., Huang, L. Subharmonics and vortex merging in mixing layers *Journal of Fluid Mechanics*, 1982, 119: 443-473.
- [16] Gutmark, E., Schadow, K., Parr, T., Parr, D., Wilson, K. Noncircular jets in combustion systems AIAA paper, 1987, 87-1379.
- [17] Crow, S., Champagne, F. Orderly Structure in Jet Turbulence *Journal of Fluid Mechanics*, 1971, 48: 547-591.
- [18] Hiley, P., Wallace, H., Booz, D. Nonaxisymmetric Nozzles Installed in Advanced Fighter Aircraft. *Journal of Aircraft*, Dec. 1976, 13, no. 12: 1000-1006.
- [19] Jou, W., Knoke, G., Ho, C.M. Entrainment Enhancement of a Supersonic Jet for Advanced Ejectors. Department of Energy Ejector Conference, 1988.
- [20] Huang, L. Small scale transition in a two-dimensional mixing layer Ph.D. Thesis, University of Southern California, 1985.
- [21] Hsiao, F. Small scale transition and preferred mode in an initially laminar plane jet Ph.D. Thesis University of Southern California, 1985.
- [22] Michalke, A. Instabilität eines kompressiblen runden Freistrahls unter Berücksichtigung des Einflusses der Strahlgrenzschichtdicke *Zeitschrift für Flugwissenschaften*, 1971, 19, no. 8/9: 319-328.
- [23] Jimenez, J., Martinez-Val, R., Rebollo, M. On the origin and evolution of three-dimensional effects in the mixing layer Internal report DA-ERO 79-G-079, Univ. Poltec., Madrid, 1979.
- [24] Breidenthal, R. Structure in turbulent mixing layers and wakes using a chemical reaction *Journal of Fluid Mechanics*, 1981, 109: 1-24.

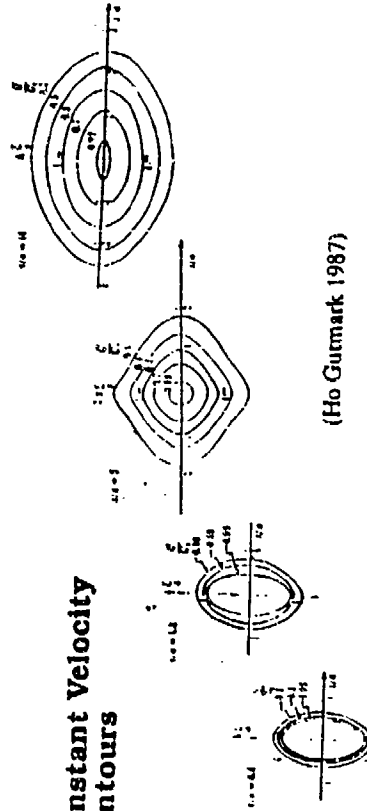
Entrainment Ratios



(Ho Gutmark 1987)

Figure 1.

Constant Velocity Contours



(Ho Gutmark 1987)

Figure 2.

Small Scale Production Enhancement by Forcing

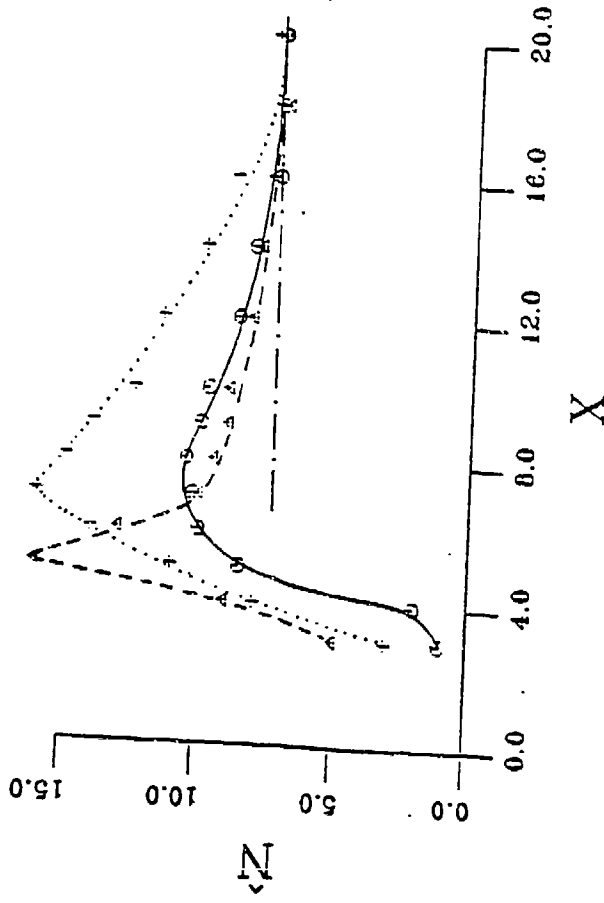


Figure 3: Forcing effect on small eddy evolution.

ϕ — Natural ; Δ — Forc'd, f_0 ; \dots ; Forc'd, $f_0 + f_0/2$.

Figure 3.

FORCING ARRANGEMENT

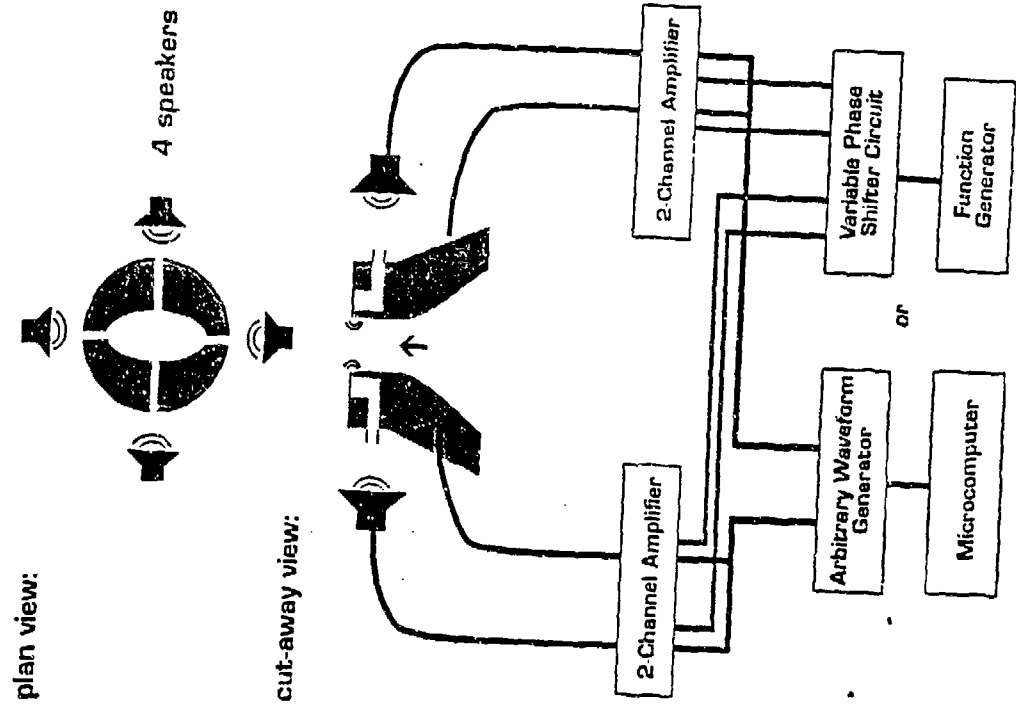


Figure 5.

2:1 Aspect Ratio Elliptic Jet Facility

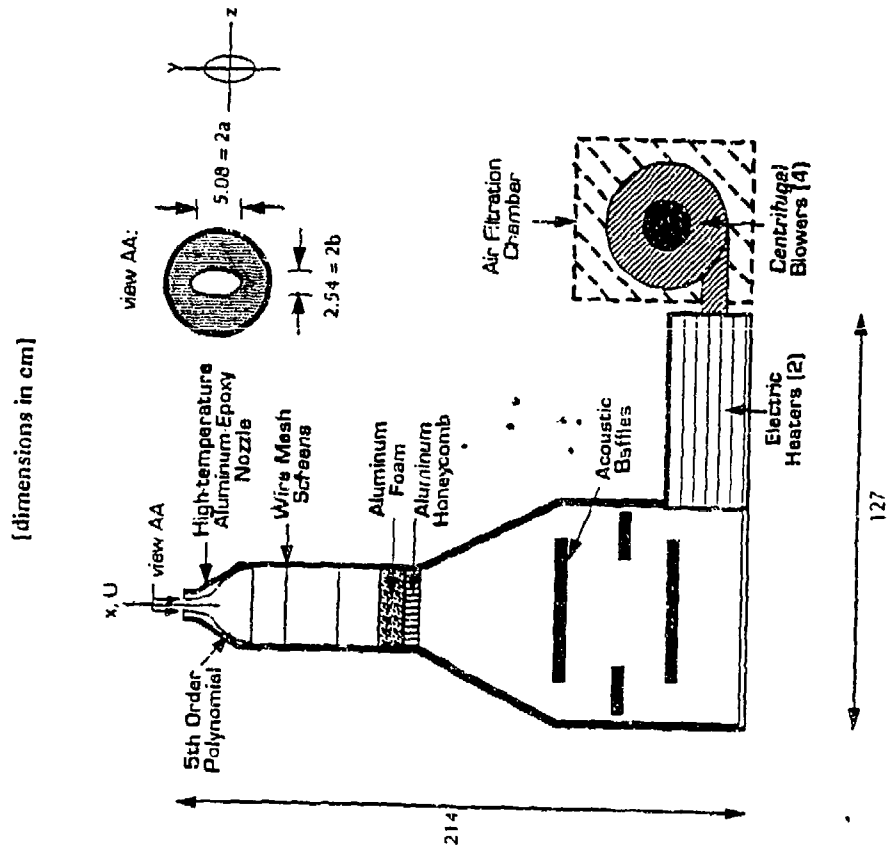
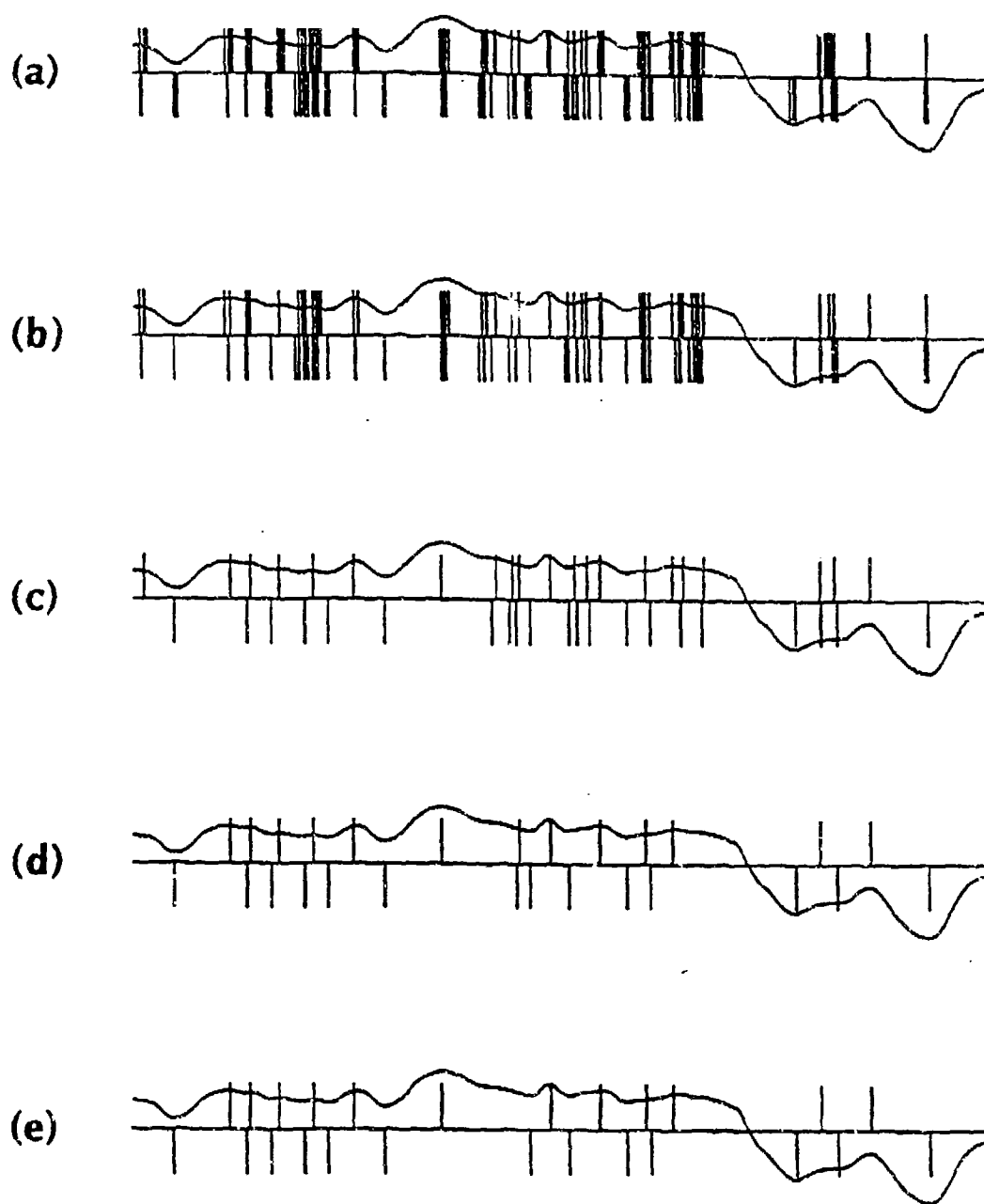


Figure 4.

Peak-Valley-Counting Method



The pulse train of peaks and valleys after the:
(a) 1st, (b) 2nd, (c) 3rd, (d) 4th and (e) 5th stage of the PVC algorithm.

Figure 6.

Unforced Case

Vortex Roll-Up Location
 $x/\lambda_0 = 2$

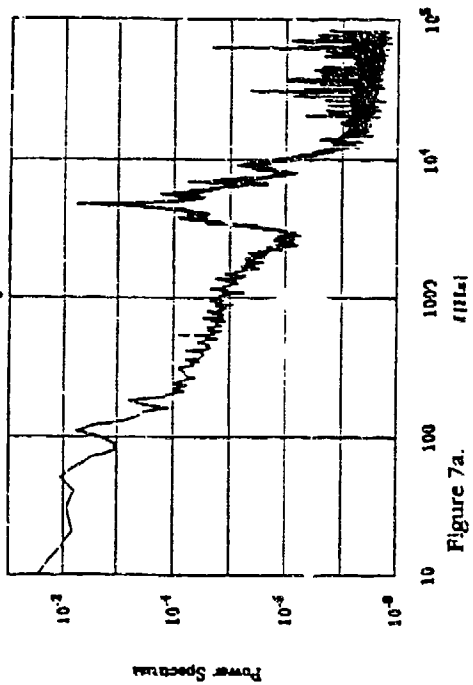


Figure 7a.

Forced Case: $f_0 = 570$ Hz

Vortex Roll-Up Location
 $x/\lambda_0 = 2$

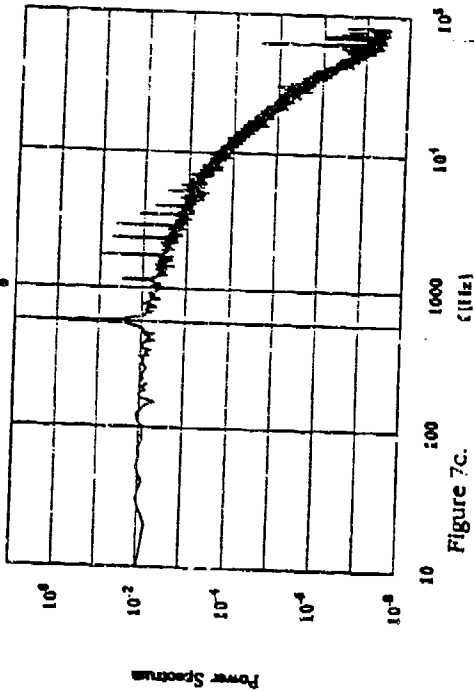


Figure 7c.

First Merging Location
 $x/\lambda_0 = 4$

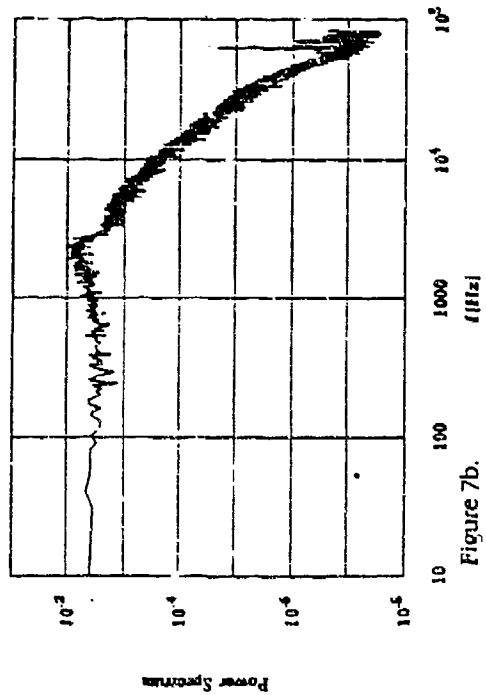


Figure 7b.

First Merging Location
 $x/\lambda_0 = 4$

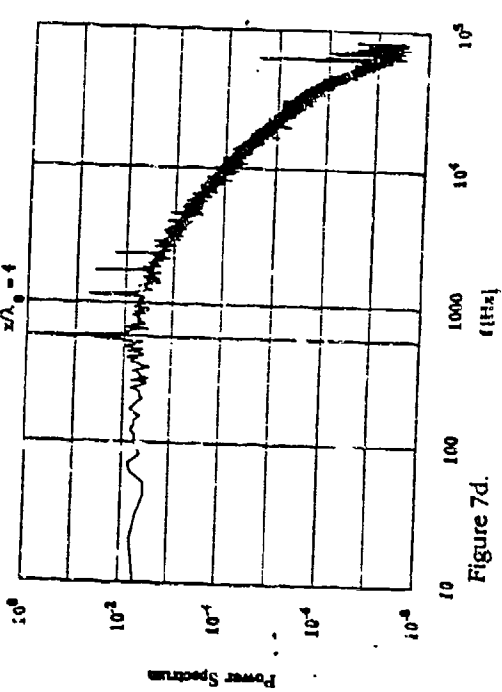


Figure 7d.

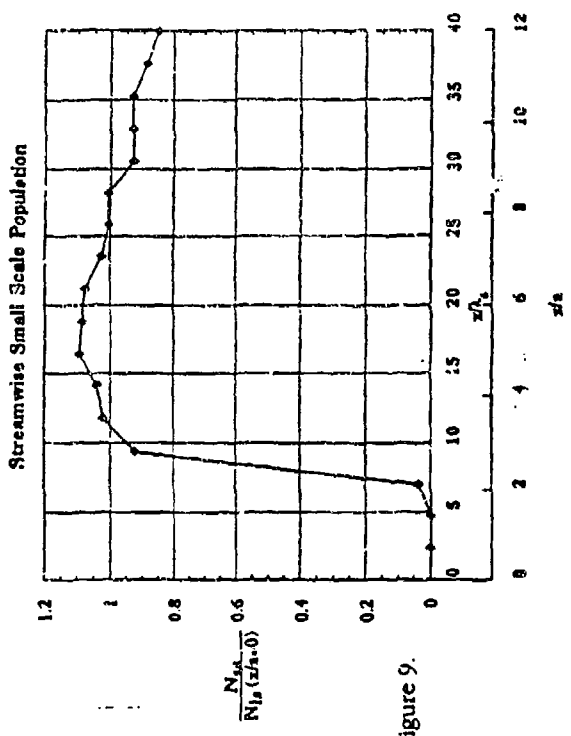


Figure 9.

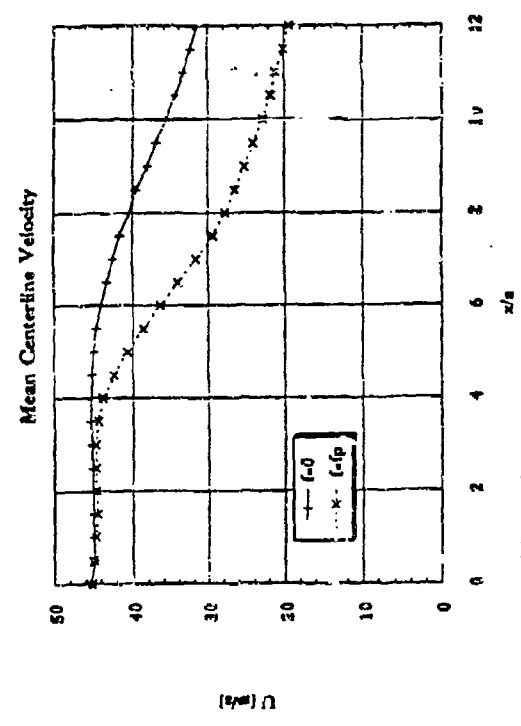


Figure 8a.

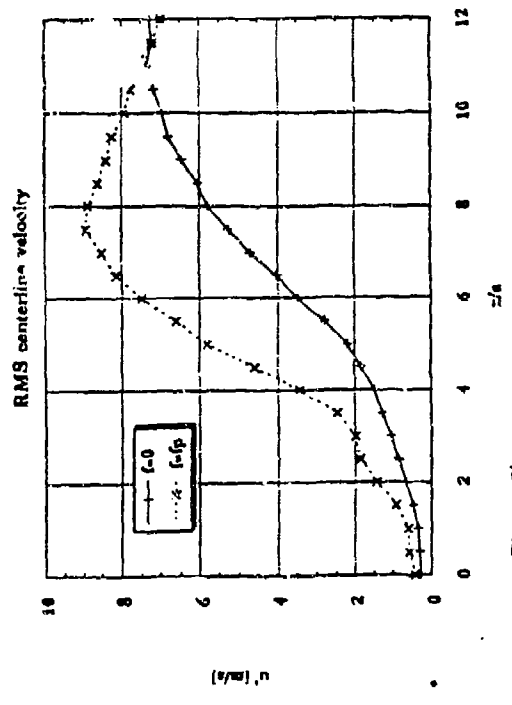


Figure 8b.

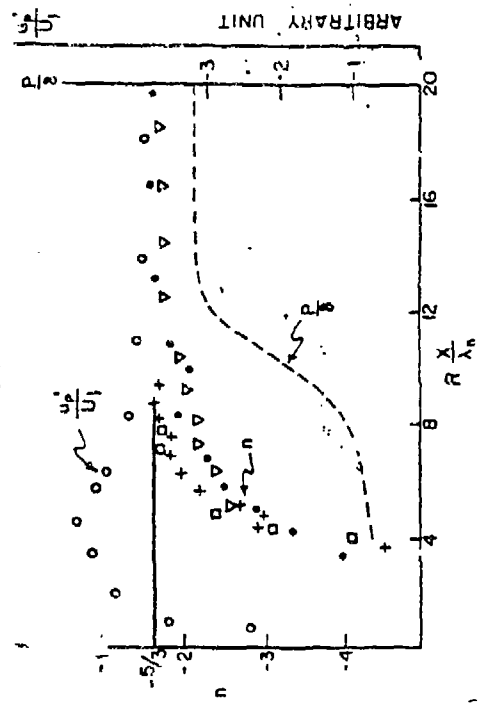


Figure 10.

(Ho Huerts 1984)

Figure 13 & experimental measures of small-scale transition as a function of streamwise distance u'_p/U_1 ; Peak turbulence level; \circ $R = 1$ (Hutchins & 2006); \square slope of the inertial subrange; \bullet $R = 1$ (Hutchins et al 1999); \triangle $R = 0.45$; ∇ $R = 1$ (Huang & Ho 1998); \diamond $R = 0.45$ (Hutchins 1983); \times $0.14 < R < 0.45$ (Hutchins 1983).

$U_0 = 45 \text{ m/s}$ $x/a = 4$
 Small Scale Topology

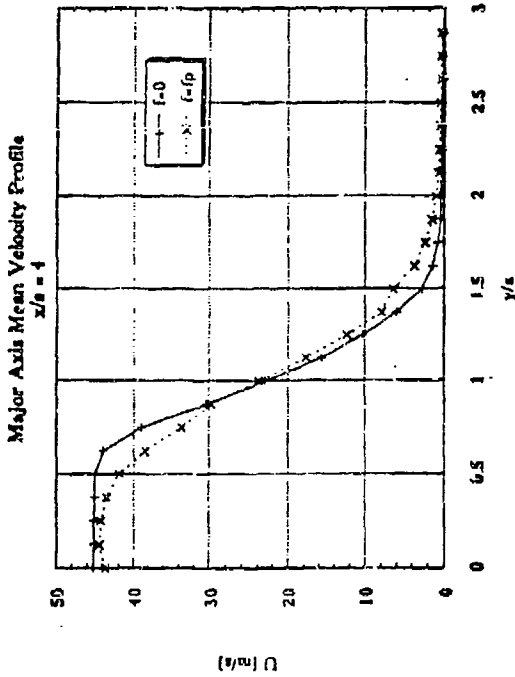


Figure 11a.

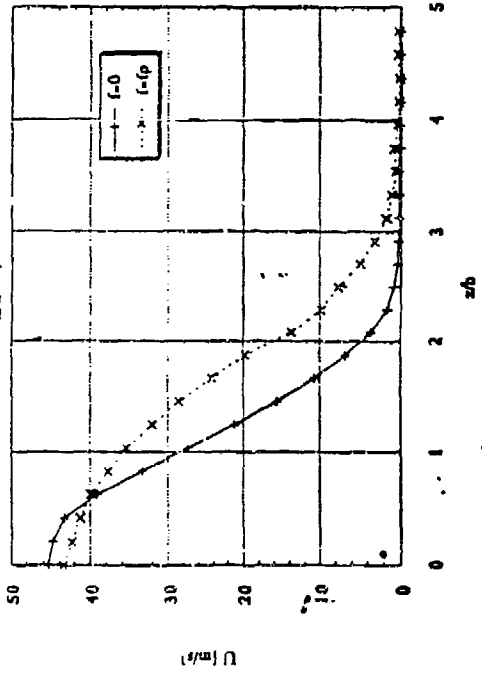


Figure 12b.

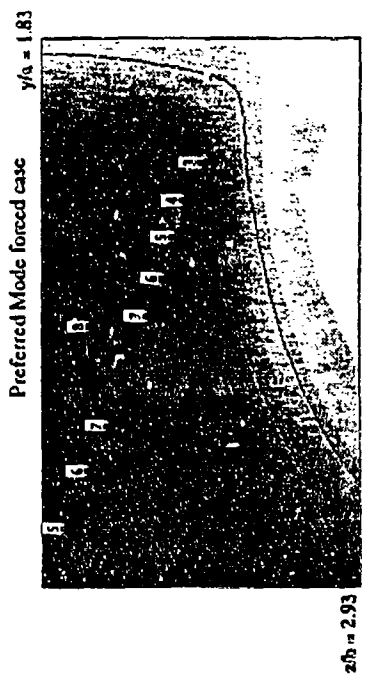
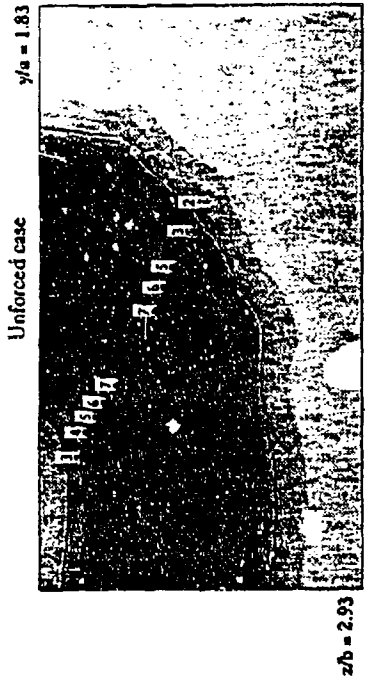


Figure 12.

Small Scale Population

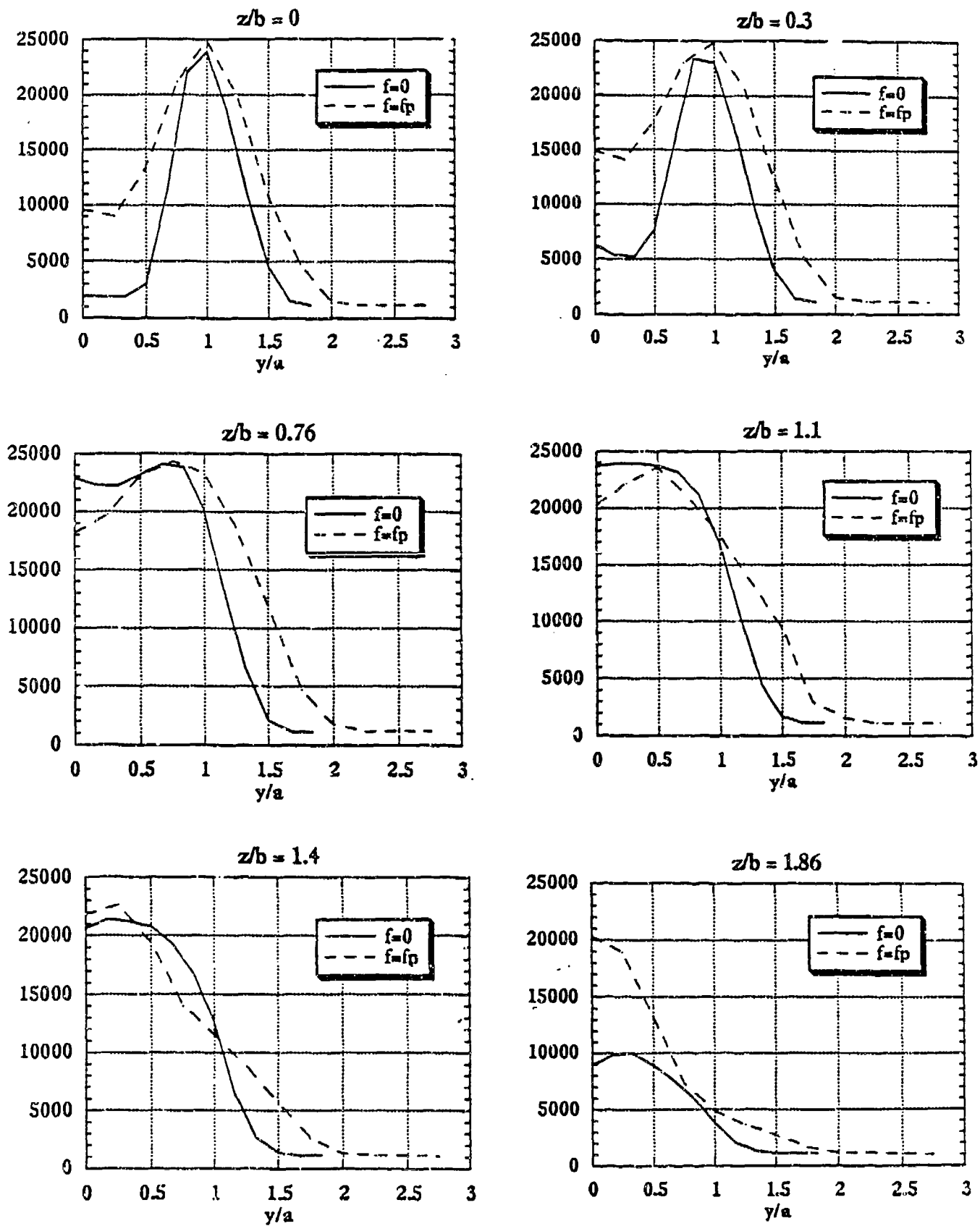
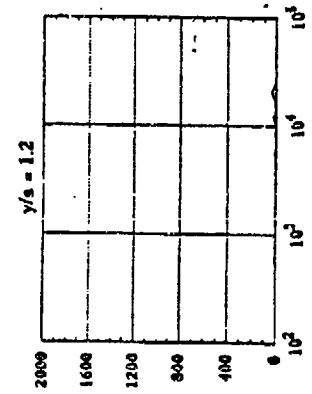
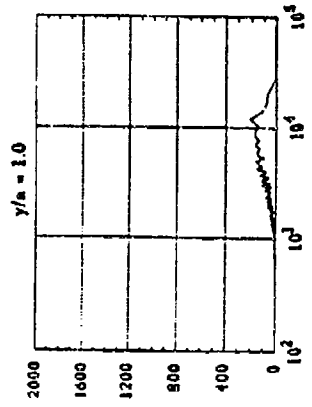
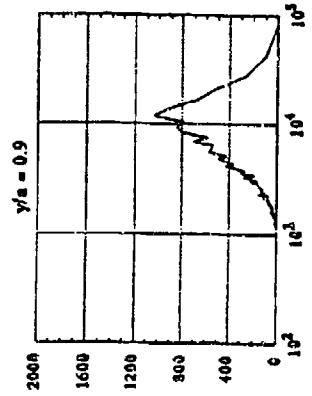
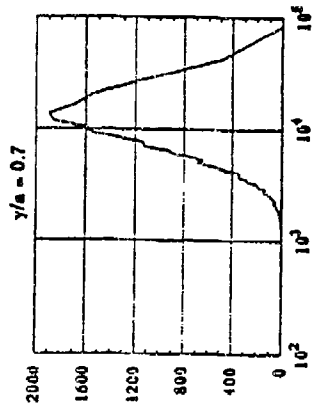
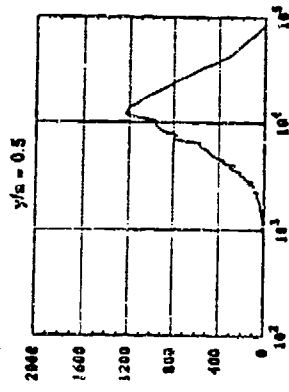
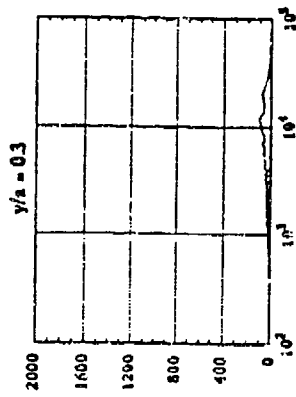


Figure 13.

Major Axis, unforced



Major Axis, forced

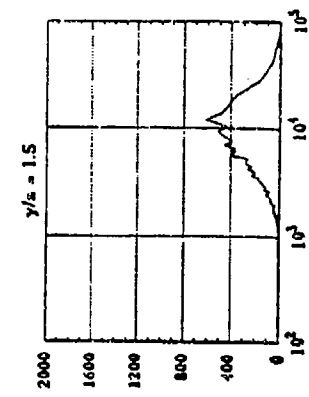
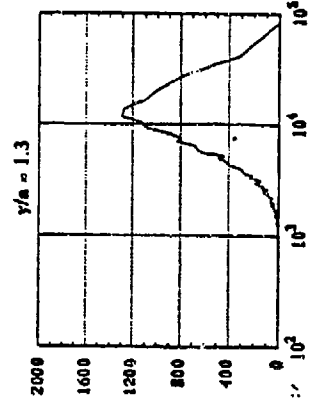
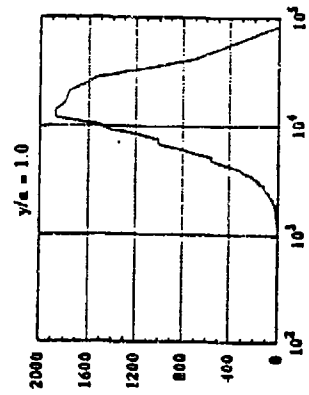
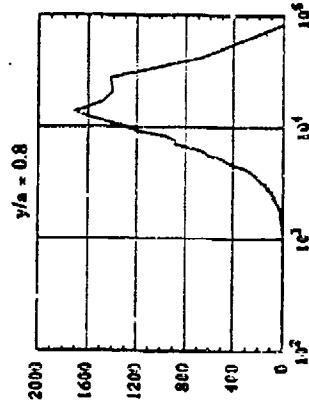
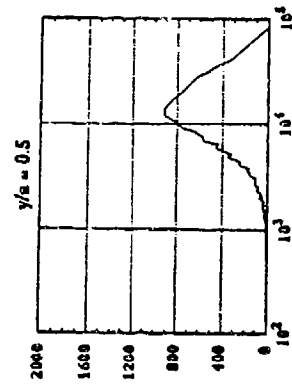
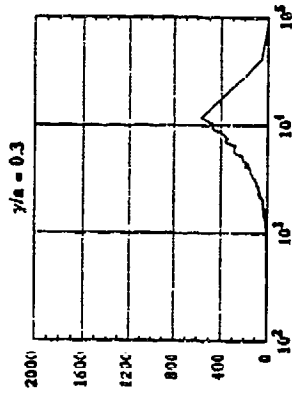


Figure 14a.

Figure 14b.

**PLANAR IMAGING OF A HEATED ELLIPTIC JET
BY THE FOCUSING SCHLIEREN METHOD**

Presented at the 1990 Fall Meeting of the
Western States Section/The Combustion Institute
La Jolla, California, October 15-16, 1990

T. Austin and S. Schreck
Department of Aerospace Engineering
University of Southern California
Los Angeles, CA

PLANAR IMAGING OF A HEATED ELLIPTIC JET BY THE FOCUSING SCHLIEREN METHOD

Thomas Austin* and Stefan Schreck†
Department of Aerospace Engineering, University of Southern California
Los Angeles, California 90089-1191
September, 1990.

* Research Assistant
† Research Associate

Abstract

The turbulent flow of a heated subsonic elliptic jet of 2:1 aspect ratio was studied experimentally. The flow structure was visualized using planar imaging by a focusing schlieren system and conventional still and motion photography. Density gradients in an inhomogeneous flow permit visualization of the resultant bending light rays by a schlieren system. Focusing Schlieren is a long overlooked improvement upon the original arrangement as it permits visualization of individual plane sections of finite depth within a stratified gas flow. Actual planar slices revealed individual cross-sections of large-scale vortical structures and small-scale three dimensional turbulence in the jet.

Introduction

Flow visualization of heated jet flow is a simple and helpful tool to aid in the analysis of the dynamics of turbulence. A heated jet can simulate the combustion process involving the mixing of hot fluid with ambient air. The ability to visualize the flow dynamics in the jet increases the overall understanding of mixing and combustion phenomena in general.

Light behaves as a series of wavefronts, such that when two plane waves at small angles propagate in the same direction, their amplitudes sum together. The resulting light wave will form light and dark fringes-- an interference pattern. Fringe separation is indicative of the difference in the optical path length which in turn is the integral of refractive index times traversed length.¹

$$\text{O.P.L.} = \int n \, ds$$

Schlieren flow visualization is based on the fundamental concept that the speed of light is inversely proportional to the index of refraction, n , of the medium. In turn, the index of refraction is directly proportional to the density of the medium, ρ , where $\beta_{\text{air}} = 0.000292$.²

$$n = 1 + \beta \frac{\rho}{\rho_0}$$

Light wave fronts turn and refract in variable density flow owing to the variation in the index of refraction. In the basic schlieren system ordinary white light is focused into parallel beams by being passed through a lens and transmitted across a test section. See figure 1. A second lens subsequently focuses the rays thereby forming a final image. By blocking part of the light at the focus of the image with a knife edge the screen visualizes the gradient of density normal to the knife edge.

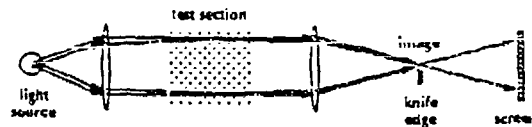


FIG. 1 Basic Schlieren System.

Therefore, the deflected light in a schlieren system is intercepted prior to the formation of its image and the sections of the field traversed by the light rays become darker. Only a single plane is focused upon in this manner, however, light is integrated along its entire path and the method does not yield a true image of a plane within the flow. A more practical albeit larger schlieren set-up replaces both lenses with inexpensive concave mirrors relocating the light source and screen off axis.³ Shadowgraphy is equivalent to schlieren visualization except there is no knife edge and the imaging displays the second derivative of the density.⁴ The schlieren method is found to be more sensitive than the shadowgraph method and is better suited towards visualizing low-temperature flows.⁵

The line-of-sight integration peculiar to conventional schlieren and shadowgraph imagery drastically limits the ability to study the inner structure of a complicated flow field. Therefore, conventional schlieren and shadowgraph methods cannot image individual planes within the flow field, whereas Focusing Schlieren depicts a more accurate image of the structures embedded within the plane of the flow. The method of Focusing Schlieren was originally developed forty years ago by Ralph Burton⁶, and Arthur Kantrowitz and Robert

Trimpi⁷, reviewed by R. Buzzard⁸ and very recently improved by Leonard Weinstein.⁹

The Focusing Schlieren system uses multiple light sources by passing light through a grating, whose lines are typically aligned parallel to the mean flow studied. In this manner many beams of light pass through any given point within the test section and subsequently there will be many beams of deflected light within the test section. Finally, there must be multiple knife edges or cutoifs to focus and filter the incoming rays. A screen receives rays which have passed through one given point. Other points intercept and deflect these rays but none of the rays focusing upon the screen will have encountered any points in common, along their respective paths. Only the deflection from the common points within a plane in the test section will contribute to the intensity of light at the screen. Other planes remain out of focus and their offset images blur out as in the focusing of ordinary lenses. There is only one moving part—the screen which is translated forwards and backwards to visualize different planes in the test section.

Focusing Schlieren Flow Diagnostic Method

Visualization was performed on a heated subsonic elliptic jet whose exit nozzle geometry was characterized by a 2:1 aspect ratio. See figure 2. Flow in an elliptic jet is highly three-dimensional establishing it as a good subject for Focusing Schlieren measurements. Maximum exit velocity of the jet was 85 m/s and exit temperature was 165 °C, respectively. The density in the potential core of the jet was low enough to enable the flow to be visualized even though its value was only 65% of ambient density.

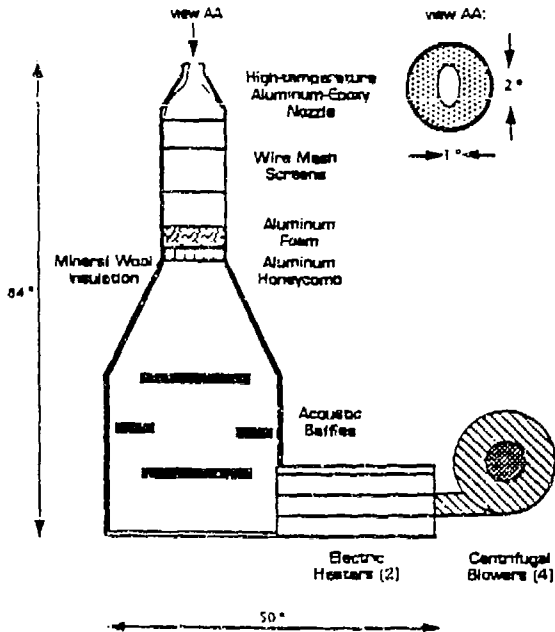


FIG. 2 2:1 Aspect Ratio Elliptic Jet Facility.

The principle viewing area of interest is shown in figure 3. The size of the flow region in the near field of the elliptic jet dictated the minimum size of the necessary optics for visualization.

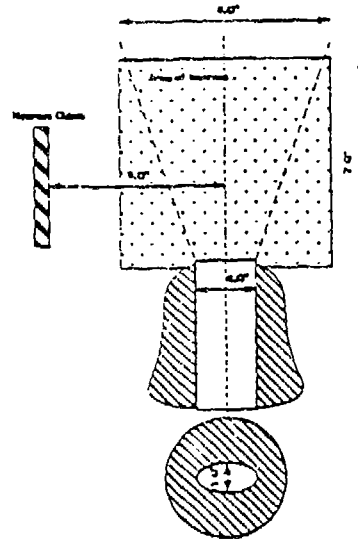


FIG. 3 Jet Exit Nozzle Facility.

Previous measurements of velocity and temperature profiles utilizing hot-wire, cold-wire, pitot tube and thermistor sensors indicated the approximate boundaries of the flow.

The laws of optics dictated the dimensions of the Focusing Schlieren flow diagnostic facility, specifically the *lens maker's formula*.¹

$$\frac{1}{d_o} + \frac{1}{d_i} = \frac{1}{f}$$

Where d_o is the distance between the first set of Ronchi Rulings and the primary lens, d_i is the distance between the second set of Ronchi Rulings and the primary lens, and f is the effective focal length of the primary lens. Weinstein obtained highest quality images with a distance ratio of $d_o/d_i = 2$. The main drawback with this ratio is that it dictates a longer facility than for a distance ratio of say, $d_o/d_i = 1$.

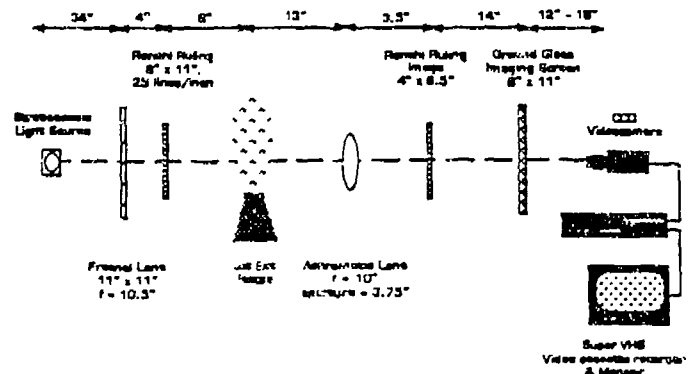


FIG. 4 Focusing Schlieren Facility.

White light is emitted from a variable strobed light source, General Radio[®] 1540 Strobolume Oscillator, controlled by a function generator. Light is collimated by a 10.5 inch focal length Fresnel Lens from Edmund Scientific and passes through Ronchi Rulings consisting of vertical 25 line per inch fringes. The fringe pattern was drawn on an Apple Macintosh[®] IIx microcomputer with Ashlar Vellum[®] drafting software and printed onto 3M[®] transparency paper by an Apple Laserwriter[®] IINT laser printer.

Light rays penetrate the jet region and are focused by a 10 inch converging lens, and then are deflected by a second set of Ronchi Rulings. The second Ronchi Rulings were created by placing Kodak Ektapan[®] 8" x 10" black and white photographic paper at the location of the second Rulings and exposing it to the image created by the first set of Rulings for one second duration under very low intensity white light in a blacked-out room. The resultant film was over developed by two extra minutes in addition to the required ten minutes in Kodak Microdol-X[®] film developer so as to obtain very dark fringe patterns.

The second set of fringes is aligned with the first set of fringes such that an interference image of moire patterns disappears. The final plane image within the flow appears on a cardboard viewing screen behind the second Ronchi Ruling or on ground glass from Edmund Scientific to enable recording of the flow by camera.

The entire system is fixed with respect to the jet nozzle except for the viewing screen which is required to move in a linear fashion so as to allow focusing of various planes within the flow. As well, the entire system is painted black to prevent stray light reflection and it rests on a sturdy steel frame to prevent bending of the optical path because the resulting interference pattern is sensitive to shifts in both Ronchi Rulings. The entire set-up was shielded from exterior light with black curtains.

Recording of the images on the ground glass screen was done by an ELMO[®] SE 301 black & white CCD TV Camera connected to a Panasonic[®] TL AG 6750 Super VHS Video Cassette Recorder and Panasonic[®] CT 2010-Y Color Video Monitor. Still black and white images were taken by a Pentax[®] Stopmatic F 35mm Camera with a Vivitar[®] 1:4.5 macro focusing zoom lens and a Nikon[®] F4S 35mm Camera with Vivitar[®] 1:4.5 macro focusing zoom lens on Kodak[®] TMAX 100 ASA and TMAX 400 ASA film. The overall sharpness of the image on film is limited due to diffraction effect and lower speed films are preferable because they have a finer grain. Final prints were developed using Kodak Polycontrast III[®] RC black and white photographic paper with 3.0 color filters and Ilford 5.1M black and white photographic paper.

Results and Discussion

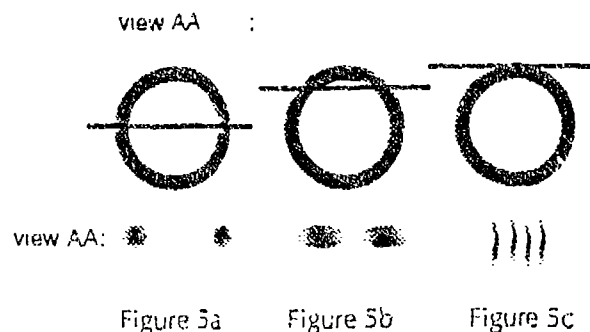
The principle focusing lens should be achromatic or employ green or yellow-orange color filters to correct

color distortions. The lens aperture should be large enough to obtain a shorter depth of focus and at the same time should have a short focal length in order to minimize the size of the entire system. A depth of focus between $1/4$ and $1/10$ of an inch was obtained. The jet region visualized was between 2 and 6 inches deep, therefore, planes occupying no more than five percent of the volume of interest could be individually visualized. Initially, an achromatic 12 inch focal length converging lens of smaller aperture than the 10 inch focal length lens created a poor depth of focus between $1/2$ and $1/4$ of an inch deep. If the lens aperture is too large it may be stopped down with an iris diaphragm.

The system was indifferent to the type of light source—both continuous rectangular white light and strobed square light sources were employed. An image formed as long as any light source was placed in the same fixed position. The intensity of the light source can be diminished with optical density filters.¹⁰

The lining up and fine adjustment of the fringe patterns was very important towards obtaining an acceptable image. It was found that 25 lines per inch was the highest ruling density that yielded the best images. A word of caution must be included about the creation of the second set of fringes: they must be properly archived by being run through film developing fixer and a water bath twice, respectively. Weinstein has developed a simple scaling rule to determine the number of fringes, (number of lines per inch on fringe) x (distance of image grid to final image in inches) ≥ 100 .¹⁰

Observations of the flow clearly revealed vortices when imaging plane cuts through the center of the jet. Otherwise, focusing at other cross-sections jet permits visualizations of vortical structures at non-perpendicular angles and the images become unrecognizable. See figures 5a and 5b. However, focusing on cross-sections near the jet edge faintly revealed streamwise vortical structures. See figure 5c.



Videotape of the flow was digitized by ImageLab[®] software and hardware on a UNIPAC[®] 386 PC micro-computer, processed on an Apple Macintosh[®] IIx microcomputer using Soyglass Transform[®] software, enhanced with Silicon Beach Digital Darkroom[®] software and printed by an Apple Laserwriter[®] IINT Post-script[®] laser printer. See Appendix A.

One of the shortcomings associated with this system is that the size of the final image is geometrically distorted. As one focuses different planes by moving the viewing screen further away from the object, the resultant image grows linearly. See figure 6.

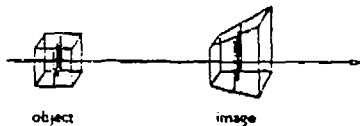


Figure 6. Image Distortion.

Single picture and video photography required that the image be recorded from behind a plate of ground glass. Super-VHS is a good video storage format because of its high-resolution, especially for digital image processing. In addition, single shot pictures required triggering of a single-flash stroboscope immediately following the opening of the camera shutter for the duration of half a second. The image cannot be directly recorded by a CCD camera, but it may be by placing 4" by 5" sheet film held in a lens-less camera at the desired focal plane of the image. The system could be improved upon by the addition of a commercially available optical bench to insure a more stable light path.

Conclusions

Focusing Schlieren yields more qualitative as well as quantitative data than conventional schlieren and shadowgraph methods. Focusing Schlieren method is a non-intrusive flow visualization method that works very well—better than conventional schlieren or shadowgraph techniques which integrate intensity along the entire light path. Conventional schlieren or shadowgraphy is only useful in flows having translational symmetry. This is why the simple layout of two-dimensional mixing layers has been the preferred choice over circular or three-dimensional jets in combustion research. A two-dimensional flow facilitates the application of line-of-sight optical diagnostic techniques. Smoke-wire techniques visualize streaklines qualitatively, but are intrusive and thus disturb the flow. They may not clearly help identifying vortical structures in the shear layer at moderate to high velocities." Fully three-dimensional turbulent flow fields can be visualized tomographically, but this is a complicated and time-consuming process. It is apparent that Focusing Schlieren will permit visual investigation of three-dimensional, and hence more realistic, flow field.

The Focusing Schlieren method also requires a smaller optical set-up than conventional schlieren or shadowgraph due to its direct light path which does not require mirrors. However, a very good quality lens is a necessity making the system more expensive. Overall, Focusing Schlieren is a more difficult system to set-up.

In the future, Super-VHS videotape images will be processed on an Apple[®] Macintosh IIx workstation or a Sun[®] 3/160 workstation driving a Gould[®] IP9515 image processor. Image frames will be digitized to display and analyze contours of constant temperature; to enhance and contrast flow structures from the background; to detect edges; smoothen and reduce noise; create graphs; and compute radiance. The fractal dimension of inhomogeneous flow could be estimated from digitized images as described by Gutmark et al.¹² Finally, Focusing Schlieren can be expanded into an elaborate three-dimensional holographic diagnostic facility.⁹

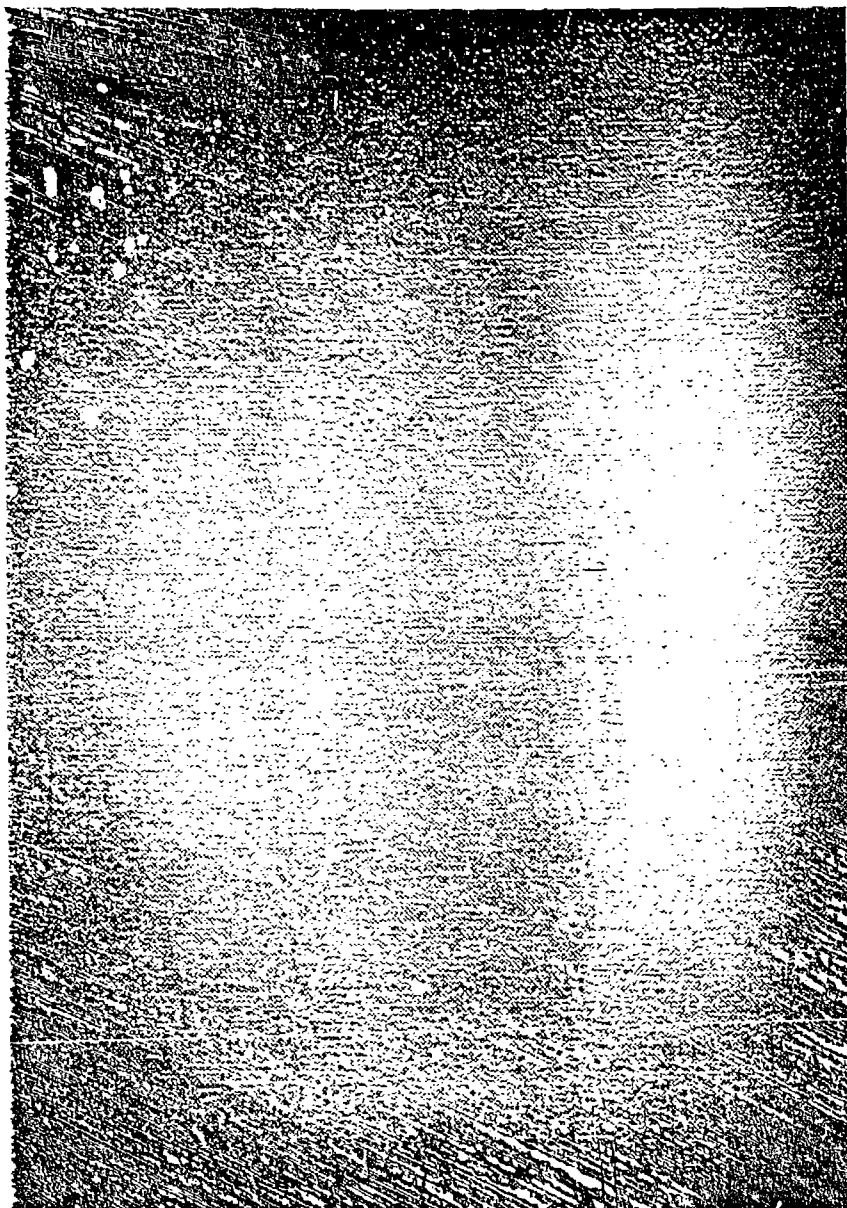
Acknowledgements

The authors benefitted from discussions of this subject with Dr. Leonard Weinstein. This work was funded by A.F.O.S.R. under contract 90-0301 and N.A.S.A. Langley contract NAG-1-1096

References

1. Miles V. Klein, *Optics* (John Wiley & Sons, New York, 1970).
2. Smithsonian Physical Tables, Washington D.C., 1954.
3. H. Liepmann, A. Roshko, *Elements of Gasdynamics* (John Wiley & Sons, New York, 1957), pp. 157-162.
4. M. S. Uberoi, L. S. Kovaszny "Analysis of Turbulent Density Fluctuations by the Shadow Method," *Journal of Applied Physics* Vol. 26, No. 1, pp. 19-24.
5. J. Hermanson, P. Dimotakis "Effects of heat release in a turbulent, reacting shear layer" *Journal of Fluid Mechanics*, 1989, Vol. 199, pp. 333-375.
6. Ralph Burton, Nov. 1949, "A Modified Schlieren Apparatus for Large Areas of Field," *Journal of the Optical Society of America*, Vol. 39, No. 11, pp. 907-908.
7. Arthur Kantrowitz, Robert Trimpf, May 1950, "A Sharp Focusing Schlieren System," *Journal of the Aeronautical Sciences*, Vol. 17, No. 5, pp. 311-319.
8. R. Buzzard, "Description of Three-Dimensional Schlieren System," *Proceedings of the 8th International Congress on High-Speed Photography*, Stockholm, Sweden, June 1968, 69V-10814 edited by N. Robert Nilsson & Lars Högberg, pp. 19-24.
9. Leonard Weinstein, June 1989, "Improved Version of a Focusing Schlieren System," Program Status: Viscous Flow Branch. NASA Langley Research Center.
10. Leonard Weinstein, August 8, 1990, Private communication.
- 11 P. Strykowski, D. Niccum, 1990. "The Stability of Countercurrent Mixing Layer in Circular Jets," submitted to *Journal of Fluid Mechanics*.
12. E. Gutmark, D. Parr, T. Parr, K. Schadow, 1990, "Fractal Behavior of a Wrinkled Annular Diffusion Flame," *Combustion and Flame*, 79, pp.7-30.

Appendix A. Digitized images.



2025 RELEASE UNDER E.O. 14176

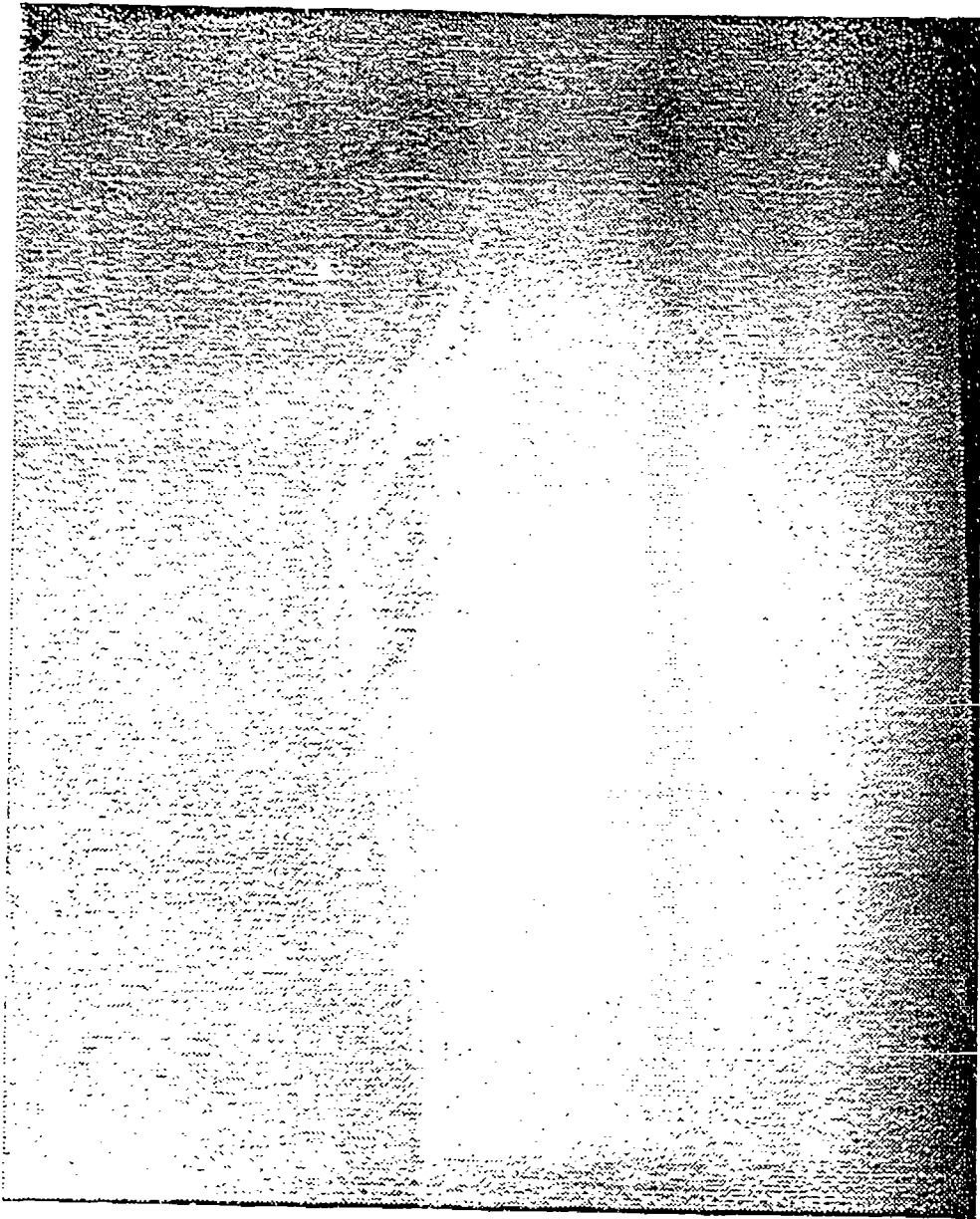
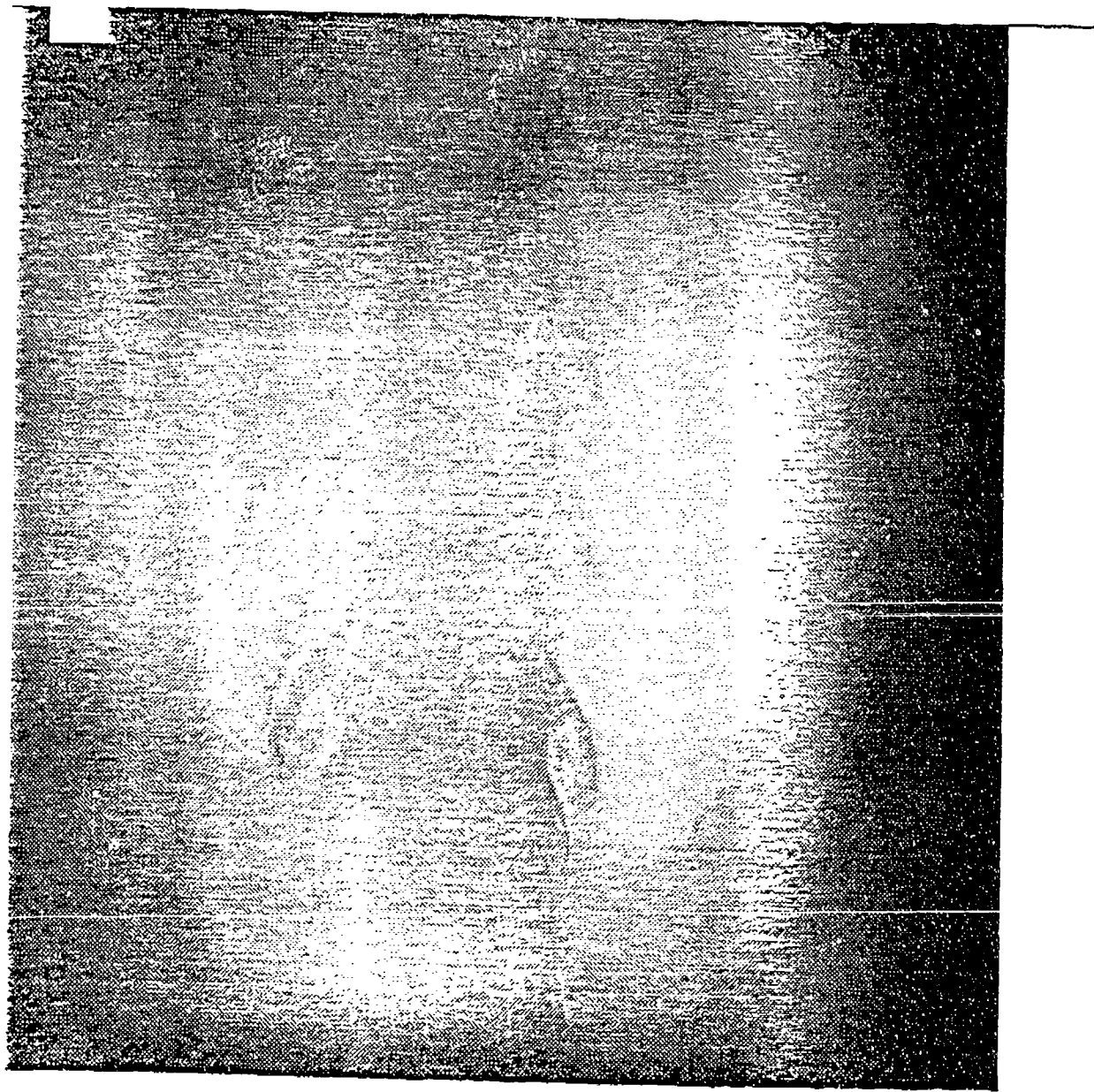


Illustration of Elliptic Jet Minor Axis



... of the ...

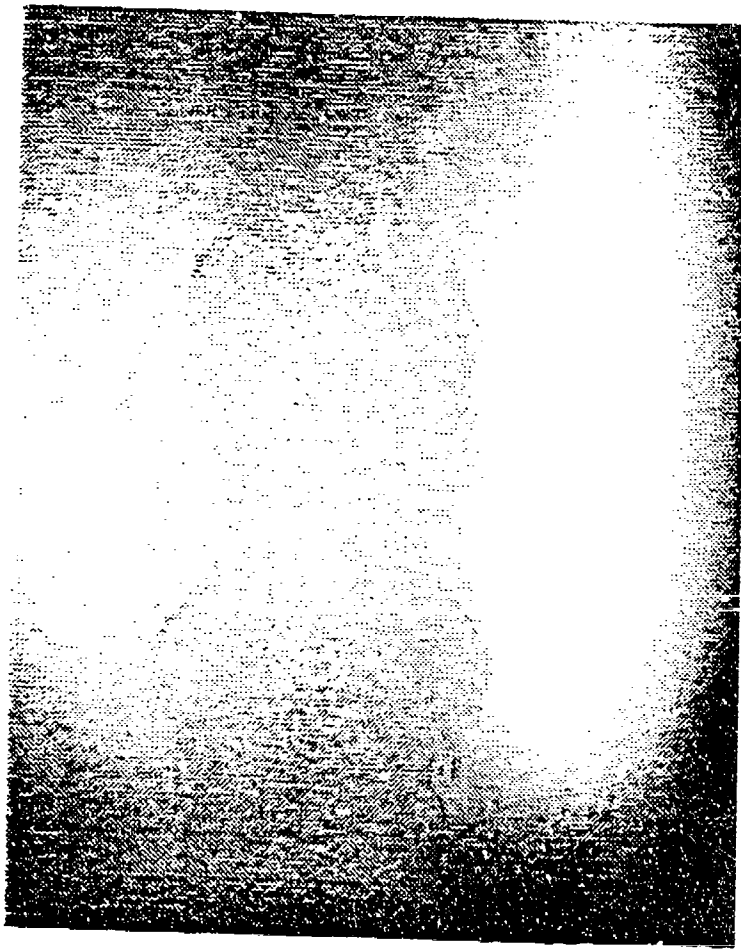
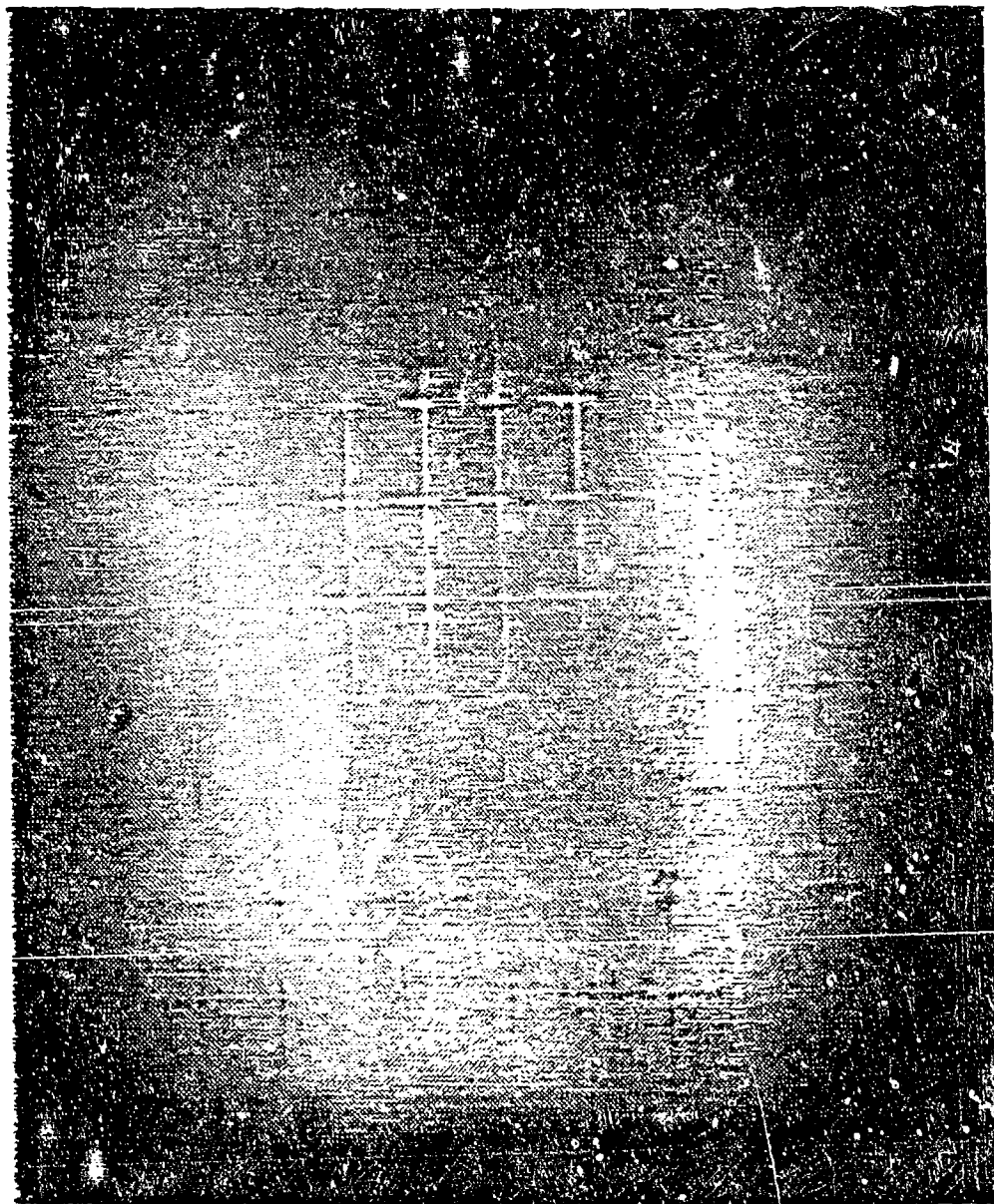


Illustration 4 - Jet Minor Axis



1950



AIAA 92-0537
CONTROLLED ENTRAINMENT IN A
2:1 ASPECT-RATIO SUBSONIC ELLIPTIC NOZZLE

T. Austin and C.M. Ho
University of Southern California,
Department of Aerospace Engineering
Los Angeles, CA

30th Aerospace Sciences
Meeting & Exhibit
January 6-9, 1992 / Reno, NV

CONTROLLED ENTRAINMENT IN A 2:1 ASPECT-RATIO SUBSONIC ELLIPTIC NOZZLE

Thomas R. Austin[†] and Chih-Ming Ho[‡]

Abstract

Large-scale and small-scale mixing processes in subsonic turbulent jet flows have been passively enhanced by the application of small aspect-ratio elliptic nozzle geometry and actively enhanced by the application of *Preferred Mode* forcing. The evolution of the asymmetrically deforming coherent elliptic vortices is responsible for large-scale mixing in asymmetric jets thereby significantly enhancing the rate of entrainment by means of the *self-induction* process. The effects of the self-induction mechanism are strongly enhanced at lower Reynolds numbers and higher temperatures. Therefore, jet spreading and entrainment are controllable by varying the exit velocity and temperature. Small-scale production occurs within the toroidal vortices principally due to self-induction unlike two-dimensional free shear layers where small scales arise through the action of *vortex merging*. The vortex merging process was suppressed by forcing the elliptic jet at the exit at the Preferred Mode frequency effectively isolating the influence of self-induction. Small-scale structures were successfully detected by processing turbulent fluctuating velocity signals with the *Peak-Valley-Code* algorithm. Preferred Mode forcing enhanced the large-scale self-induction processes and modified the small-scale mixing process but did not alter the characteristics of the small scales.

1. Introduction

The study of turbulent jet shear flow plays an important role in numerous engineering applications. Jets form due to flow issuing from a nozzle and the resultant velocity difference forms a shear layer consisting of coherent vortical structures whose dynamics are responsible for entraining surrounding fluid. Free and confined jets are common devices present in mixing processes and the production of thrust. It is therefore desirable to control mixing, or the transfer of mass, heat and momentum. Successive interactions among large scales produce smaller scales which in turn give rise towards finer mixing and initiate any possible chemical reactions at the molecular level. When heat is released in a chemically reacting turbulent shear layer the resulting flow is characterized by a nonconstant density field whose imposed nonhomogeneity couples the effects of fluid

dynamics to chemistry. It is important to understand the directly coupled effects that turbulent shear flows and combustion processes have upon each other. Therefore, to control and to improve turbulent mixing rates, and combustion properties in particular, one needs to passively, if not actively, direct the developmental processes of large- and small-scale structures in free shear flows.

1.1 The Structure of Turbulence

Turbulent shear flows are now known to be composed of structures of varying dimension and are characterized by a specific phase coherency.¹ The process of turbulent mixing begins with the entrainment of ambient fluid into the flow by either merging or self-inducing large-scale vortices. In plane mixing layers² and axisymmetric jet flows³ the dynamics of vortex merging is responsible for the growth of the turbulent shear layer in both homogeneous flows and chemically reacting mixing layers.⁴ However, in the three-dimensional flow fields characteristic of elliptic jets a second mechanism caused by the self-induction motions of the azimuthally deformed elliptic vortices controls large-scale mixing.

Successive interactions among the energetic, coherent spanwise (or toroidal) and streamwise large-scale structures, respectively, instigate the production of smaller, three-dimensional scales within the cores of the vortices coinciding with the turbulent transition region.⁵ The onset of small scales convolutes the topology of the large scales increasing their interfacial surface area. The engulfed material is broken down into smaller homogeneous parcels and the process concludes at scales below the Kolmogorov microscale where molecular diffusion smears out remaining velocity gradients and chemical processes may be initiated. The most probable length scale of the small structures lies between the Kolmogorov microscale and the Taylor microscale and this small scale appears to be responsible for dissipating most of the kinetic energy of the mean flow into heat thereby steering the mixing process towards completion.⁶ Products of chemical reactions appear to concentrate within the large scales and in particular among the small-scale regions.⁷ Planar laser induced fluorescence flow visualization of hydroxyl concentrations supports this view by revealing the existence of combustion products within vortex

[†] Research Assistant, AIAA Member, University of Southern California, Department of Aerospace Engineering, Los Angeles, CA 90089

[‡] Professor, AIAA Member, University of California Los Angeles, Mechanical, Aerospace and Nuclear Engineering Department, Los Angeles, CA 90024

cores.³ Therefore, small scale concentrations appear to overlap zones of combustion in reacting shear layers and increased small-scale production increases fine-mixing which enhances combustion.

1.2 Elliptic Jets

A *passive* method of enhancing the rate of entrainment by as much as 500% in subsonic open nozzle flows has been obtained by modifying circular nozzle geometry to a 2:1 aspect-ratio ellipse.⁹ (figure 1) This design offers a passive mixing control device and, more importantly, it is more efficient than either a conventional two-dimensional or axisymmetric nozzle. Small aspect-ratio elliptic nozzles have exhibited significantly higher spreading and entrainment rates providing improved large-scale mixing properties. Self-induction is responsible for the elliptic jet's large rate of entrainment, and its effect upon the mean flow is evident in the constant velocity contours at downstream jet cross-sections. (figure 2) This concept has been successfully demonstrated at both subsonic⁹ and supersonic conditions,¹¹ in a confined dump combustor,¹² and in high-temperature ramjet facilities yielding increased combustion efficiency.¹³

Toroidal elliptic vortices are shed at the elliptic nozzle exit. They are characterized by varying radii of curvature such that the section of the ring in the major axis plane with minimum radius of curvature is convected faster downstream by nature of the Biot-Savart Law of induction than the minor axis section with maximum radius of curvature. The faster moving section of the major axis section convects forward as it bends inward decreasing its local radius of curvature until it matches the radius of curvature of the minor axis section which is concurrently advancing outwards. This process of self-induction is the principle mechanism driving entrainment in a small aspect-ratio elliptic jet as revealed by measurements evidencing as much as ten times more entrainment in the minor axis region than the major axis region of a 2:1 aspect-ratio elliptic jet. The phenomenon of *axis switching* occurs when the initially elliptic ring momentarily sustains a circular configuration following a series of downstream distortions. These dynamics which are unique to three-dimensional nozzles dramatically enhance spreading and mixing in small aspect-ratio elliptic jet flows.

Operation of hypersonic aerospace vehicles, including the United States National Aerospace Plane and vehicles similar to it, will require supersonic mixing inside scramjet combustors. Potential benefits arising from the application of elliptic shaped nozzles include, improved combustion efficiency; the alleviation of combustion instability; subsonic and supersonic exhaust noise reduction; vectored thrust for increased aircraft agility; thrust augmentation ejectors for Vertical/Short Takeoff or Landing aircraft; turbofan engine infrared signature reduction contributing towards stealth;¹⁴ laser ejector pumps; and improved steam ejectors in heat-actuated heat pumps.¹⁵

The importance of understanding the role of the

smaller structures in mixing processes motivates our current research and their generation by large-scale vortices. In two-dimensional flows, including plane mixing layers and axisymmetric jets, the process of vortex merging is responsible for large scale growth, entrainment and small-scale production. However, in three-dimensional flow fields vortex self-induction dominates entrainment. In this light the effect of large-scale self-induction on the generation of small scales in elliptic jets is investigated for the purpose of controlling entrainment as well as small-scale mixing.

II. Experimental Procedure

II.1 Jet Facility:

The experimental subsonic jet facility is driven by multiple centrifugal blowers in parallel and operates at a maximum exit velocity of 85 m/s bordering at the upper limit of incompressibility. The flow enters an anechoically treated cylindrical chamber, contracts into an aluminum stagnation chamber of constant diameter and passes through aluminum honeycomb, aluminum foam, and a series of fine wire mesh screens where the flow field becomes more uniform and less turbulent. An aluminum composite nozzle smoothly contracts to a 2:1 aspect-ratio elliptical orifice with dimensions of 2" (major axis, 2a) by 1" (minor axis, 2b). (see figure 3).

A small azimuthally symmetric forcing chamber is machined into the nozzle exit permitting complete circumferential acoustic forcing of the initial shear layer. Four Realistic '13' speakers with a response range of 100-15,000 Hz emit at opposite ends of the major and minor axes, respectively, at the nozzle exit to perturb the flow. The speakers are powered by a pair of two-channel Carver M-200t 120W per channel power amplifiers. The output is synthesized by either a B&K function generator which sends continuous sinewaves, a simple arbitrary waveform transmitted by an RC Electronics Waveform Generator or a more complicated high-frequency waveform sent via a 12-channel Data Translation DT-2314 digital-to-analog converter. The acoustic field generated by the azimuthally positioned speakers was uniform across the nozzle exit to within 5% of the RMS pressure levels measured by a microphone at the exit.

The flow field of the elliptic jet is highly three-dimensional and is mapped out by investigating one quadrant of downstream cross-sections after performing symmetry checks. Sampling along the major and minor axes provides mean and fluctuating profiles of velocity or temperature with hot-wire and cold-wire anemometers, respectively. The velocity profiles indicate jet halfwidth spreading rates and axis switching locations. The entrainment is measured by sampling velocity and temperature across 25 by 25 grid points separated by Δx and Δy within a cross-section. The total amount of

massflow is the summation of the product of density, velocity and incremental area, $\Delta x \Delta y$. The results are verified by insuring the total momentum flux, $\sum_i \bar{p}_i(y,z) \bar{U}_i^2(y,z) \Delta y \Delta z$, is constant at the respective cross-sections. Two flow parameters, the Reynolds numbers, $Re_{D_h} = 3 \times 10^4$ and the Richardson number at maximum exit temperature, $Ri = g D_h (1-\Gamma) / (\Gamma U^2) = 10^{-3}$; where the density ratio, $\Gamma = \rho/\rho_a$ and D_h denotes the hydraulic diameter $4AP = (\pi ab) / (2\pi[(a^2-b^2)/2]^{1/2})$, clearly demonstrate the dominance of inertial forces over both viscous and buoyancy forces in the experiment.

For small scale investigations, turbulent velocity signals containing the signatures of the large and small scales in the shear layer as well as the irrotational fluctuations induced into the quiescent fluid by the passage of the large scales are sampled by two Dantec 55P71 hot-wire probes connected to a constant-temperature circuit with a flat frequency response to 30 kHz. The sensor consists of a 0.0001" diameter platinum-10% rhodium wire attached to 0.7 mm wide probes mounted on a microcomputer controlled traverse system translatable in three-dimensions. Hence, small scales larger than the probe separation with frequencies smaller than the operating range of the hot-wire circuit are resolvable. This places an effective upper limit of 55 m/s at the exit upon the operation of the facility. The fluctuating data is digitized, recorded and analyzed by a 80386 PC AT microcomputer-controlled analog-digital converter at acquisition rates up to 1 MHz. The fast-fourier transform implementing Welch's 4-point algorithm calculates the one-dimensional energy spectra from which peak frequencies of the appropriate fluid structures may be inferred. Streamwise velocity fluctuations are measured and analyzed by phase-averaging and Peak-Valley-Counting methods. Final processing is performed on a Macintosh IIx workstation.

II.2 Peak Valley-Counting Method

Measurements of longitudinal velocity fluctuations are undertaken throughout cross-sectional cuts orthogonal to the mean flow at varying distances downstream. Every data time record contained at least 15,000 small scales and 2,000 large scale structures to insure statistical reliability. The velocity traces contain low-frequency fluctuations caused by the large-scale structures and higher frequency fluctuations some of which are due to the presence of small scales. Phase-averaged data from the second hot-wire provides local large-scale statistics allowing for the purposes of conditional averaging. The Peak-Valley-Counting method developed by Huang¹⁶ and Hsiao¹⁷ and improved by Zohar⁶ was used to detect the small-scale structures. This algorithm generates a pulse train corresponding to the proper local extrema associated with small-scale fluctuations in a turbulent velocity signal by employing a series of logical conditions. The final locations of the actual small-scale fluctuations are obtained by discriminating among the 'peaks' and

'valleys' of the time signal which includes the removal of false fluctuations, erroneous consecutive maxima (or minima), analog-digital-converter noise components and random high-frequency noise by incorporating specific amplitude and temporal threshold levels throughout the five stages of the algorithm.

III. Experimental Results

III.1 Self-Induction Dynamics

Measurements have been carried out in the steady state flow of a homogeneous 2:1 aspect-ratio elliptic jet and have confirmed the findings of Ho & Gutmark (1987) verifying the elliptic jet to have increased mixing qualities over an axisymmetric jet. The addition of heat further intensifies the spreading and mixing characteristics of the elliptic jet. The experiments were performed on the same facility employing elliptic and axisymmetric nozzles of equal exit areas and operating at equal exit massflow rates thereby removing any potential bias. The parameter space of the current study included subsonic velocities from 20 m/s to 85 m/s and temperatures ranging from the ambient to 220° C.

The velocity profiles emerge at the exit with a top-hat profile and evolve into bell-shaped profiles downstream resembling asymmetric and axisymmetric jets in general. The spreading of the flow is different between the major and minor axes. At low velocities the shear layer in the minor axis region expands by spreading out into the ambient region as evidenced by the increasing velocity profiles. Velocity contour plots clearly indicate larger spread rates in the minor axis direction and illustrate a nearly circular mean velocity distribution between four and eight semi-major axis lengths downstream. (figure 4) The velocity halfwidths emphasize the linear growth of the minor axis region and indicate an unchanging state of affairs in the major axis region. The first axis switching location is evident in the neighborhood of $x/a = 7$. Downstream of the first eight semi-major axis lengths both regions grow at a nearly equivalent linear rate. At higher exit velocities the differences between the respective spreading rates become less pronounced as corroborated by the velocity halfwidths showing the minor axis region to be spreading only slightly more than the major axis region. The location of the first axis switching location depends upon the jet exit velocity (or exit Reynolds number). Centerline mean velocity plots show velocity to remain constant up to five semi-major lengths confirming the length of the potential core to be in agreement with conventional jet properties.

Temperature was increased inside the facility to investigate nonhomogeneous effects on the development of an elliptic jet. Heating the elliptic jet moderately enhanced the spreading rates by modifying the self-induction dynamics and the velocity profiles indicated an inner growth in the major axis region of the shear

layer and an outer growth in the minor axis region similar to the homogeneous low-speed case. The corresponding velocity halfwidths point out that the location of axis switching for a heated elliptic jet with the exit velocity kept constant is shifted upstream to $x/a = 5.7$. (figure 5) The spreading characteristics of higher velocity elliptic jets indicate the location of axis switching to scale with the exit Reynolds number, and nonhomogeneous density effects suggest an inverse dependency upon the density ratio, Γ . A good fit results when the axis switching location is plotted versus Re_{D_e}/Γ . Nonhomogeneous centerline mean velocities are virtually identical to their homogeneous counterparts and the length of the potential core remains unchanged.

Turbulence transports heat similarly as it transports momentum. Heat diffuses more rapidly than momentum due to a larger turbulent diffusivity of heat than momentum. Subsequently, the mean temperature distributions, albeit broader and flatter, closely resemble the mean velocity distributions and, hence, a universal behavior of mean quantities exists throughout the jet. In the case of the elliptic jet, the mean temperature profiles mimic mean velocity profiles as they grow inward along the major axis and grow outward in the minor axis region. A temperature halfwidth may be measured like its velocity counterpart, and the location where the major and minor axes regions have equal halfwidths occurs upstream from the axis switching location at $x/a = 4$. It appears that the spreading rate in the elliptic jet's minor axis is retarded at higher exit velocities (or Reynolds number) and on the other hand is enhanced by higher exit temperatures (or lower density ratios). This pattern is exhibited by the mean velocity contours for a high velocity (85 m/s) and high temperature (185 C) flow field where similar growth is apparent in the major and minor axes regions as for the low-speed homogeneous case.

The primary purpose of investigating the elliptic jet is to measure the mass entrainment and, hence, large scale mixing. The entrainment ratio is defined as the ratio of the local massflow at a cross-section to the massflow at the nozzle exit normalized with respect to the exit massflow, $Q(x) = (Q(x) - Q_0)/Q_0$. The local massflow is defined as, $Q(x) = \sum_i \bar{\rho}_i(y,z) \bar{U}_i(y,z) \Delta y \Delta z$ [kg/s], and the density and velocity components are summed over all grid locations across a jet cross-section. Entrainment measurements for varying velocities in the homogeneous elliptic jet agreed with the earlier spectacular results of Ho & Gutmark (1987). The minor axis region, defined by diagonal borders set at 45° with respect to the major and minor axes, entrains at least five times more fluid than the major axis region. (figure 6) These massflow measurements add credence to the proposed entrainment mechanism by the self-induction of asymmetric vortices.

The nonhomogeneous elliptic jet entrained as much as 25% more than the homogeneous case.¹⁰ The axisymmetric nozzle also showed a small improvement in the entrainment under nonhomogeneous conditions.

Nevertheless, in the first two semi-major axis lengths the nonhomogeneous elliptic jet entrains up to six times more than a homogeneous axisymmetric jet and entrains up to three and a half times more than a nonhomogeneous axisymmetric jet. The near-field of the homogeneous and nonhomogeneous small aspect-ratio elliptic jet was found to be a region characterized by large scale mixing more intense than in an axisymmetric jet or two-dimensional jet and these findings are promising in view of the fact that this coincides with the region where combustion processes are initiated.

Constant mean temperature contours revealed the existence of temperature maxima on either side of the centerline along the major axis following $x/a = 4$ and merging into one peak beyond $x/a = 8$, in a repeatable pattern more pronounced at higher temperatures. These double peaks occur in the mixing region following the termination of the potential core where the shear layer has closed in upon itself at the centerline. Supporting evidence to this phenomena is given by contours of RMS temperature which show similarly distributed double peaks of the thermal turbulence but along the minor axis. The evolution of the turbulent temperature field downstream as shown in RMS temperature contours portrays higher intensities in the minor axis region beginning at $x/a = 3$ and become acute at $x/a = 10$.

The existence of greater thermal turbulence in the minor axis region suggests the existence of increased mixing processes engulfing more ambient fluid into the hotter inner fluid along the minor axis region. This would create cooler regions in the minor axis region and probably be responsible for the mean temperature distribution. Larger amounts of mixing are to be expected in the minor axis region where greater spreading rates and significantly larger rates of entrainment occur. Centerline mean temperatures remain constant over shorter downstream lengths at higher temperatures suggesting higher rates of mixing in inverse proportion to the density ratio. In the mixing region downstream of the end of the potential core the centerline mean temperatures are lower in the elliptic jet than an axisymmetric jet at the exit conditions of 220 C and 55 m/s perhaps indicating deeper penetrations of ambient fluid into the mixing region of the jet.

The initial momentum thickness varies with the inverse square root of the exit velocity in the same prescribed manner as axisymmetric jets. To understand the physical mechanism driving self-induction, measurements of the initial momentum thickness were performed and confirmed previous findings of the existence of a nonconstant momentum thickness about the nozzle perimeter. At low exit velocities, $U_0 = 20$ m/s, the momentum thickness in the minor axis region is one third the thickness measured in the major axis region due to a smaller radius curvature in the upstream minor axis contour of the nozzle walls inducing a larger transverse pressure gradient. At higher exit velocities the momentum thickness increases considerably in the minor

axis region and becomes nearly equivalent about the nozzle exit at $U_0 = 70$ m/s. The initial instability of the flow is modified at different Reynolds numbers. It is suggested that low exit velocities and high exit temperatures decrease the initial spatial growth rate in the minor axis section of the newly formed elliptic vortex ring⁸ thereby increasing its initial deformation and in turn vigorously enhancing the self-induction process downstream.

III.2 Small-scale Mixing

The small-scale topology of the elliptic jet was investigated at an exit velocity, $U_0 = 45$ m/s, corresponding to a Reynolds number based on hydraulic diameter of 10^5 . Two cases are considered, first the natural flow and second, the jet excited at its Preferred Mode by forcing at $f_p = 570$ Hz with an amplitude of 1.2% of the free stream mean velocity at the centerline of the jet exit. The initial momentum thickness, θ , for the unforced case is 0.12 mm corresponding to a Reynolds number based on initial momentum thickness of 10^3 , and increases to 0.33 mm under forcing.

The shear layer initially rolls-up into coherent vortices two instability wavelengths, λ_0 , downstream at the frequency corresponding to shear layer Strouhal number, $St_0 = f_0 \theta / U_0 = 0.017$ in agreement with linear instability theory.⁹ The power spectra obtained from a fast fourier transform analysis of the initial unforced flow reveals the initial frequency and its first subharmonic indicative of vortex pairing at four λ_0 downstream. (figures 7a, 7b) Preferred mode forcing effectively suppresses vortex pairing at the first instability frequency subharmonic and instead pumps energy from the mean flow to form larger coherent vortices at 570 Hz by the *collective interaction* process.²⁰ (figures 7c, 7d) Therefore, in the forced case only the effects of self-induction dictate the evolution of the flow as well as production of the small scales.

The mean centerline velocity distribution with respect to downstream distance illustrates the dramatic effect of forcing by showing a 20% reduction in the length of the *potential core* region and an overall decrease in the mean velocity in the turbulent region downstream of the core by as much as 33%. The root-mean-square velocity data shows twice as much fluctuating energy in the center of the flow in the transitional region at the end of the potential core between $x/a = 4$ to $x/a = 7$ which also coincides with the region of very large entrainment into the mean flow.

Small-scale populations in the streamwise direction for the unforced case are measured by the Peak-Valley-Counting method and reveal a similar picture similar to the plane mixing layer. The number of small scales increases sharply from the first vortex merging position at $x/\lambda_0 = 4$ to the second merging position at $x/\lambda_0 = 8$. The distribution peaks at the third merging position, $x/\lambda_0 = 16$, and gradually decreases downstream -there is no

downstream asymptotic plateau-like region. (figure 3) A plane mixing layer characterized by nonzero velocity streams supplies constant energy to the mean flow due to the constant shear imposed in the streamwise direction. A turbulent jet with zero co-flow does not receive energy beyond the exit nozzle and hence the kinetic energy of the flow field, which is imparted to the small-scale structures from the large-scale structures via an energy cascade fashion, steadily decays downstream and is dissipated into heat by the small scales.

A still unknown nonlinear secondary instability triggers production of small scales within the cores of the spanwise large scales and may be in part due to complex stretching and tilting process among the large scales. The region of transition to full turbulence appears to follow the first vortex merging and approaching completeness after the second vortex merging. Evidence of this is provided by the number of small scales per initial large scale as calculated by the Peak-Valley-Counting method, the $-5/3$ slope of the roll-off exponent of the one-dimensional energy spectrum,²¹ and increased chemical product concentration.²² Hence the location $x/a = 4$ in the elliptic jet flow was qualified for detailed investigation of the small-scale topology because it is at the third vortex merging location and is a region approaching fully turbulent conditions.

At four semimajor axis lengths downstream the small-scale population densities were mapped out over a 12 by 12 grid encompassing a spatial cross-section intersecting the entire mean flow. Following symmetry checks only one quadrant in the flow cross-section is measured. The Peak-Valley-Counting method detects and extracts spatial, temporal and velocity information associated with the small-scale structures embedded in the coherent large scales yielding population distributions, length scales and frequencies pertaining to the small-scale activity.

The mean velocity profile across the major and minor axes, respectively, at $x/a = 4$ show distortions in the profile when the flow is forced at the Preferred Mode. These distortions vary with the forcing level and one observes in general an increase in the jet width resulting in greater spreading of the flow field, in the minor axis in particular. Density plots overlaid by constant population contours of the number of small scales per local large scale show greatest concentrations of the small scales in the shear layer of the jet for both cases. (figure 9) The population distribution in the unforced case appears 'fuller' with more curvature than the forced case. In general both contour plots appear similar in shape and density strongly suggesting that self-induction dynamics govern the evolution of the elliptic jet rather than the mechanism of vortex merging. The maximum number of small scales per local large scale attains a value of 8.8 in the forced case and is 10% greater than the peak of 8.1 in the natural flow. Forcing at the frequency predicted by linear instability theory⁹ increases the coherence of the large-scale structures by phase-locking them into a more unique frequency and pattern. This would increase the capacity

of the large scale structures to contain more smaller scales as described here. It is interesting to note that for both natural and forced cases the maximum number of small scales are located in the major axis region of the shear layer rather than the minor axis. Previous measurements have shown that the minor axis region of an elliptic jet flow are characterized by larger spreading rates and consequently entrain more fluid. The Biot-Savart induction law dictates portions of the elliptic vortices in the minor axis to be expanding outward while portions in the major axis are compressed. Vortex compression may be the candidate for small-scale production. However, due to the nature of the unsteadily deforming elliptic vortices which comprise the annular shear layer other cross-sectional further measurements at upstream and downstream streamwise locations are necessary before the flow topology can be fully understood.

The volume integral of the population density contours of the total number of small-scale structures throughout the cross-section revealed that the forced case produced 25% fewer total small scales than the natural case. This finding is significant because it shows that the self-induction mechanism produces small scales. Vortex merging dictates the evolution of two-dimensional turbulent free shear layers. However, now it appears that in the case of the *forced* three-dimensional elliptic, where vortex merging is suppressed, the dynamics of vortex self-induction are responsible for generating 75% of the small-scale population. As the natural case did produce 25% more small scales than the forced case one can surmise that the strain rate produced by vortex merging is more effective in the generation of small scales than that produced by the self-induction process. To increase the production of small scales in an elliptic jet flow would therefore suggest forcing at the initial instability frequency and its related subharmonics rather than the Preferred Mode frequency thereby promoting more energetic vortex merging.

Further analysis of the small-scale populations were performed by examining slices along the major axis direction at equivalent minor axis (z/b) stations. At first glance it appears that the forced case ($f=f_p$) populations are similar if not greater than their natural ($f=0$) counterparts. Careful observation at stations within the shear layer, $z/b = 0.76$ through $z/b = 1.4$, reveal greater population levels near the core of the flow which account for the 25% larger number of small scales in the natural flow.

At every station in the measured region the Peak-Valley-Counting method builds up a statistically meaningful histogram of the number of small scales corresponding to a specific frequency associated with the fluctuations of the small scales. The small-scale frequency histograms illustrate the existence of a most probable frequency associated with the small scales and that it is constant throughout the entire cross-sectional region of the flow. In the current investigation where the $Re_D = 10^3$ the most probable frequency of the small

scales is 13,900 Hz. Previous measurements reveal the frequency to increase with Reynolds number. At the center of the flow there is little or no small-scale activity, but at increasing radially outward locations along the major axis the histogram begins to take on a recognizable shape with a discernible constant peak of the most probable small-scale frequency. Finally at towards the edge of the shear layer the small-scale frequency histograms diminish. (figures 10a, 10b) The forced case shows similar progression along the major axis with the same most probable small-scale frequency. A characteristic small-scale length can be estimated as $l_s = U/f_s = 1.6$ mm, where f_s represents the most probable small-scale frequency and convection velocity is $U_s = U_j \times 0.6$. The frequency associated with the small scales does not change under Preferred Mode forcing due to the domination of viscous forces overcoming the effects of the larger coherent structures.

IV. Conclusion

By passively changing nozzle geometry the initial conditions in three-dimensional jet nozzles profoundly alter the downstream evolution of the flow. The upstream curvature of the exit nozzle as well as the exit aspect-ratio together dictate the initial momentum thickness distribution. As a result, the initial azimuthal distribution of vorticity along the elliptical nozzle's contour strongly modifies the self-induction process. Two prominent features associated with the flow, the location of the first axis switching and mass entrainment, were found to vary significantly with exit velocity and exit temperature. The location of the first axis switching of the elliptic vortices increased downstream in direct proportion to the mean exit velocity and in inverse proportion to the mean exit temperature. Accordingly, measurements of the mass entrainment increased with higher exit temperatures and decreased with higher exit velocities. These results reaffirm the existence of a strong correlation between the dynamics of the elliptic vortex rings and their associated axis switchings with mass entrainment by the large scales verifying that the flow is driven by self-inducing elliptic vortices. Therefore, the mean velocity and temperature fields strongly affect the initial instability of the flow thereby modifying the elliptic jet's development.

The small-scale topology of a subsonic 2:1 aspect-ratio elliptic jet has been investigated by the Peak-Valley-Counting method. At an exit velocity of 45 m/s the unforced elliptic jet transitions to full turbulence at the third vortex merging. Downstream of this location energy dissipation becomes greater than the level of kinetic energy remaining in the flow. Small scales are distributed mainly within the shear layer region and exhibit a preference towards the major axis region. Acoustic forcing at the Preferred Mode effectively suppresses vortex merging and isolates the effects of

self-induction and causes greater spreading of the mean flow field. Forcing intensifies the small-scale distribution in the major axis region. Forcing created a 25% decrease in the small-scale populations but did not significantly alter the topology of the turbulent structures. Therefore, the mechanism of self-induction is more desirable than vortex merging in turbulent jet flows because it is responsible for improved large-scale mixing and appears to be the dominant mechanism in the production of small scales in the elliptic jet. These results support the encouraging reports involving elliptic nozzles over circular nozzles in chemically reacting experiments. Quantitatively, Preferred Mode forcing decreased the number of small scales by 25% thereby reducing the small-scale mixing process. The peaks of the frequency histograms throughout the entire region of interest for both natural and forced cases yielded a most probable small-scale frequency, $f_s = 13,900$ Hz, translating into a characteristic small-scale length, $\lambda_s = 1.6$ mm. Therefore the scale of fine turbulence is unchanged by forcing and it is constant at a given Reynolds number similar to the Taylor and Kolmogorov microscales.

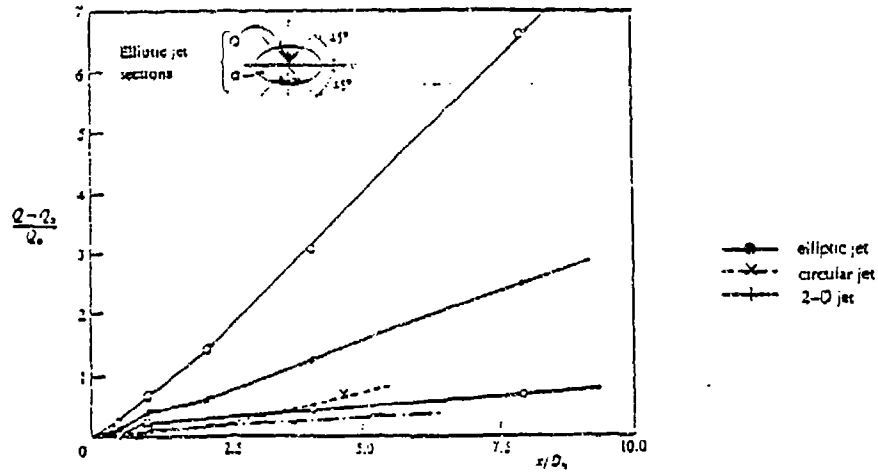
Small aspect-ratio elliptic jets appear by many accounts to be very promising improvements over axisymmetric jet configurations because of their enhanced large-scale and small-scale mixing characteristics. Coherent elliptic vortical structures which govern spreading, entrainment and large scale mixing in general have been investigated to reveal the importance of the mechanisms of vortex self-induction. Further investigation of the topology of the small-scale structures and the mechanism governing their formation by the self-interacting large-scale structures will significantly aid in the understanding of controlling and increasing production of the small scales and fine-scale mixing.

This work is supported by the Air Force Office of Scientific Research under Grant No. AFOSR-90-0301

V. References

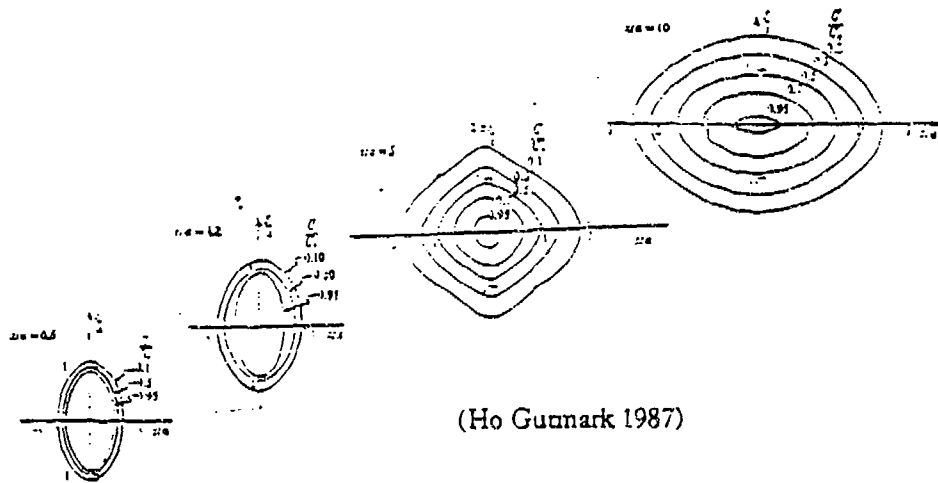
1. Ho, C. M., Huerre, P. Perturbed Free Shear Layers *Annual Review of Fluid Mechanics*, 1984, 16: 365-424.
2. Winant, C., Browand, F. Vortex pairing: the mechanism of turbulent mixing layer growth at moderate Reynolds number *Journal of Fluid Mechanics*, 1974, 63: 237-255.
3. Browand, F., Laufer, J. The Role of Large Scale Structures in the Initial Development of Circular Jets Proceedings of 4th Biennial Symposium on Turbulence in Liquids, Univ. of Missouri-Rolla, Sept. 1975: 333-344.
4. Masurani, S., Bowman, C. The structure of a chemically reacting plane mixing layer *Journal of Fluid Mechanics*, 1986, 172: 93-126.
5. Moser, R.D. & Rogers, M.M. 1991 The three-dimensional evolution of a plane mixing layer Part 2: Pairing and transition to turbulence In preparation.
6. Zohar, Y., Fine scale mixing in a free shear layer Ph.D. Thesis, University of Southern California, 1990.
7. Breidenthal, R. Structure in turbulent mixing layers and wakes using a chemical reaction *Journal of Fluid Mechanics*, 1981, 109: 1-24.
8. Gutmark, E., Parr, D., Hanson-Parr T., Schadow, K. On the Role of Large and Small-Scale Structures in Combustion Control *Combustion Science & Technology*, 1989, 66: 107-126.
9. Ho, C. M., Gutmark, E. Vortex Induction and mass entrainment in a small-aspect ratio elliptic jet *Journal of Fluid Mechanics*, 1987, 179: 383-405.
10. Austin, T., Ho, C.M. Entrainment of Asymmetric Jets A.F.O.S.R. Turbulence Research Contractor's Meeting, 1988.
11. Schadow, K., Gutmark, E. Review of Passive Shear-Flow Control Research for Improved Subsonic and Supersonic Combustion AIAA paper, 1989, 89-2736.
12. Hertzberg, J., Ho, C.M. Time averaged 3d flow in a rectangular sudden expansion AIAA paper, Jan. 1991, 91-0040.
13. Schadow, K., Wilson, K., Lee, M., Gutmark, E. Enhancement of Mixing in Ducted Rockets with Elliptic Gas-Generator Nozzles AIAA paper, 1984, 84-1260.
14. Hiley, P., Wallace, H., Booz, D. Nonaxisymmetric Nozzles Installed in Advanced Fighter Aircraft *Journal of Aircraft*, Dec. 1976, 13, no. 12: 1000-1006.
15. Jou, W., Knoke, G., Ho, C.M. Entrainment Enhancement of a Supersonic Jet for Advanced Ejectors Department of Energy Ejector Conference, 1988.
- (16) Huang, L. Small scale transition in a two-dimensional mixing layer Ph.D. Thesis, University of Southern California, 1985.
17. Hsiao, F. Small scale transition and preferred mode in an initially laminar plane jet Ph.D. Thesis University of Southern California, 1985.
18. Koshigoe, S., Ho, C.M., Tubis, A. Application of a generalized shooting method to the linear instability analysis of elliptic core jets AIAA paper, Oct. 1987, 87-2735.
19. Michalke, A. Instabilität eines kompressiblen runden Freistrahls unter Berücksichtigung des Einflusses der Strahlgrenzschichtdicke *Zeitschrift für Flugwissenschaften*, 1971, 19, no. 8/9: 319-328.
20. Ho, C. M., Huang, L. Subharmonics and vortex merging in mixing layers *Journal of Fluid Mechanics*, 1982, 119: 443-473.

21. Jimenez, J., Martinez-Val, R., Rebollo, M. On the origin and evolution of three-dimensional effects in the mixing layer Internal report DA-ERO 79- G-079, Univ. Politec., Madrid, 1979.
22. Breidenthal, R. Structure in turbulent mixing layers and wakes using a chemical reaction *Journal of Fluid Mechanics*, 1981, 109: 1-24.



(Ho Gutmark 1987)

Fig. 1. Entrainment Ratios, elliptic and circular nozzles



(Ho Gutmark 1987)

Fig. 2. Elliptic Jet $U_0 = 20$ m/s, Downstream Constant Velocity Contours

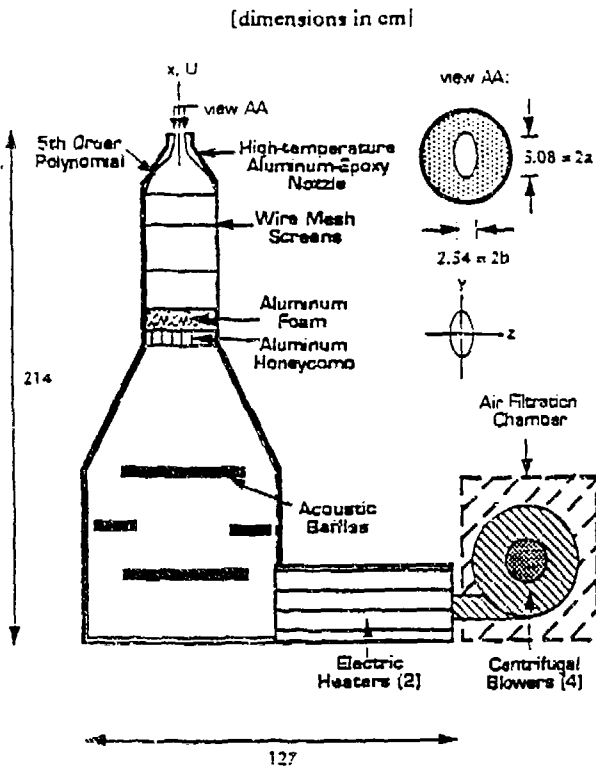


Fig. 3. Subsonic Elliptic Jet Facility

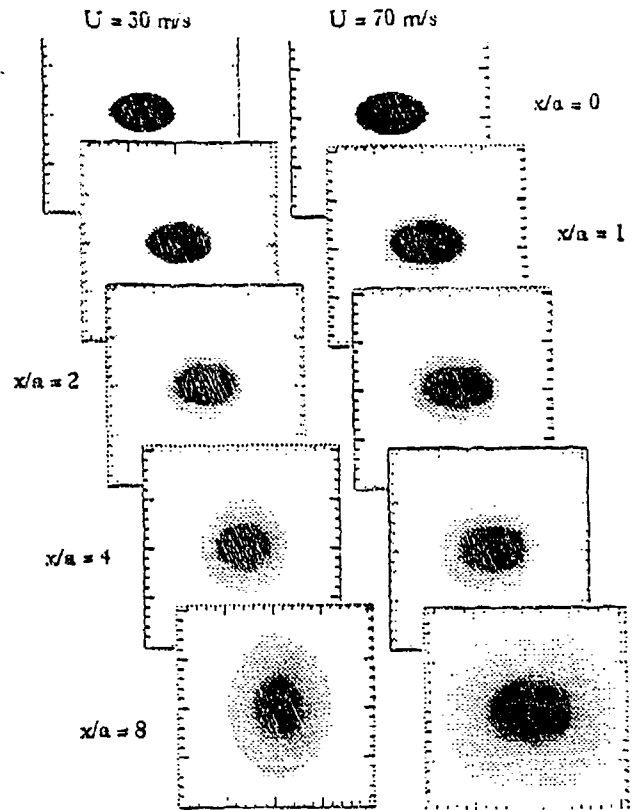


Fig. 4. Mean Exit Velocity Contours

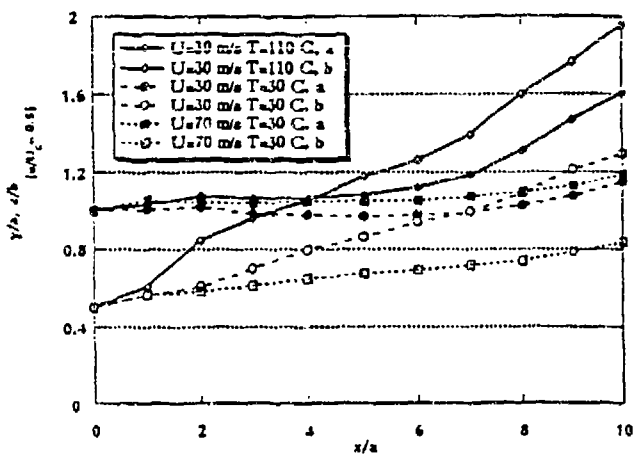


Fig. 5. First Axis Switching Location, velocity & temperature effects

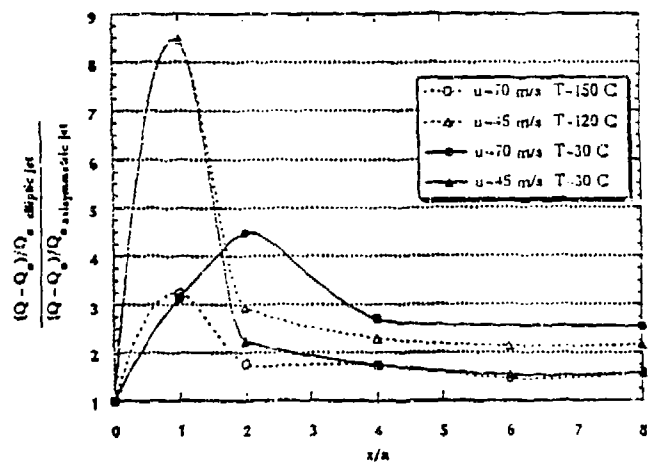


Fig. 6. Elliptic to Circular Jet Entrainment Rate Ratio

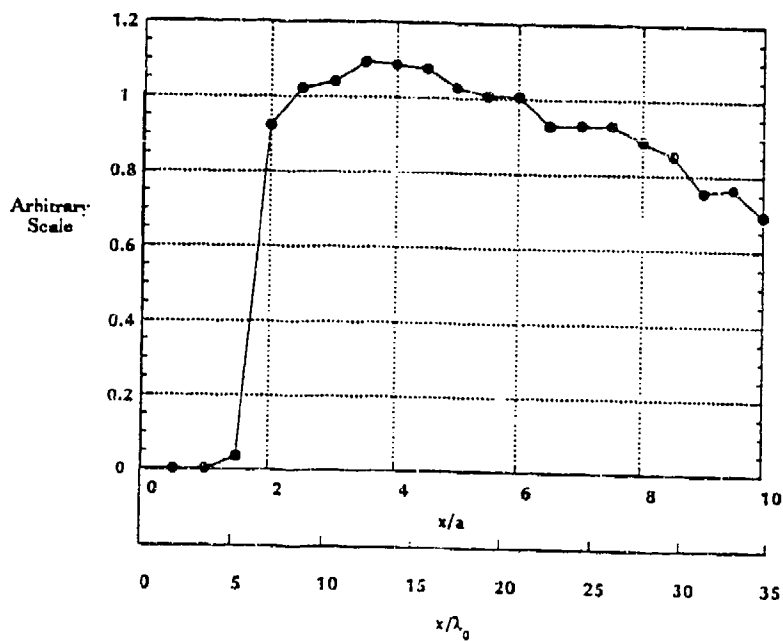
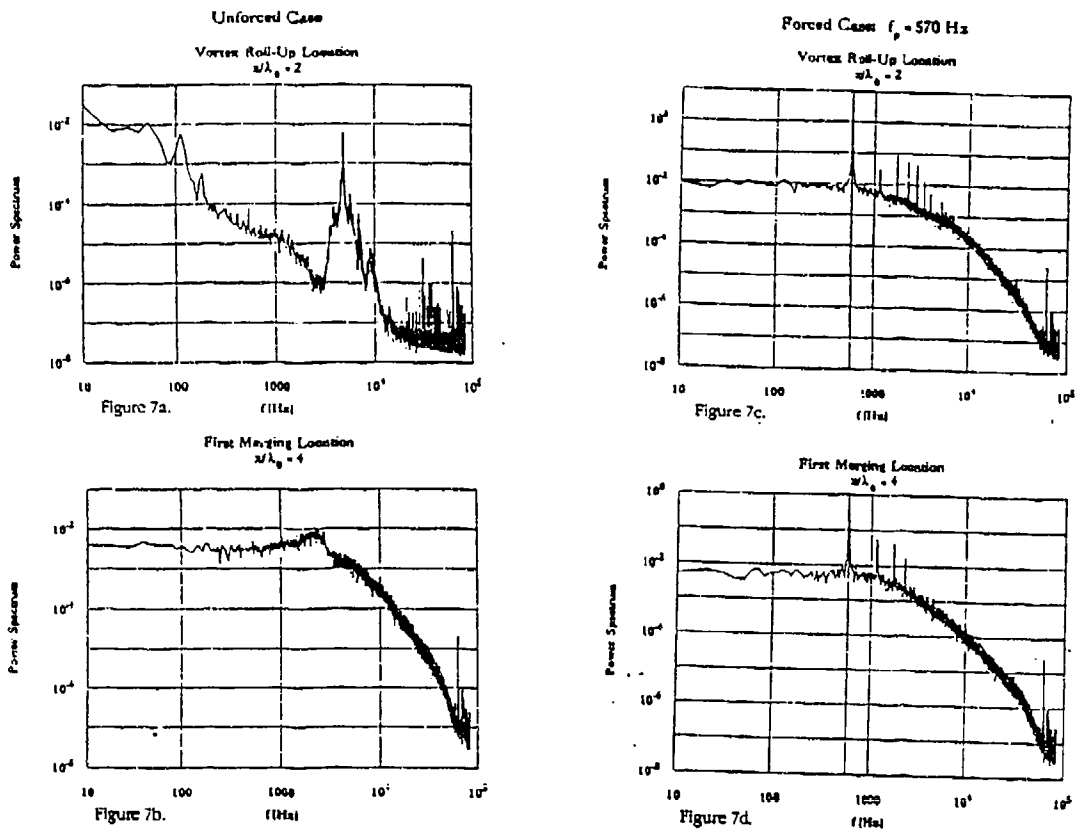


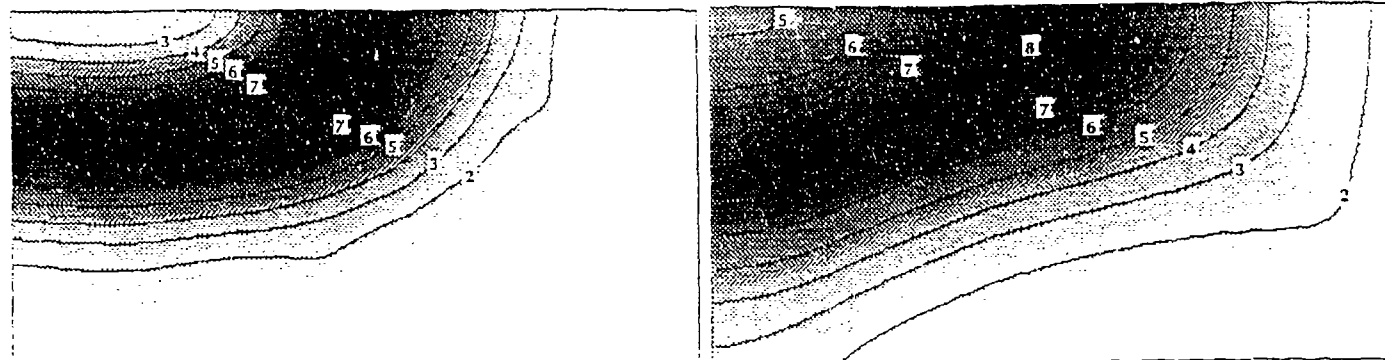
Fig. 8. Streamwise Small Scale Population, Unforced Elliptic Jet $U_0 = 45$ m/s

Unforced Case

$y/a = 1.83$

Preferred Mode forced Case

$y/a = 1.83$



2.93

$z/b = 2.93$

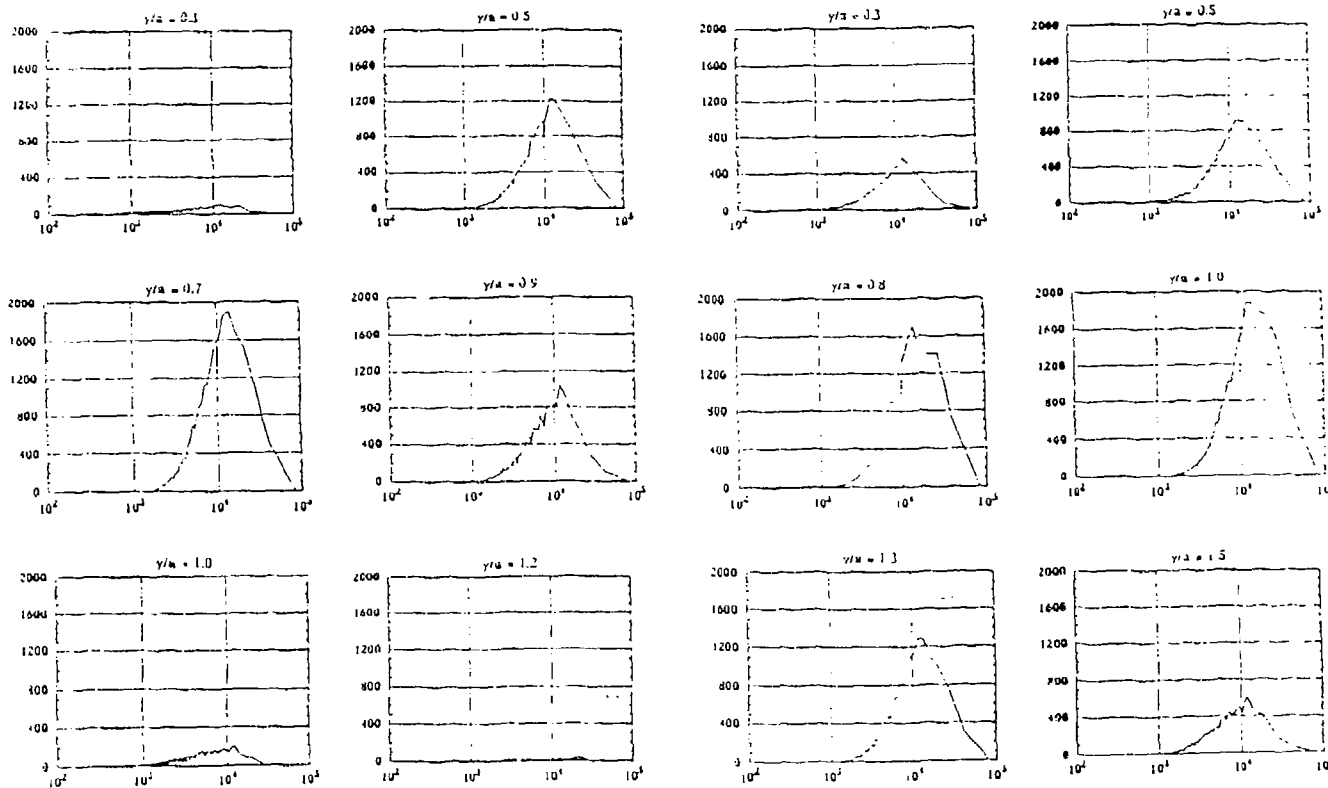
Normalized Small Scale Population per
Local Large Scale

0



21

Fig. 9. Small Scale Population Density $U_\infty = 45$ m/s, $x/a = 4$



Small-scale Frequency Histograms, $U_\infty = 45$ m/s, Major Axis

Fig. 10a. Unforced Case.

Fig. 10b. Preferred Mode Forced Case

Three-Dimensional Portraiture of a Subsonic Elliptic Jet

Thomas R. Austin

Department of Aerospace Engineering
University of Southern California
Los Angeles, CA 90089-1191
(213) 740-5320

Objective

To investigate subsonic mixing in the flow issuing from a heated 2:1 aspect-ratio elliptic nozzle. Turbulent velocity and temperature data are experimentally measured within the highly three-dimensional flowfield.

Introduction

The study of turbulent jet shear flow plays an important role in numerous engineering applications. Free and confined jets are common devices present in mixing processes and the production of thrust. It is therefore desirable to control mixing, or the transfer of mass, heat and momentum. A passive method of enhancing the rate of entrainment by as much as 500% in subsonic open nozzle flows has been obtained by modifying the nozzle geometry to a 2:1 aspect-ratio ellipse.¹ This yields a more efficient mixing control device than either a conventional two-dimensional or axisymmetric nozzle. Small aspect-ratio elliptic nozzles have exhibited significantly higher spreading and entrainment rates thereby providing improved large-scale mixing properties at both subsonic² and supersonic conditions,³ as well as in a high-temperature ramjet.⁴

Turbulent shear flows are known to be composed of structures of varying dimension and, more importantly, are characterized by phase coherency.⁵ Successive interactions among the energetic, coherent toroidal and streamwise large-scale structures, respectively, instigate the production of smaller, three-dimensional scales which in turn lead to transition towards fully turbulent flow. The importance of understanding the role of the smaller structures in mixing processes has direct applications towards improved combustion and, hence, motivates our current research. In this light, the three-dimensional portraiture is experimentally investigated in an attempt to map out the complex topology of the structure of an elliptic jet.

Visual Insight

Digitized images of streamwise slices of the flowfield reveal distorted, elliptical cross-sections of the large-scale vortices. Isocontour plots of the mean velocity and temperature fields confirm the existence of the physical phenomena of *axis switching* as well as identifying localized temperature peaks thereby providing information about the jet's evolution and mixing characteristics.

Experimental Results

Density gradients in the flowfield are visualized by means of a focusing schlieren system, recorded by conventional motion photography, digitized by a 386 PC-based Werner Frei ImageLab™ frame grabber and enhanced and analyzed with NIH Image™ and Silicon Beach Digital Darkroom® on a Macintosh® IIfx. Visualization of individual plane sections of finite depth revealed individual cross-sections of large-scale vortical structures and small-scale three dimensional turbulence in the jet. The images confirmed the *Kelvin-Helmholtz* process whereby an initially laminar jet rolls up into successive ring vortices. Observations of the flow revealed cross-sections of the large-scale vortices when imaging planar cuts through the center of the jet. The toroidal vortices are level with respect to the horizon in the major axis plane, however, when viewed from the minor axis plane they appear to be tilted at large angles with respect to each other. Quantitative measurements of the separation and size of the large-scales have been determined and were found to be in good agreement with theoretical calculations.

The mean velocity and temperature field was plotted in one-dimension with Synergy Software KaleidaGraph® and in two-dimensions with SpyGlass' Transform®, Format® and Dicer® at downstream cross-sections. Two-dimensional raster color imaging clearly illustrates the marked differences in the spreading of the flow between the major and minor axes regions. At low exit velocities the shear layer in the minor axis region expands by spreading outward into the ambient region as evidenced by the velocity contour plots indicating greater spread rates in the minor axis direction. Furthermore, a region of *axis switching* appears at low exit velocities, while at higher velocities the phenomenon is not observed and the spreading rates become less pronounced between the two axes.⁶

Adding heat to the flowfield further enhanced the already large spreading rates by modifying the self-induction dynamics of the coherent structures. This was manifested in the corresponding velocity isocontour plots for the various cases studied, whereupon the location of *axis switching* for a heated elliptic jet with the exit velocity held constant shifted upstream. At large temperatures a conspicuous temperature peak spatially bifurcates and then unites further downstream demonstrating the influence of greater mixing rates in the minor axis region.

Conclusion

2:1 aspect-ratio elliptic jets appear by many accounts to be very promising improvements over axisymmetric jet configurations because of their enhanced mixing capabilities. Coherent elliptic vortical structures which govern spreading, entrainment and large-scale mixing have been experimentally measured, visualized and analyzed with the aid of a Macintosh® to determine the mechanisms of the elliptic jet's development.

This work is supported by Air Force Office of Scientific Research grant no. 90-0301.

References

- [1] Ho, C. M., Gutmark, E. Vortex Induction and mass entrainment in a small-aspect ratio elliptic jet *Journal of Fluid Mechanics*, 1987, 179: 383-405.
- [2] Austin, T., Ho, C.M. Entrainment of Asymmetric Jets A.F.O.S.R. Turbulence Research Contractor's Meeting, 1988.
- [3] Schadow, K., Gutmark, E. Review of Passive Shear-Flow Control Research for Improved Subsonic and Supersonic Combustion AIAA paper, 1989, 89-2786.
- [4] Schadow, K., Wilson, K., Lee, M., Gutmark, E. Enhancement of Mixing in Ducted Rockets with Elliptic Gas-Generator Nozzles AIAA paper, 1984, 84-1260.
- [5] Ho, C. M., Huerre, P. Perturbed Free Shear Layers *Annual Review of Fluid Mechanics*, 1984, 16: 365-424.
- [6] Austin, T., Ho, Chih-Ming, Controlled Entrainment in a 2:1 Aspect Ratio Subsonic Elliptic Nozzle AIAA 92-0537

SMALL SCALE TOPOLOGY OF A 2:1 ASPECT-RATIO ELLIPTIC JET

Thomas R. Austin

May 1991

Department of Aerospace Engineering, University of Southern California
Supported by A.F.O.S.R.

Contents

I. INTRODUCTION	2
I.1 Free Shear Layers	2
I.2 Axisymmetric Jets	6
I.3 Three-Dimensional Jets	9
I.4 Excitation Effects	11
I.5 Small-Scale Mixing and Combustion	13
II. EXPERIMENTAL FACILITY AND TECHNIQUES	14
II.1 Jet Facility	14
II.2 Facility Modifications	15
II.3 Data Acquisition & Analysis	15
II.4 Forcing Facility	17
II.5 Optical Flow Diagnostics	17
III. CURRENT RESULTS	18
III.1 Mean Flow Field	18
III.2 Turbulent Flow Field	19
III.3 Flow Visualization	20
III.4 Forced Jet	21
III.5 Jet with Suction	21
III.6 Rectangular Orifice Jets	22
IV. PROPOSED RESEARCH	22
IV.1 Nonhomogeneous Jet	22
IV.2 Small Scale Topology	22
IV.3 Self-Induction Effects	23
IV.4 Active Control	23
V. CONCLUSION	24
BIBLIOGRAPHY	24
LIST OF FIGURES	32

I. INTRODUCTION

"Ways of improving mixing and increased spreading rate in subsonic and supersonic shear layers under study include noncircular jets."

- Panton, R., Long, L., *Aerospace America*

"Current means of reducing supersonic jet noise to meet FAR 36 Stage Three involve attempts with noncircular jets."

- Morris, P., *Aerospace America*

The study of turbulent shear flow plays an important role in numerous engineering applications. Jets are a class of unbounded shear flows that are not influenced by any physical boundary except for their orifice geometry. Jets form due to flow issuing from a nozzle and the resultant velocity difference forms a shear layer consisting of coherent structures which entrain surrounding stationary or moving fluid. The dynamics of these large scale coherent structures are chiefly responsible for jet development. In general it is desirable to control mixing, or the transfer of mass, heat and momentum, in a direction transverse to the shear layer. The earliest and simplest jets studied have been axisymmetric jets. In the search for controlled mixing of jet flows, noncircular jets, characterized by three-dimensional exit nozzles, have become recent candidates of study and they have displayed promising results. Accordingly, the large scale coherent structures have been successfully controlled by modifying initial conditions, both passively by varying exit nozzle geometry and actively with acoustic perturbations.

Turbulent mixing is a two-stage process, beginning with entrainment of ambient fluid by large scales and concluding with fine-scale mixing carried out by the small scales. The dynamics of coherent large scale toroidal rings governs large scale entrainment in jets. In particular, vortex self-induction is the principle mechanism driving entrainment in a 2:1 aspect-ratio elliptic jet. In combustion processes molecular mixing coincides with fine-scale mixing initiating exothermic chemical reactions. The investigation of small scale processes is crucial towards controlling fine-scale, or molecular, mixing and obtaining a complete understanding of mixing.

The goals of this study are to simultaneously measure both large and small scales in an incompressible subsonic jet possessing an elliptically shaped exit nozzle of 2:1 aspect-ratio. The effects of both entrainment mechanisms upon the development of small scales will be investigated. By uniformly forcing the jet with external acoustic excitation at the *Preferred Mode*, vortex pairing will be retarded thereby isolating the effects of vortex self-induction upon the shear layer. Subsequently, the contribution by self-inducting vortices to small scale production will be directly measured. Phase-averaging techniques will demarcate large scale vortices. The *Peak-Valley Counting* method combined with phase-averaging schemes will be employed to extract length and velocity gradient information of the small scales as well as their population. The *Fast Fourier Transform* algorithm will yield spectral data and the *Two-Dimensional Wavelet Transform* algorithm will be employed to simultaneously display both phase and amplitude information of structures within the flow.

APPLICATIONS

Free and confined jets are common devices present in mixing processes and the production of thrust and they have been studied theoretically, numerically and experimentally. There are numerous and immediate benefits of noncircular jet research. Operation of hypersonic aerospace vehicles, the United States National Aerospace Plane and vehicles similar to it, will require supersonic mixing inside their 'scramjet' combustors. Other benefits include, improved combustion efficiency (Schadow, Wilson, Lee & Gunmark 1984), fuel injectors inside supersonic combustors or for the alleviation of combustion instability; subsonic and supersonic exhaust noise reduction; vectored thrust for increased aircraft agility (Watts 1989); thrust augmentation ejectors for *Vertical/Short Takeoff or Landing* aircraft; the reduction of aircraft infrared signature by decreased engine exhaust temperature contributing towards *stealth*, (Hiley, Wallace & Booz 1976); laser ejector pumps; and improved steam ejectors in heat-actuated heat pumps (Jou, Knoke & Ho 1988).

1.1 Free Shear Layers

1.1.1 Foundations

The simplest free shear layer is the plane mixing layer consisting of two nearly parallel mixing streams of fluid. The flow forms at the confluence of two fluid streams far removed from the presence of solid boundaries. Solid boundaries, namely the trailing edge of an airfoil or jet exit nozzle, define the initial conditions. The velocity difference between the upper and lower streams forms a hyperbolic tangent-like velocity profile which helps create the shear layer. The profiles

are characterized by an inflection point and sizable velocity gradients whose significance to stability and turbulent energy transfer will be noted. Refer to figure 1.

The velocity ratio, R , represents the relative velocity difference between the two respective streams. Refer to Equation (1). Fractional values less than unity characterize mixing layers, jets possess values of R equal to one and velocity ratios greater than one signify the presence of reverse flows or suction. Heuristically, the shear layer spread rate, $d\theta/dx$ is proportional to R so that the velocity ratio can be viewed as a stretching parameter.

$$R = \frac{U_2 - U_1}{U_2 + U_1} = \frac{\Delta U}{2U}$$

The thickness of the shear layer at any downstream location may be represented by the momentum thickness, θ . Refer to Equation (2). This thickness decreases at higher velocities as $\theta \sim U^{-1/2}$. The initial momentum thickness will be shown to be critical towards non-dimensionalizing frequencies in stability analyses, and overall shear layer development.

Close to the trailing edge a more convenient length scale parameter is the vorticity thickness, δ . Refer to Equation (3). This scale is approximately four times the momentum thickness for a hyperbolic tangent profile, which is a good representation of the mean velocity profile in a plane mixing layer. Both length scales illustrate free shear layer growth and provide proper scaling distances for the separation between vortical structures.

$$\theta(x) = \int_{-\infty}^{\infty} \frac{U(y)}{U_{\infty}} \left(1 - \frac{U(y)}{U_{\infty}} \right) dy$$

One of the most important parameters is the Reynolds Number, $Re = U\theta/\nu$. It is a nondimensional value defining the ratio of inertial to viscous forces. Regions of self-preservation,

$$\delta = \frac{U_1 - U_2}{(\partial U(y)/\partial y)_{\max}}$$

unstable flows and transition to turbulence are marked by large Reynolds numbers. In addition, at sufficiently high Reynolds numbers the flow diverges very slowly and is primarily unidirectional or nearly parallel allowing simpler analysis. The Reynolds number classifies the 'degree' of turbulence such that as its value increases the resulting flow becomes more unstable. Large Reynolds number flow is characterized by a wide separation

of eddy length scales wherein turbulent kinetic energy cascades from larger to increasingly smaller eddies creating a *Universal equilibrium range* ($Re_{\lambda}^{3/2} \gg 1$) and at higher values ($Re_{\lambda}^{3/4} \gg 1$) the existence of an *Inertial subrange* greatly simplifies calculations by allowing isotropic conditions, where $\lambda^2 = -1/f''(0)$ is the Taylor microscale (Batchelor 1953).

Initially, mean values followed by turbulent fluctuations and eventually higher-order statistical quantities (Reynolds stresses, skewness, flatness, etc.) evolve spatially and approach a sense of uniformity whereupon each respective profile attains geometric similarity at respectively increasing locations downstream. This is the property of self-preservation and incorporates all flow parameters, velocity, temperature, stresses, correlations, etc. Ultimately, turbulent free shear layers are dissipated by very small scales converting kinetic energy in the turbulent flow into mechanical heat through the action of molecular viscosity.

In the nineteenth century, classical phenomenological theories came into acceptance coupling the assumptions of self-preservation with eddy viscosity models based upon Maxwellian statistical mechanics into the simplified Navier-Stokes Equations (Boussinesq 1877). These Boundary-Layer Equations yielded very good approximations of mean values. Early limited attempts included the Mixing Length Theory by Prandtl (1925) and the Modified Vorticity-Transport Theory by Taylor (1932) as reviewed in Tennekes & Lumley (1972). Turbulence was first considered a completely random process requiring statistical description (Monin & Yaglom 1971, 1975). Early modern experimental investigations of free shear flows were performed by Liepmann & Laufer (1947). Subsequent measurements of turbulent free shear flows included the plane jet (Bradshaw 1965), the axisymmetric jet (Wynanski & Fiedler 1969), and the plane mixing layer (Wynanski & Fiedler 1970).

Brown & Roshko (1974) confirmed the mixing layer to consist of large scale coherent structures. Concurrently, Winant & Browand (1974) showed the growth of a plane mixing layer to be due to the merging of large scale structures. Refer to figure 2. Direct numerical analyses of temporally growing mixing layers and their subsequent vortex interactions agree with experiments (Corcos & Sherman 1976; Riley & Metcalfe 1980). Ho & Huerre (1984) extensively reviewed the free shear layer.

1.1.2 Stability

Although linear in its early stages, the evolution of the mixing layer is predominantly nonlinear. Inviscid instability waves form due to the Kelvin-Helmholtz instability mechanism where small naturally occurring perturbations spontaneously arise just downstream of the trailing edge at the inflection point of the velocity profile (Drazin & Reid 1981). Free shear layers are inviscidly unstable flows shown by Rayleigh's Criteria—the existence of an inflection point in the velocity profile (Rayleigh 1880). Classical hydrodynamic stability theory has been reviewed by Lin (1955). Thus, for high Reynolds numbers free shear layer instability is due to inviscid induction effects and is stabilized by viscosity. The initial development of parallel shear flows has been studied by Betchov & Criminale (1967).

Nonlinear instabilities exponentially amplify the two-dimensional vorticity-containing structures which are composed of multiple-frequency instability waves. Any spatially coherent perturbation whose frequency is proximate to the most amplified frequency will form a dominant instability wave and its amplification rate will scale with initial conditions—the initial momentum thickness and convection velocity. Two instability wavelengths downstream of the trailing edge roll up into periodic spanwise vortices upon reaching a specific energy level. Refer to figures 3 and 4. The energy content of

the growing instability wave at a particular frequency is defined as the integral of the eigenfunctions across the mixing layer. Refer to Equation (4). The natural or most amplified frequency of the ensuing sinusoidal waves scales with a constant dimensionless frequency—the Strouhal number based on initial momentum thickness and convection velocity, $St = f_n \theta_0 / U_c = 0.017$. The wavelength of the structures is $\lambda_n = U_c / f_n$, where the convection velocity is defined as $(U_1 + U_2)/2$.

The unsteady shear layer response is modelled reasonably well by inviscid linear stability theory, and it predicts the spatial structure and the amplification rates of infinitesimally small perturbations superimposed upon a mean velocity profile. The most amplified frequency is selected according to local *spatial* stability analysis of parallel shear layers (Michalke 1965; Monkewitz & Huerre 1982). The vortex roll-up process has been numerically simulated using inviscid linear stability theory in *temporal* space (Michalke 1964). Spatial stability calculations treat wavenumbers as complex functions of real frequencies and temporal stability results are calculated with complex frequencies as functions of real wavenumbers. Measurements of amplification rates and phase velocities in mixing layers by Miksad (1972), Fiedler, Dziomba, Mensing & Rösger, (1981) and Ho & Huang (1982) agree extremely well with theory. Refer to figure 5.

$$E(f) = \int_{-\infty}^{\infty} \frac{(u'(f)/U_0)^2}{2\theta_0} dy$$

The spatial growth rate varies with Strouhal number and reveals a symmetric distribution increasing to a maximum at $St_0 = 0.017$ corresponding to the most amplified frequency or natural frequency of the initial wave and decreasing to zero at the neutral point. The phase velocity also varies with Strouhal number signifying dispersive wave action and after $St_0 = 0.017$ matches the convection velocity and the waves become non-dispersive. It is noteworthy that two amplified waves exchange energy more efficiently in non-dispersive regimes due to the fact that specific frequencies are more likely to overlap and match. Therefore a specific band of Reynolds number-dependent unstable frequencies with variable amplification exists at which a perturbed shear layer may grow spatially.

A rapidly growing subharmonic wave is generated at the neutral point where the fundamental wave has saturated, and its frequency is a subharmonic, $f_n/2$, of the natural frequency of the free shear layer (Sato 1959; Wille 1963; Browand 1966; Freymuth 1966; Miksad 1972; Ho & Huang 1982). Refer to figure 6. The fact that the stability curve for spatial growth rates in mixing layers is symmetric explains the tremendous amplification of the subharmonic frequency at the location of the neutral point. The occurrence of the subharmonic wave in the non-dispersive region is associated with the first location of vortex merging at four initial instability wavelengths downstream (Huang & Ho 1982).

Vortex merging is the process in which the induced motion of typically two and infrequently more neighboring spanwise vortices causes them to revolve about a common center-of-mass and amalgamate into a large vortex via the Biot-Savart Law (Winant & Browand 1974). It is a nonlinear process because energy is exchanged between waves of different frequencies. For pairing to occur, phase speeds and subharmonic disturbances must match between respective merging vortices (Petersen 1978; Cohen & Wygnanski 1987). Large scale structures have been numerically studied confirming the process of vortex merging (Saffman & Baker 1979).

Kelly (1967) and Monkewitz (1988) proposed a *subharmonic-resonance* model in which the subharmonic mode interacts in a weakly nonlinear fashion with the fundamental and receives energy in the process. It is the most unstable mode responsible for vortex pairing. Another provision describes the creation of a secondary instability that feeds back strengthening and amplifying the subharmonic wave. A locally new subharmonic is selected and amplified by a resonance mechanism becoming the locally most amplified wave, and the merging process is repeated downstream repeatedly at $8\lambda_n, 16\lambda_n, \dots$, albeit with some uncertainty due to phase jitter, until the respective vortices lose their coherence and breakdown. The vortices are quasi-stationary and their randomness is attributed to phase jitter due to background perturbations and varying convection velocity (Blackwelder 1987).

Gaster, Kit & Wygnanski (1985) corrected the linear stability theory allowing for a more realistic slowly-diverging shear flow. It is important to note that linear stability theory only explains local effects and amplification rates can be over predicted, Wygnanski & Petersen (1987). Since a real shear layer develops nonlinearly more accurate global results are predicted by the nonlinear instability theory which retains higher order terms (Stuart 1971; Wygnanski, Marasli & Champagne 1987).

1.1.3 Global Feedback

It is natural to expect a free shear layer to develop causally in the downstream direction. Dimotakis & Brown (1976) first suggested that large scales exert upstream influences upon their induced velocities. A global feedback mechanism hypothesizes that large scale vortices in a shear layer impose upstream influences by uniformly radiating very weak acoustic waves from merging locations. The upstream-travelling acoustic waves interact with the fundamental frequency and excite the unstable thin shear layer at the trailing edge in a resonant interaction (Laufer & Monkewitz 1980). This feedback loop explains the doubling in strength of vortex circulation at successive mergings. The associated feedback equation is defined by the distance to the j 'th merging location, x_j , where, λ_j is the subharmonic wavelength, λ_a is the acoustic wavelength and N is an integer number of waves describing ' j ' merging locations. Refer to Equation (5). The equation predicts vortex merging locations and the spreading rate in a subsonic jet (Ho & Nossair 1981, 1982).

1.1.4 Global Stability

The evolution of coherent structures has been described by propagating instability waves composed of various

frequencies. Linear hydrodynamic instability theory can be approached from a temporal or spatial point-of-view. Free shear layer experiments tend to agree with spatial calculations, however, shear layers forced periodically in time do not. Thus,



$$\frac{x_j + x_l}{\lambda_j \lambda_l} = N$$

neither approach is exact because global instabilities may amplify admitting both complex frequencies and complex wavenumbers. A combined and global spatio-temporal instability theory analyzes the dispersion relation of a given flow to determine if the system is convectively or absolutely unstable, and hence if it may be temporally or spatially calculated (Huerre &

Monkewitz 1985, 1990).

Very small amplitude disturbances for a parallel flow are assumed as in Michalke's linear hydrodynamic theory. A response in the form of a wave packet is obtained for a given initial disturbance. In convective instability all local and global modes are temporally damped such that the disturbed wave packets decay downstream with positive group velocity thereby stabilizing the flow although pressure waves may introduce upstream feedback effects (Chomaz, Huerre & Redekopp 1981). The flow is considered to be a spatial 'amplifier' of external disturbances. In absolute instability, local regions become self-excited with temporally growing oscillations but remain stationary in space such that disturbances spread both upstream and downstream contaminating and saturating the flow. Refer to figure 7. Conventional descriptions of absolutely unstable flow can not be employed, i.e. predicted merging locations. Instabilities can change locally, that is, at a particular velocity profile, from convectively to absolutely and back to convectively unstable. Therefore, local absolute instability does not necessarily imply global absolute instability. This topic will become important in the discussions regarding acoustically excited and nonhomogeneous jet flows.

1.1.5 Coherent Structures

In the fifteenth century Da Vinci recorded the earliest illustrations of vortices—the principle elements of turbulent shear layers. It is now accepted that large scale vortical structures contain most of the flow's energy—the 'energy-containing eddies' (Batchelor 1953). The Kelvin-Helmholtz mechanism distributes most of the initial vorticity downstream of the trailing edge into periodic waves which evolve into coherent structures. Coherent structures are recognizable vortices of fluid characterized by commonly aligned phase relationships that dynamically develop in space and time. Coherent large scale structures may be thought of as an evolving vorticity field in space (Ho & Huerre 1984). They are the *de facto* building blocks constituting turbulent free shear layer flow by being responsible for the transport of momentum, mass and heat. The recognition of quasi-deterministic structures dominating the free shear layer by Brown & Roshko (1974) and Winant & Browand (1974) heralded one of the biggest advances in the study of turbulent shear flows.

Inviscid, coherent spanwise structures of the order of the width of the ensuing flowfield emerge and receive energy from the mean flow via the Reynolds shear stresses. The downstream merging and subsequent growth of the large scale spanwise structures is responsible for large scale mixing and the overall development of the mixing layer. With every successive merging event, large scale passage frequencies decrease by one-half (Huang & Ho 1990), their strength and wavelength double, and the separation between large scales increases by a factor of two (Brown & Roshko 1974). The momentum thickness grows linearly and is proposed to double instantaneously at each pairing location in the *subharmonic evolution model* (Ho 1981). Refer to figure 8. Merging spanwise large scale vortices engulf large portions of ambient irrotational fluid into the shear layer producing entrainment, spreading and overall mixing. The processes of entrainment and fine-scale mixing appear to be separate at high Reynolds number (Dimotakis & Brown 1976).

Browand & Weidman (1976) found merging processes created Reynolds stress which in turn is responsible for turbulent energy production ($-\overline{u_i u_j} \partial U_j / \partial x_k$, from the dynamic equation for $-\overline{u_i u_i}$). Wygnanski & Oster (1982) measured changes in the sign of the Reynolds stress at merging locations verifying transfer of energy from fluctuating velocities to the mean flow by the stresses. This process is termed *vortex nutation* and it permits energy transfer to large scale coherent structures (Browand & Ho 1983).

Secondary instabilities initiate creation of another type of large scale coherent structures designated as streamwise vortices (Bredenthall 1978; Bernal 1981). They form in the streamwise 'braid' regions between adjacent large scale spanwise vortices which are characterized by large rates of strain. The existence of streamwise structures was theorized by Benney & Lin (1960) and Corcos (1979), measured by Konrad (1976) and Miksad (1972) and reviewed by Roshko (1981). Refer to figure 9. Threading inwards as well as overlaying spanwise vortex cores, streamwise vortices are convected downstream by the spanwise vortices (Jimenez, Cogollos & Bernal 1985). They anneal in a process similar to vortex merging in which adjacent vortices merge thereby decreasing the number of streamwise vortices. Counter-rotating streamwise vortices enhance mixing by increasing the 'mixedness' of the fluid entrained by spanwise structures and inducing ambient velocity to traverse through the shear layer. They further increase the interfacial area of the mixing layer (Bernal 1981). Nevertheless, the spanwise large scales are the major contributors towards mixing in homogeneous mixing layers (Dimotakis & Brown 1976) and chemically reacting mixing layers (Bredenthall 1978, 1981; Masutani & Bowman 1984).

Lasheras, Cho & Maxworthy (1986) found initial three-dimensional perturbations affecting streamwise vortices. It was shown that mutual influences exist between streamwise vortices, the initially two-dimensional spanwise vortices and small scales, theoretically (Pierrehumbert & Widnall 1982), experimentally (Bernal & Roshko 1986; Huang & Ho 1990), and numerically (Ho, Zohar, Moser, Rogers, Lele & Buehl 1989).

1.1.6 Small Scales

The plane mixing layer begins as a laminar flow, promptly changes into a vortical flow digesting irrotational pockets of ambient fluid and eventually becomes fully-developed turbulent flow. Throughout its existence, the turbulent shear flow consists of multiple scales of varying dimensions and associated energies. Successive interactions among spanwise and streamwise large scale structures, respectively, instigate the production of smaller, three-dimensional scales which in turn lead to transition to fully turbulent flow.

A still unknown nonlinear secondary instability triggers production of small scales within the cores of the spanwise large scales as early as the first vortex merging (Bernal 1981; Zohar 1990). Hsiao (1985), Huang (1985) and Zohar (1990) found small scale populations normalized with respect to the number of large scales to reach maxima around the second vortex merging location. Small scales appear prior to the breakdown of large scale vortices and their generation is not a result of phase decorrelation of the large scales. Although it has not been ruled out that small scales may affect the secondary instabilities leading to breakdown of the large scale vortices.

Production of the small scales may be due in part by interactions between the spanwise and streamwise large scales, or possibly due to vortex stretching and tilting of the large scales (Brachet, Orszag, Nickel, Morf & Frisch 1983). Liu (1981) showed when the large scale amplitudes saturate the transfer of energy occurs from large- to small scales. A phenomenological model about small scale mixing in a reacting turbulent shear layer was proposed by Broadwell & Breidenthal (1982).

There are various experimental methods of identifying 'signposts' marking the beginning of transition following the first vortex merging and approaching completeness after the second vortex merging. These potential indicators include in descending order of accuracy, the number of small scales per large scale as estimated by the Peak-Valley Counting method (Huang 1985; Zohar 1990), the $-5/3$ slope of the roll-off exponent of the one-dimensional energy spectrum (Jimenez, Martinez-Val & Rebollo 1979), large values of the Reynolds stress (Browand & Weidman 1976) and increased mixing (Breidenthal 1981). Refer to figure 10.

The number of small scales increase downstream, Ho & Huerre (1984) and Zohar (1990). Small scales were found to diffuse large scale structures as well as the amplification rate of pairing (Pierrehumbert & Widnall (1982). Hsiao (1985), Huang (1985) and Zohar (1990) found small scale transition location begins at $Rx/\lambda_n \approx 8$, the second vortex merging location, for both two-dimensional plane jet and mixing layer, respectively. Small scales measured in two-dimensional jet by Hsiao (1985) were close to the Kolmogorov Microscale, $(\eta = (\nu^3/\epsilon))^{1/4}$, where ϵ is the dissipation), whereas Zohar's (1990) measurements showed the values to be closer to the Taylor Microscale.

The initially coherent large scales undergo increasing levels of phase-decorrelation which may generate small scales within cores. By the third vortex merging, fully turbulent flow is achieved at the asymptotic limits of these processes (Ho, Zohar & Foss 1991). Refer to figure 11. For sufficiently high Reynolds number, $Re > 3000$, the separation of scales in wavenumber-space becomes large enough such that an inertial subrange region characterized but not necessarily defined by the $-5/3$ slope exists in the downstream region saturated by the small scales. Although not sufficiently correct, conditions of isotropy may then be invoked to more easily facilitate estimation of important length scales-- the Taylor Microscale, Kolmogorov scales, etc.

In summary, free shear layers in principle act as low-pass filters amplifying background perturbations at selectable frequencies resulting in the formation of coherent structures. The initial momentum thickness (or vorticity thickness) and velocity ratio are the controlling parameters.

1.2 Axisymmetric Jets

1.2.1 Foundations

As stated previously, jets are a basic flow configuration possessing numerous engineering applications and form due to the pressure drop through an exit nozzle. Jets are among a class of inviscidly unstable free shear flows and evolve in a fashion similar to plane mixing layers through large scale vortex merging (Bouchard & Reynolds 1972; Browand & Laufer 1975). Jets do not possess a solid boundary which may act as a vorticity source and all of the vorticity is added to the flow at the nozzle exit. A common length scale characteristic of jets and mixing layers is the initial momentum thickness, or vorticity thickness. Additionally, the existence of one extra length scale, the nozzle diameter, distinguishes jets from plane mixing layers. As the jet develops downstream the dimension characterizing the local length scale of the shear layer increases in size from being on the order of the initial momentum thickness to the order of the jet diameter.

Interior to the shear layer and separated by an unsteady intermittent surface exists the potential core, an irrotational central region of constant velocity and temperature of approximately five exit diameters in length. Refer to figure 12. In the shear layer region energy is transferred from the mean flow to the fluctuating turbulent components via the Reynolds shear stresses and the subsequent pressure-velocity gradient correlations transfer energy from the streamwise velocity fluctuations to transverse components. The shear layer continues to grow dictating flow development after the potential core terminates and the mean quantities achieve self-preservation around eight exit diameters downstream. Refer to figure 13. Farther downstream the jet continues to develop approaching a state of fully-developed turbulent flow. Even after seventy diameters turbulent properties are still not self-preserving. Refer to figure 14. No definite isotropic homogeneous

turbulent regions have been measured in axisymmetric jets.

The fact that mean quantities become self-preserving before turbulent quantities illustrates the concepts of energy transfer in turbulent shear flows and the production of turbulence. Hence similarity or equilibrium is reached in a very gradual series of steps. Self-similar velocity profiles may be conveniently non-dimensionalized by the total streamwise distance or by a local transverse length scale, the velocity 'halfwidth'. The halfwidth is the transverse distance from the centerline axis to the location where the velocity drops to half of its centerline value.

Analyses of jets using phenomenological models have been simplified by two notions at large Reynolds numbers, a narrow mean flow pattern suggesting the use of boundary-layer equations and self-preservation. The first simplification indicates zero mean transverse velocities, considerably smaller streamwise gradients ($\partial/\partial x$) than transverse ones ($\partial/\partial r$) and constant streamwise pressure. The production of turbulence is by the Reynolds stresses acting upon the mean velocity gradients and this close relationship supports similarity in mean and turbulent quantities. Therefore, self-preservation coupled with eddy viscosity models close the equations and predict gaussian-shaped mean flow distributions which are in good agreement with experiment except near the edge of the flow (Townsend 1956; Hinze 1959). See Schetz (1980) for a complete reference list. Early measurements of turbulent axisymmetric jets began with Corrsin (1943) and Corrsin & Uberoi (1949, 1950). An extensive investigation of axisymmetric jets was undertaken by Wygnanski & Fiedler (1969).

1.2.2 Stability

Initial conditions at the nozzle exit impart a longtime impression upon the flow (Townsend 1956). Measurements of the evolution of the circumferential shear layer have shown the lip of the jet nozzle to be very sensitive to initial conditions (Bradshaw 1966; Hussain & Zedan 1978). An initial velocity difference between the jet and the local ambient fluid creates a cylindrical top-hat velocity profile surrounded by a thin circular shear layer—the region of turbulent shear flow.

Laminar and turbulent free jets are inviscidly unstable flows by the presence of inflection points in their mean velocity profiles. The initially laminar axisymmetric shear layer gives rise to periodic instability waves by the Kelvin-Helmholtz instability process. Exactly like their two-dimensional counterparts, the axisymmetric waves amplify exponentially in the unstable shear layer and roll-up in a nonlinear process forming three-dimensional ring-shaped vortices approximately four initial instability wavelengths downstream. The resultant periodic vortex rings appear quasi-stationary, grow and become distorted downstream (Wille 1963; Bradshaw 1966; Becker & Massaro 1968). Refer to figure 15.

According to inviscid hydrodynamic linear instability, the initial vortex rings are built upon axisymmetric modes ($m=0$) which amplify due to the linear instability of the top-hat velocity profiles at the nozzle exit. By Michalke's (1965) linear stability theory, vortices roll-up at a most-amplified frequency downstream of the nozzle exit scaling with the initial momentum thickness and convection velocity, $St=0.017=f_c \theta_c / U_c$.

Earliest theoretical studies of axisymmetric jet instability were conducted by Tyndall (1867), who observed flames to 'dance' in response to chamber music, and Lord Rayleigh (1879). The jet instability problem is treated by the linearized inviscid Euler equations with small perturbations, the Rayleigh equation, which calculate realistic mean velocity profiles (Betchov & Criminale 1967). Sinuous and varicose modes have been likened to axisymmetric and helical modes, respectively (Sato 1960). Spatial perturbations were chosen rather than temporal ones owing to the considerations of a physical free boundary layer (Gaster 1962). Inviscid flow simplifications have been employed by Michalke & Schade (1963) and Freymuth (1966). Parallel flow and finite momentum thickness assumptions applied towards temporal (Michalke 1964), and spatial (Michalke 1965), theories, respectively, suggest better comparison of spatial instability results with experimental results than with temporal results.

Michalke (1971) performed linear inviscid instability calculation on a cylindrical vortex sheet with a finitely thin shear layer and found the amplification rate of the spreading shear layer to vary with the local shear layer thickness, θ , the reduced frequency, $2\pi f\theta/U_c$, and curvature, θ/D . The linear hydrodynamic analysis of a jet then becomes similar to that of a plane mixing layer. However, parallel flow assumptions yielded slightly incorrect results at high $\lambda_{instability}/D$ ratios (Michalke 1969) which led to a more accurate treatment of slowly diverging flow (Crighton & Gaster 1976). Treating an axisymmetric jet shear layer like a plane mixing layer creates problems because the thickening shear layer has a correspondingly larger perturbation wavelength that is on the order of the jet diameter.

The resultant toroidal vortices are coherent structures with a definite phase and they mutually interact an inviscid fashion (Lamb 1932), and undergo a merging process with neighboring vortices (Browand & Laufer 1975). Refer to figure 16. The first vortex merging of the annular vortices occurs at the saturation of the subharmonic wave in a *non-dispersive* medium (Petersen 1978). The phase velocity of higher modes is non-dispersive for all frequencies bringing about resonant interactions further amplifying the modes thereby facilitating more efficient energy transfer. This is in agreement with the subharmonic resonance mechanism (Kelly 1967; Monkewitz 1988). Refer to figure 17.

Jets possess more complicated modes of instability than plane mixing layers and undergo *symmetry-breaking* that is, their instabilities switch to higher modes downstream (Ho & Huerre 1984). Concurrent with subsequent vortex mergings downstream, the mean velocity profiles evolve into bell-shaped profiles upon which the axisymmetric modes decay and are superceded by more energetic helical ($|m| \geq 1$) modes (Batchelor & Gill 1962; Martingly & Chang 1974). Michalke (1972) showed both axisymmetric and helical modes to be amplified in a jet, albeit at different rates. Michalke (1971) calculated that the axisymmetric modes have higher amplification rates within the potential core and are therefore more unstable than higher 'spinning' or helical modes. This is in agreement with slowly diverging parallel flow theory results (Plaschko 1979).

Beyond four jet diameters downstream, helical modes dominate axisymmetric modes (Petersen & Samet 1988). At higher Reynolds numbers the helical mode appears closer to the nozzle (Fuchs & Michel 1977; Drubka 1981), possibly due to stronger global feedback effects (Ho & Huerre 1984).

Farther downstream nonlinear azimuthal instabilities grow about the circumference of the vortices forming lobes and imparting severe distortion (Browand & Laufer 1975). The structures lose phase and amplitude coherence and begin to break up. Azimuthal vortex instability modes and their induced disturbances may contribute to vortex breakdown and symmetry breaking or even encourage the overtaking of the axisymmetric modes by helical modes (Widnall, Bliss & Tsai 1974; Browand & Laufer 1975). Measurements reveal 'wavy' velocity correlations distributed circumferentially about the potential core (Sreenivasan 1984) which suggests the loss of phase coherence at progressive downstream locations possibly due to the appearance of higher order instabilities-- either azimuthal or helical. Decreasing amplification rates in the downstream direction may be responsible for the diminishing strength of the axisymmetric waves and signify the appearance of helical modes (Petersen & Samet 1988).

1.2.3 Preferred Mode

Crow & Champagne (1971) experimentally found instability waves to reach peak amplitudes around $x/D = 4$ near the end of the potential core where the flow was governed by a *preferred mode* or *jet-column mode* of constant Strouhal number based on nozzle diameter, D , $St_D = f D/U_c = 0.3$. Refer to figure 18. This is the mode of maximum growth and it differs from the *shear-layer mode* which scales with the initial most amplified frequency, $St_0 = 0.017$. This agrees with the linear stability results of Crighton & Gaster (1976) which predict a mode at Strouhal number, $f D/U_c = 0.4$, corresponding to a maximum gain in pressure amplitude. The value of the preferred mode has been found to vary between 0.25 and 0.6 in experiments and this is probably due to the existence of varying passage frequencies of acoustically untreated facilities (Gurmark & Ho 1983). Kibens (1981), Drubka (1981) and Ho & Hsiao (1983) determined the preferred mode to vary with Strouhal number at small radius-to-initial momentum thickness ratios then remain constant beyond around $150 R/\theta$.

Hence, two modes govern the local development of the structure of a free axisymmetric jet. Within the potential core region instabilities scale with the local momentum thickness and the local passage frequency, $St_\theta = f\theta/U_c$ in agreement with spatial stability theory. After four jet diameters, the preferred mode governs the flow scaling with the local momentum thickness which is on the order of the exit diameter (Petersen & Samet 1988). This location appears to coincide with the onset of helical instability modes (Michalke & Hermann 1982) inferring the preferred mode to be helical in nature. Therefore for small curvatures, θ/D , the preferred mode appears to be the natural evolution of the shear-layer mode beyond $x/D = 4$ just as the local passage frequency is a result of numerous large scale vortex mergings.

1.2.4 Global Stability

Global spatio-temporal analyses have been studied in jets. For a summary of global stability effects in jets refer to Table 4 in Huerre & Monkewitz (1990). Decreased flow densities bring about absolute instability and self-excited nonhomogeneous jets. In particular, for exit density ratios, $\rho/\rho_\infty < 0.72$, the axisymmetric mode becomes absolutely unstable prior to the appearance of the helical mode (Monkewitz & Sohn 1986; Yu & Monkewitz 1990). Experiments in heated jets reveal vortex break down immediately following the location of absolute instability (Sreenivasan, Raghu & Kyle 1989). Low-density measurements have revealed random appearances of side-jets emanating at large angles to the main flow dramatically increasing the local spreading angle (Guyon 1988; Monkewitz, Bechert, Bariskow & Lehmann 1990).

Observations of globally self-excited modes agree with spatio-temporal theory (Monkewitz, Bechert, Bariskow & Lehmann 1990). Refer to figure 19. Recent experiments indicate side-jets to be observed only in low-density axisymmetric jets, (Monkewitz, Bechert, Bariskow & Lehmann 1990; Ho 1991, private communication). Increased velocity ratios greater than one found in jets with coaxial reversed flow or suction show signs of absolute instability when $R \geq 1.3$ in agreement with spatio-temporal predictions (Strykowski & Niccum 1990).


1.2.5 Coherent Structures

Inviscid dynamics involving coherent structures occur in jets as in mixing layers. Orderly large scale structures have been identified in axisymmetric jets (Crow & Champagne 1971). The important properties related to mixing depend upon the evolution of the coherent structures. The merging dynamics of the large scale toroidal vortices govern entrainment and the added mass widens the shear layer and accordingly the shear layer spreads radially outward. Ambient fluid is entrained across the shear layer via the Biot-Savart induction mechanism (Batchelor 1967) during large scale merging and enters the potential core. Entrainment is defined as the total massflow crossing any imaginary plane orthogonal to the principle jet direction. Refer to equation (6). By similarity arguments entrainment should approach constant values far downstream because it is a mean property (Wynanski 1964) and it has been measured to be nearly constant in the potential core region (Crow & Champagne 1971).

Streamwise vortices are present in axisymmetric jets, as well. Beginning at the nozzle exit, three-dimensional secondary instabilities disturb the ring vortices and in a most nonlinear fashion develop into coherent streamwise vortices. These 'braid' regions are characterized by strong positive strain and large shear that may be stretching and aligning the vorticity

field to form these streamwise structures (Lasheras, Cho & Maxworthy 1986). The streamwise vortices connect or overlap neighboring large scale vortex cores and survive successive vortex mergings (Browand 1986). They do not appear to have as strong an effect upon entrainment as in plane mixing layers.

The actions of interacting large scale vortex rings and streamwise vortices may generate small scale three-dimensional fluctuations (Ho & Huerre 1984). Small scales begin to form following the initial vortex merging locations and their numbers realize asymptotic limits in the fully-developed region downstream of the third vortex merging (Hsiao 1985). The highly three-dimensional small scales 'wrinkle' the interfacial area of the once-coherent vortices increasing their surface areas. They proceed to carry out the final stages of mixing begun by the large scales by initiating fine-scale and molecular mixing (Broadwell & Breidenthal 1982).



$$\dot{Q}(x) = \int_0^R \rho U(r) 2\pi r dr$$

I.3 Three-Dimensional Jets

I.3.1 Foundations

Three-dimensional jets are distinguished by noncircular exit nozzles of varying geometry, i.e. elliptical, rectangular, triangular, tapered and even scalloped- or crown-shaped! By passively changing nozzle geometry the initial conditions in three-dimensional jet nozzles profoundly alter the downstream evolution of the flow. The properties of three-dimensional jets approach those of two-dimensional plane jets the limit of very large aspect-ratio. Consequently, the complicated stability modes and velocity fields in three-dimensional jets are found to be very different than axisymmetric jets. It is these properties that are responsible for significantly greater mixing processes in three-dimensional jets. Owing to their more physically intricate nature, large aspect-ratio and plane '2-D' jets were first studied, and it is only recently that small-aspect ratio and more 'irregular' jets have begun to be investigated.

I.3.2 Stability

Asymmetric jet flows display more complicated stability modes than axisymmetric flows. Michalke (1971) has remarked that the more a jet departs from axial symmetry the more unstable it becomes. Linear inviscid stability analysis of an elliptical vortex sheet indicates similarity between large aspect-ratio jets and two-dimensional jets (Crighton 1974). Measurements of velocity fields and spreading characteristics in large aspect-ratio and '2-D' jets lend support to this view (Ho & Gutmark 1987). Elliptically shaped, large scale coherent toroidal vortices are shed consecutively from the exit nozzles of three-dimensional rectangular and elliptic jets according to the previously discussed Kelvin-Helmholtz instability mechanism. The initial vorticity distributions and any intrinsic "irregularities" at the position of the formation of the shear layer help to determine its linear growth rate (Wirant 1972; Dimotakis & Brown 1976).

Morris & Miller (1984) distinguished an axisymmetric mode, helical modes which 'flap' about the major and minor axes, respectively, and even higher order 'double helix' modes in elliptic vortex sheet analyses. It is conjectured that azimuthal modes may be responsible for complicated superpositions of higher order, quasi-helical instability modes which dominate the initial axisymmetric mode in small aspect-ratio elliptic jets precluding any simple stability explanation. Elliptic ring vortices may retain their coherence and strength farther downstream than axisymmetric rings possibly due to the dynamics of self-induction, see below, resisting the higher frequency distortions of the Widnall azimuthal instability (Morris & Miller 1984; Koshigoe, Ho & Tubis 1987; Morris 1988).

Linear instability calculations found heated jets to be more unstable than cold jets (Gropengeisser 1969). More recently, analysis shows temperature to display subsonically destabilizing and conversely supersonically stabilizing effects toward the development of elliptic jets (Koshigoe, Ho & Tubis 1987). Global spatio-temporal investigations of a nonhomogeneous 2:1 aspect-ratio elliptic jet at density ratios lower than the predicted onset of absolute instability did not reveal any noticeable differences in the flow (Ho & Austin 1988). In the same facility, suction applied to increase the velocity ratio well above the predicted boundary also did not confirm the existence of absolutely unstable flow. It is possible that either spatio-temporal calculations of axisymmetric jets are not directly applicable towards small aspect-ratio elliptic jet flow fields and require re-calculation, or absolute instability may be confined to very localized regions.

I.3.3 Coherent Structures

Studies of isolated elliptically shaped vortex rings showed deforming vortices and axis switching (Viets & Sforza 1972; Dhanak & DeBernardinis 1981). The coherent elliptic vortices have varying radii of curvature such that the section of the ring in the major axis plane is convected faster downstream than the minor axis section by the inviscid nature of the Biot-Savart Law mechanism (Batchelor 1967). Refer to equation (7). The faster moving section of the major axis section convects forward as it bends inward decreasing the local radius of curvature until it matches the radius of curvature of the minor axis section which is simultaneously moving outwards. This is the process of *self-induction*. The property of *axis switching* occurs when the initially elliptic ring briefly sustains a circular configuration following a series of downstream



$$\vec{u}(\vec{x}) = -\frac{\Gamma}{4\pi} \oint \frac{\vec{r} \times d\vec{s}}{r^3}$$

distortions. Following axis switching, the major axis section becomes the 'new' minor axis section and reciprocally the minor axis section becomes the 'new' major axis section. Refer to figure 20.

These dynamics unique to three-dimensional jets only begin to uncover the highly convoluted three-dimensional evolution of the elliptic ring as it progresses downstream in comparison to the 'conventional' non-self-inductive behavior of circular toroidal rings. Viets & Sforza (1972) and Dhanak & DeBernardinis (1981) have ascribed the azimuthal distribution of vorticity along the elliptical ring's contour to be responsible for self-induction in vortex rings. Refer to figure 21. The self-induction of small aspect-ratio elliptic vortices is the cause of considerably large entrainment rates in a 2:1 aspect-ratio elliptic jet (Ho & Gutmark 1987).

Streamwise vortices, although largely undocumented, exist in three-dimensional jets and have been visualized immediately following the first vortex merging in nonhomogeneous 2:1 aspect-ratio elliptic jet flows (Huerre & Redekopp 1990). The fact that the streamwise structures are observed primarily in the major axis plane may only be a consequence of the optical flow diagnostics.

1.3.4 Large Aspect-Ratio

Early experimental studies by Trentacoste & Sforza (1967) measured mean properties of 10:1 aspect-ratio rectangular jets. Triangular and high aspect-ratio, 6:1 and greater, elliptical and rectangular jets were investigated by Sforza & Stasi (1979), Krothapalli, Baganoff & Karamcheti (1981) and Krothapalli, Hsia, Baganoff & Karamcheti (1982). Mean values approached self-similarity beyond 30 jet diameters downstream, many times farther downstream than in an axisymmetric jets (Sfeir 1978). The investigators identified four regions reflecting local stages of flow development. The first is the potential core, characterized by constant mean velocity; second, a characteristic decay region where centerline velocity decays as a negative power; third, an axisymmetric-type region where the centerline velocity decays inversely with downstream distance, and last, a fully axisymmetric region.

The first revelation distinguishing three-dimensional jets from their conventional axisymmetric counterparts was the existence of different velocity profiles and spread rates in the major and minor axes regions. The mean velocity profiles differed between the major and minor axes, respectively, indicating different spreading rates in the two planes perpendicular to the main flow. Initially, the minor axis plane would spread more than the major axis plane. The transverse location of where the local velocity equals half the local centerline velocity is termed the 'velocity halfwidth' and it characterizes jet spreading. At a particular downstream location the velocity halfwidths in both axes will be equivalent. This has been explained as the phenomenon of axis switching and its location was found to be linearly proportional to the nozzle aspect-ratio.

Entrainment values in large aspect-ratio jets were found to be similar to axisymmetric jets because axis switching and azimuthal distortion of the large-aspect ratio vortices occur further downstream. By this location the large scale structures have begun to be weakened by azimuthal instabilities dissipating their vorticity such that these 'less-coherent' rings can not engulf large amounts of ambient fluid.

1.3.5 Small Aspect-Ratio

Visualization of small 2:1 aspect-ratio elliptic jets revealed large scale vortex mergings, three-dimensionally deforming elliptic vortices, azimuthal distortions and up to three axis switching locations in the major and minor axes (Ho & Gutmark 1982; Gutmark & Ho 1986). Planar visualizations of vortex ring cross-sections showed inclined vortices with respect to the nozzle exit suggesting a helical mode nature and many prominent streamwise vortices (Austin & Schreck 1990). Refer to figure 22.

Ho & Gutmark (1987) measured up to five times greater entrainment ratios and demonstrated the small 2:1 aspect-ratio elliptic jet to be a passive means of increasing entrainment. Furthermore, ten times as much entrainment was measured in the minor axis plane than in the major axis plane. This evidence suggests a second, and perhaps more important, entrainment mechanism in addition to vortex merging—the self-induction of the asymmetric vortex rings. Specifically, the increased azimuthal deformations in the vortical structure cause the minor axis section to move outwards thereby greatly increasing the interfacial area permitting the engulfment of more irrotational ambient fluid into the jet. Refer to figure 23. Therefore, the mechanisms of shear layer growth are vortex merging and vortex self-induction. Measurements suggest optimum mixing and entrainment to exist for elliptic nozzles having aspect-ratio between 2:1 and 3:1 (Schadow, Wilson, Lee & Gutmark 1984).

There exist noticeable differences between some parameters in the major and minor axes regions. The initial momentum thickness, and hence the Strouhal number, St_0 , was found to be twenty percent smaller in the minor axis than the major axis, whereas, the most amplified frequency was constant about the nozzle exit resulting in the instantaneous shedding of single vortices. In agreement with the linear instability analyses by Michalke (1965) and Morris & Miller (1984), the frequency of the initial axisymmetric waves scale with exit velocity and the thinner initial momentum thickness in the minor axis because that section of the shear layer is associated with steeper velocity gradients and hence, maximum vorticity. The amplification rates, $-k\theta$, in both major and minor axes are equal although their peaks do not exactly coincide with predicted merging locations (Ho & Huang 1982) most likely due to increased phase jitter of the large scales brought on by severe azimuthal distortions.

Peak turbulent intensities and positive Reynolds shear stress conform to the inward motion of the major axis section and the outward motion of the minor axis section of the deforming vortex rings. The minor axis velocity profiles display considerably higher spreading than the major axis velocity profiles. Velocity halfwidths and constant-velocity contours indicate linear growth in the minor axis regions and nearly constant growth in the major axis regions. This evidence reinforces the existence of greater entrainment and spreading in the minor axis region. Refer to figure 24.

The consequences of axis switching are more dramatic in small aspect-ratio three-dimensional jets. In large aspect-ratio three-dimensional jets axis switching is only observed once, if ever. Axis switching in low velocity small aspect-ratio three-dimensional jets continues up to forty diameters downstream and then the jet becomes fully axisymmetric. The number of such locations is dependent upon the density ratio (Austin & Ho 1988a) and jet exit Reynolds number (Ho, Huerre & Redekopp 1990).

Near-field pressure fluctuations have been studied in light of noise reduction, and they are produced by the merging process at equally in both axes at subsonic velocities (Gutmark & Ho 1985). It has been shown that the source of noise in low Mach number jets has its origins in the process of nonlinear saturation of the instability waves at the vortex merging locations (Laufer & Yen 1983) and the maxima of most-amplified instability waves are associated with these locations (Ho & Huang 1982). However, recent measurements show noise to be due to the preferred mode in a high subsonic 2:1 aspect-ratio elliptic jet (Schreck & Ho 1990). In contrast, elliptic jets with aspect ratios greater than five display a difference in the pressure field between the major and minor axes regions (Voce & Simpson 1972; Browand, Chu & Laufer 1975).

1.3.6 Nonhomogeneous Flows

Turbulent measurements in a nonhomogeneous 2:1 aspect-ratio elliptic jet revealed higher mixing and entrainment in the minor axis plane, moderately higher entrainment ratios than a homogeneous elliptic jet and displacement of the axis switching location upstream (Austin & Ho 1988a, 1988b; Ho, Austin & Hertzberg 1989). Side-jets were not observed in the heated 2:1 aspect-ratio elliptic jet. Pressure and gravity forces act only through the center-of-gravity of fluid particles and cannot induce rotation. However, in a nonconstant density field the center-of-gravity does not coincide with the center-of-mass which allows pressure forces to induce rotation and generate internal vorticity. The baroclinic torque due to fluid accelerated by nonaligned pressure gradients in a varying density fluid may figure in the vorticity dynamics of a heated flow. The Helmholtz vorticity equation obtained by taking the curl of the Navier Stokes equation describes the rate of change of vorticity by stretching, tilting, thermal expansion, viscous diffusion and baroclinic torque terms (Yih 1969). Refer to equation (8). However, the baroclinic term has not been determined to be primarily



$$\frac{\partial \omega/\rho}{\partial t} + \mathbf{u} \cdot \nabla \omega/\rho = \omega/\rho \cdot \nabla \mathbf{u} - \omega/\rho \nabla \cdot \mathbf{u} + \nu \nabla^2 \omega/\rho + \frac{\nabla \rho \times \nabla P}{\rho^3}$$

responsible for increased entrainment in a heated 2:1 aspect-ratio elliptic jet. Rather, the upstream shift in the location of axis switching upon the addition of heat seems indicative that the inviscid effects of self-induction upon the vortex rings have been enhanced in an as yet unknown mechanism such that more ambient fluid is engulfed upstream.

Experiments of a confined subsonic 2:1 aspect-ratio rectangular dump jet reveal the existence of transverse velocities and the suddenly expanding recirculation zone common in axisymmetric dump combustors to be completely suppressed in the minor axis plane (Ho, Austin, & Hertzberg 1989; Hertzberg & Ho 1991). As a result combustion efficiency is improved. Schadow & Gutmark (1989) extensively reviewed propulsion research on the improvement of subsonic and supersonic combustion and determined the 3:1 aspect-ratio elliptical nozzle demonstrated higher spreading and improved combustion efficiencies over axisymmetric, square, rectangular and triangular nozzles at both subsonic and supersonic conditions. Importantly, large scale coherent structures coinciding with local combustion regions have been identified in supersonic dump combustors and ramjets admitting the possibility of controlling and enhancing real-world flows. Refer to figure 25.

Spread rates of compressible subsonic and supersonic shear layers are considerably less than in incompressible subsonic shear layer (Bogdanoff 1982; Roshko & Papamoschou 1986). It is therefore beneficial to find higher spreading and entrainment in the near field of a 2:1 aspect-ratio rectangular jet over an axisymmetric jet at supersonic conditions (Jou, Knoke & Ho 1988; Schadow & Gutmark 1989). This work extends the envelope of increased mixing performance in small aspect-ratio nozzle to supersonic conditions. However, for Mach numbers greater than 2.25 all types of jets appear to grow similarly. The expansion and compression waves further excite shear layer instabilities switching instability modes and creating more acoustic signals that feedback upstream. The geometry of the supersonic exit nozzle determines the large and small mixing characteristics (Gutmark, Wilson & Schadow 1989).

Other nonconventional and effective means of passively achieving controlled mixing and increasing entrainment rates has been to modify the jet exit boundary conditions with crown-shaped nozzle extensions (Longmire & Eaton 1990) and adding tapered nozzles of indeterminate origins (Kibens & Wlezien 1985; Schadow & Gutmark 1989).

1.4 Excitation Effects

The turbulent free shear layer is composed of quasi-deterministic large scale coherent structures whose subsequent

mergings are responsible for entrainment, growth and small scale production leading to transition. These organized structures are defined by unique passage frequencies and characteristic length scales. To increase mixing, the merging process must be controlled so as to obtain a spatially coherent merging pattern. It has been successfully demonstrated that shear layers are especially sensitive to low-level disturbances and can be excited. Existing or new perturbations can be further amplified by the influence of external acoustic waves, an embedded splitter plate or three-dimensional corrugations at the flow origin.

The phase speed of acoustic waves is much larger than phase speeds of incompressible subsonic flows thus excited acoustic waves can only impart energy at the origin by converting acoustic energy waves into vortical instability waves via the *trailing-edge receptivity* (Morkovin & Paranjape 1971; Crighton 1981). As a consequence, higher Mach number experiments can be directly excited (Tam 1978).

It is known that the most amplified wave is due to a naturally selected amplitude and phase reference. Periodic forcing smoothens phase jitter and increases coherence of the large scale structures by extracting energy from the background flow and simultaneously reducing background turbulence. This process strengthens the phase reference of the large scales permitting more convenient spatial identification of the structures. Forcing at a certain frequency with large enough amplitude leads to a response by the shear layer at that particular frequency and usually induces vortex roll-up at a frequency which is a specific harmonic of the forcing frequency.

1.4.1 Mono-Frequency Forcing

Artificial forcing was shown to 'flesh out' or strengthen vortices (Wynanski, Oster, Fiedler & Dziomba 1979; Browand & Troutt 1980). Active acoustic forcing organizes large scales and has considerable influence on the vortex merging process (Ho & Huang 1982; Oster & Wynanski 1982; Fiedler & Mensing 1985). Forcing at the fundamental or natural frequency, f_n , (mode I forcing) reinforces individual vortices and lessens influences from neighboring ones which delays vortex pairing at the first subharmonic, $f_n/2$, and discourages growth of the shear layer. This forcing arrangement increases the efficiency of energy transfer from the mean flow to the large scale structures (Zohar, Foss, Ho & Buell 1990).

In marked contrast, mode II forcing at the first subharmonic bypasses vortex merging and proceeds directly to the first vortex pairing. Numerical calculations re-affirm mode II results (Riley & Metcalfe 1980). In general, Mode "m" subharmonic forcing at the $m-1$ 'st subharmonic, $f_m = f_n/2^{m-1}$, skips the first $m-1$ mergings and introduces a frequency-locked shear layer that promotes the amalgamation of up to "m" vortices into a larger vortex at the point where the frequency, f_m , peaks in amplitude. Refer to figure 26. Hysteresis is observed between forcing modes. This mechanism, the *collective interaction*, interacts with as many as ten vortices and greatly increases spreading in the mixing layer (Ho & Nosseir 1981) and enlarges the momentum thickness (Oster & Wynanski 1982).

Subharmonic forcing induces vortex pairing under non-dispersive conditions in agreement with the dynamics of 'natural' shear layer perturbations (Ho & Huerre 1984). The phase speed of the subharmonic disturbances should match the large scales' convective speed to enable most efficient energy transfer between the modes (Petersen 1978; Cohen & Wynanski 1987).

Forcing an axisymmetric jet establishes the best response at $St=0.3$ —the preferred mode (Freymuth 1966). Crow & Champagne (1971) found similar results and observed collective interaction-like events. Forcing at the preferred mode delays subharmonic vortex roll-up and merging by locking the large scale structures into the passage frequency of large scales at the end of the potential core and causing large vortices to roll-up. The intensity peaks of the fundamental and subharmonic waves also shifted upstream with increasing forcing levels. Low-level forcing has been shown to affect the large scale coherent structures in an axisymmetric jet (Reynolds & Bouchard 1982). Forcing at the preferred mode is also the most efficient method of acoustic forcing because it requires the least energy input (Wynanski, Oster & Fiedler 1979; Gutmark & Ho 1983). Increasing the forcing amplitude by very large amounts shifts the peak of the fundamental upstream (Freymuth 1966) as well as the merging location (Ho & Huang 1982). Typical excitation forcing levels are 0.01% to 0.1% of the mean velocity. Reynolds & Bouchard (1981) forced an axisymmetric jet at extremely high levels of 17% inducing vortex rings to revolve about each other and merge into a larger structure. In general, lower forcing frequencies require larger amplitudes to affect the flow and this is visible from the instability curve showing a linear increase in growth rate at small Strouhal numbers. In an axisymmetric jet (Crow & Champagne 1971) and in a mixing layer (Zohar 1990), it was determined that forcing amplitudes saturate beyond a certain energy input level and can not further affect the flow as indicated by an asymptotic limit in the number of small scales produced in the forced mixing layer case.

Moderately forced elliptic vortices behave similarly to isolated vortex rings (Ho & Gutmark 1983a, 1983b). Schadow, Wilson, Crump, Foster & Gutmark (1984) and Gutmark, Schadow, Parr, Harris & Wilson (1985) performed subharmonic and preferred mode forcing on ramjets with three-dimensional nozzles at operational conditions to control the unsteady pressure oscillations responsible for certain combustion instability modes. Vortex roll-up occurred in a fashion similar to homogeneous non-reacting jets and the growth of the shear layer was increased. The forced coherent vortices dissipate sooner upstream regarding them unsuitable to interact with pressure oscillations in the hopes of reducing combustion instability (Schadow, Gutmark, Parr, Wilson & Crump 1987).

1.4.2 Multi-Frequency Forcing

The phase difference, ψ , between the fundamental wave and its subharmonic is crucial to vortex merging and

subharmonic growth rates decrease by varying ψ between 0 and π (Arbey & Ffowcs Williams 1984; Zhang, Ho & Monkewitz 1985) and has been numerically observed (Kelly 1967). Furthermore, numerical simulations of forcing at zero phase difference the structures are of equal size and pair normally, but at anti-phase forcing, $\psi \rightarrow \pi$, the two merging vortices are of different size and 'shred' (Riley & Metcalfe 1980) although the latter result is in dispute (Zhang, Ho & Monkewitz 1985). By varying the phase difference and amplitude ratios between fundamental and subharmonic frequencies in an axisymmetric jet yielded varying vortex pairing or shredding locations, increased momentum thickness, larger Reynolds stresses and faster shear layer growth (Ng & Bradley 1988).

Forcing at multiple frequencies increases the number of control variables— frequency, amplitude and phase reference (Wynanski & Petersen 1987). The different frequency components are known to nonlinearly interact in a type of nonlinear *mode competition* which depends upon the amplitudes and frequencies (Ho & Huerre 1984). Miksad (1972, 1973) acoustically forced a mixing layer at two frequencies and observed the nonlinear effects upon the growth and generation of various modes. Combinations of axisymmetric and helical forcing modes create 'blooming' or 'bifurcated' jets with very large spreading angles and entrainment (Lee & Reynolds 1985; Parekh, Leonard & Reynolds 1988).

Harmonic and subharmonic forcing with variable phase differences allowed for control of the nature and location of vortex pairing in crown-shaped nozzles (Longmire & Eaton 1990). Energy is transferred more efficiently from the mean flow to the vortices of the respectively forced subharmonic modes. Therefore, forcing at subharmonics of the fundamental supplies the maximum allowable energy to the frequency-locked structures (Zohar, Foss, Ho & Buell 1990).

Experimental helical forcing of axisymmetric jets at multiple frequencies radically altered the shape of the axisymmetric flow approximating an elliptical jet for modes ± 1 and to a square jet for modes ± 2 . The spreading rates and entrainment were increased and were comparable to an unforced 2:1 aspect-ratio elliptic nozzle although no axis switching was reported (Strange 1981; Long & Petersen 1989). The coupled dynamics of subharmonic forcing at multiple higher order modes and shear layer spreading processes are believed to lead to triad resonances or *controlled resonant interactions* (Long & Petersen 1989).

1.4.3 Control of Small Scales

By imparting energy to large scales through multi-spectral forcing, the resulting energetic structures should produce more small scales during merging events. Control of both the spanwise and streamwise structures as well as an increase in the number of small scales by $\approx 50\%$ were realized by harmonic plus subharmonic forcing in a mixing layer (Zohar 1990). Forcing the fuel feed of a reacting axisymmetric jet at one magnitude higher than the preferred mode shifted the transition region upstream initiating intense combustion (Gutmark, Parr, Hanson-Parr & Schadow 1989). Refer to figure 27. Increasing the production of small eddies through acoustic forcing will prove to be helpful in fine-scale and combustion processes.

All free shear layers, whether natural or forced, may be considered to be 'perturbed'. Therefore, a more consolidated overview of free shear layers, both natural and forced, can be obtained by plotting the local Strouhal number of the forced frequency versus streamwise coordinates normalized by the feedback equation integer parameter, N , along a common curve (Ho & Huerre 1984). Refer to figure 28.

1.5 Small-Scale Mixing and Combustion

Heat release in subsonic and supersonic chemically reacting flows is believed to be associated with vortex dynamics. Large scale mixing provides the bulk mixing between the fuel and oxidizer inside combustion chambers and small scale motions dynamics give rise towards finer mixing and initiate reactions leading to combustion. When heat is released in a chemically reacting turbulent shear layer the resulting flow is characterized by a nonconstant density field. This imposed nonhomogeneity couples the effects of fluid dynamics to chemistry. It is important to understand the directly coupled effects that turbulent shear flow and combustion processes have upon each other.

The reasons for controlling combustion are three-fold, to raise the amount of energy released and increase thrust, to extend flammability limits thereby broadening the operational range and to eliminate potentially disastrous combustion instabilities. Unsteady combustion combined with periodic heat release amplifies pressure oscillations of high amplitude and triggers the onset of combustion instability (Harje & Reardon 1972; Culick 1983). Therefore, to control and improve combustion characteristics one needs to passively, if not actively, direct the developmental processes of coherent structures in shear flows.

The mixing regions of fuel injectors inside combustion chambers are believed to behave like their homogeneous non-reacting counterparts. Large amounts of unmixed fluid is entrained into the shear layer by the induced velocity field of the large scale vortices and molecular diffusional mixing is accelerated by large strain fields. Refer to figure 29. Fluid may also be entrained by vortex merging superceding diffusional mixing such that low-speed, ambient fluid is ingested (Broadwell & Breidenthal 1982). The structure of chemically reacting mixing layers depends on asymmetric entrainment, mixing characteristics and finite-rate reaction kinetics (Masutani & Bowman 1986). Refer to figure 30.

Heat release from combustion decreases vortex merging and velocity gradients in plane mixing layers (Hermanson &

Dimotakis 1989). Numerical results by McMurtry, Riley & Metcalfe (1989) identified the baroclinic torque and thermal expansion terms from the Helmholtz vorticity equation for nonconstant density to be responsible for changes in the velocity profiles and reduced vorticity concentrations within the cores of the vortices. Decreased turbulent shear stress was offered as an explanation for decreased shear layer growth inferring decreased momentum transport by the vortices in the outward radial direction.

1.5.1 Coherent Structures

Products of chemical reactions concentrate within the large scales and in particular among the small scale regions (Breidenthal 1981). Combustion processes appear to be phase-locked to large scale motions which in turn modulate the dynamics of small scale mixing (Gutmark, Schadow, Parr, Parr & Wilson 1987). This reinforces the possibilities of directly controlling combustion because the methods for controlling coherent structures in homogeneous shear layers both passively and actively may be employed upon combustion systems.

Planar laser induced fluorescence flow visualization of hydroxyl concentrations indicate that combustion begins within the circumferential of large scale vortices where smaller secondary three-dimensional eddies are produced (Gutmark, Parr, Parr & Schadow 1989). As the flow develops the regions of combustion propagate into the vortex cores and heat is periodically released. Vortex merging accelerates combustion by contributing to the production of small scales.

Combustion is also measured along the streamwise vortices joining the large scales together. It is believed that the onset of small scales appears simultaneously with the beginning of transition to turbulence in homogeneous shear layers (Breidenthal 1981). The locations of small scales appear to overlap with zones of combustion in reacting shear layers and increased small scale production increases fine-mixing which enhances combustion. The combustion process has also been demonstrated to occur prior to the first vortex merging when the fuel and air mixes and burning is sustained. When the first vortex merging is delayed through preferred mode forcing, the drivers of combustion instability, pressure oscillation amplitudes, are reduced. In addition, flammability margins and overall combustion efficiency are increased (Schadow, Gutmark, Parr & Wilson 1989).

1.5.2 Excitation Effects

Strong forcing has shown to tear the 'braid' region joining adjacent large scale vortices, forming large velocity gradients, increasing stretching and straining and reducing the number of flamelets and quenching or extinguishing combustion (Givi, Jou & Metcalfe 1986; Gutmark, Parr, Parr & Schadow 1989). Active forcing of the duct acoustics in conjunction with the passive employment of small 3:1 aspect-ratio elliptic nozzles, sharp-cornered triangular nozzles, tapered slot nozzles and multi-step nozzles have all proven to enhance various combustion processes, Schadow & Gutmark (1989).

It is evident then that combustion is an extremely complicated process involving fluid dynamics, chemical kinetics and acoustic interactions. Consequently, combustion is affected by many variables—velocity, density, pressure, species concentrations, temperature, and so on. One of the principle drivers of combustion is the production of small scales, and this dictates the understanding of large-scale mixing and its relationship with fine-scale mixing. Therefore, the next best thing to the analysis of a reacting shear layer is performing fundamental research on a turbulent non-reacting free shear layer without the added complicating effects of chemistry and confinement. It is in this light that the small scale topology of a 2:1 aspect-ratio elliptic nozzle will be investigated.

II. EXPERIMENTAL FACILITY AND TECHNIQUES

II.1 Jet Facility

The experimental jet facility is driven by as many as four Winkljammer^o centrifugal blowers arranged in parallel and enclosed within a chamber which filters intaked air from the surrounding laboratory. The blowers are powered by single-phase 120V variacs that vary nozzle speed. At the nozzle exit, the maximum velocity is 85 m/s, which approaches the limit of incompressibility. In a similar vein, three-phase 60A powerstats power two parallel Western Gear^o electric heaters and supply variable heat to the flow. The heaters are located downstream of the blowers and are capable of raising the exit temperature to a maximum of 220 C which corresponds to a density ratio of 0.64. The outlet of each heater is monitored by a Fenwall^o J334 thermistor to indicate potential overheating of the jet facility. A very small temperature rise of fifteen degrees may be added to slightly contaminate the flow in order to use heat as a tracer, or temperature may be increased to isolate temperature influences on the deformation of the vortices.

Downstream of the blowers and heaters, the flow enters an anechoically treated cylindrical chamber damping 'organ-pipe' acoustic modes that might resonate with shear layer frequencies and modify the preferred mode. Perforated steel plates lined with temperature-resistant insulative mineral wool reduce passage noise from the blower blades. Hot-wire

measurements just inside the nozzle lip did not sense any acoustic frequencies at varying jet velocities verifying the 'cleanliness' of the flow. The exit flow has a low turbulence level and is 0.4% of the mean velocity. Flow visualization of the nozzle exit confirms the existence of an initially laminar flow.

The flow contracts and enters an aluminum constant diameter circular stagnation chamber where it is made more uniform and turbulence and rotational swirl are decreased by passing through aluminum honeycomb, Duocel[®] aluminum foam, and a series of fine 40 x 40 wire mesh screens. The nozzle is casted from temperature resistant PTM&W Industries[®] PR4920 aluminum filled epoxy resin composite, and the inside walls smoothly contract along a fifth-order polynomial contour to a 2:1 aspect-ratio elliptical orifice. The area contraction ratio is eighteen to one. The dimensions of the major and minor axes of the nozzle are two inches, '2a', by one inch, '2b', respectively. Refer to figure 31. The semi-major axis length, a, will be the typical scale for nondimensionalizing lengths and the hydraulic diameter, $D_h = 4A/P$, where $A = \pi ab$ and $P = 2\pi[(a^2 + b^2)/2]^{1/2}$, will be required for normalizing against axisymmetric and asymmetric jets.

II.2 Facility Modifications

Early problems plagued the jet facility provoking distortions in the mean flow field and necessitated secondary design changes. The heaters have been relocated further upstream and were replaced by different heaters that permit flow over heating plates replacing the previous arrangement where heating coils directly disturbed the flow. A butterfly diaphragm was initially located immediately downstream of the blowers acting as a passive emergency heater shut down system in the case of flow loss and preventing facility damage. The diaphragm was removed due to its negating effects upon the flow and there is no current fail-safe system in operation. The section of honeycomb was replaced upon the discovery that its cells were not properly vertically aligned and were inducing a small swirl to the flow. An anechoic chamber was inserted to dampen potential acoustic perturbations.

Ambient conditions in the Rapp Research laboratory are far from clean and a miniaturized clean room employing cotton baring filters air for the blower arrangement's intakes. Following this implementation hot- and cold-wire sensors have endured considerably longer due to fewer damaging strikes by accelerated specks of dust. The high temperatures posed a very demanding problem regarding the manufacture of sensor probes. Attempts at producing hot-wire probes with ceramics, high-temperature epoxy or silver soldering resulted in stray capacitance problems and electrical noise. Thereupon, all probes were purchased to specification. Insulation of the jet facility was initially provided by fiberglass, then mineral wool and at the present there is none for health concerns. The interior of the jet's anechoic chamber was also insulated with mineral wool to fortify acoustic damping, however this too has been removed due to portions of the material flaking off and contaminating the laboratory environment. It remains to be tested if the facility will provide a non-irritating, clean and quiet flow.

II.3 Data Acquisition & Analysis

II.3.1 Instrumentation

Instantaneous velocity signals are sampled by a high-temperature Dantec[®] 55P71 single wire hot-wire probe. A balanced-bridge constant-temperature circuit supplies current to the anemometer at a 60% overheat ratio and provides a flat frequency response to 30 kHz. Likewise, instantaneous temperature signals are sampled by the previously-stated probe or simultaneously with velocity signals by a high-temperature Dantec[®] 55A75 dual-wire parallel probe. For temperature sensitivity the hot-wire is operated at a lower overheat ratio of 0.005. The resultant cold-wire has a more limited frequency response of 300 Hz. Construction and testing of the constant current anemometer was in accord with Weidman & Browand (1975) and Antonia, Brown & Chambers (1981). The low response region between the original time constant and the noise cutoff frequency of the cold wire is extended to 3 kHz using digital frequency compensation techniques (Ho, Huerte & Redekopp 1990) and the large frequency noise is FIR filter smoothed (McClellan 1976). The sensor element consists of 0.0002" diameter platinum-10% rhodium wire soldered to a 1 mm wide probe using high-temperature 60% tin-40% lead solder.

Hot-wire voltages are calibrated in the potential core against mean pressures measured by a pitot tube connected to a Validyne[®] CD12 pressure transducer. King's Law provides the necessary relationship, $E^2 = A + B U^{1/2}$ (or Nusselt = A + B [Péclet^{1/2}]), Blackwelder (1981), and the constants of the resulting fourth order polynomial are obtained by linear least squares fitting. In the context of this investigation, the Nusselt number which is a dimensionless group of the heat transfer coefficient and length divided by the heat conductivity depends upon the Reynolds number and non-uniform temperatures. The Péclet number represents the ratio of heat advection by the heat conduction and depends upon the Reynolds number in this study (the Prandtl number remaining constant).

Temperature signals are calibrated versus mean temperature measurements by a Fenwall[®] JJ334 thermistor or an Omega[®] RTD thin film platinum resistance probe yielding nearly accurate second order fits. Hot-wire calibration becomes complicated in the presence of nonconstant density because the constants in King's relationship are instant functions of temperature. The earliest simultaneous measurements of velocity and temperature with hot- and cold-wires employing

King's Law was performed by Corrsin (1947). Recently, Ali (1975) determined a different relationship between velocity, hot-wire voltages, V_{hw} , and cold-wire voltages, V_{cw} , where, K_1 , V_0 and C_i are constants. Refer to equation (9). The unknown coefficients, C_i , are obtained by performing a least squares fit to the nonlinear equation which is initially linearized by a Taylor expansion. Refer to equation (10).

$$\sqrt{u} = \frac{1}{K_2} \left[\frac{V_{hw}^2}{(1+a)V_0 - V_{cw}} - K_1 V_0 \right] [K_3 V_{cw} + (1 - K_3) V_0]$$

$$\rightarrow \sqrt{u} = \frac{C_1 V_{hw}^2 V_{cw}}{C_3 - V_{cw}} + \frac{C_2 V_{hw}^2}{C_3 - V_{cw}} + C_4 V_{cw} + C_5$$

temperature values.

The probes are mounted on a traverse system translatable in all three-dimensions with a spatial resolution of 0.0016 mm. A PC microcomputer controls three Slo-Syn[®] DC stepper motors which drive the respective axes of the traverse system. Up to sixteen channels of data are simultaneously digitized and recorded by a PC AT microcomputer controlled RC Electronics[®] analog-to-digital converter at up to 1 MHz acquisition rates. Typically only four input signals are required: hot-wire, cold-wire, pressure and mean

II.3.2 Measurement Techniques

A-D-C sampling rates are selected to insure the acquisition of at least 10-20 samples per period and including 500-1000 periods of the passing structures to obtain a statistically meaningful population sample. Signal processing and analysis is performed on a PC AT microcomputer and image processing and final analysis is performed on an Apple[®] Macintosh IIx. Mean values and root-mean-squared fluctuations are obtained from long time-averages.

Elliptic jet flow field is highly three-dimensional and the flow field can not be realistically mapped out by radial cuts as would be the case in an axisymmetric flow. Instead, the entire cross-sectional area of the flow is investigated and after performing symmetry checks this is reduced to one quadrant of the flow. Sampling along the major and minor axes provides mean and fluctuating profiles of velocity or temperature, respectively. The velocity profiles indicate jet halfwidth spreading rates and axis switching locations. The entrainment is measured by sampling velocity and temperature (for heated flow) across 25 by 25 grid points separated by Δx and Δy at cross-sectional quadrants downstream. The total amount of massflow becomes the summation of the product of density, velocity and incremental area, $\Delta x \Delta y$. Checks can be made by insuring the total momentum flux, $\sum \rho U^2 \Delta x \Delta y$, is constant at the same cross-sections. Measurements revealed the total momentum to be constant in the potential core and to decrease no greater than five percent at locations farther downstream ($x/a > 6$). This 'missing' mass is probably due to the existence of small velocities ($u < 1$ m/s) near the edge of the flow and consequently are indistinguishable by the hot-wire or pitot tube from A-D-C bit noise.

II.3.3 Analysis Techniques

The fast-fourier transform implementing Welch's 4-point algorithm (Cooley & Tukey 1965; Brigham 1988) calculates the one-dimensional energy spectra from which peak frequencies may be inferred. Fluctuating temperature signals are statistically analyzed to obtain probability density functions of the temperature distributions. For heated measurements the density of the flow is calculated as a perfect gas. Refer to equation (11). The dynamic viscosity is then calculated using Sutherland's equation (Bertin 1984) and the kinematic viscosity becomes $\nu = \mu/\rho$. Refer to equation (12). Two flow parameters, the Reynolds numbers, $Re_a = 3 \times 10^4$ and $Re_b = 1300$, and the Richardson number at maximum exit temperature, $Ri = g'(1-S)/(S U^2) = 10^{-5}$ clearly demonstrate the dominance of inertial forces over both viscous and buoyancy forces.

$$\rho(T) [\text{kg/m}^3] = \frac{1.225 [\text{kg/m}^3] \times 288.15 [\text{K}]}{T_1 [\text{K}]}$$

$$\mu [\text{kg/s m}] = 1.458 \times 10^{-5} \frac{T [\text{K}]^{1.5}}{(T [\text{K}] + 110.4)}$$

Sources of error include measurement errors due to the accuracy of the hot-wire anemometer, ± 1 mV; the cold-wire anemometer, ± 0.01 nV; the pressure transducer, ± 0.0175 m/s; the thermistors and platinum resistance sensor, ± 0.1 C; A-D-C 'bit' noise, or minimum resolution; ± 5 mV; and randomly occurring 60-Hertz background noise. Considerable electrical noise is reduced by regulating the supplied 25V DC power

in the hot-wire anemometer circuits, and noise is virtually eliminated by powering the cold-wire anemometer circuits with 12V dry cell batteries. The reading accuracy of a water manometer used to calibrate the pressure transducer is ± 0.5 mm. The resolution of the A-D-C is the limiting point of the acquisition and analysis system and if necessary can be decreased by lowering its ± 10 V input range to ± 5 V with a resistance modification at a specific location in the circuit. The probe location in x, y and z is uncertain to ± 0.0016 mm. The jet is mounted vertically to eliminate effects of gravity and the chamber housing the facility is considerably tall enough, $> 2^{\circ}$ jet diameters, to disregard potential feedback from downstream reflections.

II.4 Forcing Facility

A small forcing chamber is machined into the nozzle exit allowing four acoustic inlets. Refer to figure 32. Four Dynaudio[®] type D-21 speakers with a response range between 100 Hz and 35 kHz acoustically perturb the flow and their output signals emit at opposed ends of the major and minor axes at the nozzle exit. This placement allows for axisymmetric, asymmetric and helical forcing modes with the phase differences between the speakers provided by a variable phase-shifting circuit. The speakers are powered by a pair of two-channel Carver[®] M-200t 120W per channel power amplifiers. The output is synthesized by either a B&K[®] function generator which sends continuous sinewaves, a simple arbitrary waveform transmitted by a PC microcomputer controlled RC Electronics[®] Waveform Generator or a more complicated high-frequency waveform may be sent via a 12-channel Data Translation[®] DT-2814 digital-to-analog converter.

II.5 Optical Flow Diagnostics

Flow visualization of heated jet flow is a simple and helpful tool to aid in the analysis of the dynamics of turbulence (Lipmann & Roshko 1957; Merzkirch 1987). Visual evidence of the small scale structure of a flow can be obtained if temperature fluctuations are present in the turbulence. Temperature gradients are steepest when they are associated with the smallest eddies, and any optical system sensitive to such fluctuating gradients 'sees' the small scale structure of turbulence. However, the usefulness of flow visualization becomes severely degraded in the near 'chaotic' three-dimensional turbulent regions downstream of the flow where higher-order instabilities increase the 'wrinkledness' of the intermittent interface.

Density gradients in the flow are visualized by means of a sharp focusing schlieren system and recorded by conventional still and motion photography. Focusing Schlieren is a non-intrusive flow visualization method (Burton 1949; Kantrowitz & Trimpi 1950; Weinstein 1991). It yields more qualitative as well as quantitative data than conventional schlieren and shadowgraph methods which are only useful in flows having translational symmetry because they integrate intensity along the entire light path. Visualization of individual plane sections of finite depth is possible within the turbulent flow. Actual planar slices reveal individual cross-sections of large-scale vortical structures and small-scale three dimensional turbulence in the jet.

In the basic schlieren system ordinary white light is focused into parallel beams by being passed through a lens and transmitted across a test section. This line-of-sight integration drastically limits the ability to study the inner structure of a three-dimensional flow field. The Focusing Schlieren system uses multiple light sources by passing light through a grating whose lines are aligned parallel to the mean flow studied. In this manner many beams of light pass through any given point within the test section and subsequently there will be many beams of deflected light within the test section. Finally, there must be multiple knife edges or cutoffs to focus and filter the incoming rays. A screen receives rays which have passed through one given point. Other points intercept and deflect these rays but none of the rays focusing upon the screen will have encountered any points in common, along their respective paths. Only the deflection from the common points within a plane in the test section will contribute to the intensity of light at the screen. Other planes remain out of focus and their offset images blur out as in the focusing of ordinary camera lenses. There is only one moving part, the screen which is translated forwards and backwards to visualize different planes in the test section.

The size of the flow region in the near field of the elliptic jet dictates the minimum size of the necessary optics for visualization. White light is emitted from a variable strobed light source, General Radio[®] 1540 Strobolume Oscillator, controlled by a function generator. Light is collimated by a 10.5" focal length Edmund Scientific[®] Fresnel Lens and passes through Ronchi Rulings consisting of vertical 25 line per inch fringes. The fringe pattern was computer generated and laserprinted onto 3M[®] transparency paper. Light rays penetrate the flow region, are focused by a 10 inch converging lens, and then are deflected by a second set of Ronchi Rulings. The second Ronchi Rulings were created by placing Kodak[®] Ektapan 8" x 10" black and white photographic paper at the location of the second Rulings and briefly exposing it to the image created by the first set of Rulings. The resultant film is developed so as to obtain very dark fringe patterns. This second set of fringes is aligned with the first set of fringes until an interference image of moire patterns vanishes. The final plane image within the flow appears on a cardboard viewing screen behind the second Ronchi Ruling or on ground glass to allow camera recording (Austin & Schreck 1990). Refer to figure 33.

Recording of the images on the ground glass screen was done by an ELMO[®] SE 301 black & white CCD TV Camera connected to a Panasonic[®] TL AG 6750 Super VHS Video Cassette Recorder and Panasonic[®] CT 2010-Y Color Video Monitor. Still black and white images were taken by a Nikon[®] F4S 35mm camera with a Vivitar[®] 1:4.5 macro focusing zoom lens on Kodak[®] TMAX 100 and 400 ASA film. Super-VHS or VHS videotape of the flow is digitized on a PC AT microcomputer, and subsequently enhanced and analyzed on an Apple[®] Macintosh IIx microcomputer or a Gould[®] IP9000 workstation in the future.

III. CURRENT RESULTS

III.1 Mean Flow Field

Measurements have been carried out in the steady state flow of a subsonic homogeneous 2:1 aspect-ratio elliptic jet and have confirmed previous results (Ho & Gutmark 1987) that reveal the elliptic jet to have markedly increased mixing qualities over an axisymmetric jet. The addition of heat was found to further modify the vorticity distribution in the coherent structures and further intensifying the spreading and mixing characteristics of the elliptic jet. All experiments were performed in the same facility, and elliptic and axisymmetric nozzles with equal exit areas and Reynolds numbers were employed thereby removing any potential bias. The parameter space of the current study included subsonic velocities from 20 m/s to 85 m/s and temperatures ranging from the ambient to 220° C. For nonhomogeneous flow the facility is allowed to warm up and reach steady state conditions (approximately one hour) in order to sample mean velocity and mean temperature measurements at the same grid locations but separately in time.

III.1.1 Mean Velocities

Mean velocity measurements in nonhomogeneous flows, whether by pitot tube or hot-wire, yield mean total pressures from which mean velocities are calculated with the knowledge of the mean temperature at that location. Refer to equations (13) & (14). The static pressure in the elliptic jet is approximately 1-2% of the total pressure throughout the flow and is deemed negligible in the velocity calculations. Measurements of the initial momentum thickness confirmed previous



$$\rho(x, y, z) = \rho_{\infty} T_{\infty} / T(x, y, z)$$



$$P - P_{\text{static}} = \frac{1}{2} \rho(x, y, z) u(x, y, z)^2$$

findings of the existence of a nonconstant momentum thickness about the nozzle perimeter: The momentum thickness is 13% thinner in the minor axis region than the major axis region. Furthermore, the momentum thickness varies with the inverse square root of the exit velocity, similar to axisymmetric jets. The most amplified frequency is determined to vary as, $U_0^{-1/2}$, and the length scale of the initial vortical structure scales as, $U_0^{-1/2}$. Nonhomogeneous flow did not noticeably affect the initial momentum thickness or the most amplified frequency.

The mean velocity profiles emerge at the exit with a top-hat profile and evolve into bell-shaped profiles downstream resembling asymmetric and axisymmetric jets in general. The spreading of the flow due to self-induction is different between the major and minor axes. At low velocities the shear layer in the minor axis region expands by spreading out into the ambient region as evidenced by the increasing velocity profiles. However, the 'narrower' velocity distribution indicates the shear layer in the major axis region spreads into the potential core. Refer to figure 34. Velocity contour plots clearly indicate larger spread rates in the minor axis direction and illustrate a nearly circular mean velocity distribution between four and eight semimajor axis lengths downstream—the region of axis switching. Refer to figure 35. Velocity halfwidths emphasize linear growth of the minor axis region and a near constant state of affairs in the major axis region. The first axis switching location is evident in the neighborhood of $x/a = 7$. Downstream of the first eight semimajor axis lengths both regions grow at a nearly equivalent linear rate. At higher exit velocities the differences between the respective spreading rates become less pronounced as evidenced by only slightly more spreading of the velocity halfwidths in the minor axis region than the major axis region. The centerline mean velocity remains constant up to five semimajor lengths confirming the length of the potential core to be in agreement with conventional jet dimensions.

III.1.2 Mass Entrainment

The primary purpose of investigating the elliptic jet is to measure the mass entrainment and, hence, large scale mixing. The entrainment ratio is defined as the ratio of the local massflow at a cross-section to the massflow at the nozzle exit, $\bar{Q}(x) = (Q(x) - Q_0)/Q_0$, where the local massflow is defined as, $Q(x) = \sum \bar{\rho}_i(y, z) \bar{U}_i(y, z) \Delta y \Delta z$ [kg/s], which is summed over all grid locations across a given jet cross-section. Entrainment measurements for varying velocities in the homogeneous elliptic jet agreed with the earlier spectacular results of Ho & Gutmark (1987). The minor axis region, defined by 'arbitrary' diagonal borders set at 45°, entrains at least five times more than the major axis region. This strongly asymmetric distribution of entrainment about the elliptic jet flow field is the primary evidence for the proposed entrainment mechanism of self-inducting azimuthally distorted elliptic vortex rings rather than the merging of vortices as found in mixing layers and axisymmetric jets.

III.1.3 Velocity Effects

Two prominent features associated with the flow, the location of first axis switching and mass entrainment, were found to vary significantly with varying exit velocity. The location of the first and only detected axis switching of the elliptic vortices increased downstream in direct proportion to the mean exit centerline velocity. Measurements of the mass entrainment decreased with increased exit velocities. Refer to figure 36. These results reaffirm the existence of a strong

correlation between the dynamics of the elliptic vortex rings and their associated axis switchings with mass entrainment by the large scales in the flow field of a 2:1 aspect-ratio elliptic jet. The maximum exit velocities correspond to Mach 0.25 so that these results hold only for a subsonic incompressible elliptic jet although these results are consistent with the fact that supersonic jets have smaller spreading rates and entrain less mass than their subsonic counterparts. These results may suggest a Reynolds number dependence in which the initial boundary layer upstream of the nozzle might be modified in both axes' regions.

III.1.4 Nonhomogeneous Effects

Temperature was increased to investigate nonhomogeneous effects on the development of an elliptic jet and heat was also employed as a contaminant to trace the large scales. Heating the elliptic jet further enhanced the already large spreading rates and the velocity profiles indicated an inner growth in the major axis region of the shear layer and an outer growth in the minor axis region similar to the homogeneous low-speed case. The resulting nonconstant density distribution in the jet modifies the dynamics of the self-inducting elliptic vortex rings. This is manifested in the corresponding velocity halfwidths whereupon the location of axis switching for a heated elliptic jet with the exit velocity held constant translates upstream from $x/a = 7$ to $x/a = 5.7$. This is a 20% reduction in the axis switching location for a 25% increase in absolute temperature. Refer to figure 37. Nonhomogeneous centerline mean velocities are virtually identical to their homogeneous counterparts and the length of the potential core remains unchanged.

Additional measurements of nonhomogeneous effects at varying exit temperatures confirmed the inverse dependency of the location of axis switching upon the density ratio, $\Gamma = \rho/\rho_0$. Evidently then, the location of axis switching depends linearly upon the ratio of Re/Γ . Refer to figure 36. Measurements of subsonic large aspect-ratio jets by other authors found the axis switching location to move downstream with increased aspect-ratio. Therefore, it is proposed that the location of the first axis switching scale with the nondimensional parameter, $Re/(\Gamma AR)$, where $AR \equiv$ aspect-ratio.

In the medium of air, turbulence transports heat similarly as it transports momentum because the Prandtl number is a constant value ~ 0.7 . Subsequently, the mean temperature distributions, albeit broader and flatter, closely resemble the mean velocity distributions and, hence, a universal behavior of mean quantities exists throughout the jet. In the case of the elliptic jet, the mean temperature profiles mimic mean velocity profiles as they grow inward along the major axis and grow outward in the minor axis region. A temperature halfwidth may be measured like its velocity counterpart, and the location where the major and minor axes regions have equal halfwidths occurs upstream from the axis switching location at $x/a = 4$. It becomes apparent that the spreading rate in the minor axis region is retarded at higher (subsonic) exit velocities while on the other hand is enhanced by higher exit temperatures. This pattern is exhibited by mean velocity contours where similar growth of the major and minor axes profiles is apparent for a high velocity (85 m/s) and high temperature (185 C) flow field as for a low-speed homogeneous case.

The nonhomogeneous elliptic jet entrained as much as 25% more mass than the homogeneous case (Ho & Austin 1988). In the first two semimajor axis lengths the nonhomogeneous elliptic jet entrains up to six times more than a homogeneous axisymmetric jet and entrains up to three and a half times more than a nonhomogeneous axisymmetric jet. Refer to figure 39. The near-field of the homogeneous and nonhomogeneous small aspect-ratio elliptic jet was found to be a region characterized by large scale mixing more intense than in an axisymmetric jet and these findings are promising in view of the fact that this coincides with the region where combustion processes are initiated. Nonhomogeneous flow in a small aspect-ratio elliptic jet is also characterized by increased large scale mixing and this is a desirous *passive* method of increasing entrainment.

III.2 Turbulent Flow Field

III.2.1 Temperature Fluctuations

Instantaneous velocity and temperature signals were measured by hot- and cold-wires, respectively, to investigate the details of the nonhomogeneous shear layer and the entrainment process. The turbulent or root-mean-square signal is extracted from the instantaneous signal statistically. Refer to equation (15). The frequency response of the cold-wire anemometer does not permit accurate measurements of the flow in the neighborhood of the nozzle exit because the characteristic frequencies are greater than the cut off frequency of the circuit. For a jet exit velocity of 70 m/s the most amplified frequency is 10,400 Hz, and the initial instability wavelength is estimated, $\lambda_n \approx U_{exit}/(2 f_n) = 0.33$ cm. The frequency of the second vortex merging is $f_n/2 = 5,200$ Hz at $x/\lambda = 8$ and the third vortex pairing, $f_n/4 = 2,600$ Hz, occurs at $x/\lambda = 16$ or 5.23 cm downstream which is at $x/a = 2.06$. Therefore, the frequency compensated cold-wire sensor is capable of resolving temperature fluctuations for all regions downstream of the first two semimajor axis lengths where characteristic frequencies are less than 3 kHz.

Mean temperature contours reveal the existence of never before seen dual temperature peaks- one on either side of the centerline along the major axis. The peaks appear after $x/a = 4$ and merge into one 'normal' peak beyond $x/a = 8$, in a

$$x_{rms} = \left\{ \frac{\sum_{i=1}^N (x_i - \bar{x})^2}{N} \right\}^{1/2}$$

repeatable pattern that is more pronounced at higher temperatures. Refer to figure 40. These 'dual peaks' occur in the mixing region following the termination of the potential core where the turbulent shear layer fills the entire flow field. Supporting evidence to this anomaly is given by contours of RMS temperature which show similarly distributed twin peaks of thermal fluctuations but along the minor axis. The evolution of the turbulent temperature field downstream as shown in RMS temperature contours portrays higher intensities in the minor axis region beginning at $x/a = 3$ and becoming acute at $x/a = 10$. The existence of greater thermal turbulence in the minor axis region indicates pronounced large scale mixing processes engulfing more ambient fluid into the hotter inner fluid along the minor axis region. This would create slightly cooler regions in the centerline and minor axis regions and probably be responsible for the unique mean temperature distribution.

Larger amounts of mixing are to be expected in the minor axis region where greater spreading rates and significantly larger rates of entrainment occur. Centerline mean temperatures remain constant over shorter downstream lengths at higher temperatures suggesting higher rates of mixing in inverse proportion to the density ratio. In the mixing region downstream of the end of the potential core the centerline mean temperatures are lower in the elliptic jet than an axisymmetric jet at the exit conditions of 220 C and 55 m/s perhaps indicating deeper penetrations of ambient fluid into the mixing region of the jet.

III.2.2 Temperature Probability Density Functions

Instantaneous temperatures were measured along the major and minor axes at downstream cross-sections in a nonhomogeneous elliptic jet with an exit temperature of 150 C and exit velocity of 70 m/s. Probability density functions, a.k.a. PDFs, were statistically obtained by building up histograms of discrete temperature ranges from the fluctuating temperature signals. These calculations depict temperature distributions and are normalized with respect to the local centerline temperature at every cross-section in the flow. The distribution of the PDF profiles along the minor axis indicate a consistently even progression. This is in marked contrast to the PDF distributions along the major axis which are skewed towards either very hot temperatures near the jet core or towards cooler ambient conditions at the jet edge. These results were repeated for all downstream locations across the major and minor shear layer regions. Refer to figure 41.

The gradual even distributions along the minor axes suggest the penetration of larger amounts of ambient fluid into the minor axis resulting in more global mixing and inducing more entrainment. The skewed arrangement of the PDFs along the major axis suggest smaller amounts of localized mixing because the regions near the centerline remain at higher temperatures than the corresponding regions along the minor axis. Measurements reveal similarly placed PDFs in cooler nonhomogeneous flows. A comparison of two PDF profiles at two similar locations in the shear layer, $y/a = 0.5$ in the major axis and $z/b = 0.5$ in the minor axis, respectively, reveals some differences for a heated flow of 130 C. A broader distribution in the minor axis is skewed towards cooler temperatures reflecting more mixing over a wider range of temperatures. In contrast, the sharp narrow peak of the major axis indicates very little mixing because the temperature of the flow remains confined to a narrow temperature range. PDF measurements of temperature fluctuations help visualize the mixing process in the elliptic jet in which the self-inducting large scale vortices engulf large amounts of ambient fluid into the mixing layer primarily in the minor axis region (Austin & Ho 1988).

III.3 Flow Visualization

The structure of the nonhomogeneous elliptic jet has been examined by standard optical methods of flow visualization, including schlieren and shadowgraph as well as by a more powerful and recently revived means— the sharp focusing schlieren. Images of the flow were recorded by still and motion picture cameras. Conventional schlieren and shadowgraph techniques display the intermittently textured surface ensconcing the flow field. The sharp focusing schlieren by definition of its name focuses upon individual thin volumetric slices within the flow field. The elliptic jet has been observed at temperatures as high as 195 C, although structures are remarkably still identifiable at lower temperatures of 45 C. The entire range of flow velocities are visualized by schlieren or shadowgraph although lower velocities yield best results. Focusing schlieren requires small density ratios (high exit temperatures) in conjunction with minimum exit velocities to enable qualitative viewing of the large scale structures. The maximum heating of the facility operated at low speed is very demanding upon the facility, and in general focusing schlieren is considerably more difficult to set up and operate efficiently than conventional schlieren or shadowgraph techniques.

Brown & Roshko (1974) and Winant & Browand (1974) primarily relied on flow visualizations of streaklines to study the motion of large scales. Optical flow diagnostics are indispensable in the analysis of experimental flows, but can not be a replacement because interpretations of flow visualization are difficult to achieve correctly. They provide a 'quick picture' to an overall flow in a brief amount of time that would otherwise require large amounts of experimental measurements to infer the observed characteristics.

III.3.1 Shadowgraph and Schlieren

Large scale toroidal vortices observed by shadowgraph and schlieren diagnostics roll up into clearly identifiable

structures in the vicinity of the nozzle exit. Additionally, a small number of streamwise vortices appear following the first vortex merging. After the first two vortex mergings, both the ring vortices and streamwise structures become obscured in a field of 'rough' turbulence. This is due to the integration of light through the entire flow field by conventional shadowgraph and schlieren methods. Nevertheless, one can appreciate the overall spreading of the jet and quantitatively the 'visual' spreading angle with respect to the centerline is as much as four times greater in the minor axis plane (25°) as compared to the major axis plane (6°). The ring vortices appear horizontal in the major axis plane and they appear 'bent' and to overlap each other somewhat in the minor axis plane. The distorted shape of the rings in the minor axis plane confirms the predicted convoluted motions of the minor axis section in the self-inducting elliptic vortices.

A non-homogeneous axisymmetric jet was also investigated and found to 'visually' spread at an approximately similar angle as in the major axis plane. The appearance of the large scales duplicated those visible in the major axis plane of the elliptic jet and few if any streamwise vortices were apparent. The existence of similar characteristics in the axisymmetric jet and major axis plane of the elliptic jet may be corollary to sensor measurements indicating similar rates of entrainment and spreading angles in the two regions. The profile of the turbulent interface appears less irregularly shaped than that of either plane in the elliptic jet. The visual evidence regarding the axisymmetric jet conclusively supports the elliptic jet's unique properties of larger spreading rates and irregularly shaped elliptic vortices.

III.3.2 Focusing Schlieren

As in the previous method of visualization, focusing schlieren confirmed an initially laminar jet rolling up into large toroidal vortices. Observations of the flow by focusing schlieren reveals cross-sections of the large scale vortices when imaging planar cuts through the center of the jet. Otherwise, focusing at other cross-sections reveal vortical structures at oblique angles. The 'rough' turbulence seen by the previous methods are not observed. Focusing schlieren allows observations of the ensuing development of the large scale structures farther downstream than conventional optical diagnostic methods. Streamwise vortices are barely distinguishable when focusing on the edge of the flow field because the 'cuts' are vertical and the jet along with its streamwise structures spreads outwards diagonally such that the entire streamwise structure is not visible in the plane of focus.

Similar to the findings made by the shadowgraph and schlieren system, the cross-sections of the large scales are horizontally situated in the major axis plane but they are tilted at large angles with respect to each other when viewed from the minor plane. Quantitative measurements of the separation and size of the large scales can be determined from digitized images of the flow and the measured scale of the initial vortex agrees with calculated values. These visualizations may suggest the onset of helical stability modes overpowering the initially axisymmetric modes of the elliptic vortices (Ho, Huerre & Redekopp 1990). Refer to figure 42. Finally, side jets were not observed for any density ratio or exit velocity and it is apparent that side jets form only in axisymmetric jets at low density ratios (Monkewitz, Bechert, Bariskow & Lehmann 1990).

III.4 Forced Jet

A brief forcing investigation was performed on a homogeneous jet operating at a low velocity of 8 m/s. Four speakers emitted sinusoidal acoustic waves into four chambers that were symmetrically located with respect to the major and minor axes. The perturbations entered the flow at the nozzle edge from four opposite directions. Forcing was done at the most amplified frequency and at very low amplitudes so as not to alter the velocity mean profile and influence the initial stability. The laminar flow at the nozzle exit exhibited a more organized pattern in that the instantaneous velocity signal displayed on an oscilloscope became more sinusoidal and less random when either or both of the major and minor pairs of opposing speakers forced the flow (in-phase forcing). The same results were observed for anti-phase forcing, when either pair of opposing speakers were operated with a 180° phase shift with respect to the other speaker pair. Under these flow and forcing conditions it appeared neither the major axis or minor axis region was more responsive to small amplitude forcing. This is interesting in light of previous measurements indicating similar near field pressure fluctuations in both the major and minor axes regions of the subsonic elliptic jet (Gutmark & Ho 1985).

III.5 Jet with Suction

The homogeneous elliptic jet is convectively unstable. Introducing nonhomogeneity into the flow by reducing the density ratio did not alter the jet's global stability modes. Subsequently, the effects of increased velocity ratio was briefly investigated by applying suction uniformly along the edge of the elliptic jet nozzle. The study was motivated by the predictions of spatio-temporal instability theory (Huerre & Monkewitz 1990) and a recent experimental study of counter-current mixing layers in an axisymmetric jet (Strykowski & Niccum 1990). Theory predicts a critical velocity ratio, $R_{crit} = 1.32$, in a mixing layer where the flow transitions from convective to absolute instability and this has been verified experimentally for axisymmetric jets. Spatio-temporal instability theory also predicts a transition to absolute instability at

density ratios < 0.7 , however absolutely unstable regions were not noticed in the nonhomogeneous elliptic jet for density ratios as low as 0.66. It is possible that asymmetric jets, specifically 2:1 aspect-ratio elliptic jets, are characterized by critical velocity and density ratios different from mixing layers.

Suction was applied along the circumference of the elliptic nozzle raising the velocity ratio up to 5 and the subsequent changes in the nonhomogeneous flow were immediately observed by means of the focusing schlieren method. It must be noted that the trailing edge separating forward and reverse flow is not ideally thin but is approximately 25 initial momentum thicknesses wide due to structural constraints imposed by heat stresses upon the aluminum-composite nozzle. Flow visualization revealed a decreased distance to the first vortex merging, the elimination of the initial laminar region and a shortening of the potential core. It appeared the virtual origin of the jet was being translated upstream by the effects of suction.

Measurements of mean quantities in a homogeneous flow were sampled at low exit velocities of 20 m/s. Reverse velocities were not measured with available sensors. Pitot tube measurements of centerline mean velocities verified a shortening of the potential core under the effects of suction from $x/a = 4$ to $x/a = 3.5$. Mean velocity profiles decreased as much as 15% and halfwidth calculations indicated decreased spreading in both axes. However, in the shear layer velocity fluctuations did not differ for all velocity ratios ≥ 1 except at the exit where the amplitudes were one order of magnitude higher in the case, $R > 1$. Massflow measurements showed that suction reduced entrainment ratios in an elliptic jet albeit higher than in an axisymmetric jet.

No firm conclusions regarding the existence of absolute instability were obtained from the study, and the configuration of the thick trailing edge may have been responsible for these results.

III.6 Rectangular Orifice Jets

Nonhomogeneous rectangular orifice jets characterized by 1:1, 2:1, 3:1 and 4:1 aspect ratios with constant hydraulic diameter were visualized by focusing schlieren. The passive and active control of the spreading of rectangular orifice jets was investigated at velocities between 30 m/s to 80 m/s and temperatures up to 150 C. For natural flows, the 'visual' jet width and overall spread angle did not exhibit significant changes in either major or minor axes. Side jets were not observed reinforcing current beliefs confining their existence to nonhomogeneous axisymmetric flows. External forcing by a single speaker located outside the near field also presented no visual change in jet width or spread angle. However, at extremely low exit velocities around 15 m/s, forcing effects became dramatically noticeable and the shear layer thickened as much as 33% and the 'visual' spreading angle increased by 25%. Evidently the amplitude of the acoustic waves was not large enough to influence jet flows at higher exit velocities. In the proposed study, stronger speakers driven by powerful amplifiers will alleviate this issue.

IV. PROPOSED RESEARCH

Investigations of the nonhomogeneous flow field will be concluded to understand the mechanism(s) driving the vorticity dynamics of the self-inducting coherent structures. The primary task will then be the investigation of the small scale topology in a homogeneous 2:1 aspect-ratio elliptic jet. The effects of self-induction and vortex merging upon the generation of small scales will be examined. The unforced elliptic jet in an addition to an axisymmetric jet will be studied initially for purposes of later comparison. Forcing the flow uniformly at the preferred mode at the exit will mask the effects of vortex merging and isolate the effects of self-induction. Measurements will be conducted of the populations, dimensions, frequencies and spatial distribution of the small scales with respect to the large scales using the Peak-Valley-Counting method. Finally, the flow will be actively controlled with acoustic forcing add the nozzle exit. Multiple frequency signals with variable phase shifts and amplitudes will be employed to increase production of small scales and enhance the small scale mixing process.

IV.1 Nonhomogeneous Jet

A dual parallel wire probe housing both a hot- and cold-wire will simultaneously measure turbulent velocity and temperature signals. Two cases will be studied, a high temperature jet at 180 C to observe strong nonhomogeneous effects and a slightly heated jet at 45 C where temperature will contaminate the flow effectively 'tagging' the large scale structures. Velocity-temperature correlations will be made to determine how nonhomogeneity modifies the dynamics of the elliptical structures and enhances the entrainment. As well, the initial boundary layer thickness will be investigated to confirm the effects of Reynolds number upon axis switching and entrainment.

IV.2 Small Scale Topology

The phase relationship between the major and minor axes sections of the distorted large scale vortical structures in an unforced natural elliptic jet will be investigated by simultaneous velocity measurements in both shear layer regions. The small scale topology of the natural elliptic jet will then be investigated. It is not known definitely at what Reynolds number elliptic jets become turbulent. The exit velocity will initially be varied to determine a velocity that is not so low that will preclude small scale production and not too high that will cause problems with the physical resolution of the 1 mm wide hot-wire sensor and the maximum 1 MHz sampling rate of the analog-to-digital converter.

Irrotational fluctuations are induced into the quiescent fluid by the passing of large scale structures in the shear layer. Quantitative knowledge regarding the large scale vortices will be obtained from the velocity signals sampled by a hot-wire anemometer in the ambient fluid adjacent to the shear layer. Simultaneously, a second hot-wire probe separated radially from the first probe will be located within the shear layer to acquire the combined turbulent signals of the large and small scales. These pairs of measurements will be undertaken at incremental downstream locations in the major and minor axes. The facility may also be heated by a few degrees to contaminate the flow using heat as a tracer and a cold-wire anemometer will sample the thermal fluctuations of the slightly heated large scales.

Phase-averaged information from the first sensor will provide the period of the large scales to help isolate the signature of the small scales. Spectral analyses of the velocity signals by a one-dimensional fast Fourier algorithm will yield the peak frequencies at the respective location in the flow. The slope of the resulting energy spectrum is not as clearly definable in jets as it is in plane mixing layers. Thus one of the 'signposts' suggesting the possible location of transition to turbulence, the '-5/3' slope, will not be employed.

Lauffer (1948) and Liepmann (1949) proposed a method for estimating the Taylor microscale by counting the number of 'zero-crossings' of a random stationary fluctuating velocity signal. Rice (1944, 1945) determined a theoretical value of the number of 'zero-crossings', N_0 , for Gaussian distributed u' and du'/dt signals. Refer to Equation 16. Gaussian characteristics occur far downstream along the centerline in axisymmetric jets (Wynanski & Fiedler 1969). A more refined method, the Peak-Valley-Counting method, incorporating specialized conditional analysis concepts will be used to determine the dimension and amount of small scales (Hsiao 1985; Huang 1985; Zohar 1990). This method generates a pulse train corresponding to the proper local extrema associated with small scale fluctuations in a turbulent velocity signal. The final result is obtained by differentiating between actual small scale fluctuations (the 'peaks' and 'valleys'), including the removal of erroneous consecutive extrema, a-d-c bit noise components and random high-frequency noise by employing appropriate amplitude and temporal threshold levels. The number of small scales will be regarded as a possible indicator of turbulent transition (Zohar 1990).

$$N_0 = \frac{1}{\pi} \frac{\left(\frac{\partial u'^2}{\partial t} \right)^{1/2}}{(u'^2)^{1/2}}$$

Analysis of the distribution of scales will incorporate a two-dimensional Wavelet Transform (Grossman & Morlet 1984). The combined Fourier and physical space properties of this method of decomposing turbulent signals provide a better view of the dynamics of coherent structures (Dallard & Spedding 1990). In contrast, the Fast Fourier Transform algorithm retains only the amplitude or phase information of the spectral components of the transformed turbulent signal.

IV.3 Self-Induction Effects

The interactions of merging vortices and streamwise structures is hypothesized to aid in the generation of small scales in the vortex cores of plane mixing layers and axisymmetric jets. The existence of a second mechanism responsible for the growth of a 2:1 aspect-ratio elliptic jet is the process of vortex self-induction. This second mechanism appears to be more responsible for increased entrainment ratios than vortex merging and may well be responsible for the generation of small scales in the elliptic jet. The flow will be forced at the preferred mode of the jet, $\Omega_d = f_d d / U_{exit}$, where ' f_d ' is obtained from the peak frequency of the 1-D energy spectrum at the end of the potential core ($x/a=5$). Forcing will inhibit the actions of vortex pairing and thereby will isolate the effects of self-induction. In this manner, the small scales will be investigated to determine how their production is modified by the presence of self-inducting vortices. Additionally, the spreading rate and entrainment ratios will be measured to confirm the importance of vortex self-induction on the development of small aspect-ratio elliptic jets.

Streamwise structures will be measured as well by hot-wire probes placed in the shear layer at a given downstream cross-section. Previous flow visualization indicates these vortices to be fairly stationary in space. It will be important to determine the distorting azimuthal effects of the streamwise upon the elliptical vortex rings and how self-induction and vortex merging modifies the streamwise structures because of the importance of interactions between these large scales towards small scale production.

IV.4 Active Control

The 2:1 aspect ratio elliptic jet was found by Ho and Gutmark (1987) to entrain considerably more mass than an ordinary axisymmetric jet due to the natural dynamics and deformations of the self-inducing elliptic vortices. It is, therefore, an efficient passive control device. From an engineering point of view, passive enhancements are more desirable than active methods. However, acoustic forcing has been demonstrated to increase the number of small scales, Zohar (1990). The elliptic jet will be actively forced to control the large and small scales to improve large and small scale mixing. It has also been discovered that increased entrainment is correlated to a shorter distance between the location of axis switching and the nozzle exit, Ho & Austin (1988). Thus, to control the location of switching by forcing the large scales, perhaps to lessen influence by vortex merging, may further enhance entrainment.

In this vein, multiple frequency forcing incorporating harmonic plus various subharmonic components with variable phase shifts and variable amplitudes will be attempted. Helically phase shifted frequencies may form 'spinning' elliptic vortices (Long & Petersen 1990) to further distort the inviscid large scales thereby increasing entrainment and, second, to increase the production of small scales and enhance fine scale mixing. The flow will be measured by hot-wires and analyzed with the Peak-Valley Counting method.

V. CONCLUSION

Jets are important fluid dynamical processes of study due to the existence of mixing regions in numerous applications. In particular, 2:1 aspect-ratio elliptic jets appear by many accounts to be very promising improvements over axisymmetric jet configurations because of their enhanced mixing capabilities. Coherent large scale structures which govern spreading, entrainment and large scale mixing in general have been investigated to reveal the importance of the mechanisms of vortex self-induction and vortex merging. It is important to continue detailed investigation of the 2:1 aspect-ratio elliptic jet aimed at the topology of the small scales and the nature of their production by the large scale structures. Methods of controlling and increasing the population of small scales will help in the understanding of their subsequent effects upon fine scale mixing in relation to combustion processes.

BIBLIOGRAPHY

- Ali, S. Hot-wire anemometry in moderately heated flow *Review of Scientific Instruments*, Feb. 1975, 46(2): 185-191.
- Antonia, A., Brown, L., Chambers, A. Determination of time constants of cold wires *Review of Scientific Instruments*, Sept. 1981, 52(9): 1382-1385.
- Arbey, H., Ffowcs Williams, J. Active cancellations of pure tones in an excited jet *Journal of Fluid Mechanics*, 1984, 149: 445-454.
- Austin, T., Ho, C.M. Entrainment of Asymmetric Jets AFOSR Turbulence Research Contractor's Meeting, 1988.
- Austin, T., Ho, C.M. Temperature Effects on Entrainment of an Elliptic Jet. *Bull. of American Physical Society*, 1988, 33: 2237.
- Austin, T., Schreck, S. Planar Imaging of a Heated Elliptic Jet by the Focusing Schlieren Method Proceedings of 1990 Fall Meeting of the Western States Section/The Combustion Institute, Oct. 1990.
- Batchelor, G. *The Theory of Homogeneous Turbulence* Cambridge University Press, Cambridge, 1953:103-105.
- Batchelor, G. *An Introduction to Fluid Dynamics* Cambridge University Press, Cambridge, 1967: 509-510.
- Batchelor, G., Gill, E. Analysis of the stability of axisymmetric jets *Journal of Fluid Mechanics*, 1962, 14: 529-551.
- Becker, H., Massaro, T. Vortex evolution in a round jet *Journal of Fluid Mechanics*, 1968, 31: 435-448.
- Betchov, R., Criminale, W. *Stability of Parallel Flows* Academic Press, New York, 1967.
- Bendat, J., Piersol, A. *Random Data: Analysis and Measurement Procedures* Wiley-Interscience, N.Y., 1971
- Benney, D., Lin, C. On the secondary motion induced by oscillations in a shear flow *Physics of Fluids*, 1960, 3: 656-657.
- Bernal, L. The coherent structure of turbulent mixing layers. I. Similarity of the primary vortex structures. II. Secondary streamwise vortex structure Ph.D. Thesis, California Institute of Technology, 1981.
- Bernal, L., Rosikco, A. Streamwise vortex structure in plane mixing layers *Journal of Fluid Mechanics*, 1986, 170: 499-525.

- Bertin, J. *Engineering Fluid Mechanics* Prentice-Hall, Englewood Cliffs, 1984: 12-13.
- Betchov, R., Criminale, W. *Stability of Parallel Flows* Academic, New York, 1967.
- Blackwelder, R. Hot wire and hot film anemometers *Methods of Experimental Physics: Fluid Dynamics*, 1981, 18A: 259-314.
- Blackwelder, R. Coherent Structures Associated with Turbulent Transport 2nd International Symposium on Transport Phenomena in Turbulent Flows, 1987.
- Blumen, W. Shear layer instability of an inviscid compressible fluid *Journal of Fluid Mechanics*, 1970, 40: 769-781.
- Bogdanoff, D. Compressibility Effects in Turbulent Shear Layers *AIAA Journal*, 1982, 21(6): 926-927.
- Bouchard, E., Reynolds, W. The Structure and Growth of the Mixing Layer Region of a Round Jet Report TF-17, Stanford University, 1982.
- Boussinesq, J. Essai sur la théorie des eaux courantes *Mém. prés. par div. savants à l'Acad. sci. Paris*, 1877, 23: 1-680.
- Brachet, M., Orszag, S., Nicke, B., Mori, R., Frisch, U. Small-scale structure of the Taylor-Green vortex *Journal of Fluid Mechanics*, 1983, 130: 411-452.
- Bradshaw, P. The effect of initial conditions on the development of a free shear layer *Journal of Fluid Mechanics*, 1966, 26: 225-236.
- Breidenthal, R. A chemically reacting turbulent shear layer Ph.D. Thesis, California Institute of Technology, 1978.
- Breidenthal, R. Structure in turbulent mixing layers and wakes using a chemical reaction *Journal of Fluid Mechanics*, 1981, 109: 1-24.
- Brigham, E. *The Fast Fourier Transform and its Applications* Prentice-Hall, Englewood Cliffs, 1983.
- Broadwell, J., Breidenthal, R. A simple model of mixing and chemical reaction in a turbulent shear layer *Journal of Fluid Mechanics*, 1982, 125: 397-410.
- Browand, F. An experimental investigation of the instability of an incompressible separated shear layer *Journal of Fluid Mechanics*, 1966, 26: 281-307.
- Browand, F. The Structure of the Turbulent Mixing Layer *Physica*, 1986, 18D: 135-148.
- Browand, F., Cnu, W., Laufer, J. Exploratory Experiments on the Entrance Effects in Subsonic Jet Flows Internal report 136, University of Southern California, 1975.
- Browand, F., Laufer, J. The Role of Large Scale Structures in the Initial Development of Circular Jets Proceedings of 4th Biennial Symposium on Turbulence in Liquids, Univ. of Missouri-Rolla, Sept. 1975: 333-344.
- Browand, F., He, C.M. The mixing layer: an example of quasi two-dimensional turbulence *Journal of Mech. Theor. Appl. Special Suppl.*, 1983: 99-120.
- Browand, F., Troutt, T. A note on spanwise structure in the two-dimensional mixing layer *Journal of Fluid Mechanics*, 1980, 97: 771.
- Browand, F., Weidman, P. Large scales in the developing mixing layer *Journal of Fluid Mechanics*, 1976, 76: 127-144.
- Brown, G., Roshko, A. On Density Effects and large structure in turbulent mixing layers *Journal of Fluid Mechanics*, 1974, 64, part 4: 775-816.
- Burton, R. A Modified Schlieren Apparatus for Large Areas of Field *Journal of the Optical Society of America*, Nov. 1949, 37(11): 907-908.
- Cohen, Z., Wignanski, I. The evolution of instabilities in the axisymmetric jet *Journal of Fluid Mechanics*, 1987, 176: 191-235.
- Cooley, J., Tukey, J. An algorithm for the machine calculation of complex fourier series *Mathematics of Computing*, April 1965, 19(30): 297-301.
- Cercos, G. The mixing layer: deterministic models of a turbulent flow U.C. Berkeley Mech. Eng. Report FM-79-2, 1979.

- Corcus, G., Sherman, F. Vorticity concentration and the dynamics of unstable free shear layers *Journal of Fluid Mechanics*, 1976, 73: 241-264.
- Corcus, G., Lin, S. The mixing layer: deterministic models of a turbulent flow. Part 2. The origin of the three-dimensional motion *Journal of Fluid Mechanics*, 1984, 139: 67.
- Corrsin, S. NACA Wartime Reports Note, No. 94, 1943.
- Corrsin, S. Extended Applications of the Hot-Wire Anemometer *Review of Scientific Instruments*, 18(7) July 1947: 469-471.
- Corrsin, S., Uberoi, M. NACA Technical Notes, No. 1865, 1949.
- Corrsin, S., Uberoi, M. NACA Technical Notes, No. 2124, 1950.
- Crighton, D. Instability of an elliptic jet *Journal of Fluid Mechanics*, 1973, 59: 665-672.
- Crighton, D. Acoustics as a branch of fluid mechanics *Journal of Fluid Mechanics*, 1981, 106: 261-298.
- Crighton, D., Gaster, M. Stability of slowly diverging jet flow *Journal of Fluid Mechanics*, 1976, 77: 397-415.
- Crow, S., Champagne, F. Orderly Structure in Jet Turbulence Boeing Sci. Res. Lab., Document D 1-82-0991, 1970.
- Crow, S., Champagne, F. Orderly Structure in Jet Turbulence *Journal of Fluid Mechanics*, 1971, 48: 547-591.
- Culick, E. Combustion Instabilities in Liquid-Fueled Propulsion Systems- An Overview Internal report, California Institute of Technology, Oct. 1983.
- Dallard, T., Spedding, G. 2-D Wavelet Transforms: Generalization of the Hardy space and application to experimental studies submitted to *SIAM J. Math. Anal.*, 1990.
- Dhanak, M., DeBernardinis, B. The Evolution of an Elliptic Vortex Ring *Journal of Fluid Mechanics*, 1981, 109: 189-216.
- Dimotakis, P., Brown, G. The mixing layer at high Reynolds number, large-structure dynamics and entrainment. *Journal of Fluid Mechanics*, 1976, 78: 535-560.
- Drazin, P., Reid, W. *Hydrodynamic Stability* Cambridge University Press, London, 1981.
- Drubka, R. Instabilities in near field of turbulent jets and their dependence on initial conditions and Reynolds number Ph.D. Thesis, Ill. Inst. Tech., 1981.
- Fiedler, H., Dziemba, B., Mensing, P., Rösgen, T. Initiation, evolution and global consequences of coherent structures in turbulent shear flows in *The Role of Coherent Structures in Turbulence and Mixing, Lecture Notes in Physics* ed. Jimenez, J., Springer, Berlin, 1981, 136: 219-251.
- Fiedler, H., Mensing, P. The plane turbulent shear layer with periodic excitation *Journal of Fluid Mechanics*, 1985, 150: 281-309.
- Freythuth, P. On the transition in a separated laminated boundary layer *Journal of Fluid Mechanics*, 1966, 25: 683-704.
- Fuchs, R., Michel, U. Experimental evidence of turbulent source coherence affecting jet noise AIAA paper, 1977, 77-1348.
- Gaster, M. A note on the relation between temporally-increasing and spatially-increasing disturbances in hydrodynamic stability *Journal of Fluid Mechanics*, 1952, 14: 222-224.
- Givi, P., Jou, W., Metcalfe, R. 21st International Symposium on Combustion, the Combustion Institute. 1986.
- Gropenzeisser, H. Contribution to the Stability of free boundary layers in compressible media Deutsche luft- und Raumfahrt, 1969, FB 69-25.
- Grossman, A., Morlet, J. Decomposition of hardy functions into square integrable wavelets of constant shape *SIAM J. Math. Anal.*, 1984, 15(4): 723-736.
- Gutmark, E., Ho, C. M. Development of an Elliptical Jet *Journal of American Physical Society*, 1982, 27: 1184.
- Gutmark, E., Ho, C. M. On a Forced Elliptic Jet Proceedings of 4th Turbulent Shear Flow Conference, Karlsruhe, Germany,

- Springer, 1983.
- Gutmark, E., Ho, C.M. Preferred modes and the spreading rates of jets *Physics of Fluids*, Oct. 1983, 2(10): 2932-2938.
- Gutmark, E., Ho, C. M. Visualization of a Forced Elliptic Jet Internal Report, University of Southern California, 1983.
- Gutmark, E., Ho, C. M. Near-Field Pressure Fluctuations of an Elliptic Jet *AIAA Journal*, 1985, 23(3): 345-358.
- Gutmark, E., Ho, C. M. Visualization of a Forced Elliptic Jet *AIAA Journal*, 1986, 24: 684-685.
- Gutmark, E., Parr, D., Hanson-Parr T., Schadow, K. On the Role of Large and Small-Scale Structures in Combustion Control *Combustion Science & Technology*, 1989, 66: 107-126.
- Gutmark, E., Parr, D., Parr, T., Schadow, K. Azimuthal Structure of an Annular Diffusion Flame *Combustion and Flame*, 1989, 75: 229-240.
- Gutmark, E., Schadow, K., Parr, D., Harris, C., Wilson, K. The mean and turbulent structure of noncircular jets AIAA paper, Mar. 1985, 85-0543.
- Gutmark, E., Schadow, K., Parr, T., Parr, D., Wilson, K. Noncircular jets in combustion systems AIAA paper, 1987, 87-1379.
- Gutmark, E., Schadow, K., Wilson, K., Bicker, C. Near-field pressure radiation and flow characteristics in low supersonic circular and elliptic jets *Physics of Fluids*, Sept. 1988, 31(9): 2524-2532.
- Gutmark, E., Wilson, K., Schadow, K. Combustion Enhancement in Supersonic Coaxial Flows AIAA paper, 1989, 89-2788.
- Guyon, E. Self-sustained oscillations in low density jets internal report, U.S.C., 1988.
- Harje, D., Reardon, F., (editors) Liquid Propellant Rocket Combustion Instability NASA SP-194, Washington, D.C., 1972.
- Hermanson, J., Dimotakis, P. Effects of heat release in a turbulent, reacting shear layer *Journal of Fluid Mechanics*, 1989, 199: 333-375.
- Hertzberg, J., Ho, C.M. Time averaged 3d flow in a rectangular sudden expansion AIAA paper, Jan. 1991, 91-0040.
- Hiley, P., Wallace, H., Booz, D. Nonaxisymmetric Nozzles Installed in Advanced Fighter Aircraft *Journal of Aircraft*, Dec. 1976, 13, no. 12: 1000-1006.
- Hinze, J. Turbulence McGraw-Hill, New York, 1959.
- Ho, C. M. Local and global dynamics of free shear layers in *Numerical and Physical Aspects of Aerodynamic Flows*, edited by Cebeci, T., New York: Springer, 1981.
- Ho, C.M., Austin, T., Hertzberg, J. Entrainment of 3-D Shear Layers The Fourth Asian Congress of Fluid Mechanics, Aug. 1989.
- Ho, C. M., Gutmark, E. Visualization of a Forced Elliptic Jet *Bull. American Physical Society*, 1982, 27: 1184.
- Ho, C. M., Gutmark, E. Vortex Induction and mass entrainment in a small-aspect ratio elliptic jet *Journal of Fluid Mechanics*, 1987, 179: 383-405.
- Ho, C. M., Hsiao, F. Evolution of coherent structures in a lip jet in *Structure of Complex Turbulent Shear Layers* ed. Dumas, R., Fulachier, L., Springer, Berlin, 1983: 121-136.
- Ho, C. M., Huang, L. Subharmonics and vortex merging in mixing layers *Journal of Fluid Mechanics*, 1982, 119: 443-473.
- Ho, C. M., Huerre, P. Perturbed Free Shear Layer *Annual Review of Fluid Mechanics*, 1984, 16: 365-421.
- Ho, C. M., Huerre, P., Redekopp, L. Unsteady Behavior of Turbulent Shear Flows Final Technical Report, A.F.O.S.R. Contract No. F49620-85-C-0080, July 1990.
- Ho, C. M., Nosseir, N. Dynamics of an impinging jet. Part 1. The feedback phenomenon *Journal of Fluid Mechanics*, 1981, 105: 119-142.
- Ho, C. M., Nosseir, N. Dynamics of an impinging jet. Part 2. The noise generation *Journal of Fluid Mechanics*, 1982, 116: 379-391.

- Ho, C.M., Zohar, Y., Foss, J. Phase Decorrelation of Coherent Structures in a Free Shear Layer submitted to *Journal of Fluid Mechanics*, 1991.
- Ho, C. M., Zohar, Y., Moser, R., Rogers, M., Lele, S., Buell, J. Phase decorrelation, streamwise vortices and acoustic radiation of mixing layers in *Studying Turbulence Using Numerical Simulation Databases II*, proceedings of 1988 summer program of the Center for Turbuence Research, report CTR-s88, 1989: 29-39.
- Hsiao, F. Small scale transition and preferred mode in an initially laminar plane jet Ph.D. Thesis University of Southern California, 1985.
- Huang, L. Small scale transition in a two-dimensional mixing layer Ph.D. Thesis, University of Southern California, 1985.
- Huang, L., Ho, C. M. Small-scale transition in a plane mixing layer *Journal of Fluid Mechanics*, 1990, 210: 475-500.
- Huerre, P., Monkewitz, P. Absolute and convective instabilities in free shear layers *Journal of Fluid Mechanics*, 1985, 159: 151-168.
- Huerre, P., Monkewitz, P. Local and global instabilities in spatially developing flows *Annual Review of Fluid Mechanics*, 1990, 22: 473-537.
- Hussain, A., Zedan, M. Effects of the initial condition on the axisymmetric free shear layer: effects of the initial momentum thickness *Physics of Fluids*, 1978, 21: 1100-1112.
- Jimenez, J. A spanwise structure in the plane shear layer *Journal of Fluid Mechanics*, 1983, 132: 319-336.
- Jimenez, J., Cogollos, M., Bernal, L. A perspective view of the plane mixing layer *Journal of Fluid Mechanics*, 1985, 152: 125-1985.
- Jimenez, J., Martinez-Val, R., Rebollo, M. On the origin and evolution of three-dimensional effects in the mixing layer Internal report DA-ERO 79-G-079, Univ. Politec., Madrid, 1979.
- Jou, W., Knoke, G., Ho, C.M. Entrainment Enhancement of a Supersonic Jet for Advanced Ejectors Department of Energy Ejector Conference, 1988.
- Kantrowitz, A., Trimpf, R. A Sharp Focusing Schlieren System *Journal of the Aeronautical Sciences*, May 1950, 17(5): 311-319.
- Kelly, R. On the stability of an inviscid shear layer which is periodic in space and time *Journal of Fluid Mechanics*, 1967, 27: 657-689.
- Kibens, V. Discrete noise spectrum generated by an acoustically excited jet *AIAA Journal*, 1981, 18: 434-441.
- Kibens, V., Wlezien, R. Active Control of Jets from Indeterminate Origin Nozzle AIAA paper, 1985, 85-0542.
- Konrad, J. An experimental investigation of mixing in two-dimensional turbulent shear flow with applications to diffusion limited chemical reactions Technical Report, California Institute of Technology-8-PU, 1976.
- Koshigoe, S., Ho, C.M., Tubis, A. Application of a generalized shooting method to the linear instability analysis of elliptic core jets AIAA paper, Oct. 1987, 87-2733.
- Krothapalli, A., Baganoff, D., Karamcheti, K. On the Mixing of a Rectangular Jet *Journal of Fluid Mechanics*, 1981, 107: 201-220.
- Krothapalli, A., Hsia, Y., Baganoff, D., Karamcheti, K. On the Structure of an Underexpanded Rectangular Jet JIAA TR-47, July, 1982.
- Lamb, H. *Hydrodynamics* Cambridge University Press, Cambridge, 1932: 242-243.
- Lasheras, J., Cho, J., Maxworthy, T. On the origin and evolution of streamwise vortical structures in a plane, free shear layer *Journal of Fluid Mechanics*, 1986, 172: 231-258.
- Laufer, J. Ph.D. Thesis, California Institute of Technology, 1948.
- Laufer, J., Monkewitz, P. On turbulent jet flow in a new perspective AIAA paper, 1980, 80-0962.
- Laufer, J., Yen, T. Noise generation by a low Mach number jet *Journal of Fluid Mechanics*, 1983, 134: 1-31.

- Lee, M., Reynolds, W. Bifurcating and Blooming Jets Report TF-22, Stanford University, 1985.
- Liepmann, H. *Hekt. Phys. Acta*, 1949, 2: 119.
- Liepmann, H., Laufer, J. Investigation of free turbulent mixing NACA Technical Note No. 1257, 1947.
- Liepmann, H., Roshko, A. *Elements of Gasdynamics* John Wiley & Sons, New York, 1957: 153-170.
- Lin, C. C. *The Theory of Hydrodynamic Stability* University Press, Cambridge 1955.
- Lin, S. The evolution of streamwise vorticity in the free shear layer Ph.D. Thesis, Univ. Cal. Berkeley, 1981.
- Lin, S., Corcos, J. The mixing layer: deterministic models of a turbulent flow. Part III: The effect of plane strain on the dynamics of streamwise vortices. *Journal of Fluid Mechanics*, 1984, 141: 139.
- Liu, J. Interactions between large scale coherent structures and fine-grained turbulence in free shear flows in *Transition and Turbulence*, Academic, N.Y., 1981.
- Longmire, E., Eaton, J. Structure and Control of a Particle-Laden Jet Report No. MD-58, Sept. 1990.
- Long, T., Petersen, R. Controlled Interactions in a Forced Axisymmetric Jet. Part I, The Distortion of the Mean Flow submitted to *Journal of Fluid Mechanics*, Dec. 1989.
- Masutani, S., Bowman, C. The structure of a chemically reacting plane mixing layer *Journal of Fluid Mechanics*, 1986, 172: 93-126.
- Mattingly, G., Chang, C. Unstable waves on an axisymmetric jet *Journal of Fluid Mechanics*. 1974, 65: 541-560.
- Maxworthy, T. Some experimental studies of vortex rings *Journal of Fluid Mechanics*, 1977, 81: 465-495.
- McClellan, P. Digital Signal Processing II, *IEEE Press*, 1976.
- McMurtry, P., Riley, J., Metcalfe, R. Effects of heat release on the large-scale structure in turbulent mixing layers. *Journal of Fluid Mechanics*, 1989, 199: 297-332.
- Merzkirch, W. *Flow Visualization* Academic Press, Orlando, 1987:115-234.
- Michalke, A. On the inviscid instability of the hyperbolic-tangent velocity profile *Journal of Fluid Mechanics*, 1964, 19: 543-556.
- Michalke, A. Vortex formation in a free boundary layer according to stability theory *Journal of Fluid Mechanics*, 1965, 22: 371-383.
- Michalke, A. On spatially growing disturbances in an inviscid shear layer *Journal of Fluid Mechanics*, 1965, 23: 521-544.
- Michalke, A. The influence of the vorticity distribution on the inviscid instability of free shear layer *Fluid Dynamics Trans.*, published by Polish Academy of Sciences, Warsaw, 1969, 4: 751-760.
- Michalke, A. A note on the spatial jet-instability of the compressible cylindrical vortex sheet. Deutsche Luft- und Raumfahrt, 1970, Mitt. 70-51.
- Michalke, A. Instabilität eines kompressiblen runden Freistrahls unter Berücksichtigung des Einflusses der Strahlgrenzschichtdicke *Zeitschrift für Flugwissenschaften*, 1971, 19, no. 8/9: 319-328.
- Michalke, A., Hermann, G. On the inviscid instability of a circular jet with external flow *Journal of Fluid Mechanics*, 1982, 114: 343-359.
- Michalke, A., Schade, H. Stability of free boundary layer *Ing.-Arch.*, 1963, 33: 521-1-23.
- Miksad, R. Experiments on the nonlinear stages of free shear layer transition *Journal of Fluid Mechanics*, 1972, 51 (4): 695-719.
- Miksad, R. Experiments on nonlinear interactions in the transition of a free shear layer *Journal of Fluid Mechanics*, 1972, 56(4): 695-719.
- Monkewitz, P. Subharmonic resonance, pairing and shredding in the mixing layer *Journal of Fluid Mechanics*, 1988, 188:

223-252.

- Monkewitz, P., Bechert, D., Bariskow, B., Lehmann, B. Self-excited oscillations and mixing in a heated round jet *Journal of Fluid Mechanics*, 1990, 213: 611-639.
- Monkewitz, P., Huerre, P. The influence of the velocity ratio on the spatial instability of mixing layers *Physics of Fluids*, 1982, 25: 1137-1143.
- Monkewitz, P., Sohn, K. Absolute Instability in Hot Jets and their Control AIAA paper, 1986, 86-1882.
- Monin, A., Yaglom, A. *Statistical Fluid Mechanics, Vol. 1* MIT Press, Cambridge, 1971.
- Monin, A., Yaglom, A. *Statistical Fluid Mechanics, Vol. 2* MIT Press, Cambridge, 1975.
- Morkovin, M., Paranjape, S. Acoustic excitation of shear layers *Zeitschrift für Flugwissenschaften*, 1971, 9: 328-335.
- Moris, P. Instability of Elliptic Jets *AIAA Journal*, Feb. 1988, 26, no. 2.
- Morris, P., Miller, D. Wavelike structures in elliptic jets AIAA paper, 1984, 84-0399.
- Ng, T., Bradley, T. Effect of Multifrequency Forcing on the Near-Field Development of a Jet *AIAA Journal*, Oct. 1988, 26, no. 10: 1201-1207.
- Orszag, S., Patera, A. Hydrodynamic stability of shear flows in *Chaotic Behavior Of Deterministic Systems*, proceedings of the Cours à l'École des Houches, North-Holland, Amsterdam, 1981: 621-662.
- Oste, D., Wygnanski, I. The forced mixing layer between parallel streams *Journal of Fluid Mechanics*, 1982, 125: 91-130.
- Parekh, D., Leonard, A., Reynolds, W. Pifureating Jets at High Reynolds Numbers Report TF-35, Stanford University, 1988.
- Petersen, R. Influence of wave dispersion on vortex pairing in a jet *Journal of Fluid Mechanics*, 1978, 89: 469-495.
- Petersen, R., Samet, M. On the Preferred Mode of Jet Instability *Journal of Fluid Mechanics*, 1988, 194: 153-173.
- Pierrehumbert, R., Widnall, S. The two- and three-dimensional instabilities of a spatially periodic shear layer *Journal of Fluid Mechanics*, 1982, 114: 59-82.
- Plaschko, P. Helical instabilities of slowly divergent jets *Journal of Fluid Mechanics*, 1979, 92: 209-215.
- Prandtl, L. Bericht über Untersuchungen zur ausgebildeten Turbulenz *Zr. angew. Math. u. Mech.*, 1925, 5: 136-139.
- Rayleigh, Lord On the instability of jets *Proc. London Math. Soc.*, 1879, 10: 4-13.
- Rayleigh, Lord On the stability, or instability, of certain fluid motions *Scientific Papers*, Cambridge University Press, 1880, 1: 474-487.
- Reynolds, W., Bouchard, E. The effect of forcing on the mixing-layer region of a round jet in *Unsteady Turbulent Shear Flows*, ed. Michel, R., Cousteix, J., Houdeville, R. Springer, Berlin, 1981: 402-411.
- Rice, S. *Bell System Technical Journal*, 1944, 23: 82.
- Rice, S. *Bell System Technical Journal*, 1945, 24: 46.
- Riley, J., Metcalfe, R. Direct Numerical Simulation of a Perturbed Turbulent Mixing Layer AIAA paper, 1980, 80-0274.
- Roshko, A., Papamoschou, D. Observation of Supersonic Free Shear Layers AIAA paper, 1986, 86-0995.
- Saffman, P. The number of waves on unstable vortex rings *Journal of Fluid Mechanics*, 1977, 84: 625-639.
- Saffman, P., Baker, G. Vortex interactions *Annual Review of Fluid Mechanics*, 1979, 11: 95-122.
- Sato, H. Further investigation on the transition of two-dimensional separated layers at subsonic speed *Journal of Physical Society of Japan*, 1959, 14: 1797-1810.
- Sato, H. The stability and transition of a two-dimensional jet *Journal of Fluid Mechanics*, 1960, 7: 53-80.

- Schadow, K., Gutmark, E. Review of Passive Shear-Flow Control Research for Improved Subsonic and Supersonic Combustion AIAA paper, 1989, 89-2786.
- Schadow, K., Gutmark, E., Parr, T., Wilson, K. Control of Turbulence in Combustion Lecture Series in Engineering, Turbulent Reactive Flows Vol. 1, *Structure*, Springer-Verlag, 1989.
- Schadow, K., Gutmark, E., Parr, T., Wilson, K., Crump, J. Large-Scale Coherent Structures as Drivers of Combustion Instability AIAA paper, 1987, 87-1326.
- Schadow, K., Wilson, K., Crump, J., Foster, J., Gutmark, E. Interaction between acoustics and subsonic ducted flow with duct AIAA paper, Jan. 1984, 84-0530.
- Schadow, K., Wilson, K., Lee, M., Gutmark, E. Enhancement of Mixing in Ducted Rockets with Elliptic Gas-Generator Nozzles AIAA paper, 1984, 84-1266.
- Schetz, J. Volume 68, Progress in Astronautics and Aeronautics: "Injection and Mixing in Turbulent Flow" American Institute of Aeronautics and Astronautics, New York, 1980.
- Schreck, S., Ho, C.M. Coherent Structure Induced Pressure Fluctuations in an Elliptic Jet AIAA paper, Oct. 1990, 90-3963.
- Sfeir, A. Investigation of Three-Dimensional Turbulent Rectangular Jets AIAA paper, July 1978, 78-1185.
- Sforza, P., Steiger, M., Trentacoste, N. Studies on Three-Dimensional Viscous Jets *AIAA Journal*, 1966, 4(5): 800-806.
- Sforza, P., Stasi, W. Heated Three-Dimensional Turbulent Jets *Journal of Heat Transfer*, 1979, 101(2): 353-358.
- Sreenivasan, K. The azimuthal correlations of velocity and temperature fluctuations in an axisymmetric jet *Physics of Fluids*, April 1984, 27(4): 867-875.
- Sreenivasan, K., Raghun, S., Kyle, D. Absolute instability in variable density round jets *Experiments in Fluids*, 1989, 7: 309-317.
- Strykowski, P., Niccum, D. The Stability of Countercurrent Mixing Layers in Circular Jets submitted to *Journal of Fluid Mechanics*, 1990.
- Strange, P. Spinning modes in orderly jet structure and jet noise Ph.D. Thesis, University of Leeds, 1981.
- Stuart, J. Nonlinear stability theory *Annual Review of Fluid Mechanics*, 1971, 3: 347-370.
- Tam, C. Excitation of instability waves in a two-dimensional shear layer by sound *Journal of Fluid Mechanics*, 1978, 89: 357-371.
- Taylor, G. *Proc. Roy. Soc. London.*, 1932, 215A:1.
- Tennekes, H., Lumley, J. *A First Course in Turbulence* MIT Press, Cambridge, 1972, 104-135.
- Townsend, A. *The structure of turbulent shear flow* Cambridge University Press, Cambridge, 1956.
- Trentacoste, N., Sforza, P. Further Experimental Results for Three-Dimensional Free Jets *AIAA Journal*, 1967, 5(5): 885-891.
- Tyndall, J. On the action of sonorous vibrations on gaseous and liquid jets *Phil. Mag.*, 1867, 3: 375-391.
- Viets, H., Sforza, P. Dynamics of Bilaterally Symmetric Vortex Rings *Physics of Fluids*, 1972, 15: 230-240.
- Voce, J., Simpson, J. Some Recent Developments in the Understanding of Jet Noise Proceedings of the 8th CAS Congress, Amsterdam, 1972: 22-25.
- Watts, M. Flight Testing *Aerospace America*, 1989, 27(12): 47.
- Weidman, P., Brownad, F. Analysis of a simple circuit for constant temperature anemometry *Journal of Physics E: Scientific Instruments*, 1975, 8: 553-560.
- Weinstein, L. An Improved Large-Field Focusing Schlieren System AIAA paper, 1991, 91-0567.
- Widnall, S., Bliss, D., Tsai, C. The Instability of Short Waves on a Vortex Ring *Journal of Fluid Mechanics*, 1974, 66: 35-47.

- Wille, R. Beiträge zur Phänomenologie der Freistrahlen *Zeitschrift für Flugwissenschaften*, 1963, 11: 222-233.
- Winant, C. Vortex pairing in a turbulent shear layer at moderate Reynolds numbers Ph.D. thesis, University of Southern California, 1972.
- Winant, C., Browand, F. Vortex pairing: the mechanism of turbulent mixing layer growth at moderate Reynolds number *Journal of Fluid Mechanics*, 1974, 63: 237-255.
- Wynanski, I., *Aeronautics Quarterly*, 1964, 15: 373.
- Wynanski, I., Fiedler, H. Some measurements in the self-preserving jet *Journal of Fluid Mechanics*, 1969, 38: 577-612.
- Wynanski, I., Petersen, R. Coherent motion in excited free shear flows *AIAA Journal*, 1987, 25: 201-213.
- Wynanski, I., Oster, D., Fiedler, H. A Forced Plane Mixing Layer: A Challenge for the Predictor proceedings of 2nd Symposium on Turbulent Shear Flows, London, (1979).
- Yih, C. S. *Fluid Mechanics* University of Michigan, 1969:62-64.
- Yu, M., Monkewitz, P. The effect of non-uniform density on the absolute instability of two-dimensional jets and wakes *Physics of Fluids*, 1990, 2(7): 1175-1181.
- Yule, A. Large scale structures in the mixing layer of a round jet *Journal of Fluid Mechanics*, 1978, 88: 413-432.
- Zhang, Y., Ho, C.M., Monkewitz, P. The Mixing Layer Forced by Fundamental and Subharmonic, proceedings of IUTAM Symposium on *Laminar-Turbulent Transition* Springer-Verlag, Berlin, 1985: 385-395.
- Zohar, Y. Fine scale mixing in a free shear layer Ph.D. Thesis, University of Southern California, 1990.
- Zohar, Y., Foss, J., Ho, C.M., Buell, J. Phase decorrelation of coherent structures in a free shear layer in preparation, 1990.

LIST OF FIGURES

- 1) Figure 1 from Browand (1986).
- 2) Figure 5 from Ho & Huerre (1984).
- 3) Figure 2 from Browand (1986).
- 4) Figure 4 from Ho & Huerre (1984).
- 5) Figure 2 from Ho & Huerre (1984).
- 6) Figure 19 from Ho & Huerre (1984).
- 7) Figure 1 from Huerre & Monkewitz (1985).
- 8) Figure 30 from Ho & Huang (1982).
- 9) Figure 10 from Lasheras, Cho & Maxworthy (1986).
- 10) Figure 12 from Huang & Ho (1990).
- 11) Figure 17 from Ho, Zohar & Foss (1991).
- 12) Axisymmetric Jet Topology Illustration.
- 13) Figure 25(a) from Strykowski & Niccum (1990).
- 14) Figure 27(a) from Crow & Champagne (1971).
- 15) Figure 4 from Wynanski & Fiedler (1969).
- 16) Figure 14 from Browand & Lauier (1975).
- 17) Figure 7 from Petersen & Samet (1988).
- 18) Figure 21 from Crow & Champagne (1971).

- 19) Figure 20 from Monkewitz, Bechert, Bariskow & Lchmann (1990).
- 20) Vortex Ring Development Illustration
- 21) Figure 3 from Dhanak & DeBernardinis (1981).
- 22) Figure 15 from Ho & Gutmark (1987).
- 23) Figure 17 from Ho & Gutmark (1987).
- 24) Figure 16 from Ho & Gutmark (1987).
- 25) Figures 21 & 22 from Schadow & Gutmark (1989).
- 26) Figures 3a, 4b & 8a from Ho & Huang (1982).
- 27) Figure 21 from Gutmark, Parr, Hanson-Parr & Schadow (1989).
- 28) Figure 24 from Ho & Huerre (1984).
- 29) Figure 3 from Schadow & Gutmark (1989).
- 30) Figure 13 from Masutani & Bowman (1986).
- 31) 2:1 Aspect Ratio Elliptic Jet Facility Illustration.
- 32) Elliptic Jet Forcing Arrangement Illustration.
- 33) Focusing Schlieren System Illustration.
- 34) Mean Velocity Profiles for $U_c=30$ m/s, $T_c=30$ C.
- 35) Mean Velocity Contours for $U_c=30$ m/s, $T_c=30$ C.
- 36) Reynolds number effects on the mass entrainment.
- 37) Nonhomogeneous effects on the location of axis switching.
- 38) The location of axis switching scaling with Reynolds number and density ratio.
- 39) Entrainment ratios of homogeneous and nonhomogeneous elliptic and axisymmetric jets.
- 40) Mean Temperature Contours for $U_c=85$ m/s, $T_c=185$ C.
- 41) Temperature PDFs for $U_c=70$ m/s, $T_c=150$ C.
- 42) Digitized Image of Elliptic Jet Minor Axis for $U_c=30$ m/s, $T_c=150$ C.

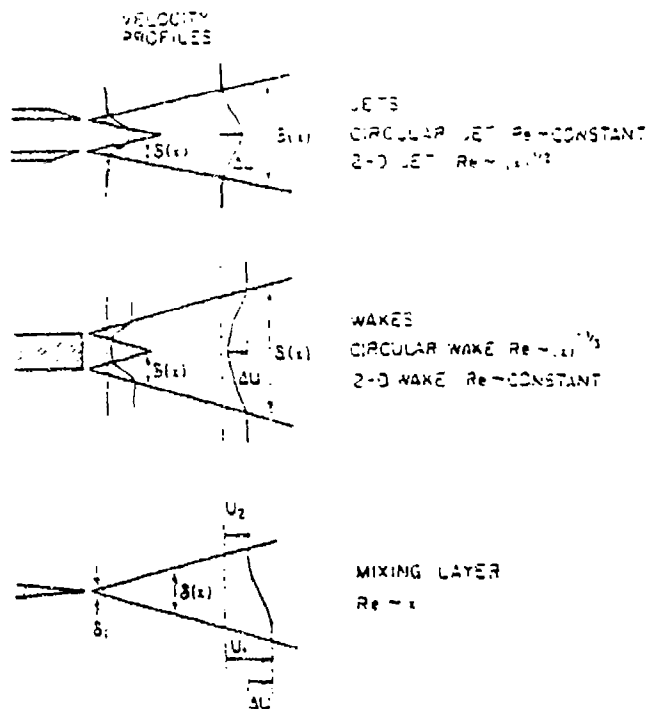


Fig. 1. The major unbounded shear flows. Local Reynolds number, $\Delta U \delta / \nu$, is based on local velocity difference, ΔU , and local turbulent layer thickness, δ . The initial layer thickness is δ_0 .

Figure 1. Free Shear Layers



Figure 2. Vortex pairing (from Winant & Browand 1974) in an unforced mixing layer. $R = 0.28$

Figure 2. Coherent Large Scale Pairing

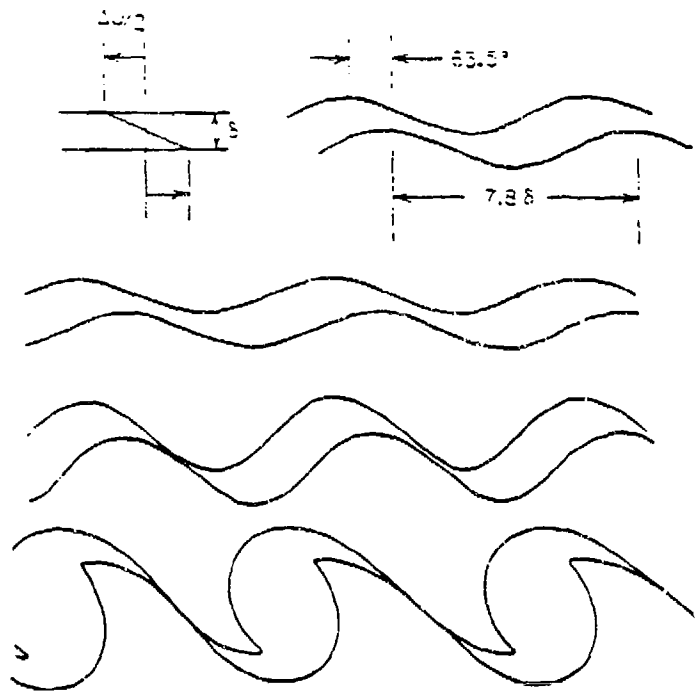


Fig. 2. Growth of the most unstable wave associated with a planar region of constant vorticity.

Figure 3. Shear Layer Formation

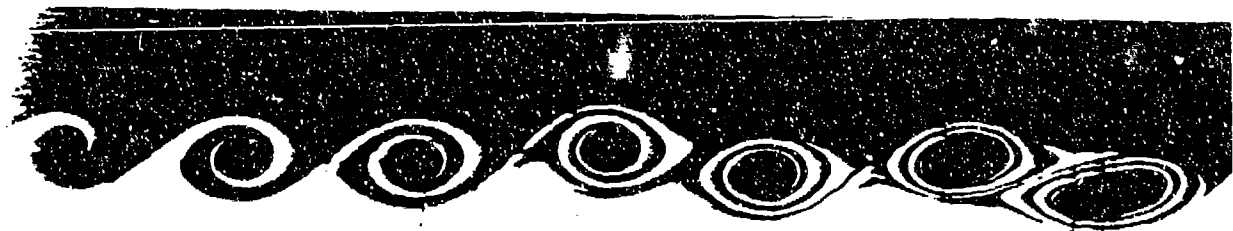
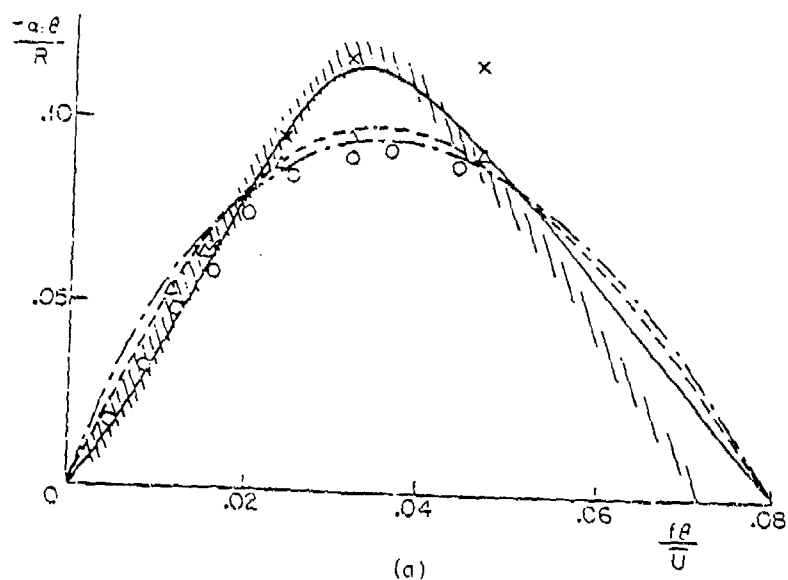
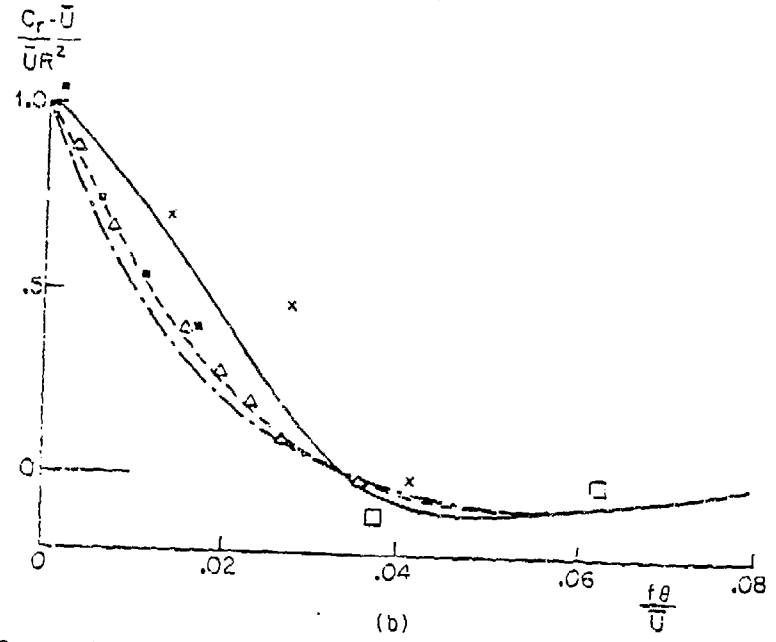


Figure 4 Roll-up of spanwise vortices (from Roberts et al. 1982). $f_t = 1/3$, $R < 1$.

Figure 4. Vortex Roll-up



(a)



(b)

Figure 2 Variations of (a) normalized amplification rate and (b) normalized phase velocity with Strouhal number $f\theta/C$. Linear stability theory (from Monkewitz & Huerre 1982). — $R = 1$; - - - $R = 0.5$; - · - · $R \ll 1$. Experiments: \square $R = 1$ (Sato 1960); \circ $R = 1$ (Freymuth 1966); \times $R = 0.72$ (Miksad 1972); \cdot $R = 1$ (Fiedler et al. 1981); \triangle $R = 0.31$ (Ho & Huang 1982); \blacksquare $R = 1$ (Drubka 1981).

Figure 5. Linear Stability Curves

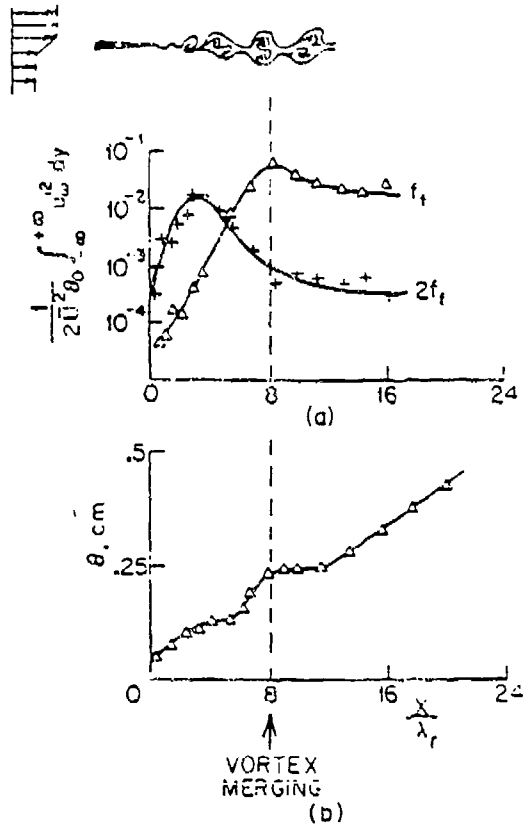


Figure 19 Evolution of (a) spectral components and (b) momentum thickness versus downstream distance (from Ho & Huang 1982). $f_n \leq f_1 \leq f_w$; $R = 0.51$, $\lambda_1 = 2\lambda_r$.

Figure 6. Vortex Merging

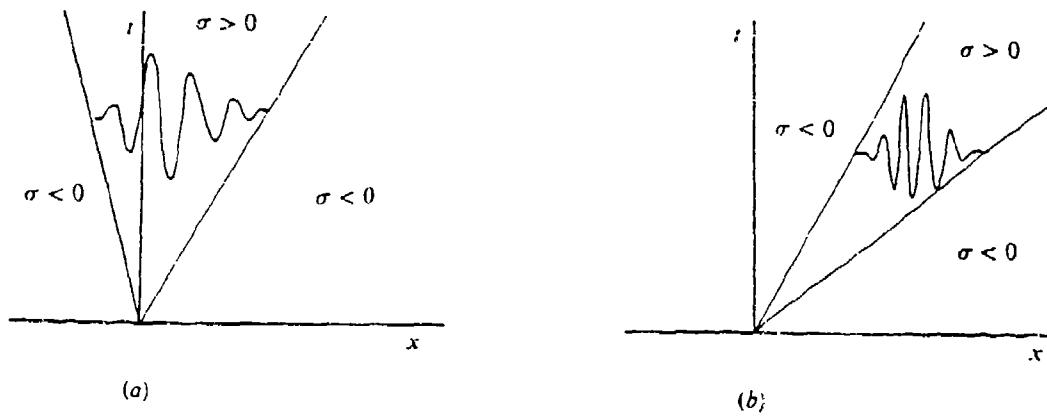


FIGURE 1. Sketch of a typical impulse response: (a) absolutely unstable flow; (b) convectively unstable flow.

Figure 7. Global Stability

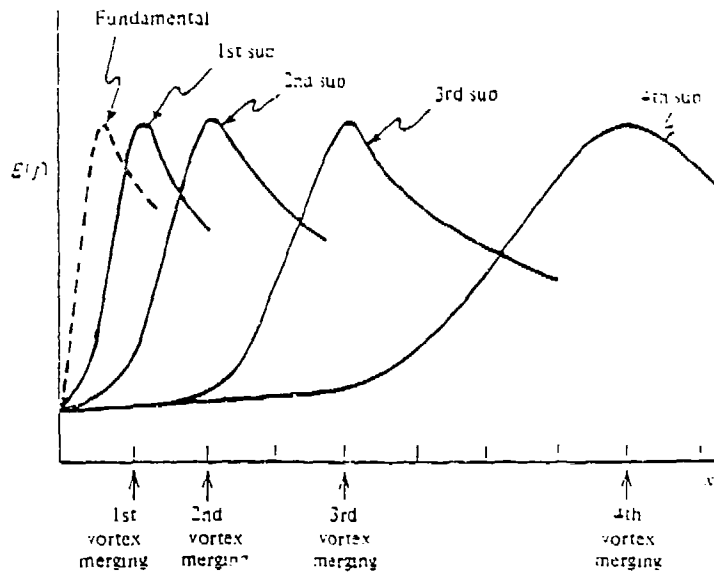


FIGURE 8. The subharmonic evolution (model Ho 1981).

Figure 8. Subharmonic Evolution

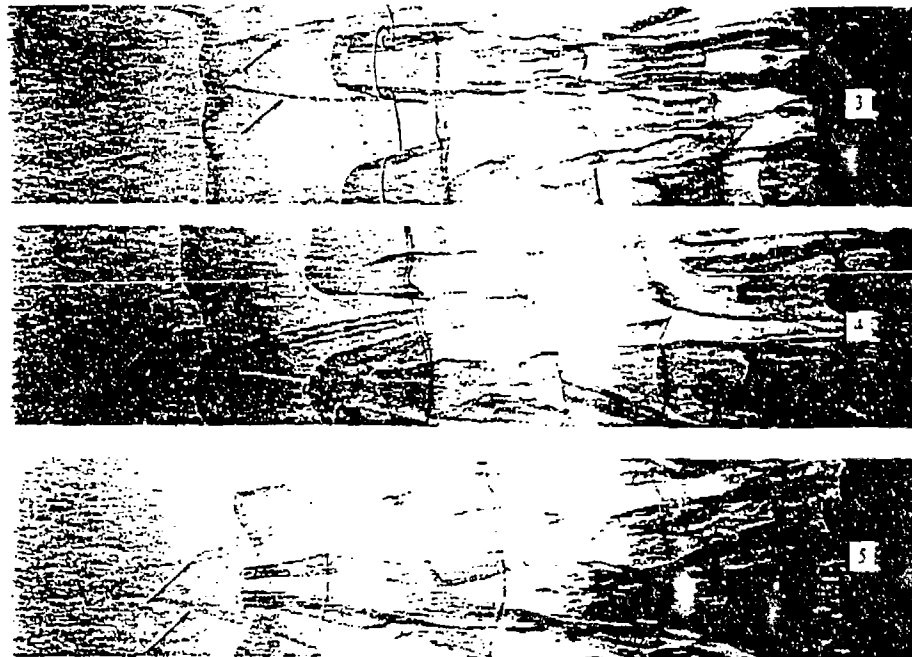


FIGURE 9. Top views showing the organization of five different streamwise vortex structures in the free shear layer ($U_1 = 6.5 \text{ cm/s}$, $U_2 = 3.5 \text{ cm/s}$). The flow is from left to right.

Figure 9. Streamwise Vortices

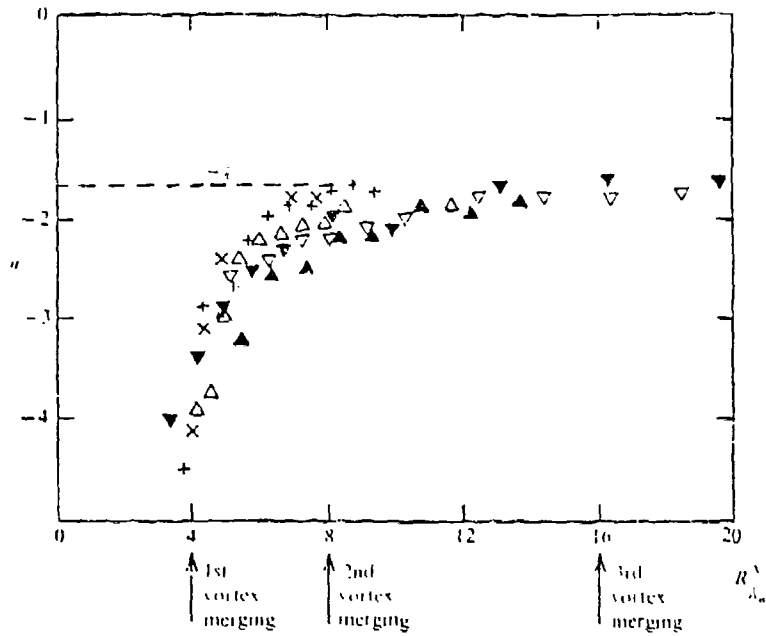


FIGURE 12. Roll-off exponent of power spectra vs. non-dimensional streamwise distance in wind tunnel tests. \times , $R = 0.45$, $U' = 10.2$ m/s; Δ , $R = 0.50$, $U' = 10.2$ m/s; $+$, $R = 0.69$, $U' = 10.2$ m/s; \blacktriangle , $R = 1.00$, $U' = 12.0$ m/s; ∇ , $R = 1.00$, $U' = 12.5$ m/s (Jimenez *et al.*, 1979), \blacktriangledown , $R = 1.00$, $U' = 8.2$ m/s (Jimenez *et al.*, 1979).

Figure 10. Power Spectra Roll-off Exponent

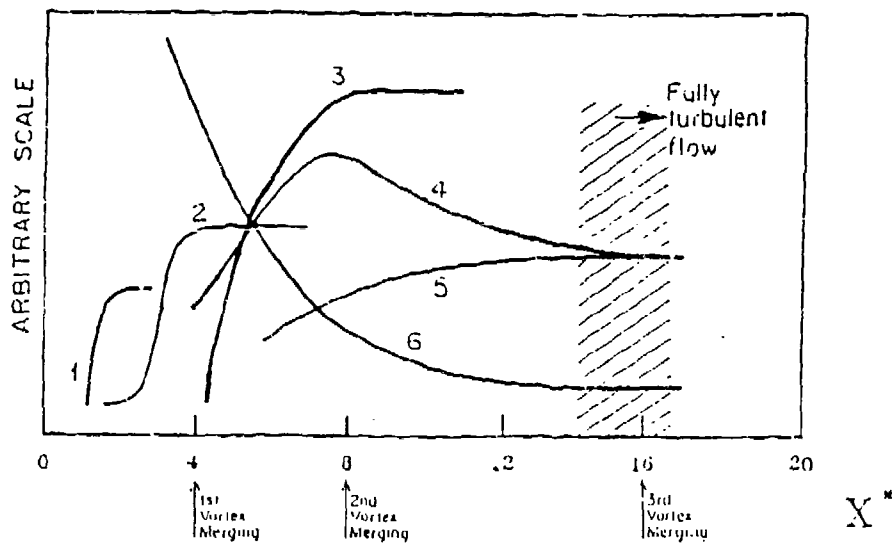


Figure 17. Sequence of transitions

- (1) growth of low frequency perturbations
- (2) phase decorrelation
- (3) small scale transition
- (4) turbulence level of initially laminar boundary layer
- (5) turbulence level of initially turbulent boundary layer
- (6) spanwise separation for 10% correlation

Figure 11. Free Shear Layer Transitions

AXISYMMETRIC JET TOPOLOGY

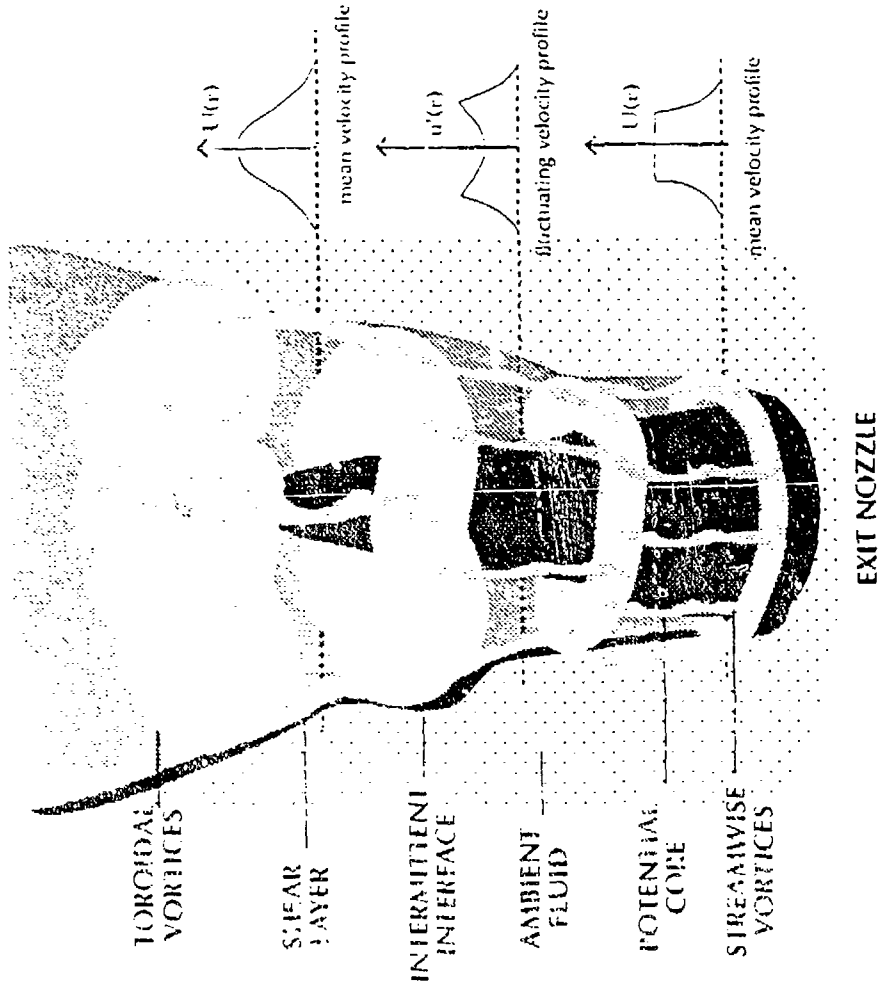


Figure 13. Axisymmetric Jet

Figure 12.

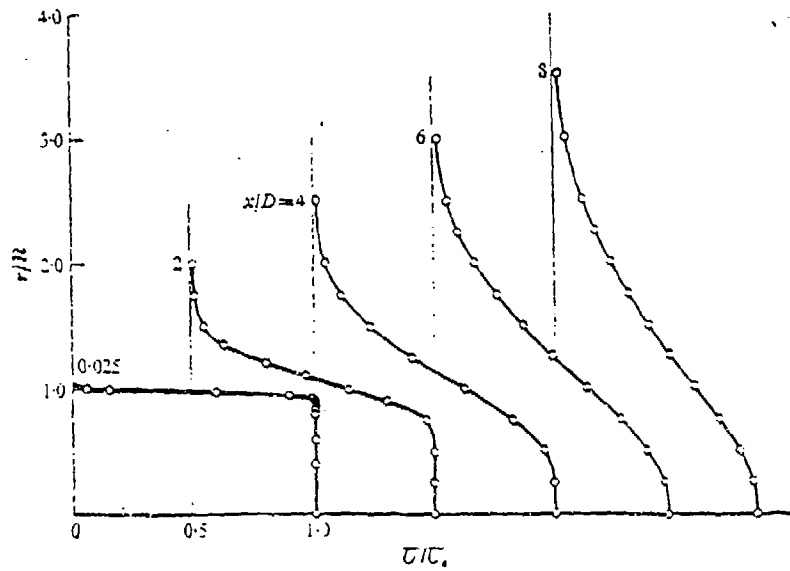


FIGURE 27. Radial mean-speed profiles at five stations along the jet axis

Figure 14. Mean Velocity Profiles

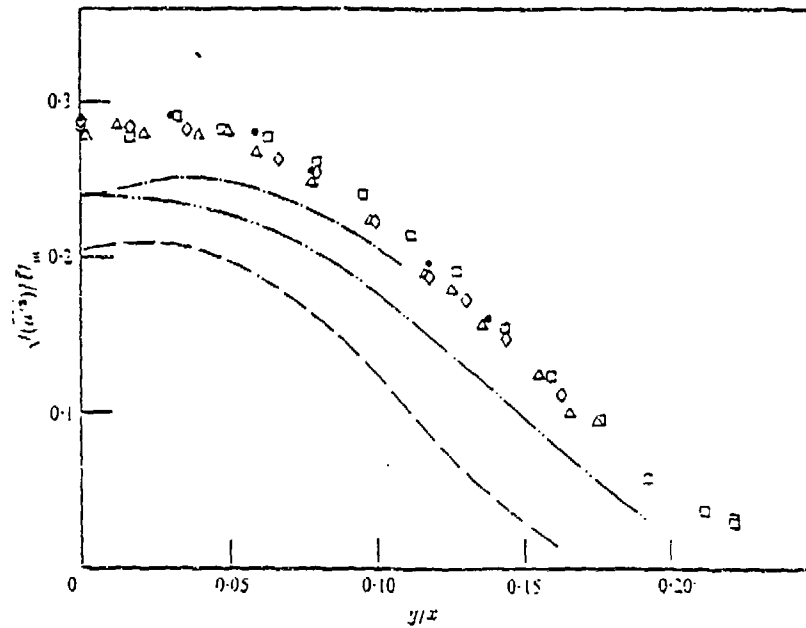


FIGURE 14. Intensity of u' fluctuation across the jet. ---, Corrsin (1949), $x/d = 20$; - · -, present investigation, $x/d = 20$; - · · -, present investigation, $x/d = 60$, using DISA correlator (flat frequency down to 5 Hz). Δ , $x/d = 50$; \square , 60; \diamond , 75; \bullet , 97.5.

Figure 15. Fluctuating Velocity Profiles

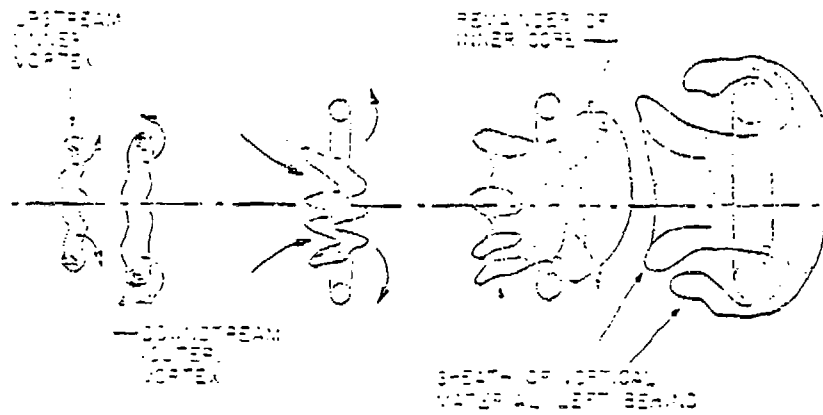


FIGURE 14. SIDE VIEW SCHEMATIC OF VORTEX SHEDDING DURING PAIRING INTERACTION.

Figure 16. Vortex Merging

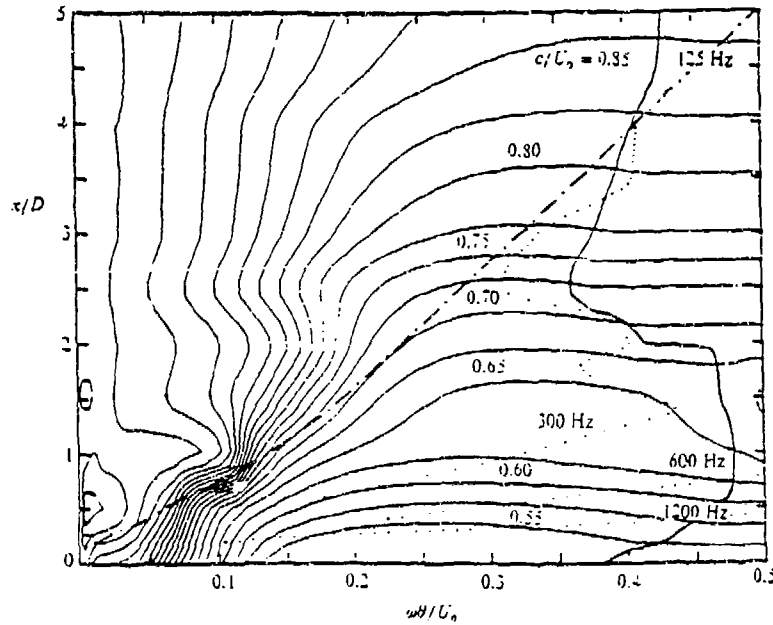


FIGURE 7. Contours of phase speeds computed from spatial stability theory.

Figure 17. Contours of Phase Velocity

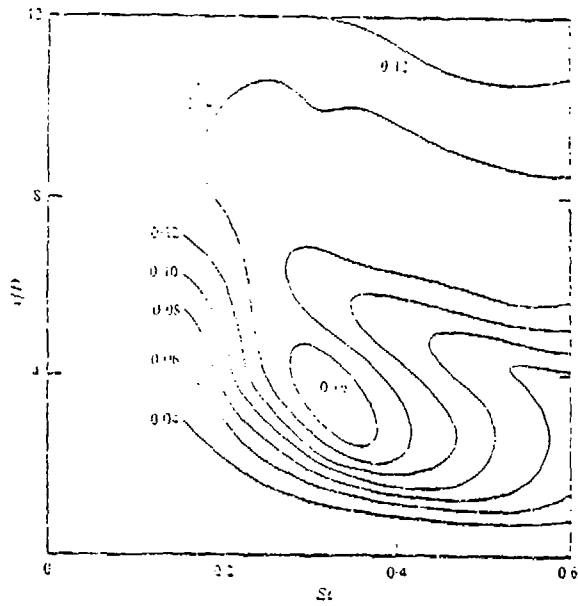


FIGURE 21. Contours of constant turbulence intensity as a function of Strouhal number of forcing and distance downstream. The forcing amplitude is fixed at 2%. The contours are labelled with w/C_u , which changes by 0.02 from one curve to the next.

Figure 18. Preferred Mode

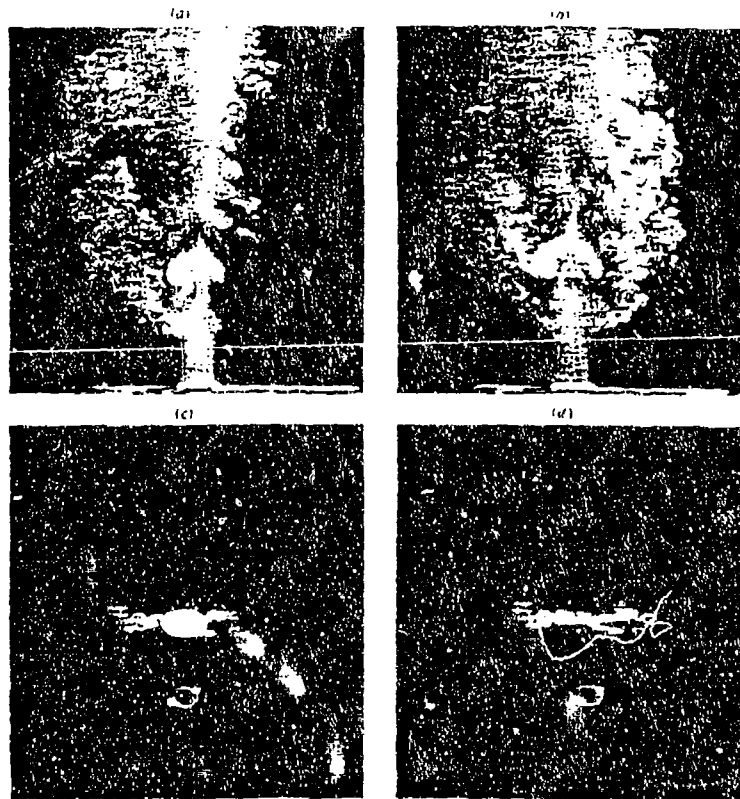


FIGURE 20. Frames from a high-speed movie (500 frames/s twice the vortex passage frequency) of a vortex tube (vortex ratio $\lambda = 0.45$, $Re = 7500$) with smoke illumination by laser sheets. (a, b) Top view of the vortex tube. (c, d) Side view. Frames showing simultaneously longitudinal and transverse views at $z/D = 2.5$ and $z/D = 3.5$.

Figure 19. Side Jets

VORTEX RING DEVELOPMENT
IN 2:1 ASPECT-RATIO ELLIPTIC NOZZLE

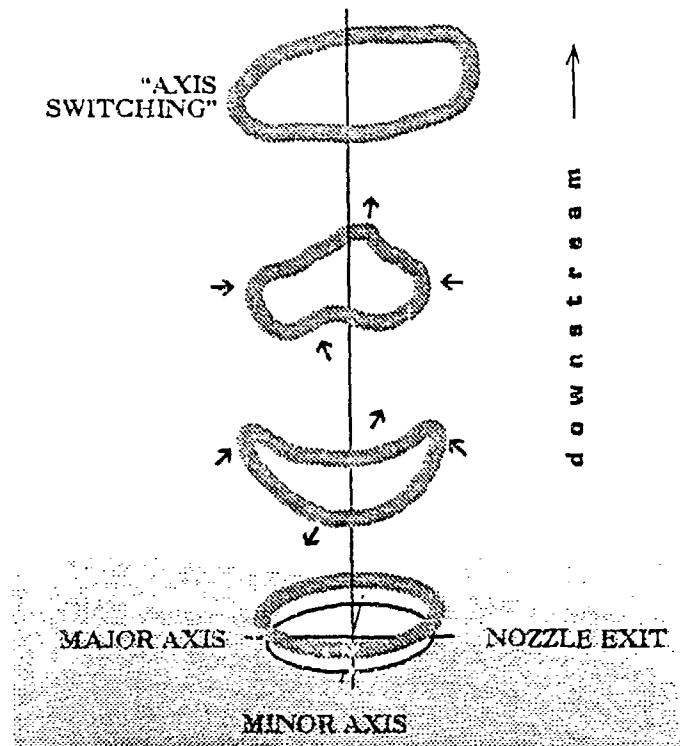


Figure 20.

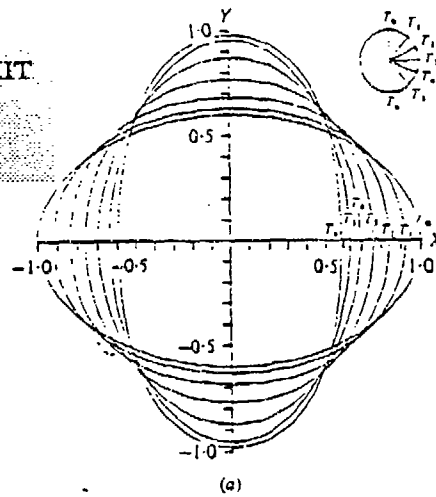


Figure 21.
Elliptic Vortex Ring Evolution

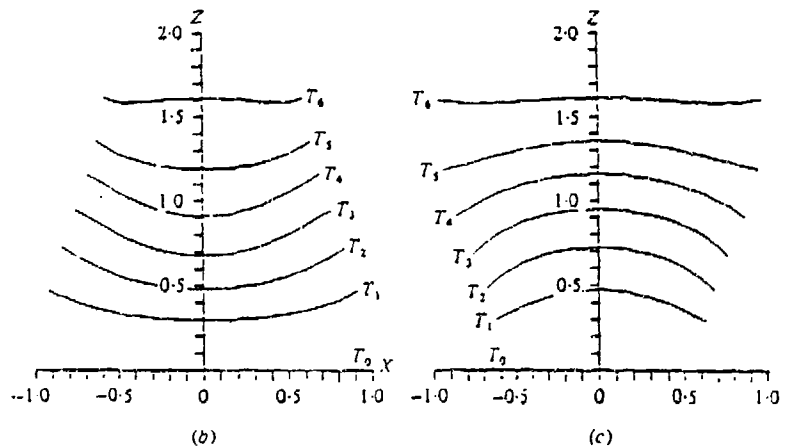


FIGURE 3. Evolution of the elliptic vortex ring of axes ratio 0.6.
(a) Plan view, (b) side view, (c) end view.

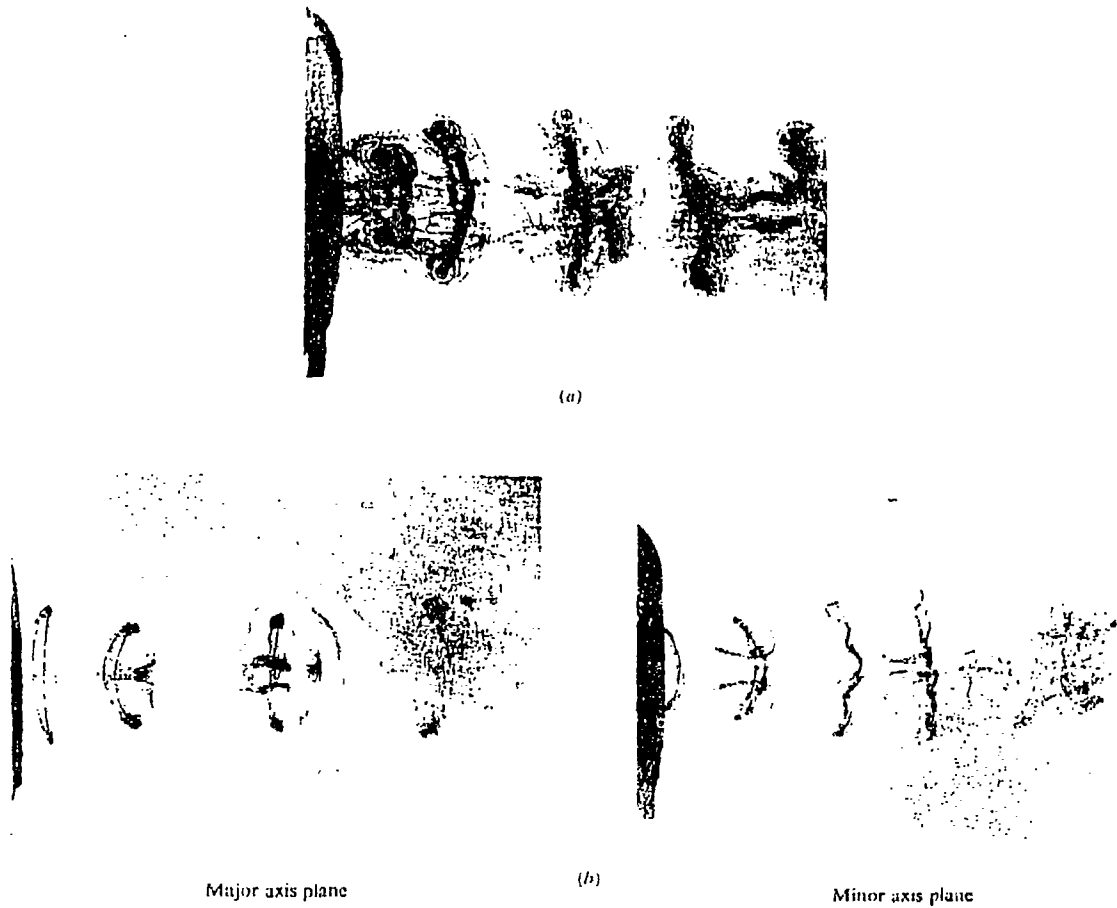


FIGURE 15. (a) Vortex merging (tagged by dye traces) in a forced elliptic jet. (b) Azimuthal deformation of vortex (tagged by dye traces) in a forced elliptic jet (Gutmark & Ho 1983, 1986).

Figure 22. Elliptic Jet Flow Visualization

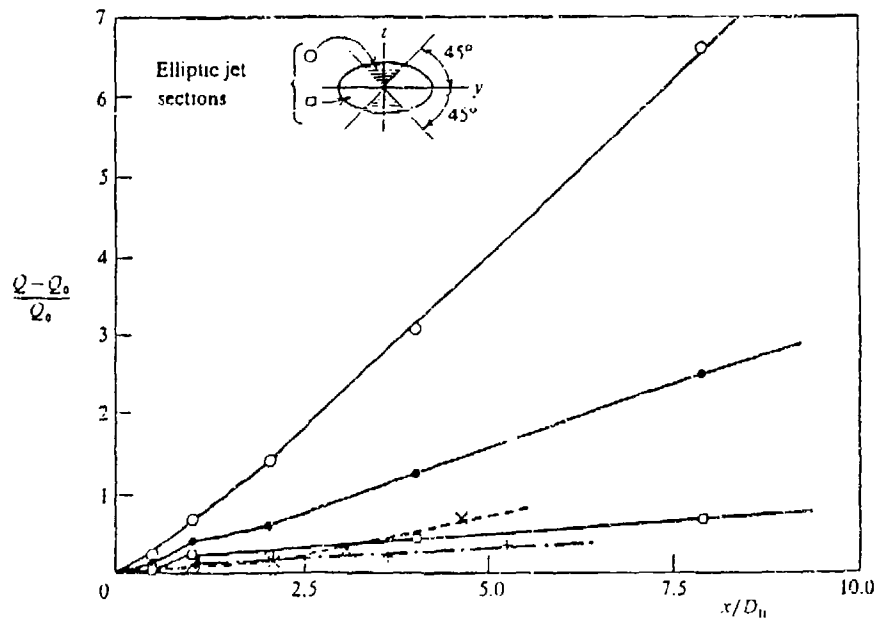


FIGURE 17. The entrainment ratio for an elliptic jet, hydraulic diameter $D_h = 3.23$ cm (\bullet); a circular jet, $D_h = 3.81$ cm (\times); and a two-dimensional jet, $D_h = 4.88$ cm (Ho & Hsiao 1982) ($+$).

Figure 23. Elliptic Jet Entrainment

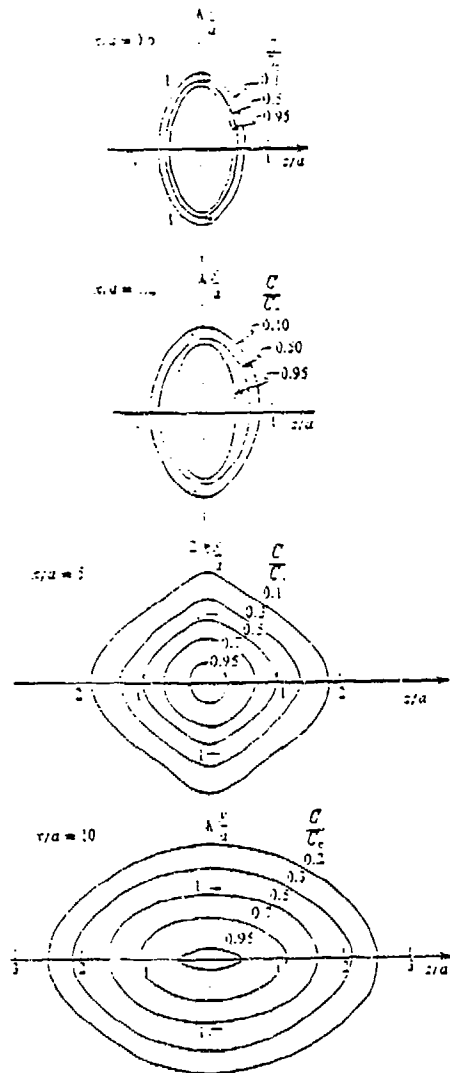
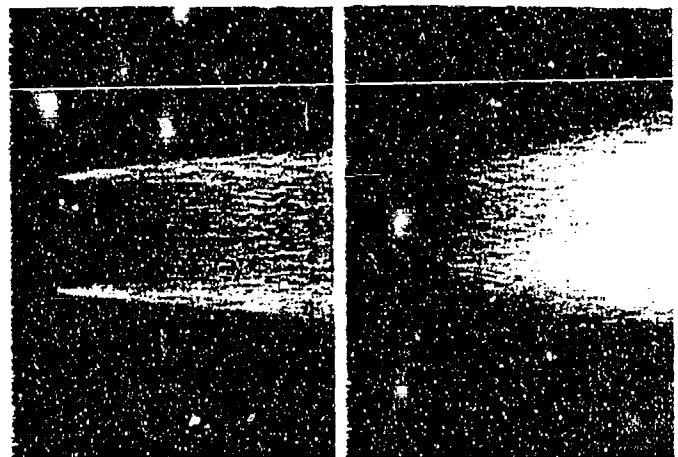


FIGURE 25. Constant-velocity contours.

Figure 25.
Nozzle Flow Visualization

Figure 24.
Elliptic Jet Mean Velocity Contours



CIRCULAR NOZZLE ELLIPTICAL NOZZLE
(MINOR AXIS)

Fig. 21. Fuel-Rich Plume Combustion -
Mixing Enhancement with Elliptical Nozzle.



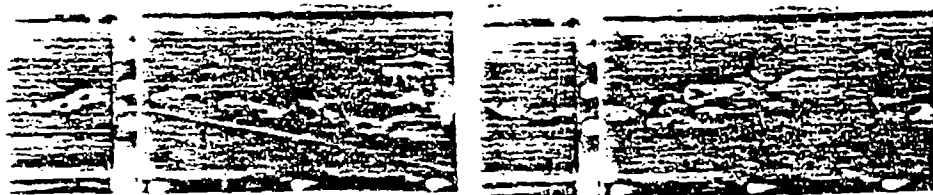
(c)

FIGURE 3. Mixing layer under mode I forcing: $f_0/f_\infty = 0.70$, $\Delta\phi = 120^\circ$.



(d)

FIGURE 4. Mixing layer under mode II forcing: $f_0/f_\infty = 0.22$, $\Delta\phi = 31.4^\circ$.



(e)

(f)

FIGURE 5. Collective interaction: $f_0/f_\infty = 0.1$, $\Delta\phi = 31.4^\circ$.

Figure 26.
Mode 'm' Forcing

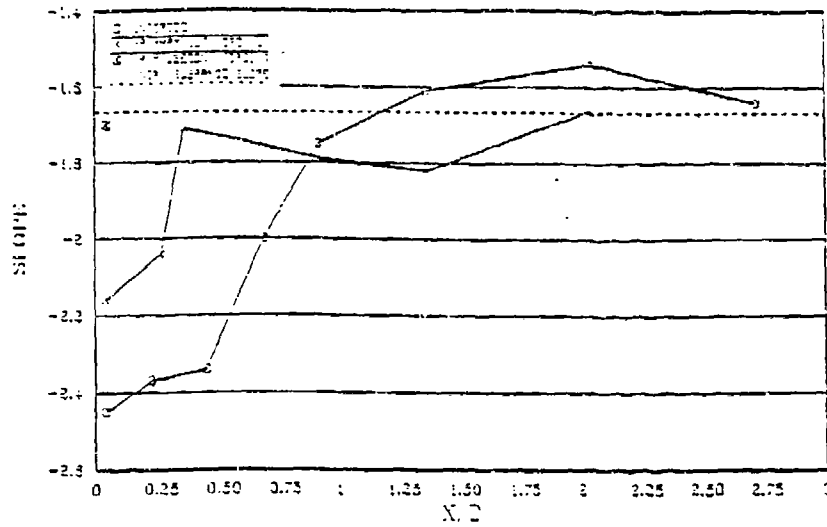


FIGURE 21. Small-scale turbulence transition as indicated by the change of the roll-off exponent in the velocity fluctuation spectrum, as a function of the streamwise distance. Unforced. \circ : Air only forcing ($St_{air} = 0.49$), \times : Air and low level fuel forcing ($St_{air} = 0.49$, $St_{fuel} = 5.91$), \square .

Figure 27. Power Spectra Roll-off Exponent

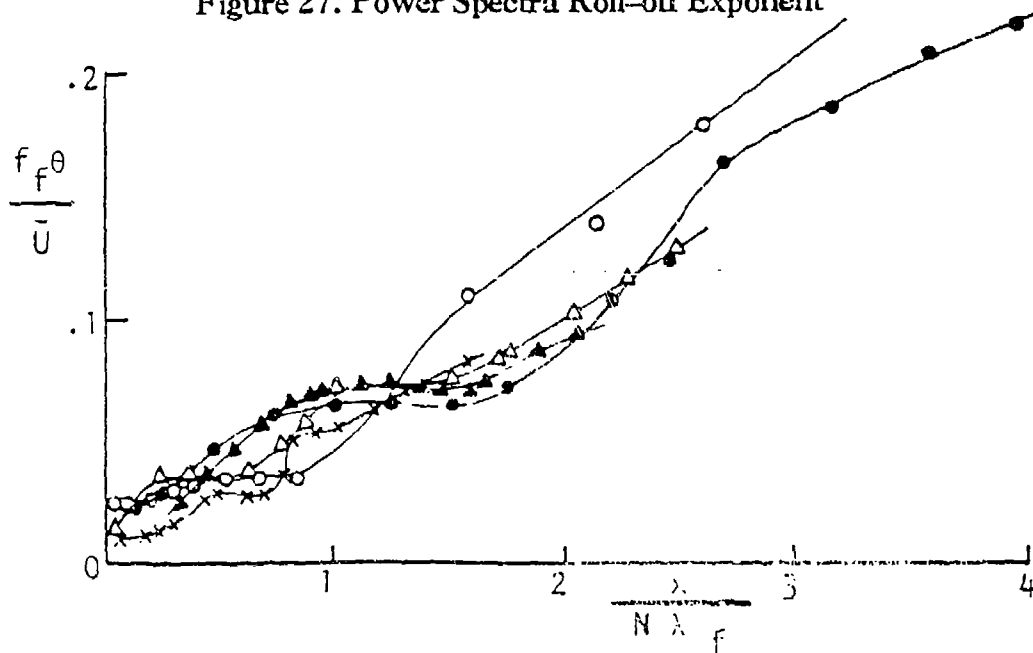


Figure 24. Rescaled free shear layer: variations of momentum thickness, with rescaled downstream distance \bullet $f_f = 0.65 f_n$, Δ $f_f = 0.43 f_n$, \times $f_f = 0.24 f_n$; $R = 0.31$, $N = 4$ (Ho & Huang 1982). \blacktriangle $f_f \ll f_n$; $R = 0.25$, $N = 4$ (Oster & Wygnanski 1982). \circ $f_f = f_n$; $R = 1$, $N = 2$, natural forcing (Drubka 1981).

Figure 28. Rescaled Free Shear Layer

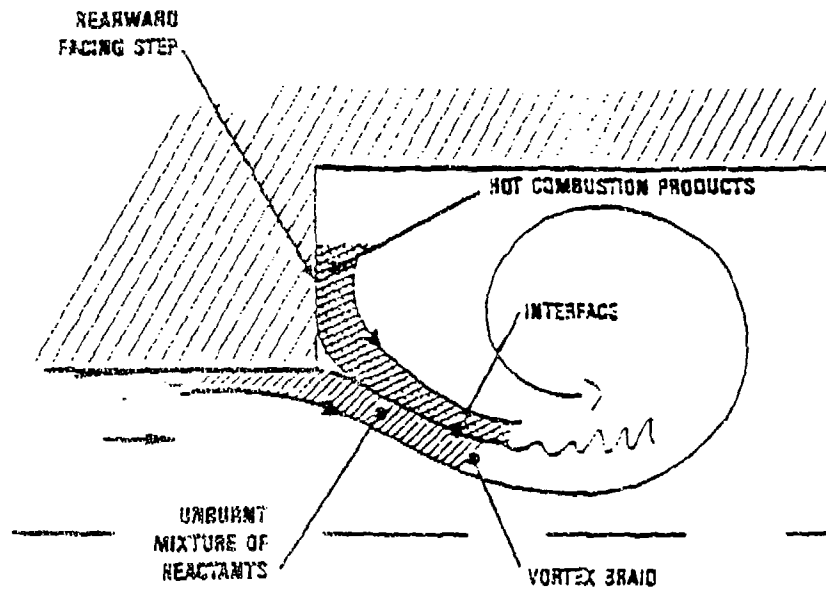


Fig. 3. Vortex Roll-Up in Dump Combustor.

Figure 29.

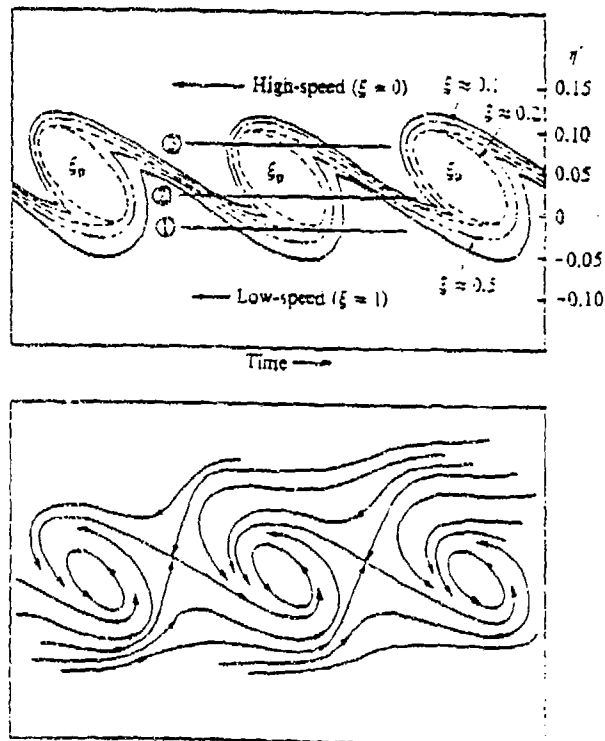


FIGURE 13. Inferred concentration structure and flow patterns of the pre-mixing transition mixing layer.

Figure 30. Shear Layer Mixing Dynamics

2:1 Aspect Ratio Elliptic Jet Facility

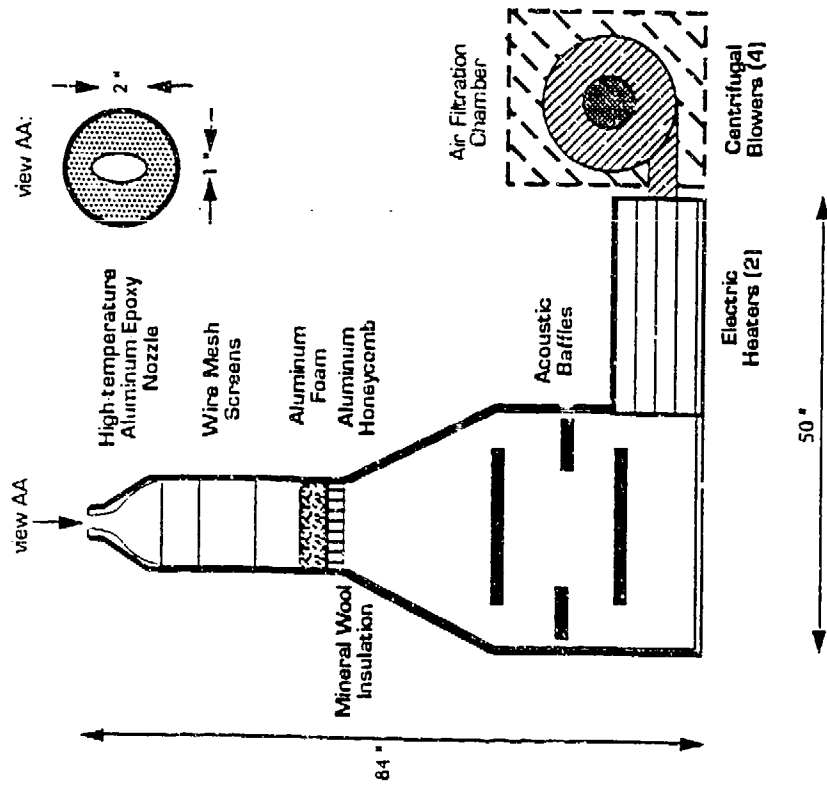


Figure 31.

Forcing Arrangement

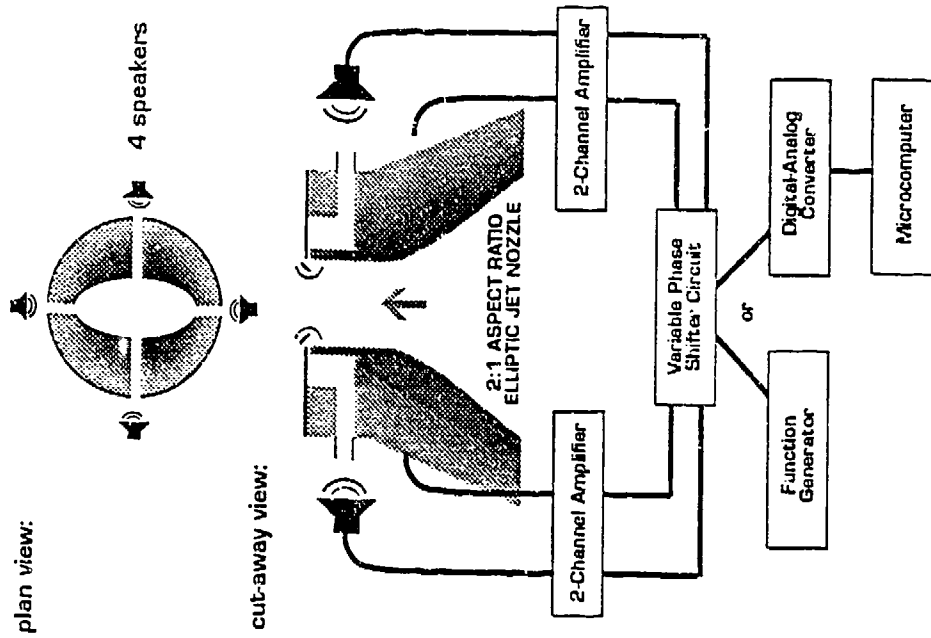


Figure 32.

Optical Flow Diagnostic Facility Focusing Schlieren System

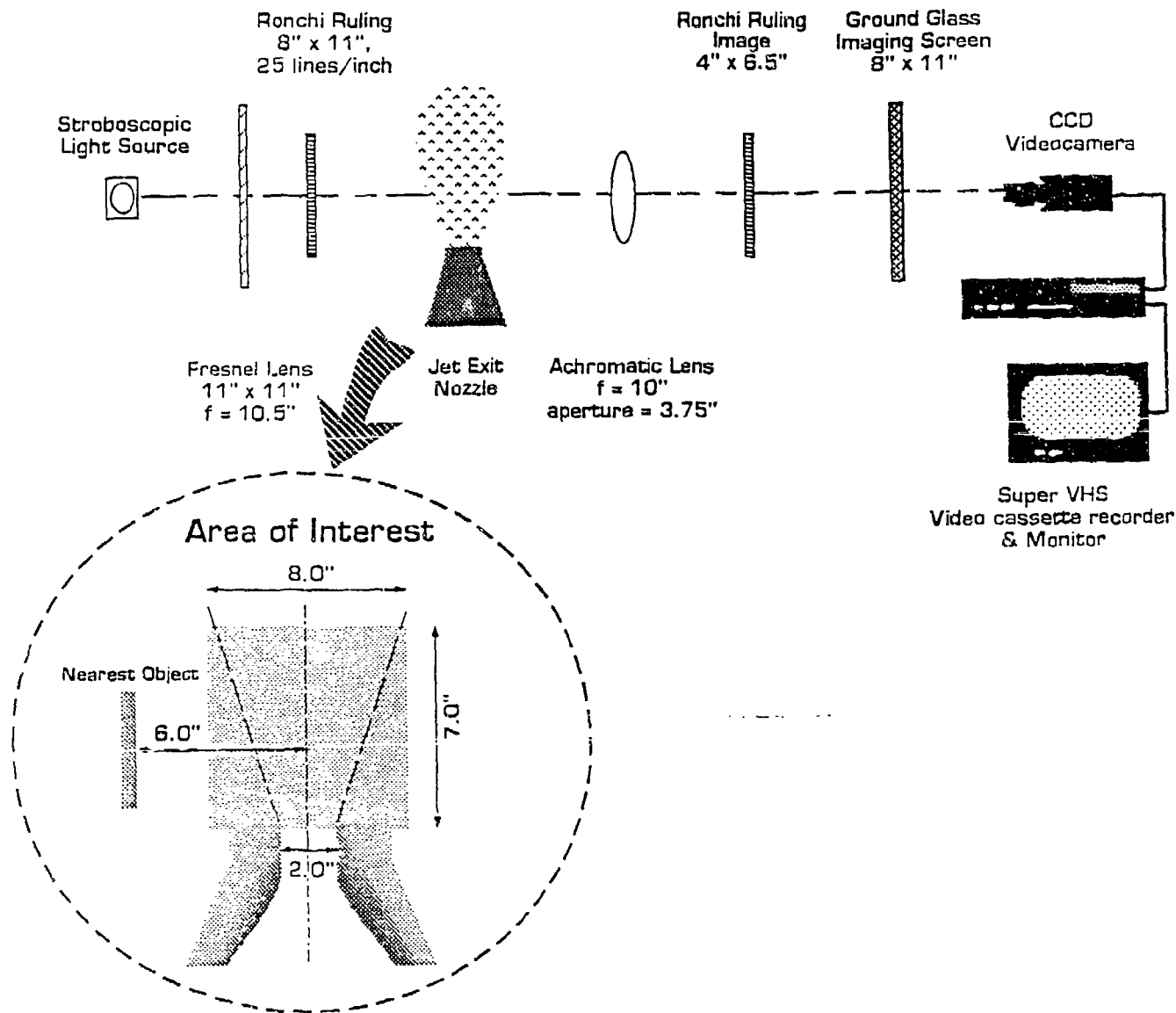


Figure 33.

Mean Velocity Profiles

$U_{\text{exit}} = 30 \text{ m/s}$ $T_{\text{exit}} = 30 \text{ C}$

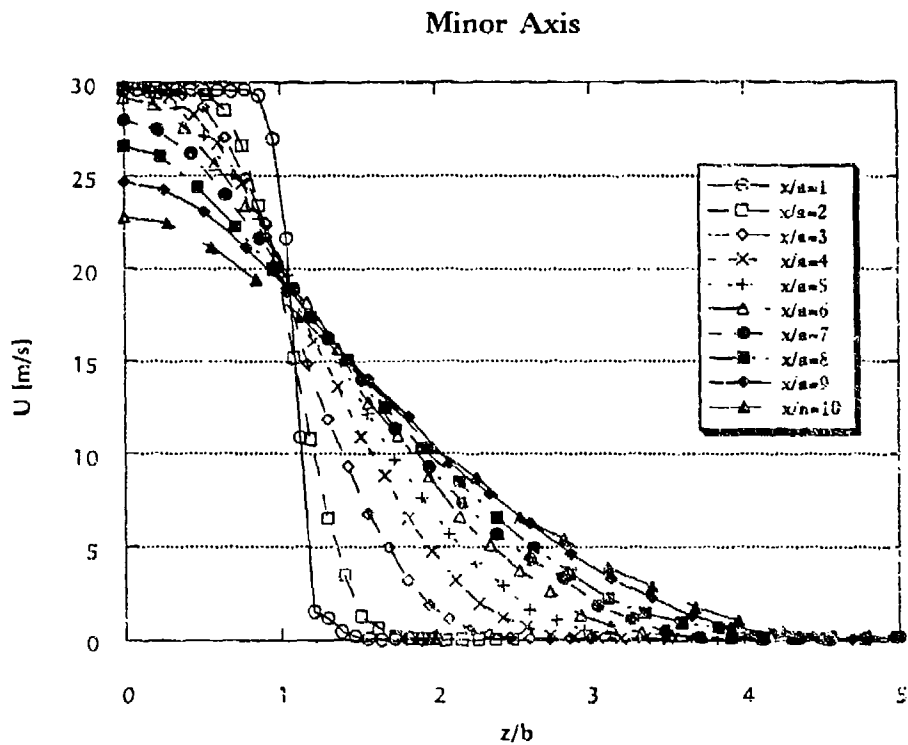
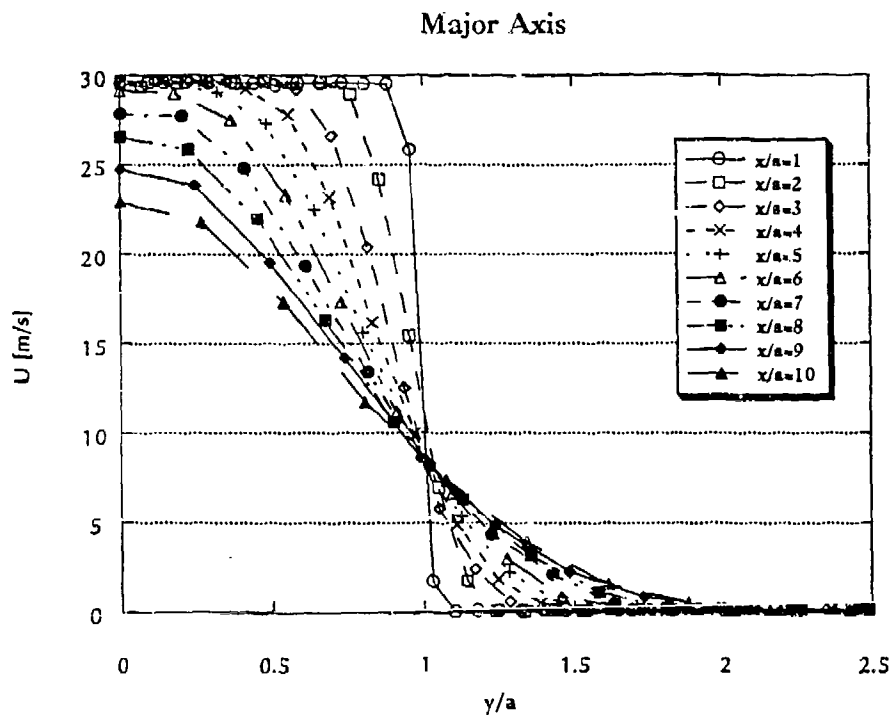
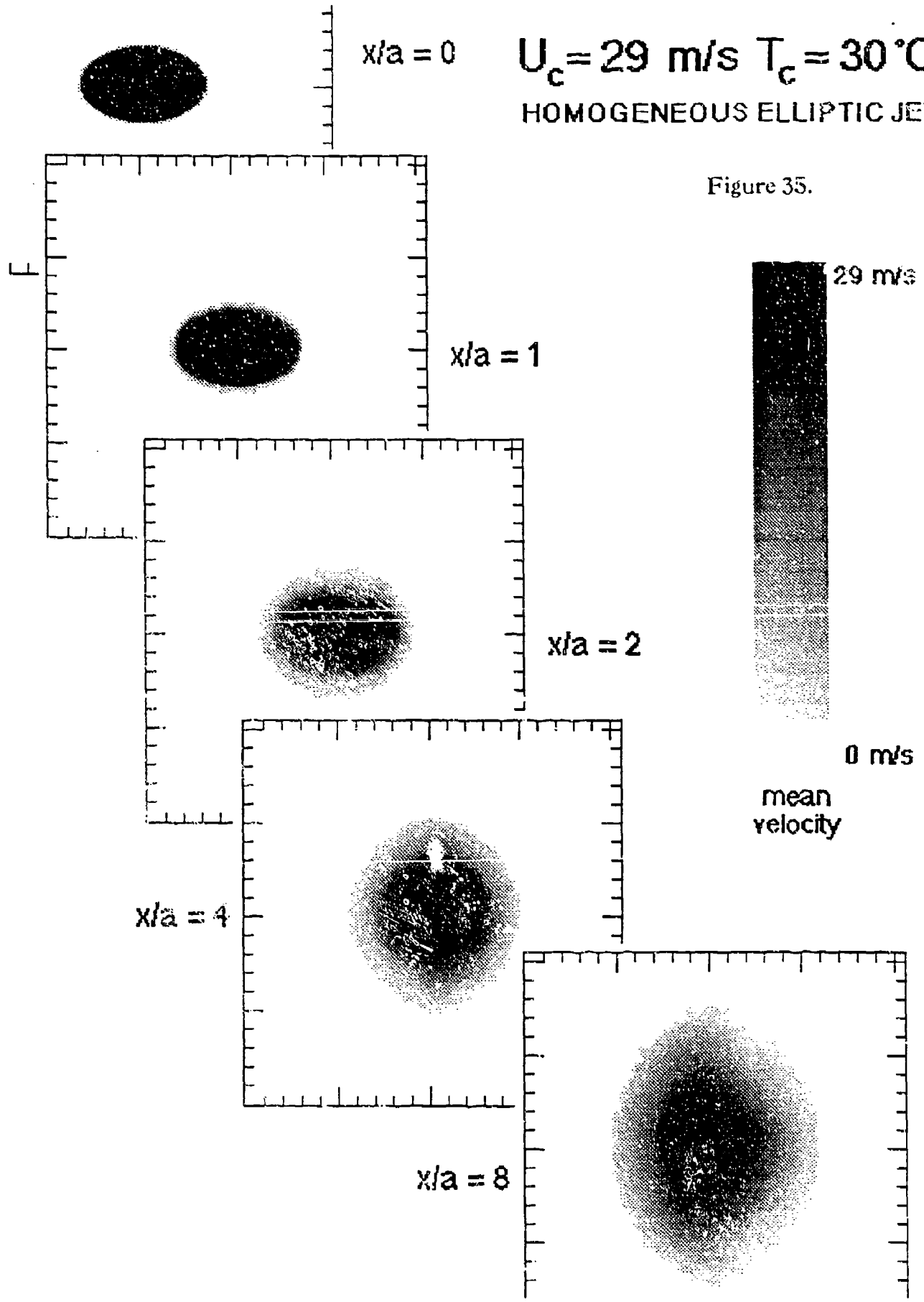


Figure 34.

$x/a = 0$

$U_c = 29 \text{ m/s}$ $T_c = 30^\circ\text{C}$
HOMOGENEOUS ELLIPTIC JET

Figure 35.



Elliptic Jet Entrainment Ratios

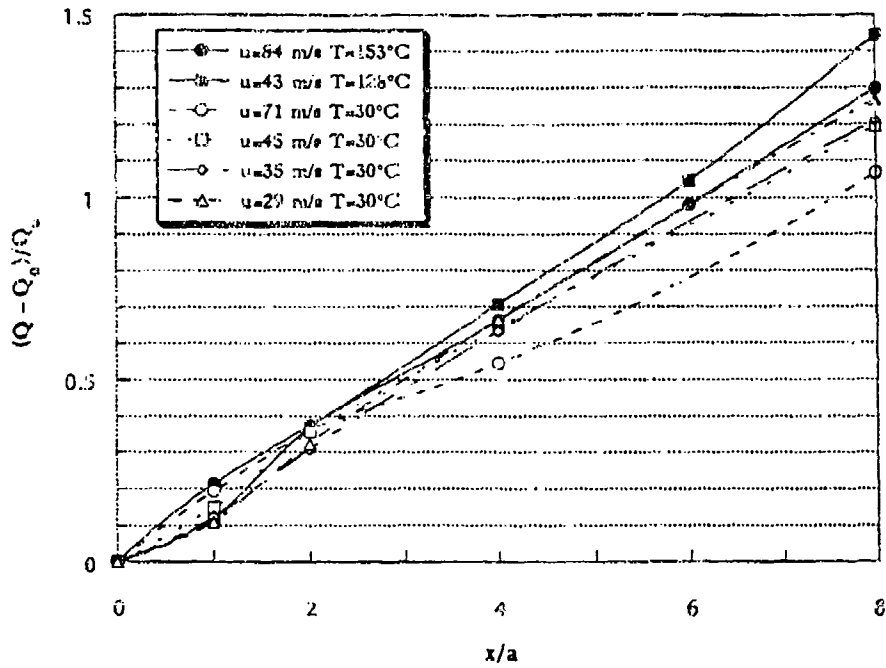


Figure 36.

Velocity Halfwidths $U_c = 30$ m/s

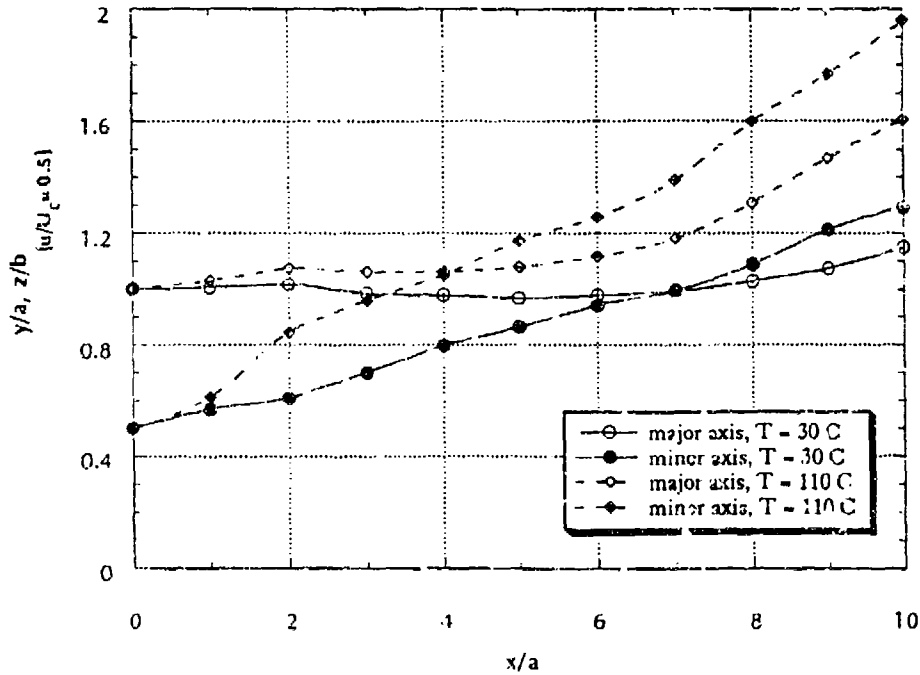


Figure 37.

Subsonic Elliptic Jet Axis Switching Location

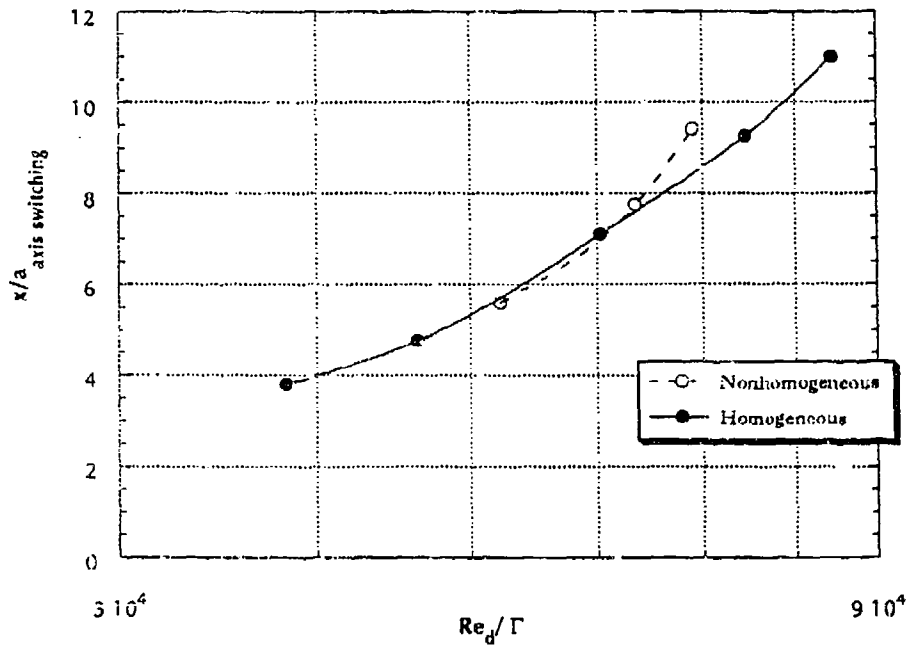


Figure 38.
Entrainment Rate Ratio

Elliptic Jet versus Axisymmetric Jet

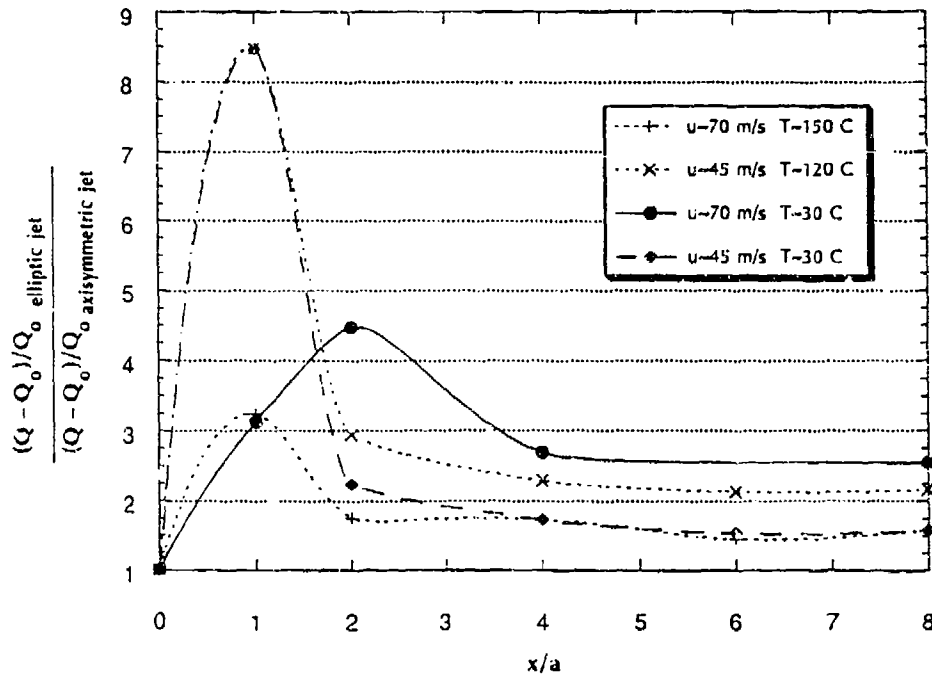
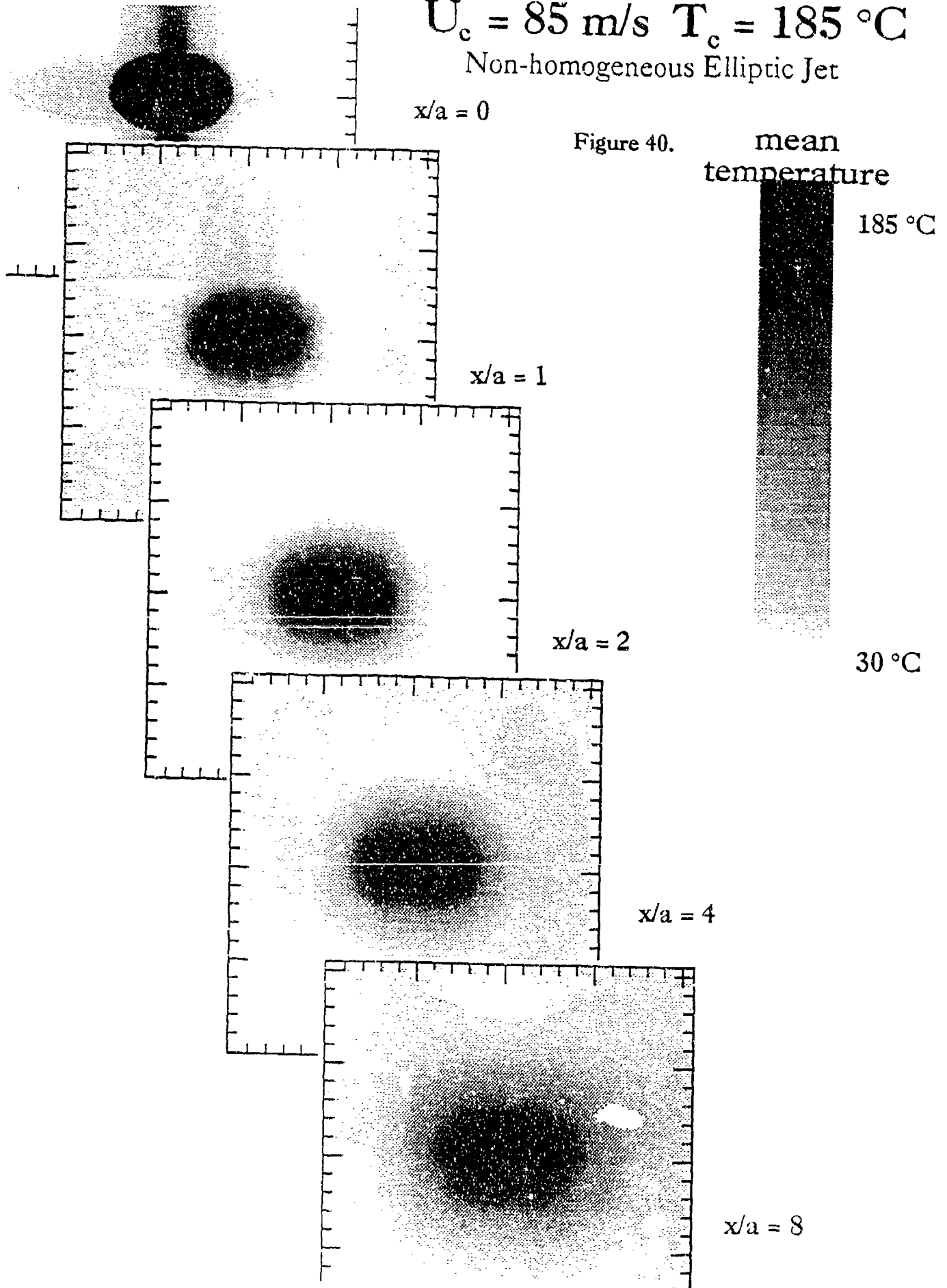


Figure 39.

$U_c = 85 \text{ m/s}$ $T_c = 185 \text{ }^\circ\text{C}$

Non-homogeneous Elliptic Jet



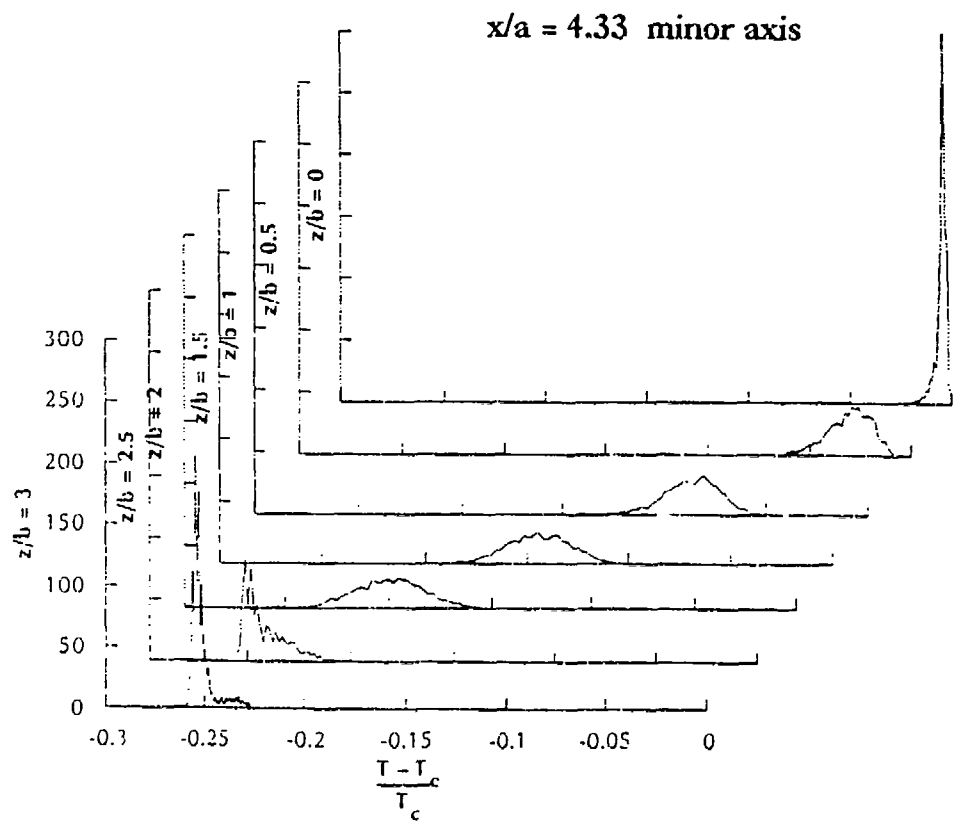
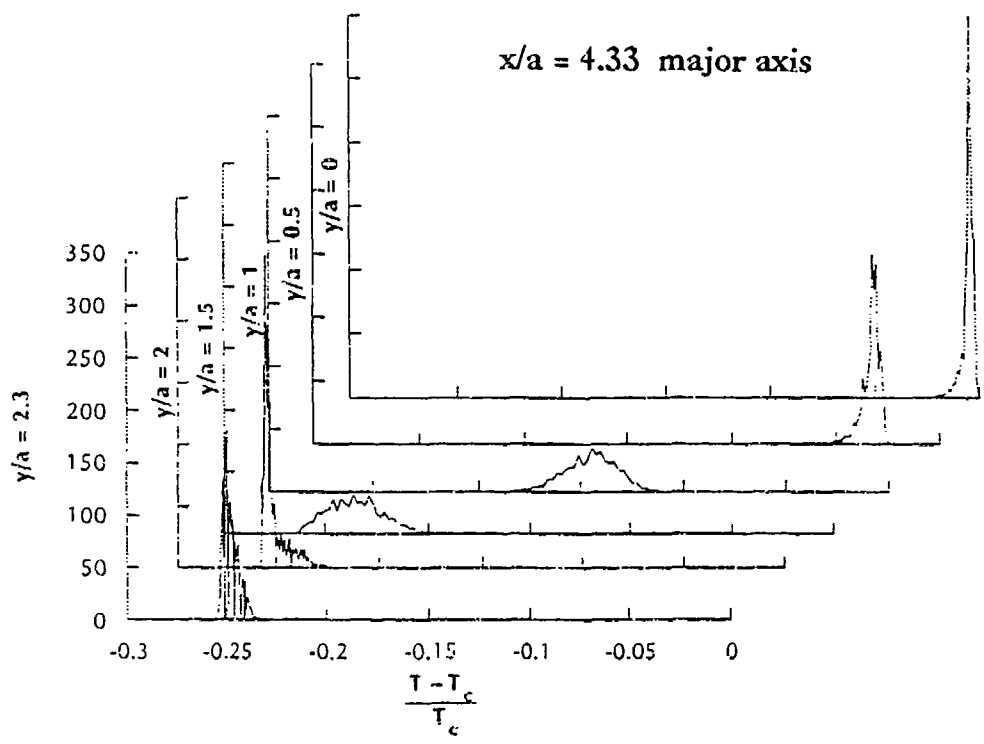


Figure 41. Temperature PDFs for $U=70$ m/s $T=150$ C



Illustration 2 Elliptic Jet Minor Axis

Figure 42. Focusing Schlieren Flow Visualization